Interplay of Higgs Phenomenology and New Physics in Supersymmetric Theories

Dissertation

zur Erlangung des Doktorgrades

an der Fakultät für Mathematik,

Informatik und Naturwissenschaften

Fachbereich Physik

der Universität Hamburg

vorgelegt von

Shruti Patel

aus

Mumbai, Indien

Hamburg

2017

Gutachter der Dissertation:	Prof. Dr. Georg Weiglein Prof. Dr. Jan Louis
Zusammensetzung der Prüfungskommission:	Prof. Dr. Georg Weiglein Prof. Dr. Jan Louis Prof. Dr. Géraldine Servant Jun.-Prof. Dr. Christian Sander Prof. Dr. Günter Sigl
Vorsitzender der Prüfungskommission:	Prof. Dr. Günter Sigl
Datum der Disputation:	16. Oktober 2017
Vorsitzender des Promotionsausschusses Physik:	Prof. Dr. Wolfgang Hansen
Leiter des Fachbereichs Physik:	Prof. Dr. Michael Potthoff
Dekan der Fakultät MIN:	Prof. Dr. Heinrich Graener

Abstract

Supersymmetric (SUSY) theories such as the Minimal Supersymmetric Standard Model (MSSM) predict a new particle spectrum, including an extended Higgs sector, in order to address fundamental questions that remain unanswered with the results obtained at the Large Hadron Collider (LHC) so far. Despite an extensive programme to search for additional Higgs bosons at the LHC, no new Higgs-like particles have been observed beyond the discovered signal at 125 GeV. Such searches have not taken into account $\mathcal{CP}$-violating effects in the Higgs sector, which are well-motivated in the light of the perceived baryon asymmetry in the universe, and which can induce significant deviations in the phenomenology of the Higgs bosons. The search for additional Higgs bosons should therefore account for the possibility that they may not necessarily be $\mathcal{CP}$-eigenstates. In the most general case where the MSSM parameters can be complex, the three neutral Higgs bosons of the theory are the loop-corrected mass eigenstates $\{h_1, h_2, h_3\}$, which are admixtures of the tree-level $\mathcal{CP}$-even and $\mathcal{CP}$-odd Higgs states. This thesis focusses on the effects of complex parameters on the production cross sections of these Higgs bosons and the interference occurring between nearly mass-degenerate Higgs states. In the first part of this thesis, we discuss higher-order corrections in the Higgs sector which give rise to $\mathcal{CP}$-violating mixing between the tree-level mass eigenstates, and present a computation of inclusive cross sections for the production of the $\mathcal{CP}$-admixed Higgs bosons through gluon fusion and bottom-quark annihilation. The predictions for the gluon-fusion process are based on an explicit calculation of the leading-order cross section for the general case of arbitrary complex parameters, supplemented by various higher-order corrections. The cross sections for the bottom-quark annihilation process are treated with a simple re-weighting procedure. In the next part, we describe the implementation of our cross-section predictions into an extension of the numerical code `SusHi`, named `SusHiMi`. In our numerical analysis, we employ `SusHiMi` to study the effects of the phase of the soft SUSY-breaking trilinear coupling of the Higgs with the top squark, and of the phase of the gluino mass parameter on the neutral Higgs cross sections, masses, and mixings. We demonstrate that squark effects can be strongly dependent on the phases of the complex parameters, and emphasise the relevance of the resummation of squark effects in the bottom-Yukawa coupling. Furthermore, we show that in a scenario where the two heavy Higgs bosons, h_2 and h_3, are strongly admixed and nearly mass-degenerate, experimentally resolving the two Higgs bosons as separate signals may not be possible. Only the sum of their cross sections including interference terms can be measured experimentally. Finally, we incorporate our cross section predictions into a formalism to account for the $\mathcal{CP}$-violating interference between the Higgs bosons. In the prediction of the process $b\bar{b} \to h_2, h_3 \to \tau^+\tau^-$, we show that strongly destructive interference arises in the benchmark scenario defined in this thesis. Consequently, considerable parameter regions escape the exclusion bounds, which would be ruled out in LHC searches which neglect these interference contributions.

Zusammenfassung

Supersymmetrische (SUSY) Theorien wie das Minimale Supersymmetrische Standardmodell (MSSM) sagen ein erweitertes Teilchenspektrum inklusive eines erweiterten Higgs-Sektors voraus, um damit Fragen zu beantworten, die nach der bisherigen Datennahme des "Large Hadron Collider" (LHC) noch offen geblieben sind. Obwohl am LHC sehr intensiv nach weiteren Higgs-Bosonen gesucht wurde, gibt es keine Anzeichen auf weitere Higgs-Bosonen neben dem beobachteten Signal bei 125 GeV. Bisher berücksichtigten die Suchen jedoch keine $\mathcal{CP}$-verletzenden Effekte im Higgs-Sektor, obwohl Letztere insbesondere durch die Baryonasymmetrie im Universum gut motiviert sind. Zudem haben sie einen erheblichen Einfluß auf die Higgs-Phänomenologie. Im allgemeinsten Fall mit komplexen MSSM-Parametern sind die drei neutralen Higgs-Bosonen schleifenkorrigierte Masseneigenzustände $\{h_1, h_2, h_3\}$, die Mischungen der $\mathcal{CP}$-geraden und -ungeraden Higgs-Zustände in niedrigster Ordnung Störungstheorie sind.

In dieser Arbeit konzentrieren wir uns auf Effekte dieser komplexen Parameter auf die Produktionswirkungsquerschnitte der Higgs-Bosonen und auf die Interferenzen, die zwischen massenentarteten Higgs-Bosonen auftreten. Die Arbeit gliedert sich in drei Teile: Im ersten Teil diskutieren wir Korrekturen höherer Ordnung im Higgs-Sektor. Wir berechnen den inklusiven Wirkungsquerschnitt für die Produktion durch Gluon-Fusion und Bottom-Quark Paarvernichtung. Die Vorhersagen für Gluon-Fusion basieren auf einer expliziten Berechnung des Wirkungsquerschnittes in führender Ordnung Störungstheorie für den allgemeinsten Fall komplexer Paramter. Dieses Resultat wird ergänzt durch Korrekturen höherer Ordnung. Die Wirkungsquerschnitte durch Bottom-Quark Paarvernichtung werden durch eine Reskalierung gewonnen. Im zweiten Teil beschreiben wir die Implementierung unserer Wirkungsquerschnittsberechnung in einer Erweiterung des numerischen Programmes `SusHi` namens `SusHiMi`. Wir nutzen `SusHiMi` um die Effekte der Phase der trilinearen Kopplung des Higgs-Bosons an Stop-Squarks und der Phase des Gluino-Massenparameters auf die neutralen Higgs-Boson Wirkungsquerschnitte, die Higgs-Massen und deren Mischung zu untersuchen. Wir zeigen, dass die Squarkeffekte stark von den Phasen der komplexen Parameter abhängen und betonen die Bedeutung der Resummation von Squarkeffekten in der Bottom-Quark Yukawa-Kopplung. Desweiteren zeigen wir in einem Szenario, in dem zwei schwere Higgs-Bosonen h_2 und h_3 stark mischen und nahezu massenentartet sind, dass die beiden Higgs-Bosonen als getrennte Signale experimentell im allgemeinen nicht auflösbar sind, sondern nur die Summe der Wirkungsquerschnitte inklusive des Interferenzterms experimentell bestimmbar ist. Zuletzt lassen wir unserere Wirkungsquerschnittsberechnung in einen Formalismus einfließen, der die hervorgerufene Interferenz zwischen den Higgs-Bosonen im Falle von $\mathcal{CP}$-Verletzung berücksichtigt. Für den Prozess $b\bar{b} \to h_2, h_3 \to \tau^+\tau^-$ zeigen wir die starke desktruktive Interferenz für ein in dieser Arbeit definiertes Szenario. In einem solchen Fall sind Parameterregionen erlaubt, die im reellen Fall der Parameter (ohne Interferenzbeiträge) durch LHC Suchen bereits ausgeschlossen wären.

List of publications

This thesis is based on the following publication:

- [1] S. Liebler, S. Patel and G. Weiglein, *Phenomenology of on-shell Higgs production in the MSSM with complex parameters*, *Eur. Phys. J.* **C77** (2017) 305, [1611.09308].

This thesis also contains results from the following ongoing work:

- [2] E. Fuchs, S. Liebler, S. Patel and G. Weiglein, *The MSSM Higgs Sector with $\mathcal{CP}$ violation at the LHC Run 2*, *in preparation.*

Contents

Chapter 1

Introduction

Search for invariances

The discovery of a Higgs boson in 2012 [3, 4] occupies a unique and essential place in the story of our pursuit for *invariances*; of lawfulness and regularities in the behaviour of the universe. That the spontaneous breaking of electroweak symmetry is realised through an $SU(2)$ doublet scalar field had evaded many attempts at experimental confirmation since the independent conception of the idea in 1964 by Robert Brout and François Englert [5], by Peter Higgs [6] and by Gerald Guralnik, Carl R. Hagen and Tom Kibble [7]. Its eventual discovery was the cumulative success of thousands of scientists and engineers who contributed not only to the knowledge that was required for the genesis of the Higgs hypothesis, but also to the theoretical and experimental expertise needed to confirm its existence.

The 125 GeV Higgs boson is the last particle that can be accommodated within the Standard Model (SM) of particle physics, a well-tested theory that has been remarkably successful in describing the electroweak and strong interactions of elementary particles. However, the SM suffers from several experimental and theoretical shortcomings, which give us ample reason to believe that it can at most be a low-energy manifestation of a more fundamental theory. The search for this underlying fundamental theory, or what is often referred to as *new physics*, continues with Run II of the Large Hadron Collider (LHC), now operating at an unprecedented centre-of-mass energy of 13 TeV and steadily increasing luminosities. Of the many new models hypothesising what may lie beyond the SM, one of the most popular and widely studied class of models proposes an extension of the direct product of a gauge symmetry with the Poincaré group, called *supersymmetry* (SUSY). Indeed, phenomenologically viable SUSY models such as the Minimal Supersymmetric Standard Model (MSSM) or its next-to-minimal extension can not only alleviate many shortcomings of the SM, but also accommodate the observed signal at 125 GeV as one of several Higgs bosons predicted by their extended Higgs sectors. The precise measurement of the properties of the discovered Higgs boson is necessary in order to detect any possible deviations from SM expectations, and therefore is as important as searching directly for additional Higgs bosons belonging to new physics models.

The possible landscape of new physics is vast, and so far undetected. The LHC experiments ATLAS and CMS have carried out extensive direct searches for signatures of new physics, including the MSSM. The failure to observe its signatures has set constraints on its parameter space and limits on the masses of SUSY particles. In the face of a seemingly shrinking parameter space that is available phenomenologically, it is important to carefully examine all the assumptions that go into the construction of the exclusion bounds and study how they are altered when some of these assumptions are modified. Most experimental analyses are optimised to search for a surplus of observed events over the background expected from the SM hypothesis. However, new physics can be detected not just in the form of an excess of measured data, but particles from beyond the SM spectrum could also cause a deficit of events due to destructive interference with the SM background. Moreover, new physics could be hidden from LHC searches due to destructive interference between closely appearing new resonances.

In the context of searches for additional Higgs bosons of the MSSM, such an effect can arise between the two neutral heavier Higgs bosons when we assume, for instance, that the $\mathcal{CP}$ symmetry is violated. In such a case, the experimental limits which have been set under the assumption of $\mathcal{CP}$ conservation may not present an accurate picture of the unambiguously excluded parameter regions and might need to be re-evaluated. Confronting the observed limits from the LHC searches with possible modifications arising due to such interference effects needs an accurate knowledge of production cross sections and branching ratios of the additional Higgs bosons, as well as the interferences that can occur between them. At the same time, computational tools need to be developed to perform and optimise theory calculations.

This forms the central theme of this thesis. The work presented in the following chapters aims to investigate the influence of $\mathcal{CP}$-violating phases of the MSSM on production cross sections of the neutral Higgs mass eigenstates, the interference effects that result from $\mathcal{CP}$-violating mixings of the neutral Higgs bosons, and their implication on Higgs searches at the LHC.

Thesis outline

The thesis begins with a theoretical introduction to the SM in **Chapter 2**, focussing on its particle content, and detailing in particular the electroweak symmetry breaking mechanism. Following a discussion on the demerits of the SM, supersymmetry is motivated in **Chapter 3**, where we describe the particle sector of the MSSM at tree level, and the complex parameters in the theory which provide additional sources of $\mathcal{CP}$ violation beyond the SM. The extended Higgs sector of the MSSM with its two Higgs doublets is discussed in detail, and we set the notations needed for the work presented in later chapters. In **Chapter 4** we briefly review the Higgs results from the ATLAS and CMS experiments, and summarise the exclusion limits from recent searches for SUSY particles and additional Higgs bosons relevant to the processes studied in this thesis.

Chapter 5 is dedicated to higher-order contributions to the Higgs sector of the MSSM with complex parameters. We begin with a discussion on the $\mathcal{CP}$-violating Higgs self-energies which give rise to mixing among the tree-level $\mathcal{CP}$-even and $\mathcal{CP}$-odd Higgs states of the MSSM. Next, we describe the use of wave function normalisation factors (or the $\hat{\mathbf{Z}}$ factors) needed to provide a correct and consistent description of the on-shell properties of external Higgs bosons, and introduce the notation for $\hat{\mathbf{Z}}$ factors which is used in Chapters 6-9. The central work of this thesis is contained in Chapters 6-8. In order to adequately study the effects of $\mathcal{CP}$-violating phases on searches for additional Higgs bosons, precise theoretical predictions for production cross sections of the Higgs bosons are required, followed by a formalism for taking into account $\mathcal{CP}$-violating interference effects that can arise between nearly mass degenerate and heavily admixed states in their production and decay. In **Chapter 6**, first the leading order calculation for Higgs production via gluon fusion in the SM is reviewed, followed by a discussion on the various ways in which $\mathcal{CP}$-violating phases modify the production cross sections of the neutral Higgs mass eigenstates of the MSSM, as compared to the $\mathcal{CP}$-conserving case. We then present the state-of-the-art gluon-fusion and bottom-quark annihilation cross sections for Higgs bosons in the MSSM for the general case of complex parameters.

Developing tools to automate calculations is crucial in making the theoretical predictions useful and accessible. In **Chapter 7**, we describe the `FORTRAN` code `SusHi` and introduce its extension `SusHiMi`, where we have implemented our predictions for production cross sections of $\mathcal{CP}$-admixed Higgs bosons in the MSSM with complex parameters. `SusHiMi` is employed in the phenomenological studies in **Chapter 8**, wherein the numerical impact of the phases of the trilinear coupling of the Higgses with the stop, and the gluino mass parameter (ϕ_{A_t} and ϕ_{M_3}, respectively) on Higgs masses, cross sections and $\hat{\mathbf{Z}}$ factors is investigated. Our studies are carried out in two scenarios where the lightest MSSM Higgs boson, interpreted to be the SM-like Higgs, is accompanied by a strong admixture of two heavy Higgs bosons nearly equal in mass. The chapter also examines the assorted theoretical uncertainties that are involved in our cross section predictions.

The cross section predictions developed in Chapter 6 and their subsequent implementation in `SusHiMi` need to be accompanied by an appropriate treatment of the interference effects that arise in the calculation of cross section times branching ratio of a full process of production and decay of the nearly mass-degenerate Higgs bosons. **Chapter 9** reviews such a formalism and describes the implementation of the relative interference factors in `SusHiMi`, which is then used to explore the implications of $\mathcal{CP}$-violating phases giving rise to Higgs mixing and interference in the process $b\bar{b} \to \tau^+\tau^-$. The resulting exclusion bounds are compared to existing bounds from Run II of the LHC which assume $\mathcal{CP}$ conservation. For this purpose, we define a benchmark scenario in accordance with the most up-to-date bounds on masses of SUSY particles and parameters described in Chapter 4. With **Chapter 10** we summarise the results presented in this thesis and conclude.

Chapter 2

The Standard Model

This chapter provides a brief introduction to the Standard Model of particle physics, describing its particle content and underlying symmetries. Subsequently the need for new physics beyond the Standard Model is motivated. This introductory chapter mainly follows Refs. [8–12].

2.1 Introduction

The history of particle physics is a long and involving tale. Attempts to deconstruct the structure of matter date back perhaps to the earliest origins of scientific thought itself. Generations of physicists have built upon the works of those who came before them, which led to a series of experimental and theoretical breakthroughs in the 20th century finally culminating in a singularly successful theory of fundamental particles and forces: The Standard Model.

The Standard Model (SM) of particle physics is a theory describing the elementary particles that make up the observed matter in the universe, along with their interactions via the electroweak and strong forces [13–20], which encompass all the known forces except gravity. Formulated in the 1970s, it accounts for practically all the experimental data from high energy physics experiments so far. The Higgs boson, whose existence is required for generating masses of the matter particles (fermions) and force carriers (bosons), was predicted as a part of the SM a little more than half a century ago [5–7,21]. The breakthrough discovery of a new scalar confirmed to be a SM-like Higgs boson at the LHC in July 2012 put in place the last missing piece of the SM and paved the way towards a new era of particle physics. In this chapter, we will describe the particles that make up the Standard Model and the underlying symmetries that drive their interactions. The primary focus will be on electroweak symmetry breaking and the Higgs mechanism, in order to set up the concepts and notations used throughout the thesis. We will then discuss the shortcomings of the theory and incite the need for searches for physics beyond the Standard Model (BSM), and in particular the role of extended Higgs sectors.

2.2 Symmetries

The SM contains fermionic (spin $\frac{1}{2}$) fields ψ, bosonic (spin 1) fields A^a_μ, and a scalar (spin 0) field Φ. Fermions make up the visible matter in the universe. They interact with each other through the intermediaries of the Yang-Mills gauge fields, the force carrying vector bosons. This means that the various gauge interactions are completely determined by the algebraic structures of certain internal symmetry groups. The remaining scalar spin 0 field is required for the Brout-Englert-Higgs (BEH) mechanism in the SM, which will be discussed in detail in Section 2.3.

The Standard Model is a renormalisable and mathematically self-consistent quantum field theory (QFT). It is invariant under the transformations defined by the Poincaré group, the full symmetry of special relativity, namely the Lorentz transformations and the inhomogeneous translations in Minkowski space-time. The gauge structure of SM is the non-Abelian group $SU(3)_C \otimes SU(2)_L \otimes U(1)_Y$. It comprises of two parts. $SU(3)_C$ with a conserved colour (C) charge is the symmetry group of Quantum Chromodynamics (QCD), the theory of strong interactions. $SU(2)_L \otimes U(1)_Y$ describes the electroweak theory, with left chiral fields charged under weak isospin (subscript L for the left-handed fermions it couples to) and the weak hypercharge (Y).

The derivatives of the fermionic fields ψ and general gauge fields A^a_μ define their kinetics and are fully determined by the global symmetries of the Poincaré group:

$$\begin{aligned}\mathcal{L}_{\text{kin}} &= \mathcal{L}^{\text{fermion}}_{\text{kin}} + \mathcal{L}_{\text{gauge}} \\ &= \bar{\psi} i \not{\partial} \psi - \frac{1}{4} F^a_{\mu\nu} F^{a\mu\nu}\end{aligned} \tag{2.1}$$

with $\bar{\psi} = \psi^\dagger \gamma^0$ and $\not{\partial} = \gamma^\mu \partial_\mu$. With the coupling of the gauge group g and the structure constants f^{abc}, the field strength tensors $F^a_{\mu\nu}$ for all gauge groups are defined as

$$F^a_{\mu\nu} = \partial_\mu A^a_\nu - \partial_\nu A^a_\mu + g f^{abc} A^b_\mu A^c_\nu \,. \tag{2.2}$$

For gauge invariance of the Lagrangian under a generic gauge group, a covariant derivative $D_\mu = \partial_\mu - igT^a A^a_\mu$ with generators[1] T^a replaces the derivatives ∂_μ in the kinetic terms.

More specifically, if we demand invariance of the SM fields under gauge transformations of the $SU(3)_C \otimes SU(2)_L \otimes U(1)_Y$ group, the derivatives ∂_μ need to be replaced by covariant derivatives D_μ as follows[2]

$$\partial_\mu \to D_\mu := \partial_\mu - i g_s \frac{\lambda^a}{2} g^a_\mu \pm i g_2 I^a W^a_\mu - i g_1 \frac{Y}{2} B_\mu$$

[1] f^{abc} are defined by T^a, the $N^2 - 1$ generators of a generic gauge group $SU(N)$: $[T^a, T^b] = i f^{abc} T^c$.
[2] the sign convention is $-$ in the SM and $+$ in the MSSM.

where g_s, g_2, g_1 are the coupling constants of the gauge groups $SU(3)_C, SU(2)_L$ and $U(1)_Y$, respectively, and summation over the gauge indices a is implied. This replacement by covariant derivatives leads to couplings of vector fields to fermions and scalars, as we will see in Section 2.3. The group $SU(3)_C$ is generated by the eight Gell-Mann matrices $\lambda^a, a \in \{1, ..., 8\}$, with the corresponding gauge fields g^a_μ called gluons, the carriers of the strong force. The Pauli matrices $\sigma^a, a \in \{1, 2, 3\}$, generate the $SU(2)_L$ group through $I^a = \frac{\sigma^a}{2}$, and define the weak isospin I^3. The gauge bosons of this group are the three W^a_μ. Finally, the Abelian group $U(1)_Y$ has the generator $\frac{Y}{2}$, defining the weak hypercharge, and one gauge field B_μ. For the strong $SU(3)_C$ interactions we define $\alpha_s = \frac{g_s^2}{4\pi}$, and for the electroweak $SU(2)_L \otimes U(1)_Y$ interactions we will use the relations

$$e = \frac{g_1 g_2}{\sqrt{g_1^2 + g_2^2}}, \quad \alpha = \frac{e^2}{4\pi}. \tag{2.3}$$

The weak isospin and hypercharge together define the electric charge by the Gell-Mann-Nishijima formula

$$Q = I^3 + \frac{Y}{2}. \tag{2.4}$$

Replacing $\not{\partial}$ with $\not{D} = \gamma^\mu D_\mu$ and using the definition of field strength tensors for g^a_μ, W^a_μ and B_μ from Eq. (2.2) in Eq. (2.1), we obtain the fermion and gauge boson dynamics encoded in the SM Lagrangian as

$$\mathcal{L}_{\text{kin}} = \bar{\psi} i \not{D} \psi - \frac{1}{4} G^a_{\mu\nu} G^{a\mu\nu} - \frac{1}{4} W^a_{\mu\nu} W^{a\mu\nu} - \frac{1}{4} B^{\mu\nu} B_{\mu\nu}. \tag{2.5}$$

2.3 Electroweak theory and the Higgs mechanism

For the SM Lagrangian to be invariant under gauge transformations there can be no explicit mass terms for the charged fermions and the gauge bosons, since they violate gauge symmetry. However, the only massless gauge bosons observed experimentally are the gluons in the strong sector and the photon in the electroweak sector. This means that the $SU(2)_L \otimes U(1)_Y$ symmetry must be broken down to the $U(1)_{\text{EM}}$ such that masses can be introduced for the gauge bosons while still maintaining the renormalisability of the electroweak theory. Moreover, a mechanism for generation of fermion masses is required as well. Therefore the theoretical explanation for the experimentally observed massive bosons and SM fermions needs a new ingredient. Such a mechanism was proposed in 1964, by introducing a new $SU(2)_L$-doublet scalar field Φ, which induces a spontaneous breaking of the $SU(2)_L \otimes U(1)_Y$ gauge symmetry via the Brout-Englert-Higgs mechanism [5–7, 21]. The complex scalar field Φ, a colour singlet with hypercharge $Y = 1$ was named

the Higgs field, and can be represented as

$$\Phi(x) = \begin{pmatrix} \phi^+(x) \\ \phi^0(x) \end{pmatrix} . \tag{2.6}$$

To obtain the masses of the gauge bosons, the Lagrangian receives the additional terms

$$\mathcal{L}_{\text{Higgs}} = (D_\mu \Phi)^\dagger (D^\mu \Phi) - V(\Phi) . \tag{2.7}$$

The most general gauge invariant scalar potential in Φ is given by

$$V(\Phi) = -\mu^2 \Phi^\dagger \Phi + \frac{\lambda}{4} (\Phi^\dagger \Phi)^2 . \tag{2.8}$$

This potential must be renormalisable, so $V(\Phi)$ cannot contain powers higher than $(\Phi^\dagger \Phi)^2$. Additionally, a stable potential must be bounded from below, which requires $\lambda > 0$ and no dependence on odd powers of Φ. Furthermore, choosing $\mu^2 < 0$ results in a minimum of the potential at $|\langle \Phi \rangle| \equiv \sqrt{\Phi^\dagger \Phi} = 0$. In this case the minimum of the potential leaves the electroweak symmetry unbroken and no mass terms emerge. In order to induce the spontaneous breaking of the $SU(2)_L \otimes U(1)_Y$ symmetry we need $\mu^2 > 0$, resulting in a non-zero vacuum expectation value (vev) v of the neutral component of the field $|\langle \Phi \rangle| \equiv \sqrt{\frac{2\mu^2}{\lambda}} = \frac{v}{\sqrt{2}}$. This choice of parameters in the Higgs potential gives rise to the famous *Mexican Hat* shape, which has an infinite set of degenerate minima lying on a circle of radius $\frac{v}{\sqrt{2}}$. These degenerate ground states rotate into each other under gauge transformations. It is now possible to obtain a physical picture of the excitations around the vacuum state. The system is free to rotate along the circumference of the circle of minima: since the potential is flat along the circle, the excitations along that direction do not cost any energy. Excitations along this circumference therefore correspond to the massless or Goldstone modes. In contrast, the potential looks approximately like that of a harmonic oscillator in the radial direction, and an excitation along a radius gives rise to the massive particles.

Following phase conventions, we can choose a specific minimum for Φ as

$$\Phi = \frac{1}{\sqrt{2}} \begin{pmatrix} 0 \\ v \end{pmatrix} . \tag{2.9}$$

The spontaneous breaking of the $SU(2)_L \otimes U(1)_Y$ symmetry of the potential to $U(1)_{\text{EM}}$ by this ground state is known as *Electroweak Symmetry Breaking* (EWSB). The full Higgs field can be written as an expansion around the minimum as

$$\Phi(x) = \begin{pmatrix} \phi^+(x) \\ \frac{1}{\sqrt{2}} (v + H^0(x) + i\chi^0(x)) \end{pmatrix} . \tag{2.10}$$

This Higgs field possesses four real degrees of freedom (dof). Here $H^0(x)$ is the physical Higgs field that predicts a massive scalar Higgs boson in the SM [21]. The other three degrees of freedom $\phi^\pm$ and χ^0 are the unphysical Goldstone bosons [22, 23] with zero vacuum expectation value. They are absent in the unitary gauge and contribute to the longitudinal dofs of the gauge bosons $W^\pm$ and Z.

2.3.1 Gauge boson masses

The masses of the gauge bosons are obtained by expanding the kinetic term $(D_\mu\Phi)^\dagger(D^\mu\Phi)$ of Eq. (2.7) around the minimum of the Higgs field. The physical mass eigenstates for charged gauge boson fields $W^\pm$ are derived from the gauge eigenstates as

$$W_\mu^\pm = \frac{1}{\sqrt{2}}(W_\mu^1 \mp iW_\mu^2)\,, \tag{2.11}$$

and the neutral mass eigenstates Z and A result from the following rotation of the neutral gauge eigenstates:

$$\begin{pmatrix} Z_\mu \\ A_\mu \end{pmatrix} = \begin{pmatrix} c_W & s_W \\ -s_W & c_W \end{pmatrix} \begin{pmatrix} W_\mu^3 \\ B_\mu \end{pmatrix} \tag{2.12}$$

with $s_W \equiv \sin\theta_W, c_W \equiv \cos\theta_W$, and θ_W is the weak mixing angle having the tree-level definition

$$s_W \equiv \frac{g_1}{\sqrt{g_1^2+g_2^2}}\,, \qquad c_W \equiv \frac{g_2}{\sqrt{g_1^2+g_2^2}}\,. \tag{2.13}$$

To understand in detail how the gauge boson masses arise, we look at the following expansion of the kinetic term:

$$\begin{aligned}(D_\mu\Phi)^\dagger(D^\mu\Phi) = \frac{1}{2}(\partial_\mu H^0)(\partial^\mu H^0) + \frac{1}{8}\, g_2^2\, (v+H^0)^2\, (W_\mu^1 - iW_\mu^2)(W^{1\mu} - iW^{2\mu}) \\ + \frac{1}{8}\, (v+H^0)^2\, (g_2W_\mu^3 + g_1B_\mu)(g_2W^{3\mu} + g_1B^\mu)\,.\end{aligned} \tag{2.14}$$

From the second term of the above equation we see that the two electrically charged mass eigenstates $W_\mu^\pm$ acquire the mass

$$m_W = \frac{v}{2}g_2\,. \tag{2.15}$$

The third term contains the masses for the neutral gauge bosons. They are the eigenvalues of the mass matrix obtained from the v^2-term:

$$\mathbf{M}_0^2 = \frac{v^2}{4}\begin{pmatrix} g_1^2 & g_1 g_2 \\ g_1 g_2 & g_2^2 \end{pmatrix}. \tag{2.16}$$

The determinant of $\mathbf{M}_0^2$, and therefore one of the eigenvalues is zero, so we get a massless photon corresponding to the gauge boson of the unbroken $U(1)_{\mathrm{EM}}$ symmetry, while the second eigenvalue gives the mass of the Z boson:

$$m_\gamma = 0, \qquad m_Z = \frac{v}{2}\sqrt{g_1^2 + g_2^2}\,. \tag{2.17}$$

Finally, expanding the Higgs potential $V(\Phi)$ around the minimum of the Higgs field, we determine the mass term for the Higgs boson, which arises from the Higgs self-coupling λ:

$$m_{H^0}^2 = \frac{\partial V(H^0)}{\partial H^{0\,2}} = \frac{\lambda}{2}v^2\,. \tag{2.18}$$

The Higgs mass in the SM is a free parameter and needs to be measured experimentally. The gauge bosons $\gamma, W^\pm$ and Z are intermediaries of the electroweak forces. All electrically charged particles interact electromagnetically by exchanging photons. The $W^\pm$ and Z bosons carry the weak force. While the Z couples to all fermions, $W^\pm$ couple only to the left-handed ones. Gluons, the gauge bosons of the strong sector, remain unaffected by electroweak symmetry breaking and are massless. They mediate interactions between coloured particles.

2.3.2 Fermion masses and Yukawa couplings

Fermions make up the visible matter in the universe. SM fermions can be classified into quarks and leptons. Quarks are $SU(3)_C$ triplets that carry a colour charge. Since all freely existing particles are colour neutral, quarks can only exist in colour-neutral bound states called hadrons. Leptons are chargeless under $SU(3)_C$ and can exist as free particles. Fermions are chiral fields, which means that left-handed quarks and leptons (q_L, l_L) transform differently from the right-handed ones (q_R, l_R). The SM contains three copies or generations of fermions ($i \in \{1, 2, 3\}$) with similar quantum numbers, each containing a collection of chiral fields (f_{i_L}, f_{i_R}) with different particle masses. The left-handed fields in each generation (q_{i_L}, l_{i_L}) transform as doublets under $SU(2)_L$ while the right-handed ones (q_{i_R}, l_{i_R}) transform as weak singlets.

Within a generation, the left-handed quark doublet q_{i_L} consists of an up-type (u_{i_L}) and a down-type (d_{i_L}) quark. The corresponding right-handed singlets are u_{i_R} and d_{i_R}. Similarly, the left-handed lepton doublet has an up-type lepton, which is a neutrino ν_i and a charged down-type lepton. The corresponding down-type right-handed leptons are

e_{i_R}. There are no right-handed neutrinos in the SM.

Fermions acquire masses in the SM through Yukawa couplings of the Higgs field to the Dirac fields, since explicit fermion mass terms break the gauge symmetry of the Lagrangian. These appear in the Lagrangian as follows:

$$\mathcal{L}_{\text{Yukawa}} = -\overline{q}_L \mathbf{y}_d \Phi d_R - \overline{q}_L \mathbf{y}_u \overline{\Phi} u_R - \bar{l}_L \mathbf{y}_l \Phi e_R + h.c\,. \tag{2.19}$$

where the charged conjugated Higgs field $\overline{\Phi} = i\sigma_2 \Phi^*$, with the neutral $\langle \phi^{0*} \rangle$ in the upper component, induces masses for the up-type fermions. As a result, just one Higgs doublet is sufficient for generating masses for both the up- and down-type fermions and the gauge bosons in the SM. The lepton mass matrix is given by

$$\mathbf{m}_l = \frac{v}{\sqrt{2}} \mathbf{y}_l\,. \tag{2.20}$$

Since there are no right-handed neutrinos to participate in the Higgs couplings, neutrinos are massless in the SM, although more recent evidence of neutrino oscillations indicates that they are in fact massive (see e.g. Ref. [24]). A diagonal mass matrix for the quarks is obtained by diagonalising the 3×3 Yukawa matrices $\mathbf{y}_f, f \in \{u, d\}$ through a unitary transformation:

$$\mathbf{m}_f = V_L^f \mathbf{y}_f V_R^{f\dagger} \frac{v}{\sqrt{2}}\,. \tag{2.21}$$

Notice that the coupling strength of the massive fermions (as well as the massive gauge bosons) to the Higgs boson is directly proportional to their masses, which is a consequence of the BEH mechanism. The product of the unitary matrices $V_L^u V_L^{d\dagger}$ appears in the couplings of the charged-current $W^\pm$ interactions to the physical states u_L, d_L and is called is the Cabibbo-Kobayashi-Maskawa (CKM) matrix [25, 26]. It contains the only complex parameter of the SM, and it is the solitary source of $\mathcal{CP}$ violation within the SM:

$$V_{\text{CKM}} = V_L^u V_L^{d\dagger}\,. \tag{2.22}$$

2.4 Full SM Lagrangian

Quantisation and higher-order corrections in the SM require gauge fixing terms in the Lagrangian, set by $\mathcal{L}_{\text{fix}}$. These terms introduce additional, unphysical degrees of freedom of the gauge bosons to the theory, which must be cancelled. This compensation necessitates the introduction of the so-called Faddeev-Popov ghost and anti-ghost terms $\mathcal{L}_{\text{ghost}}$. These ghosts are not real physical quantities, they are purely mathematical entities appearing as virtual particles within loops. Therefore the full Lagrangian of the Standard

Model is

$$\mathcal{L}_{\text{SM}} = \mathcal{L}_{\text{gauge}} + \mathcal{L}_{\text{kin}}^{\text{fermion}} + \mathcal{L}_{\text{Yukawa}} + \mathcal{L}_{\text{Higgs}} + \mathcal{L}_{\text{fix}} + \mathcal{L}_{\text{ghost}} \,. \tag{2.23}$$

2.5 Shortcomings of the Standard Model

The Standard Model has been extremely successful in the description of almost all the measurements made in high energy experiments over the past decades, with no unambiguous hints of additional physics found in these measurements even as the TeV scale is probed. However, the SM falls short of explaining several experimental observations, in addition to certain theoretical shortcomings. This suggests that the SM cannot be the complete theory of nature but it can only serve as an effective theory describing the universe at the energy scales we currently explore.

The first and most obvious indication of the SM being an inherently incomplete theory is that it cannot accommodate a description of the gravitational force. Gravitational effects in the quantum regime become discernible only at M_{P}, the Planck energy scale[3]. While these hardly have any phenomenological impact at the current energy scales investigated by particle physics experiments, a new framework is certainly required at M_{P}, which serves as the maximal cut-off scale for the validity of the SM.

The SM is a renormalisable QFT, which means that even if no new physics exists between the electroweak scale (M_{EW}) and the Planck scale, it can be run all the way up to the highest cut-off $\Lambda \sim M_{\text{P}}$. If we treat the SM as an effective theory, one would expect the Higgs mass to be a prediction of the full theory above M_{P}, which is 17 orders of magnitude higher than M_{EW}. This hierarchy of scales can drastically effect the stability of the Higgs mass in the presence of quantum corrections. The mass of the Higgs boson receives radiative corrections from every particle that can couple to it, either directly or indirectly, giving rise to a term $\Delta M_{H^0}^2$ which is independent of the bare mass of the Higgs:

$$M_{H^0}^2 = M_{H^0,0}^2 + \Delta M_{H^0}^2 \,. \tag{2.24}$$

These correction terms are quadratically dependent on the ultraviolet momentum cut-off Λ. For example, a one-loop correction to the Higgs mass from a fermion loop takes the form

$$\Delta M_{H^0}^2 = -\frac{y_f^2}{8\pi^2}\Lambda^2 + \cdots \tag{2.25}$$

The ellipsis represents terms proportional to m_f^2 which grow logarithmically with Λ. Setting the cut-off to the Planck scale makes the quantum correction around 30 orders

[3] $M_{\text{P}} = \mathcal{O}(10^{19})$ GeV.

of magnitude larger than the measured $M_{H^0} \sim 125$ GeV, which then requires the bare mass $M_{H^0,0}$ in Eq. (2.24) to be extremely fine-tuned. This instability is unique for scalar masses. The masses of fermions and gauge bosons are protected by symmetries such that they are not quadratically divergent with the cut-off momentum. Furthermore, there can be contributions similar to Eq. (2.25) from virtual effects of any new heavy particles that might exist and couple to the Higgs. Such contributions are sensitive to the masses of the heavy particles, not just the cut-off. While within the SM itself such a cancellation is technically possible since the Higgs mass is a free parameter, for a UV completion of the SM where the Higgs mass is a predicted quantity, it is considered highly unnatural to have such an enormously precise cancellation without a symmetry reason, and is called the *Hierarchy Problem*. It motivates new physics below the Planck scale which can regulate these radiative corrections.

If one demands theoretical elegance from the SM, then an explanation for fractional electric charges of the quarks giving rise to accidental cancellation of gauge anomalies is missing, as is an explanation for the hierarchy in masses of fermions. In addition, if we expect the gauge couplings g_1, g_2, g_3 to unify at the GUT scale, then new particles need to be introduced to alter the running of the couplings [27].

It would seem fair to conclude that worrying about perceived imperfections of a theory, even a phenomenologically successful one, can pay off. However, the shortcomings of the SM are not just limited to aesthetics. As mentioned earlier, the observation of non-zero neutrino masses leading to neutrino oscillations [24] is not explained by the SM. Furthermore, the only source of $\mathcal{CP}$ violation in the SM is the single phase of the CKM matrix. $\mathcal{CP}$ violation, along with baryon number violation and departure from thermal equilibrium, is a condition required for the observed baryon asymmetry in the universe [28–30]. However, the one complex parameter in the SM is not adequate to explain the perceived matter-antimatter asymmetry, and additional $\mathcal{CP}$-violating parameters are needed. Evidence from astrophysical observations points to the existence of Dark Matter (DM) and Dark Energy (DE), which make up $\sim 27\%$ and $\sim 68\%$ of total energy density of the universe, respectively [31], whereas ordinary matter only constitutes $\sim 5\%$. For DM to be made up of elementary particles, not only does it need to have no electromagnetic or strong interactions with the SM particles, it also needs to be stable on cosmological time scales. The SM does not offer a viable candidate for cold DM, or an explanation for DE.

In recognition of these shortcomings, there are several extensions of the Standard Model that attempt to tackle a combination of these problems. They include ideas proposing composite Higgses, extended Higgs sectors, additional space-time dimensions, new symmetries etc. Even though there has been no evidence of new physics beyond the SM so far, the search for new particles continues as we probe higher energies with greater luminosities in present day particle accelerators.

This thesis focuses on one such BSM theory, Supersymmetry (SUSY), which introduces

a new symmetry relating fermions and bosons. As one of the most widely studied BSM theories, it offers solutions to the fine-tuning of the Higgs mass, provides candidates for DM, enables the unification of the gauge couplings and can provide additional sources of $\mathcal{CP}$ violation which contribute to the matter-antimatter asymmetry in the universe, making it a compelling phenomenological theory.

Chapter 3

The MSSM with complex parameters

This chapter discusses the basic features of supersymmetry, with focus on the physics of the MSSM, and is based on Refs. [12, 32–38]. In particular the properties of the Higgs sector and the role of complex parameters relevant for this thesis are outlined. Similarities to Ref. [1] are intended and reflect the contributions of the author.

3.1 The Minimal Supersymmetric Standard Model

In the early 1900s, only three types of particles had been discovered: photons, electrons and protons. Wolfgang Pauli addressed his now famous letter suggesting the existence of a new kind of weakly interacting particles, the neutrinos, to the *Radioactive Ladies and Gentlemen* [39], who would meet in Tübingen to discuss beta decays, at a time when conception of new particles was not considered a popular solution to fundamental problems. However, neutrinos were indeed the correct solution to the problem of the continuous beta decay spectrum. Problem solving paradigms in particle physics have changed since then; new particles are suggested in most of the prominent models of new physics in order to overcome the shortcomings in the field. Perhaps the boldest of these models is supersymmetry, which proposes a vast and new, yet undiscovered particle spectrum which could solve many of the problems that plague the Standard Model today.

In this section we give a brief historical perspective to the motivations for developing SUSY and its resulting implications on particle physics phenomenology. We will discuss how weak scale supersymmetry provides solutions to the shortcomings of the SM and subsequently we will describe the particle content of the minimal realisation of SUSY: The Minimal Supersymmetric Standard Model (MSSM).

3.1.1 A brief history of supersymmetry

It is a plausible assertion that a dominant theme in twentieth century physics was that of symmetry, the pursuit of which was heuristically very successful. Symmetries are often

the primary feature of nature that constrain the allowed dynamics of an interaction, and have proved to be a reliable concept for exploring and formulating physical laws.

In Chapter 2 we saw that the interactions of the SM are driven by symmetries and the subsequent breaking of some of them. However, the SM does not encompass all the symmetries of nature that are compatible with Lorentz invariance. This can serve as a motivation for studying extensions of the SM symmetries that can manifest physically. Nonetheless, space-time symmetries and internal, local symmetries cannot be combined arbitrarily. Every realistic quantum field theory can only have a Lie group symmetry that is the direct product of the Poincaré group and the internal symmetry groups. This was proven in the landmark "no-go" theorem by Sidney Coleman and Jeffrey Mandula in 1967 [40] which stated the "*impossibility of combining space-time and internal symmetries in any but a trivial way*". In 1971, Y.A. Golfand and E.P. Likhtman introduced four anti-commuting spinor generators in 3+1 dimensions that can extend the Poincaré group [41], which came to be known as supercharges. In 1972, D.V. Volkov and V.P. Akulov independently suggested non-linear realisations of supersymmetry [42]. Rudolf Haag, Jan Łopuszanski and Martin Sohnius analysed all possible superalgebras in the general form and showed that by weakening the assumptions of the Coleman-Mandula theorem and allowing both commuting and anticommuting symmetry generators such that the ordinary Lie algebra was replaced by a Lie superalgebra, it was possible to non-trivially bypass the no-go theorem [43].

In 1974, Julius Wess and Bruno Zumino introduced the simplest interacting supersymmetric quantum field theory with a free chiral supermultiplet [44]. The minimal supersymmetric extension of the Standard Model proposed in order to address the shortcomings of the SM was developed starting in the late 1970s and early 1980s. While the number of viable supersymmetric models has greatly increased over the last decades; with several models containing additional symmetries and ingredients, as well as non-minimal extensions, the non-observation of SUSY has severely constrained the parameters of the theory.

3.1.2 A symmetry of fermions and bosons

Supersymmetry is a space-time symmetry that relates a fermionic state to a bosonic state and vice versa. Even though the initial reasons for studying SUSY were purely mathematical, it is well motivated in the light of the shortcomings of the SM. SUSY predicts new scalar particles for each SM fermion, and a fermionic particle for each SM gauge boson. These new particles are called *superpartners*. The supersymmetric operator $\mathcal{Q}$ generating such a transformation is an anti-commuting spinor which changes the spin of a particle by $\frac{1}{2}$. The single particle states of a supersymmetric theory are contained in irreducible representations of the supersymmetry algebra, called *supermultiplets*. A supermultiplet contains both fermionic and bosonic states with equal degrees of freedom. $\mathcal{Q}$ and its hermitian conjugate $\mathcal{Q}^\dagger$, also a supersymmetric operator, must satisfy the

commutation and anti-commutation algebra defined by

$$[P^\mu, \mathcal{Q}_\alpha] = [P^\mu, \mathcal{Q}^\dagger_{\dot\alpha}] = 0\,, \tag{3.1}$$

$$\{\mathcal{Q}_\alpha, \mathcal{Q}^\dagger_{\dot\alpha}\} = -2\sigma^\mu_{\alpha\dot\alpha} P_\mu\,, \tag{3.2}$$

$$\{\mathcal{Q}_\alpha, \mathcal{Q}_\beta\} = \{\mathcal{Q}^\dagger_{\dot\alpha}, \mathcal{Q}^\dagger_{\dot\beta}\} = 0\,, \tag{3.3}$$

where P^μ is the 4-momentum generator of space-time translations with Lorentz index μ, σ^μ are the Pauli matrices, and $\alpha, \dot\alpha, \beta, \dot\beta$ are the spinor indices. $\mathcal{Q}$ and $\mathcal{Q}^\dagger$ also commute with generators of all the gauge transformations, so that the particles housed in a single supermultiplet have the same quantum numbers for electric charge, weak isospin and colour. Furthermore, we see from Eq. (3.1) that the squared mass operator $-P^2$ commutes with $\mathcal{Q}$ and $\mathcal{Q}^\dagger$:

$$[\mathcal{Q}_\alpha, P^2] = [\mathcal{Q}_\alpha, P_\mu]P^\mu + P^\mu[\mathcal{Q}_\alpha, P_\mu] = 0\,. \tag{3.4}$$

This relation implies that all the fields in a supermultiplet have equal eigenvalues of $-P^2$ and are mass degenerate in unbroken supersymmetric models.

We can already notice hints of how a supersymmetric extension of the Standard Model can alleviate some of its shortcomings. As discussed in Section 2.5, each fermion loop in the Higgs self-energy contributes a quadratically divergent term proportional to $-y_f^2\Lambda^2$, where y_f is the Yukawa coupling and Λ is the momentum cut-off of the integral. The predicted existence of a scalar partner $\tilde{f}_{L/R}$ for each fermion chirality state $f_{L/R}$ means then that the Higgs self-energy receives quadratically sensitive contributions from the scalar loops, which are proportional to $y_{\tilde f}^2\Lambda^2$. As a result, the quadratically divergent contributions from the fermions are cancelled by those from the scalar loops if $y_f = y_{\tilde f}$. The complete quantum corrections to the Higgs mass also contain logarithmically divergent terms, which vanish entirely if the masses of the SM particles and their superpartners are equal. However, SUSY cannot be realised in nature as an exact symmetry, as we discuss in more detail in Section 3.1.5. SUSY breaking results in a mass splitting between fermions and their superpartners, $m_{\tilde f}^2 = m_f^2 + \Delta^2$. As long as the relationship between the dimensionless couplings $y_f = y_{\tilde f}$ is maintained, Δ^2 does not spoil the cancellation of the quadratically divergent terms. This is known as *soft* breaking of SUSY. However, even though the mass split is performed such that it does not affect the quadratically divergent terms in the renormalised self-energy corrections to the Higgs mass, it induces correction terms of the form $\ln\left(\frac{m_{\tilde f}^2}{m_f^2}\right)$. These corrections can be kept small enough such that fine-tuning is not reintroduced if the masses of the superpartners are not too separate from those of the SM particles and appear at $\mathcal{O}$(TeV).

TeV scale masses of the superpartners can additionally improve the unification of the strong, weak and electromagnetic couplings [27]. SUSY not only addresses the theoretical shortcomings of the SM, but can also provide explanations for experimental observations

not predicted by the SM. The new SUSY particle spectrum contains a light, stable, weakly interacting state which could be a candidate for cold dark matter. Finally, several parameters of the theory may be complex, opening up new portals to $\mathcal{CP}$ violation. We will discuss the last feature in greater detail in Section 3.3.

Incorporating the SM into SUSY

In a supersymmetric extension of the SM, the known fermions and bosons are embedded into chiral or gauge supermultiplets, with a superpartner having a spin differing by $\frac{1}{2}$. We saw that Standard Model quarks and leptons have left- and right-handed parts that transform differently under gauge transformations, therefore they must be a part of chiral supermultiplets. Since these left- and right-handed components are separate Weyl spinors ψ, each of them has its own complex spin 0 scalar partner (called a scalar fermion or *sfermion*). On-shell, this complex field has two real propagating degrees of freedom, similar to the two spin polarization states of ψ. However, off-shell the Weyl fermion is a complex object with two components and four real degrees of freedom, two of which are eliminated on-shell. We see that there is a mismatch in the fermionic and bosonic degrees of freedom off-shell. The chiral supermultiplet therefore also contains an auxiliary complex scalar field F which closes the supersymmetry algebra off-shell. This field vanishes on-shell and does not propagate. The chiral Lagrangian including auxiliary terms is given by

$$\mathcal{L}_{\text{chiral}} = -D^\mu \phi^{*i} D_\mu \phi_i + i\psi^{\dagger i}\bar{\sigma}^\mu D_\mu \psi_i + F^{*i}F_i + \left[\left(-\frac{1}{2}W^{ij}\psi_i\psi_j + W^i F_i\right) + h.c.\right] . \quad (3.5)$$

The W_i and W_{ij} are the first and second derivatives of the superpotential with respect to the complex scalar fields:

$$W_i = \frac{\partial W}{\partial \phi_i} , \quad W_{ij} = \frac{\partial^2 W}{\partial \phi_i \partial \phi_j} . \quad (3.6)$$

The Euler-Lagrange equations of motion for the auxiliary fields give $F_i = -W_i^*, F^{i*} = -W^i$, which can be replaced accordingly. In the above equations W is the superpotential containing the most general set of renormalisable, SUSY-invariant non-gauge interactions:

$$W = L^i\phi_i + \frac{1}{2}M^{ij}\phi_i\phi_j + \frac{1}{6}y^{ijk}\phi_i\phi_j\phi_k . \quad (3.7)$$

Here, L_i are parameters with mass dimension 2 and only affect the scalar potential part of the Lagrangian. They are allowed only when ϕ_i are gauge singlets and can play an important role in spontaneous supersymmetry breaking.

Analogously, the gauge supermultiplet contains the SM vector bosons A^a_μ along with their fermionic superpartners λ^a (called *gauginos*), and a real bosonic auxiliary field D^a, included for the same reasons as F. The Lagrangian describing the vector supermultiplets

is

$$\mathcal{L}_{\text{gauge}} = -\frac{1}{4}F^a_{\mu\nu}F^{a\mu\nu} + \frac{1}{2}D^aD^a + i\lambda^{a\dagger}\bar{\sigma}^\mu D_\mu\lambda^a\,, \tag{3.8}$$

with the field strength tensors $F^a_{\mu\nu}$ defined in Eq. (2.2). Finally, the complete SUSY Lagrangian is expressible as

$$\mathcal{L}_{\text{SUSY}} = \mathcal{L}_{\text{chiral}} + \mathcal{L}_{\text{gauge}} - \sqrt{2}g\left((\phi^*T^a\psi)\lambda^a + \lambda^{\dagger a}(\psi^\dagger T^a\phi)\right) + g(\phi^*T^a\phi)D^a\,, \tag{3.9}$$

where T^a are the gauge group generators. The additional terms in the Lagrangian consist of all possible gauge invariant and renormalisable interaction terms, and the equation of motion for D^a turns out to be $D^a = -g(\phi^*T^a\phi)$.

The scalar potential of the supersymmetric Lagrangian can be split into "F"-terms, determined by the Yukawa interactions, and "D"-terms determined by the gauge interactions, and is bounded from below:

$$V(\phi,\phi^*) = V_F + V_D = F^{i*}F_i + \frac{1}{2}D^aD^a = W_i^*W^i + \frac{1}{2}g_a^2(\phi^*T^a\phi)^2\,. \tag{3.10}$$

3.1.3 The MSSM superpotential

The MSSM is the simplest phenomenologically viable SUSY model. The SM particle spectrum is more than doubled, with each left- and right-handed fermion and gauge bosons getting their corresponding superpartners. The gauge and chiral multiplets are detailed in Table 3.1. By convention, the chiral multiplets are defined in terms of the left-handed Weyl spinors, with the right-handed fermions and their superpartners being the conjugate of the left-handed ones. With a generation index $i \in \{1,2,3\}$, the left-handed quark doublets are denoted as $q_i = (u_{i_L}, d_{i_L})$. Their scalar superpartners (or *squarks*) are $\tilde{q}_i = (\tilde{u}_{i_L}, \tilde{d}_{i_L})$. Transforming under the same representation of the gauge groups, both q_i and $\tilde{q}_i$ are contained in a chiral supermultiplet Q_i. The right-handed up-type quark singlet $u^\dagger_{i_R}$, denoted in our convention as $\bar{u}_{i_L}$, and its superpartner $\tilde{\bar{u}}_{i_L}$ are contained in the supermultiplet $\bar{u}_i$. Similarly the multiplet $\bar{d}_i$ contains the down-type quark singlet $\bar{d}_{i_L}$ along with its superpartner $\tilde{\bar{d}}_{i_L}$.

The supermultiplet L_i contains the left-handed lepton doublets $e_i = (\nu_i, e_{i_L})$ along with the corresponding scalar leptons (*sleptons*) $\tilde{e}_i = (\tilde{\nu}_i, \tilde{e}_{i_L})$. Finally, $\bar{e}_i$ contains the charged lepton singlets $(e^\dagger_R, \tilde{e}^*_R)$, owing to the absence of right-handed neutrinos in the SM or the MSSM.

The gauge bosons and their superpartners occur in three supermultiplets: one each for the B-boson and the *bino* $\tilde{B}$, the $\{W^\pm, W^3\}$ bosons and the *winos* $\{\widetilde{W}^\pm, \widetilde{W}^3\}$, and the gluon g with the *gluino* $\tilde{g}$.

The Higgs sector of the MSSM is richer than that of the SM. The MSSM is a two-Higgs doublet model that is constrained by supersymmetry. Constraints imposed by SUSY, as

Table 3.1: Chiral and gauge supermultiplets of the MSSM [36, 37].

Chiral	**Label**	**Spin-0**	**Spin-1/2**	$(\mathbf{SU(3)_C}, \mathbf{SU(2)_L}, \mathbf{U(1)_Y})$
(S)quarks	Q	$(\tilde{u}_L, \tilde{d}_L)$	(u_L, d_L)	$(\mathbf{3}, \mathbf{2}, 1/3)$
	$\bar{u}$	$\tilde{u}_R^*$	$u_R^\dagger$	$(\bar{\mathbf{3}}, \mathbf{1}, -4/3)$
	$\bar{d}$	$\tilde{d}_R^*$	$d_R^\dagger$	$(\bar{\mathbf{3}}, \mathbf{1}, 2/3)$
(S)leptons	L	$(\tilde{\nu}_L, \tilde{e}_L)$	(ν_L, e_L)	$(\mathbf{1}, \mathbf{2}, -1)$
	$\bar{e}$	$\tilde{e}_R^*$	$e_R^\dagger$	$(\mathbf{1}, \mathbf{1}, 2)$
Higgs(inos)	$\mathcal{H}_1$	(h_d^0, h_d^-)	$(\tilde{h}_d^0, \tilde{h}_d^-)$	$(\mathbf{1}, \mathbf{2}, -1)$
	$\mathcal{H}_2$	(h_u^+, h_u^0)	$(\tilde{h}_u^+, \tilde{h}_u^0)$	$(\mathbf{1}, \mathbf{2}, 1)$
Gauge		**Spin-1/2**	**Spin-1**	
Gluino, gluon		$\tilde{g}$	g	$(\mathbf{8}, \mathbf{1}, 0)$
Bino, B-boson		$\widetilde{B}$	B	$(\mathbf{1}, \mathbf{1}, 0)$
Winos, W-bosons		$\{\widetilde{W}^\pm, \widetilde{W}^3\}$	$\{W^\pm, W^3\}$	$(\mathbf{1}, \mathbf{3}, 0)$

will be discussed subsequently, dictate that at least two Higgs doublets are required to provide masses for both the up- and down-type fermions and the gauge bosons. In the SM, these masses are generated by the scalar doublet Φ and its complex conjugate $\overline{\Phi}$. The two complex Higgs doublets of the MSSM have a total of eight degrees of freedom. Three of these dof lend longitudinal components to the massive gauge bosons via the EWSB mechanism. The remaining physical dof manifest themselves as five Higgs bosons. Each of these Higgses have corresponding spin $\frac{1}{2}$ superpartners called *Higgsinos*. We discuss the mixings of the particles described in Table 3.1 into mass eigenstates and their manifestation as physical fields in Section 3.2.

The chiral and gauge supermultiplets appear in the R-parity (see Section 3.1.4) conserving superpotential containing the non-gauge interactions as follows:

$$W_{\text{MSSM}} = \overline{u}\mathbf{y_u}Q \cdot \mathcal{H}_2 - \overline{d}\mathbf{y_d}Q \cdot \mathcal{H}_1 - \overline{e}\mathbf{y_e}L \cdot \mathcal{H}_1 + \mu\ \mathcal{H}_1 \cdot \mathcal{H}_2\,. \tag{3.11}$$

The dot operator is the $SU(2)_L$-invariant product contracted by the total anti-symmetric tensor $\epsilon_{\alpha\beta}$, and the gauge indices and generations of the supermultiplets have been suppressed. The $\mathbf{y_{u,d,e}}$ are the 3×3 Yukawa matrices in family space as described in Section 2.3.2. Here we see two separate Higgs doublets that couple to the up- and down-type fermions, in contrast to the SM where the doublet Φ with a vev in the lower component and $\overline{\Phi}$ with a vev in the upper component render both the up-type and down-type fermions massive. However, it is not possible to replace $\mathcal{H}_2$ by $\overline{\mathcal{H}}_1$, since W_{MSSM} is a holomorphic function that cannot contain complex conjugates in order to preserve SUSY. Furthermore, we also need two Higgsinos and therefore two Higgs doublets with hypercharges $Y_{\mathcal{H}_{1,2}} = \pm 1$ to facilitate the cancellation of gauge anomalies that would occur in

a scenario where only one fermionic Higgsino existed. In Eq. (3.11), μ, the only SUSY conserving parameter later appears as the potentially complex Higgsino mass parameter.

3.1.4 R-parity

Experimental searches have not shown deviations from lepton (L) and baryon (B) number conservation so far. In the SM, their conservation occurs accidentally, since all possible renormalisable terms exclude ones that violate L and B. Even though W_{MSSM} in Eq. (3.11) conserves lepton and baryon number, L- and B-violating terms are not excluded from the renormalisable and gauge invariant MSSM, which can lead to an unstable proton. In order to safeguard the MSSM from the consequences of B and L violation, a new symmetry called R-symmetry [45] is introduced. We require that every coupling preserves R-parity, which is defined as

$$R = (-1)^{3B+L+2S}\,, \tag{3.12}$$

where S is the spin of the particle. This assigns $R = +1$ for SM particles and $R = -1$ for their superpartners. It allows all interactions in Eq. (3.11) but forbids the baryon- and lepton-number violating terms. Mathematically, it can be motivated as the discrete subgroup $\mathbb{Z}_2$, a remnant of the continuous $U(1)$ gauge symmetry. If R-parity is conserved, SUSY particles can only be produced in pairs, and the lightest supersymmetric particle (LSP) is completely stable. This has phenomenological importance: if the LSP is colour and charge neutral as well as weakly interacting, it is an ideal candidate for cold non-baryonic dark matter [46, 47]. In the MSSM the lightest neutralino $\tilde{\chi}^0$ can play this role. Additionally, any sparticle can only decay into an odd number of LSPs. There exist phenomenological SUSY models that allow for R-parity violation, however all the interactions considered in this thesis preserve R-parity.

3.1.5 SUSY breaking

As discussed in Section 3.1.2, unbroken SUSY interactions would imply that the SM particles and their SUSY counterparts are mass degenerate. However, the fact that we have not detected SUSY particles in experiments so far means that supersymmetry is not realised exactly in nature. Any phenomenologically viable model must therefore involve SUSY breaking. From a theoretical perspective, one would expect SUSY to be broken spontaneously in the manner of EWSB. Spontaneous breaking of SUSY could occur in a hidden sector which has no direct renormalisable couplings to the visible sector and could be mediated to the visible sector through different mechanisms. From a practical point of view, the exact SUSY breaking mechanism does not have much phenomenological impact. It is therefore useful to parametrise our ignorance of the exact dynamics of supersymmetry breaking by introducing terms that break the symmetry explicitly in the

Lagrangian. As argued in Section 3.1.2, the SUSY breaking couplings must be soft, which means that the relations between the dimensionless couplings must remain unmodified in order to avoid reintroducing the quadratic divergences in the Higgs mass correction terms.

The most general renormalisable Lagrangian for soft SUSY breaking terms with gauge invariance and R-parity conservation is [36, 37]

$$\begin{aligned}\mathcal{L}_{\text{soft}} = &-\frac{1}{2}\left(M_3\tilde{g}^a\tilde{g}^a + M_2\tilde{W}^a\tilde{W}^a + M_1\tilde{B}\tilde{B} + h.c.\right)\\ &-\left(\tilde{\bar{u}}\mathbf{a_u}\tilde{Q}\cdot\mathcal{H}_2 - \tilde{\bar{d}}\mathbf{a_d}\tilde{Q}\cdot\mathcal{H}_1 - \tilde{\bar{e}}\mathbf{a_e}\tilde{Q}\cdot\mathcal{H}_1 + h.c.\right)\\ &-\tilde{Q}^\dagger\mathbf{m^2_{\tilde{Q}}}\tilde{Q} - \tilde{L}^\dagger\mathbf{m^2_{\tilde{L}}}\tilde{L} - \tilde{\bar{u}}\mathbf{m^2_{\tilde{\bar{u}}}}\tilde{\bar{u}}^\dagger - \tilde{\bar{d}}\mathbf{m^2_{\tilde{\bar{d}}}}\tilde{\bar{d}}^\dagger - \tilde{\bar{e}}\mathbf{m^2_{\tilde{\bar{e}}}}\tilde{\bar{e}}^\dagger\\ &-m^2_{\mathcal{H}_1}\mathcal{H}_1^*\cdot\mathcal{H}_1 - m^2_{\mathcal{H}_2}\mathcal{H}_2^*\cdot\mathcal{H}_2 - (m^2_{12}\mathcal{H}_1\cdot\mathcal{H}_2 + h.c.)\,. \end{aligned} \tag{3.13}$$

Here, a is the gauge index, and $M_{1,2,3}$ are the bino, wino and gluino masses, respectively. The second line contains the dimensionful trilinear interaction terms $\mathbf{a_u}, \mathbf{a_d}$ and $\mathbf{a_e}$ of the Higgs boson with two sfermions. Each $\mathbf{a_u}, \mathbf{a_d}$ and $\mathbf{a_e}$ is a complex 3×3 matrix in family space, with a one-to-one correspondence to the Yukawa couplings of the superpotential [36]. In the third line are the soft sfermion squared masses $\mathbf{m^2_{\tilde{f}}}$ with $\tilde{f} \in \{\tilde{Q}, \tilde{L}, \tilde{u}, \tilde{d}, \tilde{e}\}$, which, along with $M_{1,2,3}$ from the first line, break the mass degeneracy between the SM particles and their superpartners. The last line introduces the squared mass terms of the Higgs supermultiplets $m^2_{\mathcal{H}_{1,2}}$ and the bilinear term in the Higgs field with the soft breaking mass parameter m^2_{12}.

We see that while the superpotential (which conserves SUSY) introduces only one new parameter, μ, the SUSY breaking Lagrangian introduces a number of masses, mixing angles and couplings with potentially complex values that are not present in the SM. The MSSM contains 105 new parameters in the most general case, in addition to 19 from the SM. It is useful to impose an organizing principle on the SUSY breaking Lagrangian, since several of the new parameters in Eq. (3.13) are severely constrained by experiment. Therefore, in phenomenological studies of the MSSM, one imposes simplifying assumptions motivated by experimental constraints that can reduce the parameter space considerably.

In this thesis, we will assume that SUSY breaking is "universal" with respect to flavour. In an idealised limit where the squark and slepton squared mass matrices are flavour diagonal, one can assume

$$\mathbf{m^2_{\tilde{Q},\tilde{L}}} = m^2_{\tilde{Q},\tilde{L}}\mathbf{1}, \quad \mathbf{m^2_{\tilde{\bar{u}}}} = m^2_{\tilde{\bar{u}}}\mathbf{1}, \quad \mathbf{m^2_{\tilde{\bar{d}}}} = m^2_{\tilde{\bar{d}}}\mathbf{1}, \quad \mathbf{m^2_{\tilde{\bar{e}}}} = m^2_{\tilde{\bar{e}}}\mathbf{1}\,. \tag{3.14}$$

This ensures that SUSY contributions to the severely constrained flavour-changing neutral currents are minimal. Assuming minimal flavour violation (MFV) [48–50], which means that SUSY does not introduce any flavour violating interactions beyond those already

present in the SM, renders the trilinear couplings proportional to the corresponding Yukawa couplings:

$$\mathbf{a}_u = A_u \mathbf{y_u}, \qquad \mathbf{a}_d = A_d \mathbf{y_d}, \qquad \mathbf{a}_e = A_e \mathbf{y_e}\,. \tag{3.15}$$

As a consequence of this structure in the MFV case, only squarks and sleptons of the third generation have large couplings to the Higgs boson. Another simplifying assumption to further shrink the parameter space in the MSSM is to assume $\mathcal{CP}$ conservation. However, as we will demonstrate in Chapter 5 and onwards, $\mathcal{CP}$-violating terms can give rise to rich phenomenological features and we therefore allow parameters to be complex throughout this thesis. Lastly, along with the unification of gauge couplings, one can also assume that the gaugino masses unify at GUT scale, which leads to the following relation for the electroweak soft-breaking mass parameters:

$$M_1 = \frac{5}{3}\frac{s_W^2}{c_W^2} M_2\,. \tag{3.16}$$

3.2 The mass spectrum of the MSSM

The gauge eigenstates of the sfermion and gaugino sectors mix into and propagate as physical mass eigenstates as a result of electroweak symmetry breaking. In the subsequent sections, we describe the physical fields of the MSSM, especially the ones relevant to this thesis. A significant portion of this section will be dedicated to detailing the Higgs sector and the electroweak symmetry breaking mechanism in the MSSM.

3.2.1 Sfermion sector

In the MSSM without flavour mixing in the sfermion sector, sfermions $\tilde{f}_{L,R}$ of one generation mix into mass eigenstates $\tilde{f}_{1,2}$. The term of the Lagrangian containing the sfermion mass matrix of one generation is given by [51]

$$\begin{aligned}
&\mathcal{L}_{\tilde{f}} \supset -(\tilde{f}_L^\dagger, \tilde{f}_R^\dagger) M_{\tilde{f}}^2 \begin{pmatrix} \tilde{f}_L \\ \tilde{f}_R \end{pmatrix} \qquad \text{with} \\
&M_{\tilde{f}}^2 = \begin{pmatrix} M_{\tilde{f}_L}^2 + m_f^2 + m_Z^2 \cos 2\beta (I_f^3 - Q_f s_W^2) & m_f X_f^* \\ m_f X_f & M_{\tilde{f}_R}^2 + m_f^2 + m_Z^2 \cos 2\beta Q_f s_W^2 \end{pmatrix}.
\end{aligned} \tag{3.17}$$

Here m_f is the corresponding fermion mass and $X_f := A_f - \mu^* \cdot \{\cot\beta, \tan\beta\}$, where $\cot\beta$ and $\tan\beta$ apply to up- and down-type sfermions, respectively. The soft-breaking masses $M_{\tilde{f}_L}^2$ and $M_{\tilde{f}_R}^2$, the third component of the weak isospin I_f^3, the electric charge Q_f and the mass of the fermion m_f are real parameters. This also applies to the Z-boson mass m_Z and the sine of the weak mixing angle $s_W \equiv \sin\theta_W$. Contrarily, in the $\mathcal{CP}$-violating MSSM the trilinear couplings of the Higgs to the sfermions $A_f = |A_f| e^{i\phi_{A_f}}$ and

the Higgsino mass parameter $\mu = |\mu| e^{i\phi_\mu}$, and hence X_f, can be complex. These complex parameters enter the Higgs sector via the Higgs–sfermion couplings, see Appendix A, and are thus also of direct relevance for Higgs boson production.

For minimal flavour violation, the mass matrix is diagonalised for all f separately through the unitary matrix $U_{\tilde{f}}$ having real diagonal elements and complex off-diagonal elements,

$$\begin{pmatrix} \tilde{f}_1 \\ \tilde{f}_2 \end{pmatrix} = U_{\tilde{f}} \begin{pmatrix} \tilde{f}_L \\ \tilde{f}_R \end{pmatrix} . \tag{3.18}$$

The sfermion masses $m_{\tilde{f}_1}$ and $m_{\tilde{f}_2}$, using the convention $m_{\tilde{f}_1} \leq m_{\tilde{f}_2}$, are calculated as the eigenvalues of Eq. (3.17). Explicitly, these are given by

$$\begin{aligned} m^2_{\tilde{f}_{1,2}} = \; & m_f^2 + \frac{1}{2}\Bigg[M^2_{\tilde{f}_L} + M^2_{\tilde{f}_R} + I_3^f m_Z^2 \cos 2\beta \\ & \mp \sqrt{\left[M^2_{\tilde{f}_L} - M^2_{\tilde{f}_R} + m_Z^2 \cos 2\beta (I_f^3 - Q_f s_W^2) \right]^2 + 4 m_f^2 |X_f|^2} \Bigg] . \end{aligned} \tag{3.19}$$

The fact that the left-handed soft-breaking parameter $M^2_{\tilde{f}_L}$ is the same for the fields in an $SU(2)_L$ doublet gives rise to a tree-level relation between masses of up-type and down-type squarks.

3.2.2 Gluino sector

The gluino $\tilde{g}$, a colour octet fermion with spin $s = \frac{1}{2}$, does not mix with other fields and enters the tree-level Lagrangian in the form

$$\mathcal{L}_{\tilde{g}} \supset -\frac{1}{2} \overline{\tilde{g}} m_{\tilde{g}} \tilde{g} \, , \tag{3.20}$$

where $m_{\tilde{g}}$ is the absolute value of the possibly complex soft-breaking parameter $M_3 = m_{\tilde{g}} e^{i\phi_{M_3}}$. In the Feynman diagrams for the Higgs boson self-energies and the Higgs boson production via gluon fusion, the gluino only contributes beyond the one-loop level. However it affects the bottom-quark Yukawa coupling already at the one-loop level, where it enters the leading corrections to the relation between the bottom-quark mass and the bottom-quark Yukawa coupling which can be resummed to all orders. A more detailed discussion of this will follow in Section 6.4.1.

3.2.3 Neutralino sector

The Higgsinos and electroweak gauginos mix with each other as a result of electroweak symmetry breaking. The neutral Higgsinos $(\tilde{h}_u^0, \tilde{h}_d^0)$ and the neutral gauginos $(\tilde{B}, \tilde{W}^3)$

combine into four neutral eigenstates called *neutralinos*. Their gauge eigenstates

$$\tilde{G}^0 = \begin{pmatrix} \tilde{B} \\ \tilde{W}^3 \\ \tilde{h}_d^0 \\ \tilde{h}_u^0 \end{pmatrix}, \tag{3.21}$$

appear in the MSSM Lagrangian as

$$\mathcal{L}_{\tilde{\chi}^0} \supset \frac{1}{2} \tilde{G}^{0^T} \mathbf{M}_{\tilde{\chi}^0} \tilde{G}^0 + h.c.\,, \tag{3.22}$$

where the $\tilde{\chi}^0$ denote the neutralinos,

$$\begin{pmatrix} \tilde{\chi}_1^0 \\ \tilde{\chi}_2^0 \\ \tilde{\chi}_3^0 \\ \tilde{\chi}_4^0 \end{pmatrix} = N \begin{pmatrix} \tilde{B} \\ \tilde{W}^3 \\ \tilde{h}_d^0 \\ \tilde{h}_u^0 \end{pmatrix}. \tag{3.23}$$

$\mathbf{M}_{\tilde{\chi}^0}$ is the symmetric neutralino mass matrix given by

$$\mathbf{M}_{\tilde{\chi}^0} = \begin{pmatrix} M_1 & 0 & -m_Z s_W \cos\beta & m_Z s_W \sin\beta \\ 0 & M_2 & m_Z c_W \cos\beta & -m_Z c_W \sin\beta \\ -m_Z s_W \cos\beta & m_Z c_W \cos\beta & 0 & -\mu \\ m_Z s_W \sin\beta & -m_Z c_W \sin\beta & -\mu & 0 \end{pmatrix}, \tag{3.24}$$

and the complex, unitary matrix N diagonalises the mass matrix[1]:

$$N^* \mathbf{M}_{\tilde{\chi}^0} N^{-1} = \text{diag}\,(m_{\tilde{\chi}_1^0}, m_{\tilde{\chi}_2^0}, m_{\tilde{\chi}_3^0}, m_{\tilde{\chi}_4^0})\,, \tag{3.25}$$

such that $m_{\tilde{\chi}_1^0} \leq m_{\tilde{\chi}_2^0} \leq m_{\tilde{\chi}_3^0} \leq m_{\tilde{\chi}_4^0}$. The gaugino mass parameters M_1 and M_2, in addition to the Higgsino mass parameter μ, can also be complex. However, one of the phases of M_1 and M_2 can be rotated away by an $\mathbb{R}_2$ transformation without loss of generality and the other only has a minor impact on the Higgs sector. We will therefore neglect their phase dependence in this thesis.

3.2.4 Chargino sector

Analogous to the mixings that result in neutralinos, the charged Higgsinos $(\tilde{h}_u^+, \tilde{h}_d^-)$ and the charged winos $(\widetilde{W}^\pm)$ mix into *charginos*, $\tilde{\chi}_{1,2}^\pm$. The mass eigenstates are related to

[1] $\mathbf{M}_{\tilde{\chi}^0}$ can have negative mass eigenstates, which is fixed by applying the Takagi factorisation. A unitary transformation T rotates the eigenvalue resulting in $m_{\tilde{\chi}_i^0} \geq 0$ [52, 53].

the gauge eigenstates by

$$\begin{pmatrix}\tilde{\chi}_1^+\\ \tilde{\chi}_2^+\end{pmatrix} = V\begin{pmatrix}\widetilde{W}^+\\ \tilde{h}_u^+\end{pmatrix}, \quad \begin{pmatrix}\tilde{\chi}_1^-\\ \tilde{\chi}_2^-\end{pmatrix} = U\begin{pmatrix}\widetilde{W}^-\\ \tilde{h}_d^-\end{pmatrix}. \tag{3.26}$$

Notice that the mixing matrix for the positively charged and negatively charged fermions is different. The gauge eigenstates can be defined as

$$\tilde{g}^+ = \begin{pmatrix}\widetilde{W}^+\\ \tilde{h}_u^+\end{pmatrix}, \qquad \tilde{g}^- = \begin{pmatrix}\widetilde{W}^-\\ \tilde{h}_d^-\end{pmatrix}, \tag{3.27}$$

and the MSSM Lagrangian containing the chargino mass terms is

$$\mathcal{L}_{\tilde{\chi}^\pm} \supset \frac{1}{2}[\tilde{g}^{+^T}\mathbf{M}_{\tilde{\chi}^\pm}^T\tilde{g}^- + \tilde{g}^{-^T}\mathbf{M}_{\tilde{\chi}^\pm}\tilde{g}^+] + h.c.\,, \tag{3.28}$$

with the tree-level chargino mass matrix $\mathbf{M}_{\tilde{\chi}^\pm}$ governed by the Higgsino mass parameter μ and the gaugino mass parameter M_2 as follows,

$$\mathbf{M}_{\tilde{\chi}^\pm} = \begin{pmatrix} M_2 & \sqrt{2}m_W\sin\beta\\ \sqrt{2}m_W\cos\beta & \mu\end{pmatrix}. \tag{3.29}$$

The masses of the charginos are obtained by diagonalising $\mathbf{M}_{\tilde{\chi}^\pm}$ using the two 2×2 unitary matrices U and V:

$$U^*\mathbf{M}_{\tilde{\chi}^\pm}V = \text{diag}\,(m_{\tilde{\chi}_1^\pm}, m_{\tilde{\chi}_2^\pm}) \tag{3.30}$$

such that $m_{\tilde{\chi}_1^\pm} \leq m_{\tilde{\chi}_2^\pm}$. This results in the eigenvalues

$$m_{\tilde{\chi}_{1,2}^\pm} = \frac{M_2^2 + |\mu|^2 + 2m_W^2}{2} \mp \sqrt{\left(\frac{M_2^2 + |\mu|^2 + 2m_W^2}{2}\right) - |\mu M_2 - m_W^2\sin 2\beta|^2}\,. \tag{3.31}$$

3.2.5 Higgs sector and EWSB in the MSSM

As discussed in Section 3.1.3, the MSSM contains two Higgs doublets with opposite hypercharges $Y_{\mathcal{H}_{1,2}} = \pm 1$ in order to introduce masses for both the up- and down-type fermions:

$$\mathcal{H}_1 = \begin{pmatrix}h_d^0\\ h_d^-\end{pmatrix}, \quad \mathcal{H}_2 = \begin{pmatrix}h_u^+\\ h_u^0\end{pmatrix}. \tag{3.32}$$

The Higgs potential consists of Higgs-specific F- and D-terms, and the soft-breaking terms from the last line of Eq. (3.13):

$$\begin{aligned} V_H &= (V_F + V_D - \mathcal{L}_{\text{soft}}) \Big|_H \\ &= (|\mu|^2 + m_{\mathcal{H}_2}^2)(|h_u^0|^2 + |h_u^+|^2) + (|\mu|^2 + m_{\mathcal{H}_1}^2)(|h_d^0|^2 + |h_d^-|^2) \\ &\quad + \left[m_{12}^2(h_u^+ h_d^- - h_u^0 h_d^0) + h.c.\right] + \frac{g_1^2 + g_2^2}{8}\left[|h_u^0|^2 + |h_u^+|^2 - |h_d^0|^2 - |h_d^-|^2\right]^2 \end{aligned} \tag{3.33}$$

where we employed

$$V_F = \left|\frac{\partial W}{\partial \mathcal{H}_1}\right|^2 + \left|\frac{\partial W}{\partial \mathcal{H}_2}\right|^2, \tag{3.34}$$

$$V_D = \frac{g_2^2}{2}\sum_{a=1}^{3}\left(\mathcal{H}_1^\dagger \frac{\sigma^a}{2}\mathcal{H}_1 + \mathcal{H}_2^\dagger \frac{\sigma^a}{2}\mathcal{H}_2\right)^2 + \frac{g_1^2}{2}\left(\mathcal{H}_2^\dagger \frac{1}{2}\mathcal{H}_2 - \mathcal{H}_1^\dagger \frac{1}{2}\mathcal{H}_1\right)^2. \tag{3.35}$$

The quadratic terms of V_H contain the SUSY parameter $|\mu|^2$ and the real soft breaking terms $m_{\mathcal{H}_1}$, $m_{\mathcal{H}_2}$. The full scalar potential of the MSSM also contains terms that involve squark and slepton fields that are ignored here since they do not get vevs. The bilinear terms have the soft coefficient m_{12}^2, which can be complex, but whose phase can be absorbed by redefining the phases of μ and m_{12}^2 through a Peccei-Quinn transformation [54, 55].

So far, we have encountered the possible complex parameters M_1, M_2, M_3, A_f, μ and m_{12}^2. In Section 3.3, we will describe the $\mathbb{R}_2$ and Peccei-Quinn (PQ) transformations used to absorb the phases of M_2 and m_{12}^2 and discuss the experimental bounds on the rest of the phases.

Electroweak symmetry breaking in the MSSM

In order to obtain massive fermions and gauge bosons, we require that the minimum of Eq. (3.33) should break down the symmetry to $SU(2)_L \otimes U(1)_Y \to U(1)_{\text{EM}}$ in accordance with observations in nature. However the presence of an additional complex Higgs doublet makes the EWSB mechanism more complicated than in the SM.

In order to simplify the EWSB mechanism in the MSSM, one can take advantage of the freedom to use gauge transformations, and carry out an $SU(2)_L$ transformation to rotate away h_u^+ at the minimum such that we can assume without loss of generality that $\left\langle h_u^+ \right\rangle = 0$ [36]. A potential satisfying this minimising condition also has $\left\langle h_d^- \right\rangle = 0$. This implies that the $U(1)_{\text{EM}}$ symmetry is unbroken in the vacuum state since the charged components of the Higgs doublets have vanishing vevs.

We can now express the Higgs potential V_H in terms of the neutral Higgs states:

$$V_H^0 = (|\mu|^2 + m_{\mathcal{H}_2}^2)|h_u^0|^2 + (|\mu|^2 + m_{\mathcal{H}_1}^2)|h_d^0|^2 - [m_{12}^2 h_u^0 h_d^0 + h.c.] + \frac{g_1^2 + g_2^2}{8}[|h_u^0|^2 - |h_d^0|^2]^2 \,. \tag{3.36}$$

For the MSSM scalar potential to successfully induce EWSB, it must satisfy the same properties that we imposed on the SM scalar potential in Eq. (2.8). Not only must it have a stable minimum that does not lie at the origin, but it must also be bounded from below. The quartic interactions of V_H are able to stabilise the potential for arbitrarily large values of h_u^0 and h_d^0. However, when $h_u^0 = h_d^0$, the quartic D-term (proportional to $g_1^2 + g_2^2$) is identically zero. This is called the D-flat direction in field space, and for the scalar potential to be bounded from below we require the quadratic part of the potential to be positive in this direction. This imposes the following relation on μ, $\mathcal{H}_{1,2}$ and m_{12}^2:

$$0 < 2m_{12}^2 < 2|\mu|^2 + m_{\mathcal{H}_1}^2 + m_{\mathcal{H}_2}^2 \,. \tag{3.37}$$

The second condition on the scalar potential is that it needs to have a saddle point at the origin $|h_u^0| = |h_d^0| = 0$. This unstable origin is achieved when the linear combination of h_u^0 and h_d^0 has a negative mass squared:

$$m_{12}^2 > (|\mu|^2 + m_{\mathcal{H}_1}^2) + (|\mu|^2 + m_{\mathcal{H}_2}^2) \,. \tag{3.38}$$

It is clear that Eq. (3.37) and Eq. (3.38) cannot be simultaneously fulfilled if $m_{\mathcal{H}_1}^2 = m_{\mathcal{H}_2}^2$ and especially for $m_{\mathcal{H}_1}^2 = m_{\mathcal{H}_2}^2 = 0$, which means SUSY breaking is necessary for successful EWSB in the MSSM. There exist models with boundary conditions derived from Minimal SUper GRAvity (MSUGRA) or Gauge-Mediated Supersymmetry Breaking (GMSB) wherein $m_{\mathcal{H}_1}^2 = m_{\mathcal{H}_2}^2$ holds at the GUT scale, but radiative corrections involving large top-Yukawa couplings can drive $m_{\mathcal{H}_2}^2$ to small values, unequal to $m_{\mathcal{H}_1}^2$, at the electroweak scale. In such models electroweak symmetry breaking is induced by quantum radiative corrections proportional to the squared masses of SUSY particles via a mechanism known as radiative EWSB, which generates EWSB dynamically for universal boundary conditions. Naturally, in order to prevent the reintroduction of large fine tuning of the bare Higgs mass in such a case, the SUSY particle masses should not be larger than $\mathcal{O}$(TeV).

Having established the conditions necessary for h_u^0 and h_d^0 to have real non-vanishing vevs, we can write

$$\left\langle h_u^0 \right\rangle = v_u \,, \qquad \left\langle h_d^0 \right\rangle = v_d \,. \tag{3.39}$$

Their ratio is written as

$$\tan\beta = \frac{v_u}{v_d} \tag{3.40}$$

and is one of the primary input parameters describing MSSM phenomenology. The values of v_u and v_d must satisfy the observed phenomenology of the Higgs sector, and hence we

define their relation to the SM vev

$$v^2 = v_u^2 + v_d^2 = \frac{4m_Z^2}{g_1^2 + g_2^2} \approx (246\ \text{GeV})^2\,, \tag{3.41}$$

where m_Z is the mass of the Z-boson.

The μ problem

The minimisation condition for the scalar potential leads to the relation

$$\frac{m_Z^2}{2} = -\mu^2 + \frac{m_{\mathcal{H}_1}^2 - m_{\mathcal{H}_2}^2 \tan^2\beta}{\tan^2\beta - 1}\,. \tag{3.42}$$

The left-hand side of this equation resides at the electroweak scale. On the other hand, μ is a SUSY conserving parameter, and $m_{\mathcal{H}_{1,2}}^2$ are soft-breaking parameters with m_{soft} as their mass scale. These parameters on the right-hand side of Eq. (3.42) with a priori separate origins must combine to result in the electroweak scale. Unless their mass scales are within a couple of orders magnitude of m_Z, additional cancellations will be required to fulfil the above relation. The MSSM does not provide an explanation for why μ^2 must be small compared to, say, M_{P}^2 and in particular why it should be of the order of 10^2 or 10^3 GeV. This is known as the "μ problem" [56, 57] and serves as a motivation for next-to-minimal supersymmetric models, where μ naturally arises at the electroweak scale as the vev of an additional singlet. However, in this thesis we will limit ourselves to the MSSM.

Tree-level masses and mixings

In an expansion around the minimum, the neutral fields of the two Higgs doublets can be decomposed into $\mathcal{CP}$-even (ϕ_1^0, ϕ_2^0) and $\mathcal{CP}$-odd (χ_1^0, χ_2^0) components as follows[2]

$$\mathcal{H}_1 = \begin{pmatrix} v_d + \frac{1}{\sqrt{2}}(\phi_1^0 + i\chi_1^0) \\ \phi_1^- \end{pmatrix}, \quad \mathcal{H}_2 = e^{i\xi} \begin{pmatrix} \phi_2^+ \\ v_u + \frac{1}{\sqrt{2}}(\phi_2^0 + i\chi_2^0) \end{pmatrix}. \tag{3.43}$$

Here ξ is a possible relative phase between the two doublets. Inserting this expansion into the scalar potential we obtain

$$V_H \supset -\sum_i T_i \Phi_i^0 + \frac{1}{2}\Phi^0 \mathbf{M}_{\phi\phi\chi\chi} \Phi^{0T} + \frac{1}{2}\Phi^- \mathbf{M}_{\phi^\pm\phi^\pm} \Phi^{+T} \cdots\,, \tag{3.44}$$

[2] We note that the convention differs from the convention employed by `FeynHiggs` by a different sign of χ_1^0 and ϕ_1^-, which induces different signs in the corresponding elements of the matrices in Eq. (3.44), Eq. (3.46) and Eq. (3.47) and the χ_1^0 couplings to (s)quarks displayed in Appendix A.

with $\Phi^0 := (\phi_1^0, \phi_2^0, \chi_1^0, \chi_2^0)$ and $\Phi^\pm := (\phi_1^\pm, \phi_2^\pm)$. T_i are the tadpole coefficients, $\mathbf{M}_{\phi\phi\chi\chi}$ is the mass matrix of the neutral degrees of freedom,

$$\mathbf{M}_{\phi\phi\chi\chi} = \begin{pmatrix} M^2_{\phi\phi} & M^2_{\phi\chi} \\ M^{\dagger 2}_{\phi\chi} & M^2_{\chi\chi} \end{pmatrix}, \tag{3.45}$$

and $\mathbf{M}_{\phi^\pm\phi^\pm}$ is the 2×2 Hermitian mass matrix of the charged Higgs components. At tree level, the minimisation conditions for V_H require the tadpole coefficients and the relative phase ξ between the Higgs doublets to vanish. Consequently, the Higgs sector of the MSSM is $\mathcal{CP}$-conserving at lowest order. This also implies that $\mathbf{M}_{\phi\phi\chi\chi}$ is block diagonal. The two complex Higgs doublets of Eq. (3.43) contain eight degrees of freedom. In analogy to the SM, EWSB results in three of these degrees of freedom contributing to the longitudinal polarisation components of Z and $W^\pm$ bosons. The remaining five degrees of freedom manifest themselves as five physical Higgs bosons of the MSSM: $\mathcal{CP}$-even h, H, a $\mathcal{CP}$-odd A and two charged Higgses $H^\pm$ at lowest order. The tree-level neutral mass eigenstates $\{h, H, A, G\}$, where G is the unphysical Goldstone boson, are obtained from the tree-level neutral gauge eigenstates $\{\phi_1^0, \phi_2^0, \chi_1^0, \chi_2^0\}$ through a unitary matrix as follows:

$$\begin{pmatrix} h \\ H \\ A \\ G \end{pmatrix} = \begin{pmatrix} -s_\alpha & c_\alpha & 0 & 0 \\ c_\alpha & s_\alpha & 0 & 0 \\ 0 & 0 & s_{\beta_n} & c_{\beta_n} \\ 0 & 0 & -c_{\beta_n} & s_{\beta_n} \end{pmatrix} \begin{pmatrix} \phi_1^0 \\ \phi_2^0 \\ \chi_1^0 \\ \chi_2^0 \end{pmatrix}. \tag{3.46}$$

Similarly, for the charged Higgs states one obtains

$$\begin{pmatrix} H^\pm \\ G^\pm \end{pmatrix} = \begin{pmatrix} s_{\beta_c} & c_{\beta_c} \\ -c_{\beta_c} & s_{\beta_c} \end{pmatrix} \begin{pmatrix} \phi_1^\pm \\ \phi_2^\pm \end{pmatrix}, \tag{3.47}$$

where $s_x \equiv \sin x, c_x \equiv \cos x$. α, β_n and β_c are the mixing angles for the $\mathcal{CP}$-even Higgs bosons (h, H), the neutral $\mathcal{CP}$-odd states $(A,\ G)$, and the charged states $(H^\pm,\ G^\pm)$, respectively. Minimising the Higgs potential leads to $\beta := \beta_n = \beta_c$ at tree level, with the following relation between the mixing angles

$$\tan(2\alpha) = \frac{m_A^2 + m_Z^2}{m_A^2 - m_Z^2} \tan(2\beta)\,. \tag{3.48}$$

The masses of the Higgs bosons at tree level are given by the relations

$$m^2_{h/H} = \frac{1}{2}\left(m_A^2 + m_Z^2 \mp \sqrt{(m_A^2 + m_Z^2)^2 - 4 m_A^2 m_Z^2 \cos^2(2\beta)}\right) \tag{3.49}$$

$$m^2_{H^\pm} = m_A^2 + m_W^2, \qquad m_A^2 = \frac{2m_{12}^2}{\sin(2\beta)}\,, \tag{3.50}$$

Table 3.2: A summary of physical states of the MSSM [36] excluding the SM fermions and gluons.

Names	Gauge eigenstates	Physical states
Sfermions	$\tilde{f}_L, \tilde{f}_R^*$	$\tilde{f}_1, \tilde{f}_2$
Neutralinos	$\tilde{B}, \tilde{W}^3, \tilde{h}_u^0, \tilde{h}_d^0$	$\tilde{\chi}_1^0, \tilde{\chi}_2^0, \tilde{\chi}_3^0, \tilde{\chi}_4^0$
Charginos	$\tilde{W}^\pm, \tilde{h}_u^+, \tilde{h}_d^-$	$\chi_1^\pm, \chi_2^\pm$
Gluino	$\tilde{g}$	$\tilde{g}$
Gauge bosons	B, W^1, W^2, W^3	$\gamma, Z, W^\pm$
Higgs bosons	$h_u^0, h_d^0, h_u^+, h_d^-$	$h, H, A, H^\pm$

with $m_h < m_H$. The Higgs sector of the MSSM at lowest order is fully determined (besides the gauge couplings) by two parameters, which are usually chosen as m_A (or equivalently, $m_{H^\pm}$) and $\tan\beta(\equiv t_\beta)$ for the case of the MSSM with real parameters. For the MSSM with complex parameters, we choose the mass $m_{H^\pm}$ instead of m_A as the input parameter, since beyond tree-level, $\mathcal{CP}$-violating mixings give rise to $\mathcal{CP}$-admixed Higgs bosons and A is no longer a mass eigenstate. At higher orders as particles from other sectors contribute to loop-induced effects, also other SUSY parameters affect the Higgs boson masses and mixings.

Eq. (3.49) gives the upper bound $m_h \leq m_Z$ at tree level, which had already been excluded at LEP for a SM-like Higgs boson [58]. We must take into consideration higher order corrections to the Higgs mass; while the 1-loop contributions from third generation (s)quarks are substantial and can shift the upper bound to about 140 GeV [59–63], leading 2-loop corrections reduce this bound to about 130 GeV for TeV scale SUSY masses [64]. For the latest developments in Higgs mass calculations we refer the reader to Refs. [65–69] and references therein. The discovery of the SM-like Higgs signal at ∼125 GeV by ATLAS and CMS in 2012 is therefore a priori compatible with the lightest MSSM Higgs boson h. While there exist scenarios wherein the heavier $\mathcal{CP}$-even Higgs boson H can be interpreted as the SM-like discovered state [70–74], in this thesis we will mainly consider scenarios where the lightest MSSM Higgs boson is SM-like.

A summary of the mass eigenstates of the MSSM resulting from mixings of the gauge eigenstates is presented in Table 3.2.

The decoupling limit

In the MSSM, the tree-level couplings of the neutral Higgs bosons to the up and down-type fermions and gauge bosons depend on the mixing angles α and β. These couplings, relative to those of the SM Higgs, are summarised in Table 3.3. Eq. (A.1) in Appendix A illustrates how they explicitly appear in the Lagrangian.

In models with an extended Higgs sector, the SM Higgs coupling to gauge bosons is

Table 3.3: Tree-level couplings of the neutral MSSM Higgs bosons to SM massive fermions and gauge bosons relative to the couplings of the SM Higgs.

	ϕ	g_u^ϕ	g_d^ϕ	g_V^ϕ
SM	H^0	1	1	1
MSSM	h	c_α/s_β	$-s_\alpha/c_\beta$	$\sin(\beta-\alpha)$
	H	s_α/s_β	c_α/c_β	$\cos(\beta-\alpha)$
	A	$1/t_\beta$	t_β	0

distributed among the neutral BSM Higgs bosons to maintain unitarity. For example, the MSSM features the following sum rule for the relative gauge boson (V) couplings to the three neutral Higgs bosons [75]:

$$\sum_{\phi\in\{h,H,A\}} (g_V^\phi)^2 = 1\,, \tag{3.51}$$

. These couplings of the Higgs bosons of the MSSM relative to SM values are

$$g_V^h = \sin(\beta-\alpha), \quad g_V^H = \cos(\beta-\alpha)\,, \tag{3.52}$$

with no tree-level couplings of the $\mathcal{CP}$-odd A or $H^\pm$ to VV. When $m_A \gg m_Z$, the Higgs masses and mixing angles simplify:

$$m_h^2 \approx m_Z^2 \cos^2 2\beta\,, \quad m_H^2 \approx m_A^2 + m_Z^2 \sin^2 2\beta\,, \quad \cos^2(\beta-\alpha) \approx \frac{m_Z^4 \sin^2 4\beta}{4m_A^4}\,. \tag{3.53}$$

In this limit, it is apparent that $m_A \simeq m_H \simeq m_{H^\pm}$, and $\cos(\beta-\alpha) \to 0$ up to corrections of $\mathcal{O}(m_Z^4/m_A^4)$. Consequently, the tree-level mixing angles α and β approach the limiting values

$$\sin(\alpha) \to -\cos(\beta), \quad \cos(\alpha) \to \sin(\beta), \quad \sin(\beta-\alpha) \to 1, \quad \cos(\beta-\alpha) \to 0\,. \tag{3.54}$$

This results in H and A decoupling from VV, and the hAZ coupling $g_{AZ}^h = \cos(\beta-\alpha)$ vanishes. The h coupling to VV and the fermions behaves like that of the SM Higgs boson. This is called the *decoupling limit* [76]. In this limit, the MSSM Higgs sector behaves SM-like, and the heavy Higgs bosons searches in the production and decay channels with gauge bosons become difficult because of small rates. The couplings of the heavy Higgses to the fermions may either be suppressed or enhanced depending on the angles α and β.

As the discovered 125 GeV scalar has yet to show any significant deviation from SM properties, limits such as the decoupling limit or the more general alignment limit[3] [77–79]

[3]Here an SM-like Higgs boson arises if one of the neutral Higgs mass eigenstates is approximately aligned with the direction of the Higgs vev in field space.

where one of the Higgs bosons can be interpreted as the SM-like discovered state are crucial for benchmark scenarios for MSSM Higgs searches. The scenarios investigated in this thesis will largely lie in the decoupling region.

3.3 $\mathcal{CP}$-violating phases in the MSSM

In Section 3.1.5 we discussed the introduction of 105 additional parameters in the MSSM parametrising our ignorance of the precise SUSY breaking mechanism. Assuming MFV restricts the total number of new MSSM parameters to 41. Along with a mass in the Higgs sector[4] M_A (or $M_{H^\pm}$), they are: $\tan\beta$, the gaugino mass parameters $|M_1|, |M_2|, |M_3|$ and $|\mu|$, the sfermion masses $m_{\tilde{u}_i}, m_{\tilde{d}_i}, m_{\tilde{e}_i}, m_{\tilde{L}_i}, m_{\tilde{Q}_i}$ for the three generations, and the trilinear couplings $|A_f|$, $f \in \{e, \mu, \tau, u, d, c, s, t, b\}$ of the sfermions.

In addition to these real parameters, there are also 14 possible $\mathcal{CP}$-violating phases: the Higgsino mass parameter phase ϕ_μ, the gluino mass parameter phase ϕ_{M_3}, the phase of the soft-breaking bilinear mass term $\phi_{m_{12}^2}$, the phases of the gaugino mass parameters, ϕ_{M_1}, ϕ_{M_2} and the phases of the trilinear couplings ϕ_{A_f}, $f \in \{e, \mu, \tau, u, d, c, s, t, b\}$. However, as we have already mentioned in Section 3.2.3 and Section 3.2.5, not all of the 14 phases are physical. The phases of m_{12}^2 and M_2 (or M_1) can be rotated away, leaving us with 12 independent $\mathcal{CP}$-violating phases.

To absorb the phases of M_2 and m_{12}^2, we perform two $U(1)$ transformations: $\mathbb{R}_2$ and Peccei-Quinn (PQ), as follows [32]. The transformation of parameters $M_{1,2,3}, A_f, m_{12}^2$ and μ is defined such that the Lagrangian remains invariant. Quantities are multiplied by $e^{iq\varphi}$ under a general $U(1)$ transformation, where φ is the rotation angle and q is the $U(1)$ charge. The U(1) charges of the parameters $M_{1,2,3}, A_f, m_{12}^2$ and μ under an $\mathbb{R}_2$ transformation are $q_{\mathbb{R}_2} = -1, -1, 0, 1$, respectively. Similarly, their charges under a PQ transformation are $q_{PQ} = 0, 0, -1, -1$, respectively. First, an $\mathbb{R}_2$ transformation with the angle ϕ_{M_2} is performed on each of the parameters and fields, followed by a PQ transformation with the angle $\phi_{m_{12}^2}$. This has the following effect on the phases:

$$\{\phi_\mu, \phi_{M_1}, \phi_{M_2}, \phi_{M_3}, \phi_{m_{12}^2}, \phi_{A_f}\}$$

$$\downarrow \mathbb{R}_2(\phi_{M_2})$$

$$\{\phi_\mu + \phi_{M_2}, \phi_{M_1} - \phi_{M_2}, 0, \phi_{M_3} - \phi_{M_2}, \phi_{m_{12}^2}, \phi_{A_f} - \phi_{M_2}\}$$

$$\downarrow PQ(\phi_{m_{12}^2})$$

$$\{\phi_\mu + \phi_{M_2} - \phi_{m_{12}^2}, \phi_{M_1} - \phi_{M_2}, 0, \phi_{M_3} - \phi_{M_2}, 0, \phi_{A_f} - \phi_{M_2}\}$$

The remaining non-vanishing phases and fields are redefined to absorb ϕ_{M_2} and $\phi_{m_{12}^2}$. The phases of M_2 and m_{12}^2 are thus rotated away. If we attempt further $U(1)$ transformations

[4] We use capital letters to denote loop-corrected Higgs masses.

on the remaining angles, no more phases can be absorbed. Note that the phases of M_1 or M_3 could also have been chosen for the $\mathbb{R}_2$ transformation but ϕ_{M_2} is chosen as a matter of convention.

The complex parameters in the MSSM provide additional sources of $\mathcal{CP}$ violation beyond the single phase of the CKM matrix [25,26]. Such additional sources are needed to explain the observed baryon asymmetry in the universe. However, this thesis will concentrate on investigating the impact of these complex parameters on the Higgs phenomenology of the MSSM applied to key processes at the LHC. In particular, we concentrate on parameters that have a significant impact on Higgs boson production via gluon-fusion and bottom-quark annihilation. The most important of these are the phases of the trilinear couplings of the Higgs to the third generation fermions ϕ_{A_t,A_b}, owing to potentially large stop and sbottom loop effects arising from large top- and bottom-Yukawa couplings. We also investigate the effect of the phase of the gluino mass parameter and the Higgsino mass parameters ϕ_{M_3} and ϕ_μ, respectively. While ϕ_{M_3} affects the bottom-Yukawa coupling at one-loop level and the Higgs boson self-energies at two-loop level, ϕ_μ affects both at one-loop level.

However, the phases of these parameters face experimental constraints. The most restrictive constraints on the phases arise from bounds on the electric dipole moments (EDMs) of the electron and the neutron [80–82]. EDMs from heavy quarks [83, 84] and the deuteron [85] also have an impact. MSSM contributions to these EDMs already contribute at the one-loop level and primarily involve the first two generations of sleptons and squarks. Thus, EDMs lead to severe constraints on the phases of A_q for $q \in \{u, d, s, c\}$ and A_l for $l \in \{e, \mu\}$. Using the convention that the phase of the wino soft-breaking mass M_2 is rotated away, one finds tight constraints on the phase of μ [86]. On the other hand constraints on the phases of the third-generation trilinear couplings are significantly weaker. Ref. [87] provides a comprehensive review of the same. While recent constraints from EDMs [88] taking into account two-loop contributions [89] have the potential to rule out the largest values of the phase of A_t, there is still significant room for variation of the phases of A_t and M_3.

In this thesis, we will therefore display the full range of the phases of A_t and M_3 in our considered scenarios without explicitly imposing EDM constraints, following the common approach in benchmark scenarios for Higgs phenomenology (Ref. [90] provides a recent discussion). In Chapter 5, the impact of the complex parameters giving rise to $\mathcal{CP}$-violating self-energies which induce a mixing between the tree-level mass eigenstates h, H and A will be discussed. In Chapter 6 we will investigate the effects of $\mathcal{CP}$-violating couplings and mixings on gluon-fusion and bottom-quark annihilation cross sections for neutral Higgs production, and provide a numerical and phenomenological study of the processes in Chapter 8.

Chapter 4

Experimental status at the LHC

This chapter provides a brief review of the current experimental status for a selection of measurements and searches at the LHC relevant for the work in this thesis. Note that it is in no way an overview of all the important results and measurements made by high-energy experiments in the past years, and more recently at Run II of the LHC. Other than the sources cited in the text, Refs. [91–96] have been used for this chapter.

4.1 Introduction

The Large Hadron Collider builds on the successes of collider experiments such as the Large Electron-Positron Collider (LEP), the Tevatron, and the DESY colliders HERA, DORIS, and PETRA. The LHC at the European Laboratory for Particle Physics (CERN) is a circular proton–proton collider with a circumference of 27.6 km. It is housed in the tunnel that was built for the LEP, and is placed at a depth ranging from 50–175 m. The tunnel has two beamlines intersecting at four points. Particle collisions are analysed by seven experiments: ATLAS and CMS, the biggest of these, use general purpose detectors to study a wide range of physics. The LHC started up in the fall of 2008 and in the years 2010–12 ran at centre-of-mass (com) energies $\sqrt{s} = 7$ TeV and $\sqrt{s} = 8$ TeV. At design luminosity, the LHC can allow more than 2800 bunches of protons to circulate in each beam with the nominal intensity of 10^{11} protons per bunch. In the first years of Run I of the LHC, ATLAS and CMS had collected more than 20 fb^{-1} of integrated luminosity. In 2015, the LHC started to collide protons at the centre-of-mass energy of 13 TeV, which substantially improves the reach of searches for BSM physics. The anticipated integrated luminosity for Run II of the LHC, scheduled to end in 2018, is around 120 fb^{-1} per experiment, leading to much larger sets of available data.

In the following sections, we present a summary of the measurements of the SM Higgs production and decay rates made by ATLAS and CMS, following which we will discuss the relevant results for SUSY and heavy Higgs searches. In particular, we will discuss the exclusion limits on the masses of stops and gluinos from direct SUSY searches, and the bounds on the MSSM parameter space from searches for additional Higgs bosons.

4.2 Experimental results

4.2.1 Higgs production and decay at the LHC

In 2012, ATLAS and CMS announced the discovery of a new particle with a mass of 125 GeV compatible with the properties of the SM Higgs boson. With its measured properties, the discovered particle can also be interpreted to be a Higgs boson belonging to new physics models having extended Higgs sectors, such as the MSSM. The neutral Higgs bosons h, H and A of the MSSM can be produced via the main SM Higgs production channels (Fig. 4.1):

$$\begin{aligned} \text{gluon fusion :} \quad & gg \to h/H/A \\ \text{associated production with heavy quarks :} \quad & gg \to q\bar{q} + h/H/A \\ \text{associated } h/H \text{ production with } W/Z \text{ (Higgsstrahlung) :} \quad & q\bar{q} \to V + h/H \\ \text{vector boson fusion for } h/H \text{ production :} \quad & qq \to VV \to qq + h/H \end{aligned}$$

However, due to modified couplings of the MSSM Higgs bosons to the fermions and gauge bosons, as well as the presence of additional SUSY particles that couple to the Higgses and participate in the loops, the production rates and cross sections of the MSSM Higgs bosons are significantly different than for the SM case. The differences that arise in the gluon-fusion and bottom-quark annihilation cross sections of the MSSM Higgs bosons in comparison to the SM Higgs will be discussed in detail in Chapter 6. For low and

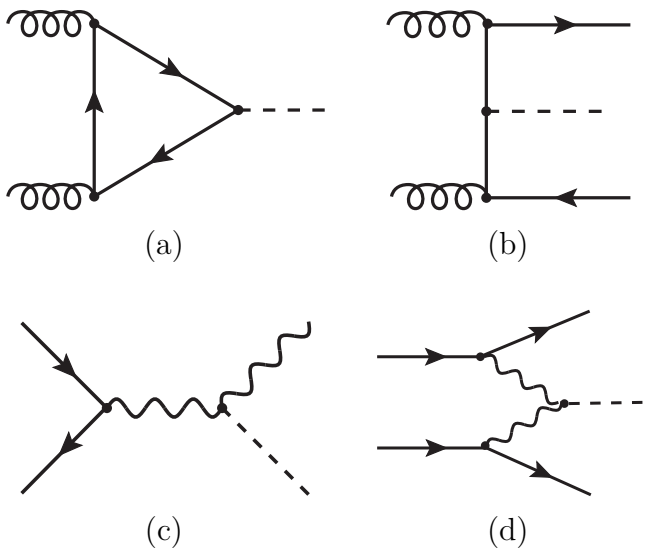

Figure 4.1: The dominant neutral Higgs production mechanisms in hadronic collisions are (a) gluon fusion (b) associated production with heavy quarks (c) Higgsstrahlung and (d) vector boson fusion.

medium values of $\tan\beta$, the MSSM Higgs bosons are predominantly produced through gluon fusion. At high $\tan\beta$, the production in association with a pair of bottom quarks is the dominant process, due to the enhanced bottom-Yukawa coupling to the Higgs bosons. Additionally, at tree level, only the $\mathcal{CP}$-even MSSM Higgs bosons h and H can be produced in the Higgsstrahlung and vector boson fusion processes, since there are no tree-level couplings of the $\mathcal{CP}$-odd A to $V = W, Z$. The lowest-order cross sections in these processes are those of the SM Higgs boson folded with the square of the normalised g_V^ϕ couplings to the MSSM Higgs bosons h and H. Beyond tree level, couplings of the $\mathcal{CP}$-odd Higgs A to the vector bosons can also be induced. Moreover, SUSY particles participating in the loops can alter the production rates of the MSSM Higgs bosons compared to the SM case. There are also other mechanisms for the production of the MSSM Higgses, as in the SM. The processes for the production of two Higgs particles,

$$\text{Higgs boson pair production :} \qquad q\bar{q}, gg \to \phi_i\phi_j \,,$$

with $\phi_{i,j} \in \{h, H, A\}$ are naturally more numerous for extended Higgs sectors than in the SM, and can be enhanced due to resonant heavy Higgs bosons. In the MSSM, two of these processes, the production of hA and HA, can occur at tree level through $q\bar{q}$ annihilation, and at one loop in the $gg \to hA, HA$ mechanisms. The other pair production processes $gg \to hh, HH, hH, AA$, are loop induced, as in the case of the SM [97].

For the 125 GeV Higgs, H^0, at the LHC, the dominant production channel is the gluon-fusion process. This can be seen from Fig. 4.2 (a) which shows the inclusive Standard Model Higgs boson production cross sections at 13 TeV for various production modes. The Higgs is detected through its final state decay products F, and can decay via several modes, each of which is quantified by its *branching ratio*:

$$\mathrm{BR}^F = \Gamma^F / \Gamma^{\mathrm{tot}} \,, \tag{4.1}$$

where Γ^F is the partial width of the process $H^0 \to F$ and Γ^{tot} is the total width. A 125 GeV Higgs provides an excellent opportunity to explore Higgs couplings to many SM particles. The dominant decay modes for a 125 GeV SM-like Higgs are $H^0 \to b\bar{b}$ and $H^0 \to WW^*$ followed by $H^0 \to gg$, $H^0 \to \tau^+\tau^-$, $H^0 \to c\bar{c}$ and $H^0 \to ZZ^*$, as seen in Fig. 4.2 (b). The rates of $H^0 \to \gamma\gamma, H^0 \to \gamma Z$ and $H^0 \to \mu^+\mu^-$ are much smaller. However large the branching ratio for $H^0 \to b\bar{b}$ is, for any given M_{H^0}, the sensitivity of a search channel depends not only on the production cross section and the branching ratio of the decay channel, but also on the reconstructed mass resolution, selection efficiency of the detector, and the amount of background in the final state. The $H^0 \to b\bar{b}$ and $H^0 \to \tau^+\tau^-$ channels suffer from large backgrounds — with the QCD backgrounds for the former being much more overwhelming — and a relatively poor mass resolution. The $H^0 \to W^+W^- \to l^+\nu_l l'^-\bar{\nu}_{l'}$ channel has a relatively large branching fraction but the presence of neutrinos spoils the mass resolution. The channels where the signal has been

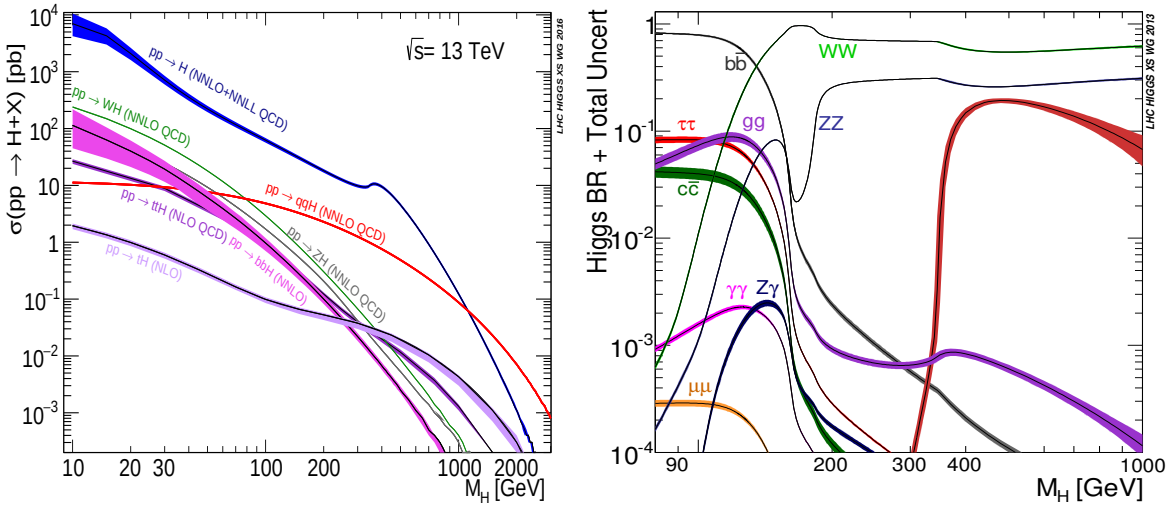

(a) (b)

Figure 4.2: (a) Inclusive production cross sections at the LHC for the SM Higgs boson [92] and (b) the SM Higgs boson decay branching ratios at 13 TeV [91].

discovered first, therefore, are $H^0 \to \gamma\gamma$ and $H^0 \to ZZ^* \to 4l$, where all the final state particles are measured very precisely and the M_{H^0} resolution is very good. For $M_{H^0} \geq 150$ GeV, the most sensitive search channels are $H^0 \to WW^*$ and $H^0 \to ZZ^*$, with W and Z decaying into several leptonic and hadronic final states. With the combined 2011–12 dataset at 7 and 8 TeV com energy and an integrated luminosity 25 fb^{-1}, the excess in $H^0 \to \gamma\gamma$ had a local significance of 7.4σ as measured by ATLAS [98], and 4.2σ as measured by CMS [99], for a background only hypothesis. In the $H^0 \to ZZ^* \to 4l$ channel the values were 6.6σ in the ATLAS measurement [100], and 6.8σ in the CMS measurement [101]. The 125 GeV Higgs boson was "rediscovered" by ATLAS and CMS in 2016 with the 13 TeV dataset in Run II of the LHC, and so far no significant deviation from the properties predicted for the SM Higgs have been found.

One possibility for characterising Higgs boson yields is by using the signal strength μ, defined as the ratio of the measured Higgs boson rate to its SM prediction. For a specific production process $I \to H^0$ and decay mode $H^0 \to F$, the signal strengths for the production μ_I and decay μ^F are defined as

$$\mu_I = \frac{\sigma_I}{(\sigma_I)_{\text{SM}}} \qquad \text{and} \qquad \mu^F = \frac{\text{BR}^F}{(\text{BR}^F)_{\text{SM}}}, \tag{4.2}$$

where σ_I and BR^F are the production cross sections for $I \to H^0$ and branching fractions for $H^0 \to F$, respectively. The data does not allow the quantities μ_I and μ^F to be measured separately for a given process, and the experimentally measured quantity is

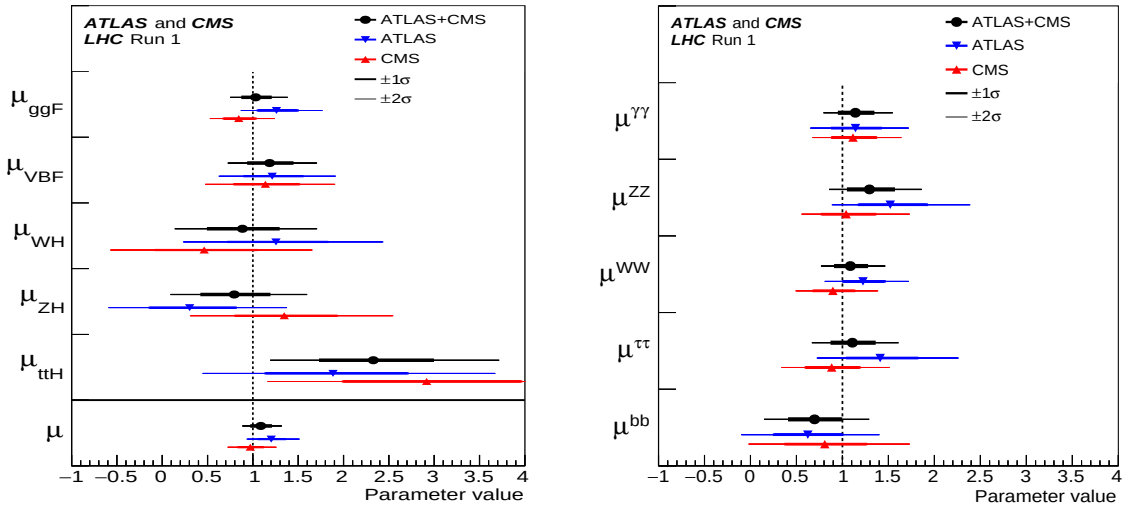

Figure 4.3: Run I legacy: Best fit for (a) the production and (b) the decay signal strength parameter μ in individual channels for the combination of ATLAS and CMS data. The thick error bars indicate 1σ, and the thin bars indicate 2σ intervals. For the production signal strength, an extrapolation from fiducial to the inclusive cross section was performed. Figures from Ref. [102].

the product $\mu_I \cdot \mu^F$. This gives the combined signal strength

$$\mu_I^F = \frac{\sigma_I \cdot \mathrm{BR}^F}{(\sigma_I)_{\mathrm{SM}} \cdot (\mathrm{BR}^F)_{\mathrm{SM}}} = \mu_I \cdot \mu^F \,. \tag{4.3}$$

All combined fits of signal strengths therefore make assumptions about the relationship between μ_I of different production processes or similarly between μ^F of different decay modes. Thus the meaning of the signal strength depends on the assumptions made. The signal strengths for individual production and decay channels are shown for combined ATLAS and CMS data at 8 TeV in Fig. 4.3. While they show a great degree of agreement to the SM prediction, the measurements are still affected by considerable uncertainties. The mass of the discovered Higgs boson determined from combined measurements from ATLAS and CMS is [102]

$$M_{H^0} = 125.09 \pm 0.21(\mathrm{stat.}) \pm 0.11(\mathrm{syst.})\ \mathrm{GeV}\,. \tag{4.4}$$

In order to probe the spin and $\mathcal{CP}$-properties of the discovered Higgs, systematic analyses of its production and decay angles are needed. Most of these analyses are based on the discrimination of distinct hypothesis for the spin and $\mathcal{CP}$-properties. The experiments so far provide evidence of the spin-0 nature of the Higgs [103, 104]. The detected signal disfavours the pure $\mathcal{CP}$-odd hypothesis, but the experimental measurements have a very

limited sensitivity to a possible admixture of $\mathcal{CP}$-even and $\mathcal{CP}$-odd components.

4.2.2 Direct SUSY searches

Among the results from the ATLAS and CMS experiments are a multitude of searches for supersymmetric particles. The programmes for SUSY searches in both experiments are based on a wide range of techniques that measure SM background contributions and a plethora of final states. No evidence of the SUSY sparticle spectrum has been detected so far [94,96]. However, unlike the SM, SUSY has different possibilities for mass hierarchies, decay patterns etc., which can give rise to a variety of signatures. The reported limits on masses of SUSY particles are therefore reliant on specific assumptions placed on the model parameters. Consequently, the results presented cannot be interpreted in a wholly generic way and one must be careful when making use of these limits in a particular SUSY model. One approach is to conduct the search in specific models with a reduced set of free parameters. The phenomenological MSSM or pMSSM assumes no R-parity violation, no new sources of $\mathcal{CP}$ violation, mass degenerate first and second generation scalars and no flavour changing neutral currents. These assumptions reduce the parameter set of SUSY to 19. Another popular approach is to present the experimental results within the

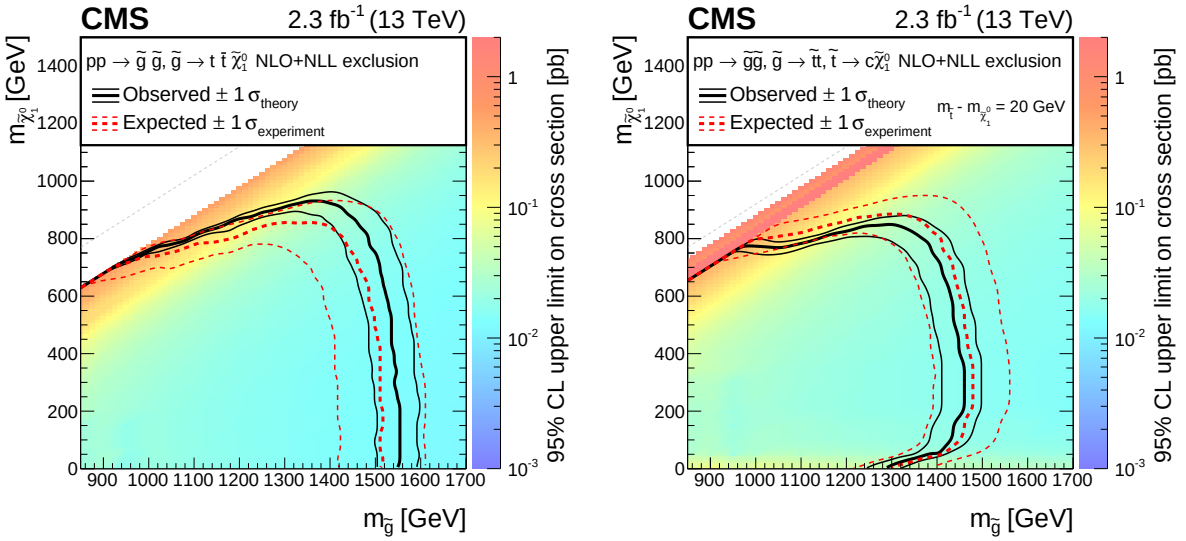

Figure 4.4: Exclusion limits at 95% CL for simplified models of top (s)quarks produced via decays of gluino pairs in the (a) T1tttt and (b) T5ttcc scenarios. The solid black curves represent the observed exclusion contour with respect to NLO+NLL cross section calculations and the accompanying ±1 standard deviation uncertainties. The dashed red curves represent the expected exclusion contour and the ±1 standard deviation uncertainties including experimental uncertainties. Figures from Ref. [105].

constrained MSSM or the CMSSM, which only has 4 parameters, and a sign.

A complementary approach to searches in specific models is to present search results in terms of simplified models [106–111]. These are effective models built with a minimal set of particles necessary to produce SUSY-like final states, with a specific sequence of their production and decay contributing to the channels of interest. They are parametrised directly in terms of sparticle masses. The simplified model approach can quantify the dependence of an experimental limit on the particle spectrum or a certain sequence of particle production and decay more generally than a specific model [109]. Confronting the limits obtained in simplified models with the predictions of a realistic model, one needs to take into account the fact that the sensitivity in a simplified model is in general higher, since the considered decay chain is assumed to occur with 100% branching ratio.

As an example, in Fig. 4.4 (a) and (b) we show exclusion limits at 95% CL for simplified models of top quarks and squarks produced via decays of gluino pairs in the T1tttt and T5ttcc scenarios, presented by CMS for a dataset at 13 TeV com energy and an integrated luminosity of 2.3 fb^{-1}. The T1tttt is a scenario in simplified models of gluino pair production where each gluino decays into a top-antitop pair and a neutralino, whereas in T5ttcc the gluino decays to an on-shell top squark and a top quark, and the top squark decays to a charm and a neutralino [105, 108]. The colour spectrum depicts the 95% CL upper limit on the cross section values in pb. As described in the plot, the observed exclusion contour with respect to NLO+NLL cross section calculations [112] and corresponding ± 1 standard deviation uncertainties are represented by the solid black curves. The dashed red curves indicate the expected exclusion contour for the background-only hypothesis with the ± 1 standard deviation uncertainties. For the T1tttt scenario shown in Fig. 4.4 (a), gluino masses up to 1550 GeV and neutralino masses up to 900 GeV are excluded[1]. In the depicted T5ttcc scenario in Fig. 4.4 (b), gluino masses up to 1450 GeV and neutralino masses up to 820 GeV are excluded.

In a similar vein, Fig. 4.5 shows a summary of ATLAS searches for stop pair production [94]. The dashed and solid lines show the expected and observed limits, respectively, including all uncertainties except the theoretical signal cross section uncertainty (PDF and scale uncertainty). Four decay modes have been considered separately with the assumption of a 100% branching ratio: $\tilde{t} \to W + b + \tilde{\chi}_1^0$ which is a three-body decay for $m_{\tilde{t}} < m_t + m_{\tilde{\chi}_1^0}$, $\tilde{t} \to f + f' + b + \tilde{\chi}_1^0$ which is a four-body decay, $\tilde{t}_1 \to t + \tilde{\chi}_1^0$ and $\tilde{t} \to c + \tilde{\chi}_1^0$. These exclusion plots are an overlay of contours resulting from different stop decay channels which have different sparticle mass hierarchies and simplified decay scenarios, so their interpretation in a realistic model is not straightforward. The full understanding of the implications of these searches requires the interpretation of the experimental results in the context of all kinds of theoretical models. A description of one of the several methods to use simplified model limits to constrain general SUSY models can be found in

[1] A Moriond 2017 update from CMS to the gluino mass limits in the T1tttt scenario with data from 35.9 fb^{-1} of integrated luminosity excludes gluino masses up to a little more than 2 TeV, see Ref. [96].

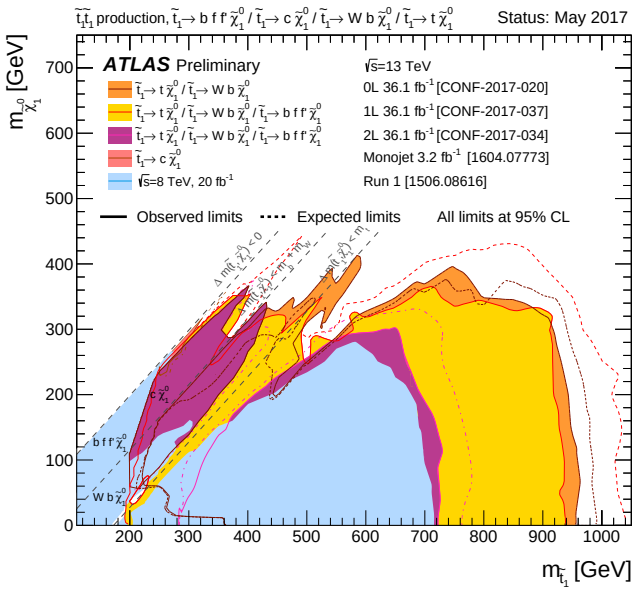

Figure 4.5: Summary of the dedicated ATLAS searches for top squark pair production based on 3.2 to 36.1 fb^{-1} of pp collision data taken at $\sqrt{s} = 13$ TeV. Exclusion limits at 95% CL are shown in the $m_{\tilde{t}_1} - m_{\tilde{\chi}_1^0}$ mass plane. Figure from Ref. [94].

Ref. [113]. There are many publicly available tools that have been developed for recasting results from LHC searches for BSM physics, such as `CheckMATE` [114,115], `RIVET` [116], `XQCAT` [117,118], `ATOM/Fastlim` [119], `SModelS` [120,121], and the more recently released `GAMBIT` [122], among others.

4.2.3 Searches for heavy Higgs bosons

The first run of the LHC in 2011–12 imposed strong constraints on the allowed MSSM parameter space, arising from the discovery of a scalar boson at 125 GeV, with couplings that are compatible with the SM predictions, the non-observation of SUSY particles and the non-observation of additional neutral Higgs bosons in direct searches [123–126]. As discussed in Section 3.2.5, the discovered Higgs can be interpreted as the lightest neutral Higgs h of the MSSM, while interpreting it as the heavier scalar H of the MSSM is under pressure from the data [125, 126]. If we consider the discovered state to be the lightest MSSM Higgs h, the predicted existence of heavier Higgses H, A and $H^{\pm}$ needs to be probed. In this interpretation, M_A must be large so that the theory is in the decoupling limit. In the decoupling limit for $t_\beta \gtrsim 10$, the mass of the lightest scalar is bound at tree level by $m_h < m_Z$ and a SUSY mass scale of $\sim$1 TeV is required in the maximal mixing case to obtain the observed Higgs mass of 125 GeV, whereas, when the value of $|X_t|$ is small, multi-TeV stops are necessary [129]. However, the $\tan\beta$-enhancement of the couplings of the heavy Higgs bosons to bottom quarks and τ-leptons leads to significant

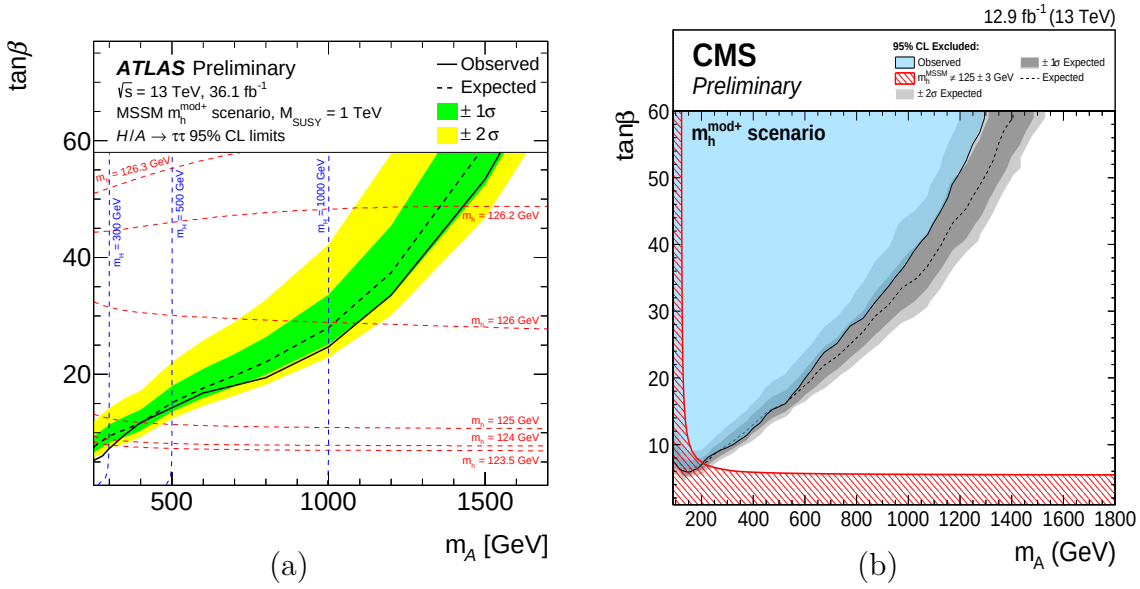

Figure 4.6: (a) The observed (black) and expected (dashed) limits at 95% CL on $\tan\beta$ as a function of M_A are shown in the $m_h^{\text{mod+}}$ scenario of the MSSM, measured by ATLAS in the $H/A \to \tau^+\tau^-$ channel for $\sqrt{s} = 13$ TeV and 36.1 fb^{-1} of integrated luminosity [127]. (b) Exclusion limits combining all channels in the $m_h^{\text{mod+}}$ scenario of the MSSM measured by CMS for $\sqrt{s} = 13$ TeV and 12.9 fb^{-1} of integrated luminosity [128].

constraints on the $(M_A, \tan\beta)$ plane from direct searches by ATLAS and CMS [123–126].

Searches for SUSY Higgs bosons are typically carried out in benchmark scenarios, described for example, in Ref. [130]. Fig. 4.6 shows the exclusion contours in one such benchmark in the MSSM, called the $m_h^{\text{mod+}}$ scenario. In Fig. 4.6 (a) regions in the $(M_A, \tan\beta)$ plane excluded at 95% CL in the $m_h^{\text{mod+}}$ scenario of the MSSM measured by ATLAS for $\sqrt{s} = 13$ TeV and 36.1 fb^{-1} of integrated luminosity are shown. Dashed lines of constant M_h and M_H are shown in red and blue, respectively. The observed (expected) 95% CL upper limits exclude $\tan\beta > 5.3$ (7.5) for $M_A = 0.25$ TeV and $\tan\beta > 54$ (60) for $M_A = 1.5$ TeV. Fig. 4.6 (b) shows the model exclusion limits in the $(M_A, \tan\beta)$ plane combining all channels, for the same scenario in the MSSM, measured by CMS for $\sqrt{s} = 13$ TeV and 12.9 fb^{-1} of integrated luminosity. The red contour indicates the region which does not yield a Higgs boson consistent with a mass of 125 GeV within the theoretical uncertainties of ±3 GeV.

It is pertinent to note that these exclusion limits assume that all parameters in the MSSM are real and $\mathcal{CP}$-symmetry is conserved. Recall from our discussion in Section 3.3 that in the most general case, the MSSM can have 12 physical $\mathcal{CP}$-violating phases. Their inclusion in the predictions of observables such as masses, cross sections, and decay rates leads to significant changes in the phenomenology of the MSSM, and is necessary for the general case of the MSSM with complex parameters to have an accurate compari-

son of theoretical predictions with experimental results. We presented a brief overview of experimental constraints on the phases of the complex parameters of the MSSM in Section 3.3. In Chapter 5, we will describe the Higgs sector of the MSSM with complex parameters beyond the lowest order and show that at higher orders an admixture of all three neutral Higgs bosons, i.e. the two $\mathcal{CP}$-even Higgs bosons h, H and the $\mathcal{CP}$-odd Higgs boson A, is induced. In Chapter 8, we will analyse scenarios where the light Higgs boson describes the SM-like Higgs at $\sim 125\,\text{GeV}$ and the heavy Higgs bosons are strongly admixed. For a proper prediction in such a case, $\mathcal{CP}$-violating interference effects need to be taken into account in the full process involving production and decay of the Higgs bosons, which requires going beyond the usual narrow-width approximation (see also Refs. [131–135]). A convenient way to incorporate interference effects is a generalised narrow-width approximation for the production and decay of on-shell particles as described in Refs. [32, 136, 137], where in Ref. [136] only lowest-order contributions have been considered, while in Refs. [32, 137] also the inclusion of higher-order corrections has been addressed. In Chapter 9, we will review such a formalism and define benchmark scenarios with $\mathcal{CP}$ violation to describe the effect of the interferences on the exclusion limits for Higgs searches at the LHC.

Chapter 5

Higgs mixing at higher orders

In this chapter, we discuss the higher-order corrections that give rise to $\mathcal{CP}$-violating mixings in the Higgs sector of the MSSM with complex parameters. We will set up the notations for the calculation of $\hat{\mathbf{Z}}$ factors which are used throughout the thesis. This review largely follows Refs. [33, 138] and references therein. Similarities to Ref. [1] in parts of this chapter are intended and reflect the contributions of the author.

5.1 Introduction

In Chapter 3, the Higgs sector of the MSSM was reviewed, along with a discussion on the possible complex parameters of the theory which could give rise to interesting phenomenological implications. The Higgs sector of the MSSM is $\mathcal{CP}$-conserving at tree level. Higher-order corrections in the MSSM Higgs sector have a huge impact on its phenomenology, with particles from other sectors contributing significantly to observables such as masses, widths, and cross sections via loop diagrams. In particular, we must account for higher-order corrections in order to study the impact of $\mathcal{CP}$-violating phases. Beyond the lowest order, the Higgs sector receives contributions from loop corrections and all possible mixings with other particles that are $\mathcal{CP}$-violating in the most general case. In the following sections, we present a discussion on $\mathcal{CP}$-violating effective self-energies in the general case of complex parameters, and the treatment of masses of the resultant physical eigenstates. We will then introduce the non-unitary $\hat{\mathbf{Z}}$ matrix which is required for the correct on-shell properties of incoming and outgoing loop-corrected mass eigenstates.

$\mathcal{CP}$-violating mixing between the neutral Higgs bosons $\{h, H, A\}$ arises as a consequence of radiative corrections and results in the neutral mass eigenstates $\{h_1, h_2, h_3\}$. The full mixing at higher orders takes place not just between $\{h, H, A\}$, but also with the Goldstone boson and the electroweak gauge bosons. In general, 6×6 mixing contributions involving the fields $\{h, H, A, G, Z, \gamma\}$ need to be taken into account. However, for the calculation of the Higgs boson masses and wave function normalisation factors at the considered order it is sufficient to restrict ourselves to a 3×3 mixing matrix among $\{h, H, A\}$, since mixing effects with $\{G, Z, \gamma\}$ only appear at the sub-leading two-loop

level and beyond. In processes with external Higgs bosons, on the other hand, mixing contributions with G and Z already enter at the one-loop level, but the numerical effect of these contributions has been found to be very small, see e.g. Refs. [51, 139–141]. In the description and numerical analysis of Higgs production through gluon fusion and bottom-quark annihilation presented in Chapters 6 and 8 respectively, we will therefore neglect these kinds of (electroweak) mixing contributions of the external Higgs bosons with Goldstone and gauge bosons.

Concerning electroweak corrections, we only incorporate the potentially numerically large contributions to the Higgs boson masses and wave function normalisation factors as well as the electroweak contribution to the correction affecting the relation between the bottom-Yukawa coupling and the bottom-quark mass (detailed in Section 6.4.1). All other contributions considered here such as the electroweak corrections to gluon fusion involve at least one power of the strong coupling. For the contribution of the Z boson and the Goldstone boson to the gluon-fusion process via $gg \to \{Z^*, G^*\} \to h_i$ (the photon only enters at higher orders) it should be noted that contributions from mass-degenerate quark weak-isodoublets vanish and only top- and bottom-quark contributions proportional to their masses are of relevance, as can be inferred from the discussion of the Higgsstrahlung process in Refs. [142,143]. This is a consequence of the fact that only the axial component of the quark–quark–Z boson coupling contributes to the loop-induced coupling of the Z boson to two gluons. Similarly, squark contributions in $gg \to \{Z^*, G^*\}$ are completely absent at the one-loop level, even in case of $\mathcal{CP}$ violation in the squark sector. The one-loop contributions to $gg \to \{Z^*, G^*\}$ therefore have no dependence on the phases of complex parameters. Thus, for the remainder of this chapter, we focus our discussion on the contributions to the 3×3 mixing between the lowest-order mass eigenstates $\{h, H, A\}$ giving rise to the loop-corrected $\mathcal{CP}$-admixed mass eigenstates $\{h_1, h_2, h_3\}$.

5.2 Effective self-energies

The 3×3 mass matrix $\mathbf{M}$ contains the tree-level masses m_i^2 on the diagonal and has non-zero (off-)diagonal self-energies involving the Higgs states [144]. It enters the Lagrangian, with $\Phi \in \{h, H, A\}$, as follows

$$\mathcal{L} \supset -\frac{1}{2}\Phi \mathbf{M} \Phi^T , \tag{5.1}$$

with

$$\mathbf{M}(p^2) = \begin{pmatrix} m_h^2 - \hat{\Sigma}_{hh}(p^2) & -\hat{\Sigma}_{hH}(p^2) & -\hat{\Sigma}_{hA}(p^2) \\ -\hat{\Sigma}_{Hh}(p^2) & m_H^2 - \hat{\Sigma}_{HH}(p^2) & -\hat{\Sigma}_{HA}(p^2) \\ -\hat{\Sigma}_{Ah}(p^2) & -\hat{\Sigma}_{AH}(p^2) & m_A^2 - \hat{\Sigma}_{AA}(p^2) \end{pmatrix} . \tag{5.2}$$

When all the parameters are real, the $\mathcal{CP}$-even Higgs bosons h and H do not mix with the $\mathcal{CP}$-odd A and therefore $\hat{\Sigma}_{hA} = \hat{\Sigma}_{HA} = 0$. However, allowing for certain parameters to have $\mathcal{CP}$-violating phases permits all self-energies $\hat{\Sigma}_{ij}(p^2)$ for $i, j \in \{h, H, A\}$ to be in general non-zero. The propagator matrix (up to contributions from Goldstone bosons and gauge bosons that are neglected here, see above) is then given by

$$\mathbf{\Delta}_{hHA}(p^2) = -\left[\hat{\mathbf{\Gamma}}_{hHA}(p^2)\right]^{-1}, \tag{5.3}$$

where the irreducible 2-point vertex functions

$$\hat{\Gamma}_{ij}(p^2) = i\,[(p^2 - m_i^2)\delta_{ij} + \hat{\Sigma}_{ij}(p^2)] \tag{5.4}$$

form the elements of the matrix

$$\hat{\mathbf{\Gamma}}_{hHA}(p^2) = i\,[p^2\mathbf{1} - \mathbf{M}(p^2)]\,. \tag{5.5}$$

Therefore the 3×3 propagator matrix can be written as

$$\begin{aligned}\mathbf{\Delta}_{hHA}(p^2) &= \begin{pmatrix} \Delta_{hh}(p^2) & \Delta_{hH}(p^2) & \Delta_{hA}(p^2) \\ \Delta_{Hh}(p^2) & \Delta_{HH}(p^2) & \Delta_{HA}(p^2) \\ \Delta_{Ah}(p^2) & \Delta_{AH}(p^2) & \Delta_{AA}(p^2) \end{pmatrix} \\ &= i \begin{pmatrix} p^2 - m_h^2 + \hat{\Sigma}_{hh}(p^2) & \hat{\Sigma}_{hH}(p^2) & \hat{\Sigma}_{hA}(p^2) \\ \hat{\Sigma}_{Hh}(p^2) & p^2 - m_H^2 + \hat{\Sigma}_{HH}(p^2) & \hat{\Sigma}_{HA}(p^2) \\ \hat{\Sigma}_{Ah}(p^2) & \hat{\Sigma}_{AH}(p^2) & p^2 - m_A^2 + \hat{\Sigma}_{AA}(p^2) \end{pmatrix}^{-1}. \end{aligned} \tag{5.6}$$

The individual components of $\mathbf{\Delta}_{hHA}$ are the propagators $\Delta_{ij}(p^2)$, which result from the matrix inversion in Eq. (5.3). The diagonal Higgs propagators are therefore given by the following expression:

$$\begin{aligned}\Delta_{ii}(p^2) &= \frac{\hat{\Gamma}_{jj}\hat{\Gamma}_{kk} - \hat{\Gamma}_{jk}^2}{-\hat{\Gamma}_{ii}\hat{\Gamma}_{jj}\hat{\Gamma}_{kk} + \hat{\Gamma}_{ii}\hat{\Gamma}_{jk}^2 - 2\hat{\Gamma}_{ij}\hat{\Gamma}_{jk}\hat{\Gamma}_{ki} + \hat{\Gamma}_{jj}\hat{\Gamma}_{ki}^2 + \hat{\Gamma}_{kk}\hat{\Gamma}_{ij}^2} \\ &= \frac{i}{p^2 - m_i^2 + \hat{\Sigma}_{ii} - i\frac{2\hat{\Gamma}_{ij}\hat{\Gamma}_{jk}\hat{\Gamma}_{ki} - \hat{\Gamma}_{jj}\hat{\Gamma}_{ki}^2 - \hat{\Gamma}_{kk}\hat{\Gamma}_{ij}^2}{\hat{\Gamma}_{jj}\hat{\Gamma}_{kk} - \hat{\Gamma}_{jk}^2}} = \frac{i}{p^2 - m_i^2 + \hat{\Sigma}_{ii}^{\text{eff}}(p^2)}\,. \end{aligned} \tag{5.7}$$

All the 2-point vertex functions depend on p^2 through Eq. (5.4), which we have dropped for ease of notation, and i, j, k are all different with no summation over them. The diagonal propagator obtained in the last line of Eq. (5.7) has the same structure as for the case without any $\mathcal{CP}$-violating mixing, but the self-energy is replaced by the effective

self-energy $\hat{\Sigma}^{\text{eff}}_{ii}(p^2)$,

$$\hat{\Sigma}^{\text{eff}}_{ii}(p^2) = \hat{\Sigma}_{ii}(p^2) - i\frac{2\hat{\Gamma}_{ij}\hat{\Gamma}_{jk}\hat{\Gamma}_{ki} - \hat{\Gamma}_{jj}\hat{\Gamma}^2_{ki} - \hat{\Gamma}_{kk}\hat{\Gamma}^2_{ij}}{\hat{\Gamma}_{jj}\hat{\Gamma}_{kk} - \hat{\Gamma}^2_{jk}}\,, \tag{5.8}$$

which is defined such that it also includes the mixing contributions in the off-diagonal elements. Notice that it separates the diagonal self-energy $\hat{\Sigma}_{ii}$ already existing at 1-loop order from the mixing 2-point functions whose products contribute to $\hat{\Sigma}^{\text{eff}}_{ii}$ only at 2-loop level. When there is no $\mathcal{CP}$-violating mixing, the second term in Eq. (5.8) is zero and we obtain the result for the $\mathcal{CP}$-conserving propagator matrix.

Similarly, for $i \neq j$, the propagator entries are

$$\Delta_{ij}(p^2) = \frac{\hat{\Gamma}_{ij}\hat{\Gamma}_{kk} - \hat{\Gamma}_{jk}\hat{\Gamma}_{ki}}{\hat{\Gamma}_{ii}\hat{\Gamma}_{jj}\hat{\Gamma}_{kk} + 2\hat{\Gamma}_{ij}\hat{\Gamma}_{jk}\hat{\Gamma}_{ki} - \hat{\Gamma}_{ii}\hat{\Gamma}^2_{jk} - \hat{\Gamma}_{jj}\hat{\Gamma}^2_{ki} - \hat{\Gamma}_{kk}\hat{\Gamma}^2_{ij}}\,. \tag{5.9}$$

Using the notation $D_i(p^2) = p^2 - m_i^2$, the ratios of the propagators can be written as,

$$\frac{\Delta_{ij}}{\Delta_{ii}} = -\frac{\hat{\Gamma}_{ij}\hat{\Gamma}_{kk} - \hat{\Gamma}_{jk}\hat{\Gamma}_{ki}}{\hat{\Gamma}_{jj}\hat{\Gamma}_{kk} - \hat{\Gamma}^2_{jk}} = -\frac{\hat{\Sigma}_{ij}(D_k + \hat{\Sigma}_{kk}) - \hat{\Sigma}_{jk}\hat{\Sigma}_{ki}}{(D_j + \hat{\Sigma}_{jj})(D_k + \hat{\Sigma}_{kk}) - \hat{\Sigma}^2_{jk}}\,. \tag{5.10}$$

The above equation can be used to express the effective self-energy alternatively as

$$\hat{\Sigma}^{\text{eff}}_{ii}(p^2) = \hat{\Sigma}_{ii}(p^2) + \frac{\Delta_{ij}(p^2)}{\Delta_{ii}(p^2)}\hat{\Sigma}_{ij}(p^2) + \frac{\Delta_{ik}(p^2)}{\Delta_{ii}(p^2)}\hat{\Sigma}_{ik}(p^2)\,, \tag{5.11}$$

with $i \neq j \neq k$. In Eq. (5.11), we see that the ratio of the off-diagonal and diagonal propagators are weights of the off-diagonal self-energies, and the total effective self-energy appears as a sum of the diagonal and weighted off-diagonal self-energies.

5.3 Higgs masses

Since the renormalised self-energies are complex in general, the propagator poles can lie on the complex momentum plane. The neutral Higgs masses are determined as the complex poles of the propagators,

$$\mathcal{M}^2 = M^2 - iM\Gamma, \tag{5.12}$$

where M are the loop-corrected masses extracted from the real parts of the complex pole, and Γ are the total widths obtained from the imaginary parts of $\mathcal{M}^2$. These complex poles are the roots of the determinant of the matrix $\hat{\mathbf{\Gamma}}_{hHA}(p^2)$,

$$\det\left[\hat{\mathbf{\Gamma}}_{hHA}(p^2)\right] = -\left(\det[\mathbf{\Delta}_{hHA}(p^2)]\right)^{-1} = 0\,. \tag{5.13}$$

It is straightforward to ascertain the masses at tree level when there are no self-energy contributions to the 2-point vertex functions,

$$\hat{\Gamma}_{ij}(p^2) = i(p^2 - m_i^2)\delta_{ij}\,, \tag{5.14}$$

and the matrix $\hat{\mathbf{\Gamma}}$ is diagonal,

$$\hat{\mathbf{\Gamma}}^{(0)}_{hHA}(p^2) = i\begin{pmatrix} D_h(p^2) & 0 & 0 \\ 0 & D_H(p^2) & 0 \\ 0 & 0 & D_A(p^2) \end{pmatrix}. \tag{5.15}$$

In this case, the solutions to Eq. (5.13) are the tree-level masses m_i^2 for the lowest-order mass eigenstates h, H and A. One can now go beyond the lowest order and consider the case where self-energies are restricted to just the diagonal elements, i.e. $\hat{\Sigma}_{ij} = 0$ for $i \neq j$. In this case where no mixing is allowed, we determine the masses from the roots of the determinant of the matrix

$$\hat{\mathbf{\Gamma}}^{(\text{no mixing})}_{hHA}(p^2) = i\begin{pmatrix} D_h(p^2) + \hat{\Sigma}_{hh}(p^2) & 0 & 0 \\ 0 & D_H(p^2) + \hat{\Sigma}_{HH}(p^2) & 0 \\ 0 & 0 & D_A(p^2) + \hat{\Sigma}_{AA}(p^2) \end{pmatrix}. \tag{5.16}$$

The condition

$$\det\left[\hat{\mathbf{\Gamma}}^{(\text{no mixing})}_{hHA}(p^2)\right] = \prod_{i\in\{h,H,A\}} D_i(p^2) + \hat{\Sigma}_{ii}(p^2) = 0 \tag{5.17}$$

is fulfilled for any $p^2 - m_i^2 + \hat{\Sigma}_{ii}(p^2) = 0$, and there is one pole $p^2 = \mathcal{M}_i^2$ for each propagator $\Delta_{ii}(p^2)$, which yields the loop-corrected masses M_i^2 for $i \in \{h, H, A\}$. In the absence of mixing self-energies among the lowest-order mass eigenstates h, H, A, the loop-corrected mass eigenstates h_1, h_2, h_3 maintain their pure $\mathcal{CP}$-even and -odd nature. As a result, there is a clear one-to-one correspondence such that h_1, h_2 and h_3 can be identified as h, H and A respectively.

The case for a $\mathcal{CP}$-conserving 2×2 mixing between h and H is more involved. In this case, the matrix $\hat{\mathbf{\Gamma}}$ is block diagonal,

$$\hat{\mathbf{\Gamma}}^{(2\times2)}_{hHA}(p^2) = \begin{pmatrix} \hat{\mathbf{\Gamma}}_{hH}(p^2) & 0 \\ 0 & \hat{\Gamma}_A(p^2) \end{pmatrix}, \tag{5.18}$$

where $\hat{\mathbf{\Gamma}}_{hH}(p^2)$ is the 2×2 matrix,

$$\hat{\mathbf{\Gamma}}_{hH}(p^2) = i\begin{pmatrix} D_h(p^2) + \hat{\Sigma}_{hh}(p^2) & \hat{\Sigma}_{hH}(p^2) \\ \hat{\Sigma}_{Hh}(p^2) & D_H(p^2) + \hat{\Sigma}_{HH}(p^2) \end{pmatrix}, \tag{5.19}$$

and $\hat{\Gamma}_A(p^2) = i[p^2 - m_A^2 + \hat{\Sigma}_{AA}(p^2)]$. Since A does not participate in the mixing, we can infer right away that the pole $\mathcal{M}_A^2$ fulfils $\mathcal{M}_A^2 - m_A^2 + \hat{\Sigma}_{AA}(\mathcal{M}_A^2) = 0$, and results in the loop-corrected mass M_A for the lowest-order mass eigenstate A.

The other two masses are determined from the poles of the propagators from the 2×2 matrix $\hat{\mathbf{\Gamma}}_{hH}(p^2)$. Its determinant, given by

$$\det\left[\hat{\mathbf{\Gamma}}_{hH}(p^2)\right] = \left[D_h(p^2) + \hat{\Sigma}_{hh}(p^2)\right]\ \left[D_H(p^2) + \hat{\Sigma}_{HH}(p^2)\right] - \hat{\Sigma}_{hH}^2(p^2) \tag{5.20}$$

has two roots. However, unlike the previous cases, we do not have a trivial one-to-one correspondence between the lowest-order mass eigenstates $\{h, H\}$ and the loop-corrected mass eigenstates $\{h_1, h_2\}$. This can be understood by inverting the 2×2 matrix to obtain the individual propagators:

$$\Delta_{ii}(p^2) = \frac{i\left[D_j(p^2) + \hat{\Sigma}_{jj}(p^2)\right]}{\left[D_i(p^2) + \hat{\Sigma}_{ii}(p^2)\right]\left[D_j(p^2) + \hat{\Sigma}_{jj}(p^2)\right] - \hat{\Sigma}_{ij}^2(p^2)} \tag{5.21}$$

$$= \frac{i}{D_i(p^2) + \hat{\Sigma}_{ii}(p^2) - \frac{\hat{\Sigma}_{ij}^2(p^2)}{D_j(p^2)+\hat{\Sigma}_{jj}(p^2)}} \tag{5.22}$$

$$= \frac{i}{p^2 - m_i^2 + \hat{\Sigma}_{ii}^{\text{eff}}(p^2)}\,, \tag{5.23}$$

where the effective self-energy is described as

$$\hat{\Sigma}_{ii}^{\text{eff}}(p^2) = \hat{\Sigma}_{ii}(p^2) - \frac{\hat{\Sigma}_{ij}^2(p^2)}{D_j(p^2) + \hat{\Sigma}_{jj}(p^2)} \tag{5.24}$$

and $i \neq j$ in all of the above. On comparing Eq. (5.20) and Eq. (5.21), we notice that the inverse diagonal propagators are proportional to the determinant of the 2×2 matrix,

$$\frac{1}{\Delta_{ii}(p^2)} = \frac{i}{D_j(p^2) + \hat{\Sigma}_{jj}(p^2)} \det\left[\hat{\mathbf{\Gamma}}_{hH}(p^2)\right]\,. \tag{5.25}$$

The above equation tells us that the two roots of the determinant are poles for *both* Δ_{hh} and Δ_{HH}. If we label the two poles $\mathcal{M}_1$ and $\mathcal{M}_2$, then the equation

$$p^2 - m_i^2 + \hat{\Sigma}_{ii}^{\text{eff}}(p^2) = 0 \tag{5.26}$$

is satisfied by $p^2 = \mathcal{M}_a$, $a \in \{1, 2\}$ for each $i \in \{h, H\}$. As a result, the straightforward correspondence between $\{h, h_1\}$ and $\{H, h_2\}$ no longer holds, since the loop-corrected mass eigenstates $\{h_1, h_2\}$ are admixtures of the lowest-order mass eigenstates $\{h, H\}$. From Eq. (5.26) we deduce the loop-corrected masses M_{h_1} and M_{h_2}. By convention we choose $M_{h_1} \leq M_{h_2}$. However, note that they are still both purely $\mathcal{CP}$-even and it is therefore often convenient for a $\mathcal{CP}$-conserving 2×2 mixing to label h_1 as h, and h_2 as

the heavy state H.

One can now extend these results to the general case of 3×3 mixing in the MSSM where the $\mathcal{CP}$-violating self-energies $\hat{\Sigma}_{hA}$ and $\hat{\Sigma}_{HA}$ participate in the loop-corrections as well. In this case, the loop-corrected mass eigenstates h_a, $a \in \{1,2,3\}$ are admixtures of the lowest-order mass eigenstates h, H and A. The determinant of $\hat{\mathbf{\Gamma}}_{hHA}(p^2)$ now has three roots. Following the same procedure as in the case for 2×2 mixing, the diagonal propagator can be written as

$$\frac{1}{\Delta_{ii}} = \frac{\det\left[\hat{\mathbf{\Gamma}}_{\mathrm{hHA}}(\mathrm{p}^2)\right]}{\left(D_j + \hat{\Sigma}_{jj}\right)\left(D_k + \hat{\Sigma}_{kk}\right) - \hat{\Sigma}_{jk}^2}\,. \tag{5.27}$$

Similarly, the off-diagonal propagator is

$$\frac{1}{\Delta_{ij}} = \frac{\det\left[\hat{\mathbf{\Gamma}}_{\mathrm{hHA}}(\mathrm{p}^2)\right]}{\hat{\Sigma}_{jk}\hat{\Sigma}_{ki} - \hat{\Sigma}_{ij}\left(D_k + \hat{\Sigma}_{kk}\right)}\,. \tag{5.28}$$

Both the inverse diagonal and the off-diagonal propagators are proportional to the determinant of $\hat{\mathbf{\Gamma}}_{hHA}$, analogous to the case for the 2×2 mixing. Consequently, all the three roots of the determinant are poles of each propagator i.e. the three poles $p^2 = \mathcal{M}_a^2$, $a \in \{1,2,3\}$ satisfy the equation

$$\mathcal{M}_a^2 - m_i^2 + \hat{\Sigma}_{ii}^{\mathrm{eff}}(\mathcal{M}_a^2) = 0 \tag{5.29}$$

for any $i \in \{h, H, A\}$. Therefore, there is no one-to-one mapping between the lowest-order and loop-corrected mass eigenstates. Each loop-corrected mass eigenstate h_a is an admixture of *all* three lowest-order mass eigenstates h, H, A. Finally, we obtain the loop-corrected masses M_{h_a} from Eq. (5.29), which are ordered such that $M_{h_1} \leq M_{h_2} \leq M_{h_3}$.

5.4 Wave function normalisation factors for external Higgs bosons

In the Feynman-diagrammatic approach, a physical process that involves external Higgs bosons is defined in terms of the tree-level mass eigenstates $i \in \{h, H, A\}$. However, as we saw in Section 5.3, $\mathcal{CP}$-violating higher-order contributions induce mixings between the tree-level mass eigenstates and they are no longer the physical states. Instead, the physical states are the $\mathcal{CP}$-admixed h_a, $a \in \{1,2,3\}$. In evaluating processes with external Higgs bosons beyond lowest order, an appropriate prescription to account for the mixings is required so that the outgoing particle has the correct on-shell properties, and the S-matrix is properly normalised. This is fulfilled if the fields are renormalised according to the full on-shell conditions, where it is ensured that all the different fields do not mix on

their mass shells at the loop level. The on-shell renormalisation conditions also result in a unit residue for the fields. However, in the Higgs sector of the MSSM we adopt the $\overline{\text{DR}}$ scheme for $\tan\beta$ and field renormalisation [144][1]:

$$\delta \tan\beta^{\overline{\text{DR}}} = \frac{1}{2}(\delta Z_{\mathcal{H}_2}^{\overline{\text{DR}}} - \delta Z_{\mathcal{H}_1}^{\overline{\text{DR}}}) \qquad \text{with} \tag{5.30}$$

$$\delta Z_{\mathcal{H}_1}^{\overline{\text{DR}}} = -\,\text{Re}\left[\Sigma'^{(\text{div})}_{HH}(m_H^2)\right]_{\alpha=0}\,, \tag{5.31}$$

$$\delta Z_{\mathcal{H}_2}^{\overline{\text{DR}}} = -\,\text{Re}\left[\Sigma'^{(\text{div})}_{hh}(m_h^2)\right]_{\alpha=0}\,. \tag{5.32}$$

The field renormalisation constants in this scheme do not ensure that all mixing contributions between the mass eigenstates $\{h_1, h_2, h_3\}$ vanish on-shell and the propagators of the external particles have unit residue. As a result, the correct on-shell properties need to be established via the introduction of finite wave function normalisation factors, denoted as the so-called $\hat{\mathbf{Z}}$ factors [145–147]. The matrix of those $\hat{\mathbf{Z}}$ factors contains the correction factors for the external Higgs bosons $\{h_1, h_2, h_3\}$ relative to the lowest-order mass eigenstates $\{h, H, A\}$. The (non-unitary) matrix elements $\hat{\mathbf{Z}}_{aj}$ [138] (see also Refs. [51, 139]) are composed of the root of the external wave function normalisation factor $\hat{Z}_i^a$, and the on-shell transition ratio $\hat{Z}_{ij}^a$ which are evaluated at the complex pole $\mathcal{M}_a^2$. The wave function normalisation factors for an external Higgs boson $i \in \{h, H, A\}$ are defined as the residue of the propagators at the complex pole $\mathcal{M}_a$ according to the LSZ formalism [148],

$$\hat{Z}_i^a := \text{Res}_{\mathcal{M}_a^2}\{\Delta_{ii}(p^2)\}\,. \tag{5.33}$$

They are obtained by expanding $\hat{\Sigma}_{ii}^{\text{eff}}(p^2)$ around the complex pole $p^2 = \mathcal{M}_a^2$ in the diagonal propagator in Eq. (5.7),

$$\begin{aligned}
\Delta_{ii}(p^2) &= \frac{i}{p^2 - m_i^2 + \hat{\Sigma}_{ii}^{\text{eff}}(p^2)} \\
&= \frac{i}{p^2 - m_i^2 + \hat{\Sigma}_{ii}^{\text{eff}}(\mathcal{M}_a^2) + (p^2 - \mathcal{M}_a^2)\cdot\hat{\Sigma}_{ii}^{\text{eff}\prime}(\mathcal{M}_a^2) + \mathcal{O}((p^2-\mathcal{M}_a^2)^2)} \\
&= \frac{i}{p^2 - \mathcal{M}_a^2}\cdot\frac{1}{1 + \hat{\Sigma}_{ii}^{\text{eff}\prime}(\mathcal{M}_a^2) + \mathcal{O}(p^2 - \mathcal{M}_a^2)}\,,
\end{aligned} \tag{5.34}$$

which gives the following residue at $p^2 \to \mathcal{M}_a^2$,

$$\hat{Z}_a^i = \frac{1}{1 + \hat{\Sigma}_{ii}^{\text{eff}\prime}(\mathcal{M}_a^2)}\,. \tag{5.35}$$

For going from the second to the third line of the equation in Eq. (5.34) we used the pole condition to substitute $\mathcal{M}_a^2 = m_i^2 - \hat{\Sigma}_{ii}^{\text{eff}}(\mathcal{M}_a^2)$. Since the propagator for Higgs boson i on

[1] A summary of renormalisation schemes for the Higgs sector of the MSSM is given in Appendix C.

an external line has three poles $\mathcal{M}_a^2$, $a \in \{1,2,3\}$ there are three choices of $\mathcal{M}_a^2$ at which the residue of $\Delta_{ii}(p^2)$ can be computed for each i. If we evaluate the amputated Green's function at $\mathcal{M}_a^2$, the correct S-matrix normalisation is given by $\sqrt{\hat{Z}_i^a}$, and the outgoing mass eigenstate is h_a. Similarly, if the amputated Green's function is evaluated at $\mathcal{M}_b^2$, the normalisation factor is $\sqrt{\hat{Z}_i^b}$ with h_b as the outgoing particle. Thus, the factor $\sqrt{\hat{Z}_i^a}$ accounts for the normalisation of each external particle $i \in \{h, H, A\}$ at the mass shell $p^2 = \mathcal{M}_a^2, a \in \{1,2,3\}$. Furthermore, the mixing between i and j on an external line at $\mathcal{M}_a^2$ needs to be accounted for as well. For this, the factor $\sqrt{\hat{Z}_i^a}$ needs to be multiplied by the transition ratio $\hat{Z}_{ij}^a$ which occurs in a diagram where h_a is the external particle but i couples to the vertex. It is defined as

$$\hat{Z}_{ij}^a = \left.\frac{\Delta_{ij}(p^2)}{\Delta_{jj}(p^2)}\right|_{p^2=\mathcal{M}_a^2} . \tag{5.36}$$

The indices $\{a, b, c\}$ refer to the loop-corrected mass eigenstates, while $\{i, j, k\}$ label the lowest-order mass eigenstates. As before, there are three possible poles $\{\mathcal{M}_a^2, \mathcal{M}_b^2, \mathcal{M}_c^2\}$ at which $\{\hat{Z}_i, \hat{Z}_{ij}, \hat{Z}_{ik}\}$ can be computed. Similarly, $\{\hat{Z}_j,\ \hat{Z}_{ji},\ \hat{Z}_{jk}\}$ and $\{\hat{Z}_k,\ \hat{Z}_{ki},\ \hat{Z}_{kj}\}$ can also be evaluated at all possible poles $\{\mathcal{M}_a^2, \mathcal{M}_b^2, \mathcal{M}_c^2\}$. Even though all possibilities allowed by the mixing can be used because of the pole structure of each propagator, it is necessary to be consistent and define at which pole to evaluate the factors $\hat{Z}_{ij}^a$ for any given state i. Moreover, a particular choice can be numerically more convenient than another one. Throughout the thesis, we follow the index scheme defined in Ref. [138], unless stated otherwise. Under this scheme $\hat{Z}_i, \hat{Z}_{ij}$ and $\hat{Z}_{ik}$ are evaluated at $\mathcal{M}_a^2$; $\hat{Z}_j, \hat{Z}_{ji}$ and $\hat{Z}_{jk}$ are evaluated at $\mathcal{M}_b^2$; and finally $\hat{Z}_k, \hat{Z}_{ki}$ and $\hat{Z}_{kj}$ are evaluated at $\mathcal{M}_c^2$. Using this scheme we will employ the notation [33, 138]

$$\hat{Z}_a := \hat{Z}_i^a\,, \quad \hat{Z}_{aj} := \hat{Z}_{ij}^a\,, \quad \hat{Z}_{bi} := \hat{Z}_{ji}^b\,, \quad \hat{Z}_{ci} := \hat{Z}_{ki}^c\,. \tag{5.37}$$

The $\hat{\mathbf{Z}}$ factors are therefore written as

$$\hat{\mathbf{Z}}_{aj} = \sqrt{\hat{Z}}_a \hat{Z}_{aj}\,, \tag{5.38}$$

corresponding to the non-unitary matrix

$$\hat{\mathbf{Z}} = \begin{pmatrix} \sqrt{\hat{Z}}_1\hat{Z}_{1h} & \sqrt{\hat{Z}}_1\hat{Z}_{1H} & \sqrt{\hat{Z}}_1\hat{Z}_{1A} \\ \sqrt{\hat{Z}}_2\hat{Z}_{2h} & \sqrt{\hat{Z}}_2\hat{Z}_{2H} & \sqrt{\hat{Z}}_2\hat{Z}_{2A} \\ \sqrt{\hat{Z}}_3\hat{Z}_{3h} & \sqrt{\hat{Z}}_3\hat{Z}_{3H} & \sqrt{\hat{Z}}_3\hat{Z}_{3A} \end{pmatrix} . \tag{5.39}$$

The non-unitarity of the matrix results from the imaginary parts of the self-energies of unstable particles evaluated at a non-vanishing incoming momentum. As a result we do not get a unitary transformation between the lowest-order mass eigenstates $\{h, H, A\}$

and the loop-corrected mass eigenstates $\{h_1, h_2, h_3\}$. As explained above, these $\hat{\mathbf{Z}}$ factors provide the correct normalisation of a matrix element with an external on-shell Higgs boson h_a, $a \in \{1,2,3\}$, at $p^2 = \mathcal{M}_a^2$. Consequently, they satisfy the condition of unit residue and vanishing mixing on-shell [32, 51, 139],

$$\lim_{p^2 \to \mathcal{M}_a^2} -\frac{i}{p^2 - \mathcal{M}_a^2} \left(\hat{\mathbf{Z}} \cdot \hat{\mathbf{\Gamma}}_{hHA} \cdot \hat{\mathbf{Z}}^T\right)_{hh} = 1\,, \tag{5.40}$$

$$\lim_{p^2 \to \mathcal{M}_b^2} -\frac{i}{p^2 - \mathcal{M}_b^2} \left(\hat{\mathbf{Z}} \cdot \hat{\mathbf{\Gamma}}_{hHA} \cdot \hat{\mathbf{Z}}^T\right)_{HH} = 1\,, \tag{5.41}$$

$$\lim_{p^2 \to \mathcal{M}_c^2} -\frac{i}{p^2 - \mathcal{M}_c^2} \left(\hat{\mathbf{Z}} \cdot \hat{\mathbf{\Gamma}}_{hHA} \cdot \hat{\mathbf{Z}}^T\right)_{AA} = 1\,. \tag{5.42}$$

Starting with Eq. (5.40)–Eq. (5.42) and deriving the elements of the $\hat{\mathbf{Z}}$ matrix works equally well. The application of the $\hat{\mathbf{Z}}$ factors yields an expression of the amplitude $\mathcal{A}_{h_a}$ for an external on-shell Higgs boson h_a in terms of a linear combination of the amplitudes resulting from the one-particle irreducible diagrams for each of the lowest-order mass eigenstates $\{h, H, A\}$ according to

$$\mathcal{A}_{h_a} = \hat{\mathbf{Z}}_{ah}\mathcal{A}_h + \hat{\mathbf{Z}}_{aH}\mathcal{A}_H + \hat{\mathbf{Z}}_{aA}\mathcal{A}_A + \ldots = \sqrt{\hat{Z}_a}\left(\hat{Z}_{ah}\mathcal{A}_h + \hat{Z}_{aH}\mathcal{A}_H + \hat{Z}_{aA}\mathcal{A}_A\right) + \ldots\,, \tag{5.43}$$

which can be written more succinctly in matrix form as

$$\begin{pmatrix} \mathcal{A}_{h_1} \\ \mathcal{A}_{h_2} \\ \mathcal{A}_{h_3} \end{pmatrix} = \hat{\mathbf{Z}} \begin{pmatrix} \mathcal{A}_h \\ \mathcal{A}_H \\ \mathcal{A}_A \end{pmatrix} + \cdots\,. \tag{5.44}$$

The ellipsis indicates additional mixing effects with Goldstone bosons and gauge bosons, which we neglect in our numerical analysis, following the discussion in Section 5.1. The sum arises because contributions from each lowest-order mass eigenstate need to be taken into account for each loop-corrected mass eigenstate h_a. Eq. (5.43) is pictorially represented in Fig. 5.1. Thus, we see that the propagator corrections at the external legs

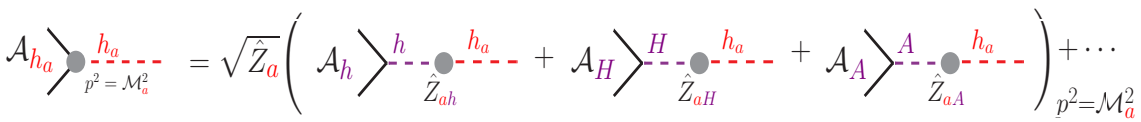

Figure 5.1: A diagrammatic representation depicting the use of $\hat{\mathbf{Z}}$ factors for external Higgs bosons. The amplitude $\mathcal{A}_{h_a}$ is composed of a combination of the individual amplitudes of the tree-level mass eigenstates computed on the mass shell of h_a, along with the transition ratios $\hat{Z}_{aj}$ and the overall normalisation factor $\hat{Z}_a$.

are absorbed into the vertices of the neutral Higgs bosons h_a. The calculation of $\hat{\mathbf{Z}}$ factors for the MSSM Higgs bosons can be performed using the code `FeynHiggs` [64, 67, 144, 149, 150], where these results are obtained for the general case of complex parameters.

In Section 6.3.2, we will detail the application of the $\hat{\mathbf{Z}}$ factors in the analytical calculation of gluon-fusion and bottom-quark annihilation cross sections for the $\mathcal{CP}$-admixed Higgs states h_1, h_2 and h_3, and we will study their numerical impact in Chapter 8. In Chapter 9 we will discuss them in the context of internal propagators and investigate their role in interferences between the Higgs bosons being exchanged in a full process of production and decay.

Chapter 6

Higgs cross sections in the MSSM with complex parameters

In this chapter, we will present the results for the gluon-fusion and bottom-quark annihilation cross sections in the MSSM with complex parameters. The chapter begins with an illustrative procedure for calculating the gluon-fusion process in the Standard Model and subsequently presents the cross section for neutral Higgs production in the MSSM with real parameters. Finally, results for the cross section for gluon fusion and bottom-quark annihilation in the MSSM with complex parameters including higher-order contributions are presented. These results have been published in Ref. [1].

6.1 Motivation

As we have discussed previously, the 125 GeV Higgs signal observed by ATLAS and CMS can easily be accommodated in extended Higgs sectors like a Two-Higgs-Doublet Model (2HDM) or supersymmetric extensions, e.g. the Minimal Supersymmetric Standard Model. Therefore, an essential part of the programme of the LHC experiments in the upcoming years will be the search for additional Higgs bosons predicted by such models. For this purpose, and in order to test possible deviations from the SM expectations for the SM-like Higgs boson, the precise knowledge of production cross sections through gluon fusion and bottom-quark annihilation for these Higgs bosons is a key ingredient. For a detailed summary of current efforts in this direction, the reader is referred to the reports of the LHC Higgs Cross Section Working Group, see Refs. [91, 92, 151, 152].

We saw in Chapter 4 that the searches for additional Higgs bosons have been interpreted in various scenarios beyond the Standard Model, including several supersymmetric ones. However, there have been no analyses so far for the most general case where $\mathcal{CP}$ is violated and leads to mixing between $\mathcal{CP}$-even and -odd eigenstates. This is mainly due to the lack of appropriate theoretical predictions for the Higgs production rates at the LHC for complex parameters in the MSSM and of a practical prescription for taking into account relevant interference effects in Higgs production and decay. A discussion of the latter has recently been given in Ref. [137].

Therefore the primary goal of this thesis has been to provide state-of-the-art cross-section predictions in the MSSM, taking into account $\mathcal{CP}$-violating effects, for the two main Higgs production channels at the LHC, which can be used as input for future experimental analyses in $\mathcal{CP}$-violating Higgs scenarios. We present in this chapter precise predictions for neutral Higgs boson production through gluon fusion and bottom-quark annihilation in the MSSM with complex parameters, in which $\mathcal{CP}$-even and $\mathcal{CP}$-odd Higgs states form three admixed Higgs mass eigenstates $h_a, a \in \{1, 2, 3\}$.

Early investigations of Higgs production through gluon fusion at hadron colliders in the MSSM with complex parameters were carried out in Refs. [153–155]. A thorough analysis taking different production channels into account was presented in Ref. [156], and results for Higgsstrahlung can be found in Ref. [157]. Large effects of stops on the cross section for a $\mathcal{CP}$-odd Higgs boson neglecting $\mathcal{CP}$-even and -odd Higgs mixing were discussed in Ref. [158]. Refs. [159, 160] discuss the production of a light Higgs through gluon fusion including its decay into two photons in the MSSM with complex parameters. It should be noted that the mentioned references were published before the Higgs discovery in 2012 and mostly employ only the lowest order in perturbation theory for the production processes. It is therefore timely to improve these predictions by including up-to-date higher-order corrections and to investigate the compatibility with the experimental results obtained for the observed signal at 125 GeV.

For this purpose, the results presented in this chapter for cross section predictions in the MSSM with complex parameters were implemented into the numerical code `SusHi` (SUperSymmetric HIggs) [161, 162], which calculates Higgs production cross sections through gluon fusion and heavy-quark annihilation [163] in the SM, the MSSM, the Two-Higgs-Doublet-Model (2HDM) and the Next-to-Minimal Supersymmetric Standard Model (NMSSM) [164]. However, until now, `SusHi` did not support complex parameters in the MSSM and thus did not provide predictions for $\mathcal{CP}$-admixed Higgs bosons.

The structure of the chapter is as follows: We start by presenting the calculation for the gluon-fusion cross section for the SM Higgs in Section 6.2. This will be followed by discussing the additional ingredients that modify this cross section for neutral Higgs bosons in the MSSM with real parameters in Section 6.3.1. In Section 6.3.2, we will then present the full leading order cross section for gluon fusion in the MSSM with $\mathcal{CP}$ violation considering the mixing of Higgs bosons (discussed in Chapter 5), the complex Yukawa couplings, and resummation of SUSY QCD corrections. Higher-order corrections to this gluon-fusion cross section are modified and adapted for the complex case from results available for the case of the MSSM with real parameters.

These cross section predictions have been implemented into an extension of `SusHi`, named `SusHiMi` (SUperSymmetric HIggs MIxing) [1]. `SusHiMi` will be released as a part of `SusHi-1.7.0`, the next update of `SusHi`. Higher-order corrections and the scope of their implementation in `SusHiMi` are discussed in detail in Section 6.4. Finally, we discuss the calculation and implementation of bottom-quark annihilation cross sections in the

MSSM with complex parameters, which have been treated with a simple re-weighting procedure.

Program packages for cross section calculations

In the following, a number of particle physics program packages have been employed at various steps of the calculations. We make use of the `Mathematica` package `FeynArts` [165–169] to generate the processes considered here. The package `FormCalc` [170–174] has been used to compute amplitudes and cross sections for the processes. Furthermore, we employ the package `FeynCalc` [175, 176] for the reduction of tensor integrals. To obtain cross sections for the $\mathcal{CP}$-violating MSSM, we made use of the `MSSMCT` model file available within `FeynArts` [169]. For the calculation of the masses and the wave function normalisation factors ensuring the correct on-shell properties of external Higgs bosons, which involves the evaluation of Higgs boson self-energies and their renormalisation (see Chapter 5), we use the code `FeynHiggs` [64, 67, 144, 149, 150]. The numerical evaluation of cross sections is carried out using `SusHi` [161, 162]. The exclusion bounds for heavy Higgs searches in the MSSM with complex parameters are obtained using `HiggsBounds` [177–180].

For the calculations presented in Section 6.2 and Section 6.3 we use `FeynArts-3.9`, `FormCalc-8.4` and `FeynCalc-8.2.0`. In our phenomenological studies in Chapter 8 we use `SusHiMi` within `SusHi-1.7.0` (to be released) and `FeynHiggs-2.11.2`. For the implementation of interference factors and the study of their phenomenological impact in Chapter 9, we use `SusHiMi` along with `FeynHiggs-2.13.0` and `HiggsBounds-5.1.1beta`.

6.2 Gluon-fusion cross section in the SM

Neutral Higgs production at the LHC mainly takes place via five channels, as described in Section 4.2.1, with the main channel being gluon fusion due to high gluon luminosity. In the SM, there is no direct coupling between the Higgs boson and the gluons. The gluon-fusion process is therefore loop mediated, with quarks running in the loops. We know from Section 2.3.2 that the Higgs–quark Yukawa coupling is directly proportional to the quark masses. This means that the biggest contribution to the gluon-fusion cross section comes from third generation quarks coupling to the Higgs. The Higgs boson Yukawa coupling is 35 times larger for the top quark in comparison to the next heaviest fermion, the bottom quark. The top-loop coupling corresponds to an effective Lagrangian that is given by

$$\mathcal{L} = H^0 \; G_{\mu\nu} G^{\mu\nu} \,, \tag{6.1}$$

with the Higgs field H^0 and the QCD field strength tensor $G^{\mu\nu}$. At leading order (LO), the gluon-fusion cross section has been known since a long time [181,182]. In this section, we will present those results for the lowest order calculation in the SM with only the top quark running in the loop, as an illustrative procedure. The derivation and notations used largely follow the detailed review in Ref. [183].

At the lowest order, there are two Feynman diagrams that contribute to the process, shown in Fig. 6.1. The momentum definitions have been labelled in the figure. The kinematic relations are

$$k_1^2 = k_2^2 = 0 \tag{6.2}$$

$$(k_1 + k_2)^2 \equiv q^2 = \hat{s} = m_{H^0}^2 \,. \tag{6.3}$$

The colour of the gluons in the $SU(3)$ adjoint representation is denoted by the indices a, b; the colour of quarks in the fundamental $SU(3)$ representation is denoted by i, j.

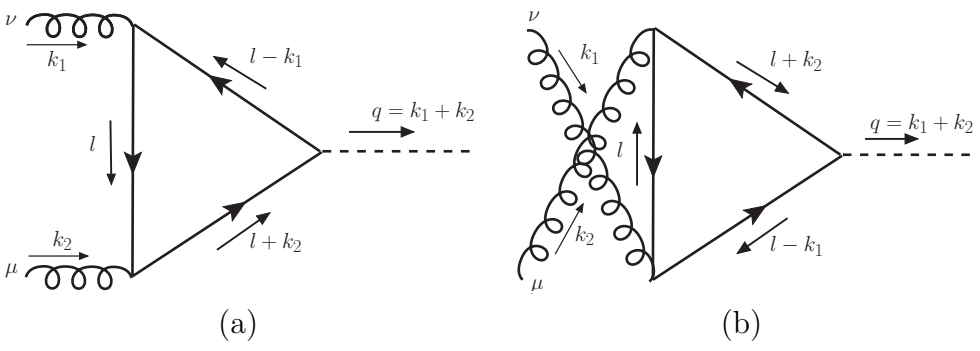

Figure 6.1: The two contributing diagrams along with the notation used for momenta and indices. Charge flow is indicated by arrows on spinor fields and momentum flow is denoted by separate arrows.

Lorentz group indices for gluons are given by μ, ν and spinor indices by α, β. Next, we need the Feynman rules to write down the matrix elements of the diagrams:

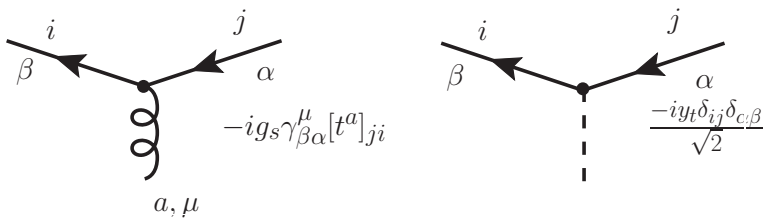

The top quark propagator, neglecting width effects, is therefore given by

$$\frac{i(\not{p}+m)_{\beta\alpha}\delta_{ij}}{p^2-m^2+i\epsilon}\,. \tag{6.4}$$

With the polarisation of external gluons given by $\epsilon_\mu(\lambda, k)$ with spin λ and momentum k, the momentum in the loop l, the mass in the loop m, and the loop integral regularised in $d = 4 - 2\varepsilon$ dimensions, the matrix element for the two diagrams is as follows,

$$\begin{aligned}\mathcal{M} = (-ig_s)^2\left(-i\frac{y_t}{\sqrt{2}}\right) i^3\mathrm{Tr}[t_a t_b](-1)\epsilon_\nu(\lambda_1,k_1)\epsilon_\mu(\lambda_2,k_2)\\ \int\frac{d^dl}{(2\pi)^d}\frac{1}{D_1D_2D_3}\mathrm{Tr}[(\not{l}+\not{k}_2+m)\gamma^\mu(\not{l}+m)\gamma^\nu(\not{l}-\not{k}_1+m)\\ +(-\not{l}+\not{k}_1+m)\gamma^\nu(-\not{l}+m)\gamma^\mu(-\not{l}-\not{k}_2+m)]\,.\end{aligned} \tag{6.5}$$

Here, the propagators in the denominator are

$$\begin{aligned}D_1 &= l^2-m^2\,,\\ D_2 &= (l-k_1)^2-m^2\,,\\ D_3 &= (l+k_2)^2-m^2\,.\end{aligned} \tag{6.6}$$

The trace in Eq. (6.5) can be simplified using `FORM`, and results in [183]

$$\begin{aligned}&\mathrm{Tr}[(\not{l}+\not{k}_2+m)\gamma^\mu(\not{l}+m)\gamma^\nu(\not{l}-\not{k}_1+m)+\\ &\quad(-\not{l}+\not{k}_1+m)\gamma^\nu(-\not{l}+m)\gamma^\mu(-\not{l}-\not{k}_2+m)] =\\ &\quad 8m\,[k_1^\mu k_2^\nu - k_1^\nu k_2^\mu + 2k_2^\mu l^\nu - 2k_1^\nu l^\mu + 4l^\mu l^\nu - g^{\mu\nu}k_1\cdot k_2 - g^{\mu\nu}l\cdot l + g^{\mu\nu}m^2]\,.\end{aligned} \tag{6.7}$$

The principal complexity of the calculation comes from the fact that this expression needs to be integrated over the loop integral l. Inserting Eq. (6.7) in Eq. (6.5) requires

us to calculate the tensor integral[1]

$$C_{\mu\nu} = \int \frac{d^d l}{(2\pi)^d} \, \frac{l_\mu l_\nu}{D_1 D_2 D_3} \,. \tag{6.8}$$

Using the method of Passarino-Veltman reduction of tensor integrals [185, 186] it can be shown that $C_{\mu\nu}$ can be written in terms of the scalar two- and three-point functions B_0 and C_0:

$$C_0 = \int \frac{d^d l}{(2\pi)^d} \, \frac{1}{D_1 D_2 D_3} \,, \tag{6.9}$$

$$B_0(p,q) = \int \frac{d^d l}{(2\pi)^d} \, \frac{1}{D_p D_q} \,, \tag{6.10}$$

with $p, q \in \{1,2,3\}$ and $p \neq q$. Carrying out the Passarino-Veltman reduction of $C_{\mu\nu}$ and expanding the dependence on the dimension d in terms of ε as $1/(d-2) \sim \frac{1}{2}(1+\varepsilon+\varepsilon^2+\cdots)$ the complete integral of the trace is[2]

$$\begin{aligned}
\mathcal{M} = & \int \frac{d^d l}{(2\pi)^d} \, \frac{1}{D_1 D_2 D_3} \, \mathrm{Tr}[(\not{l} + \not{k}_2 + m)\gamma^\mu \cdots (-\not{l} - \not{k}_2 + m)] \\
= & \, (\epsilon_1 \cdot \epsilon_2) \, \left[8m(\varepsilon + \varepsilon^2) B_0(2,3) - 4m C_0 m_{H^0}^2 + 16m^3(1 + \varepsilon + \varepsilon^2) C_0 \right] \\
& + (k_1 \cdot \epsilon_2)(k_2 \cdot \epsilon_1) \left[\frac{16m}{m_{H^0}^2}(-\varepsilon - \varepsilon^2) B_0(2,3) + 8m C_0 + \frac{32m^3}{m_{H^0}^2}(-1 - \varepsilon - \varepsilon^2) C_0 \right] .
\end{aligned} \tag{6.11}$$

Here we have redefined $\mathcal{M}$ by leaving out all the pre-factors before the integral in Eq. (6.5) for ease of expression. We will take them into account again in the end. The above result can then be expressed as

$$\mathcal{M} = (\epsilon_1 \cdot \epsilon_2) \; a + (k_1 \cdot \epsilon_2) \; (k_2 \cdot \epsilon_1) \; b \,, \tag{6.12}$$

with

$$\begin{aligned}
a = & \; 8m \; (\varepsilon + \varepsilon^2) \; B_0(2,3) - 4m \; C_0 m_{H^0}^2 + 16m^3(1 + \varepsilon + \varepsilon^2) \; C_0 \,, \\
b = & \; - \frac{2a}{m_{H^0}^2} \,.
\end{aligned} \tag{6.13}$$

Evaluating the scalar integral B_0 and applying the limit $\varepsilon \to 0$ simplifies the coefficients

[1] A detailed description of the scalar one loop integrals can be found in Ref. [184].

[2] See Ref. [183] for a step-by-step derivation. This reduction was re-derived using `FeynCalc` as a cross check.

to

$$a = \frac{8m}{16\pi^2}\left(1 - \frac{1}{2}m_{H^0}^2(1-\tau)16\pi^2 C_0\right),$$
$$b = -\frac{2a}{m_{H^0}^2}. \tag{6.14}$$

where $\tau = \frac{4m^2}{m_{H^0}^2}$. Finally, the cross section can be written as

$$\hat{\sigma} = \frac{1}{2\hat{s}}\int d\mathrm{PS}\,\overline{\sum}_{\mathrm{spin,colour}}|\mathcal{M}|^2, \tag{6.15}$$

with the $2 \to 1$ phase space

$$\begin{aligned}\int d\mathrm{PS} &= \int \frac{d^4q}{(2\pi)^4}\,(2\pi)\,\delta_+(q^2 - m_{H^0}^2)\,(2\pi)^4\delta^4(k_1 + k_2 - q)\\ &= 2\pi\delta(\hat{s} - m_{H^0}^2).\end{aligned} \tag{6.16}$$

Averaging over colour gives a factor of $(\frac{1}{8})^2$ and averaging over initial state spin gives a factor of $(\frac{1}{2})^2$. Furthermore, we use $m \equiv m_t$, $(g_s^2)^2 = 16\pi^2\alpha_s^2$ and $\frac{y_t^2}{(\sqrt{2})^2} = \frac{m_t^2}{v^2} = \sqrt{2}G_F m_t^2$, where G_F is Fermi's constant. The square of trace of the colour factor ($\mathrm{Tr}[t_a t_b] = \frac{1}{2}\delta_{ab}$) contributes a factor 2. Therefore the total cross section, using Eq. (6.12) and Eq. (6.14), is

$$\begin{aligned}\hat{\sigma} &= \frac{\alpha_s^2(\mu_R)\pi^3\sqrt{2}G_F}{8m_{H^0}^2}\,\frac{m_t^2}{m_{H^0}^2}\sum_{\mathrm{spins}}|\mathcal{M}|^2\; m_{H^0}^2\;\delta(\hat{s} - m_{H^0}^2)\\ &= \frac{\alpha_s^2(\mu_R)G_F}{128\sqrt{2}\pi}\tau^2\left|1 - \frac{1}{2}m_{H^0}^2(1-\tau)16\pi^2 C_0\right|^2\; m_{H^0}^2\;\delta(\hat{s} - m_{H^0}^2),\end{aligned} \tag{6.17}$$

where μ_R is the renormalisation scale, which at LO only enters through the scale dependence of the strong coupling constant α_s. In the last line, we used the fact that summing the squared matrix element over the gluon polarisation gives us a factor of $2|a|^2$. C_0 is the scalar three-point function given by [185]:

$$C_0 = \frac{i}{16\pi^2\hat{s}}\begin{cases}\frac{1}{2}\left[\ln\left(\frac{1+\beta}{1-\beta}\right) - i\pi\right]^2 & \beta = \sqrt{1-\tau}, \quad \tau < 1\\ -2\arcsin^2\left(\frac{1}{\sqrt{\tau}}\right), & \tau > 1.\end{cases} \tag{6.18}$$

Therefore, the complete result of the lowest order partonic cross section is expressed as [182]:

$$
\begin{aligned}
\hat{\sigma} \equiv \sigma_{\mathrm{LO}} &= \frac{\sigma_0^{H^0}}{m_{H^0}^2}\,\delta(\hat{s}-m_{H^0}^2),\\
\sigma_0^{H^0} &= \frac{G_F\alpha_s^2(\mu_R)}{288\sqrt{2}\pi}\,\left|\mathcal{A}^{H^0}\right|^2,\\
\mathcal{A}^{H^0} &= \frac{3}{2}\tau[1+(1-\tau)f(\tau)],\\
f(\tau) &= \begin{cases} \arcsin^2\frac{1}{\sqrt{\tau}}, & \tau \geq 1\\ -\frac{1}{4}\left(\log\frac{1+\sqrt{1-\tau}}{1-\sqrt{1-\tau}}-i\pi\right)^2, & \tau<1\,. \end{cases}
\end{aligned}
\tag{6.19}
$$

With increasing mass, the width of the Higgs boson of the SM becomes broader as it approaches W^+W^-, ZZ thresholds. In the lowest order approximation, it is possible to incorporate this effect by replacing the zero-width δ-distribution with the Breit-Wigner function and changing the kinematic factors $m_{H^0}^2 \to \hat{s}$ appropriately [182]:

$$
\delta(\hat{s}-m_{H^0}^2) \to \frac{1}{\pi}\frac{\hat{s}\Gamma_h/m_{H^0}}{(\hat{s}-m_{H^0}^2)^2+(\hat{s}\Gamma_{H^0}/m_{H^0})^2}\,. \tag{6.20}
$$

So far we have discussed the calculation of the partonic cross section. However, gluons are a part of the colliding protons and therefore a convolution with the parton distribution functions (PDFs) needs to be performed in order to obtain the hadronic cross section. This also induces a dependence on the factorisation scale μ_F. If we denote the gluon luminosity as

$$
\mathcal{L}^{gg}(\tau) = \int_\tau^1 \frac{dx}{x} g(x)g(\tau/x)\,, \tag{6.21}
$$

the lowest-order proton–proton cross section in the narrow-width approximation is

$$
\sigma_{\mathrm{LO}}(pp\to H^0) = \sigma_0\tau_{H^0}\mathcal{L}^{gg}(\tau_{H^0}) \tag{6.22}
$$

where $\tau_{H^0} = m_{H^0}^2/s$ and s is the hadronic centre of mass energy.

6.3 Gluon-fusion cross section in the MSSM

In this section we discuss the calculation of the gluon-fusion cross section in the MSSM with particular emphasis on the effects of complex parameters. In Section 6.3.1, we will review the lowest order gluon-fusion cross section for the case of the MSSM with real parameters, where no $\mathcal{CP}$ violation is allowed. A detailed discussion of this process can be found in Ref. [182] and references therein. Our notation closely follows Ref. [161] and Ref. [1]. In Section 6.3.2 we will present the results for the leading order cross section in the $\mathcal{CP}$-violating case of the MSSM.

6.3.1 Cross section in the MSSM with real parameters

We saw in Section 4.2.1 that the main mechanisms for production of neutral Higgs bosons in the MSSM are the same as those in the SM, with gluon fusion being the dominant one as before. Since the leading order process for gluon fusion starts at one-loop level, it is a production mechanism where new physics can play a significant role in changing the production cross section by entering the loop and couplings with the Higgs. In the MSSM, in addition to the quark induced contributions, the squark induced contributions to the gluon-fusion process also participate, even though they are suppressed by inverse powers of the supersymmetric particle masses if those masses are heavy. However, these contributions become significant and even comparable to quark contributions when the squarks have sub-TeV masses as predicted in several benchmark scenarios for the MSSM [130], as well as many supergravity-inspired models, see for instance Ref. [187]. While these benchmark scenarios with light squarks in the MSSM are in tension with current exclusion limits from squark searches, there exist parameter regions where they haven't been completely ruled out.

In the calculation for the gluon-fusion cross section in the MSSM, differences from the expression for the SM cross section arise not just from the squark loops, but also from the weights of the top- and bottom-loop contributions which have to be modified by the relative couplings to the MSSM Higgs bosons presented in Table 3.3, since the mixing angles of the Higgs sector can alter the hierarchy of the couplings. For example, the coupling of the bottom quarks to the Higgs states is strongly enhanced for large $\tan\beta$ compared with the coupling to the heavier top quark[3].

When $\mathcal{CP}$ is conserved, the physical Higgs states are the $\mathcal{CP}$-eigenstates h, H and A. There are no $\mathcal{CP}$-violating mixings between the three neutral Higgses, and at tree level only the $\mathcal{CP}$-even eigenstates mix[4], which is controlled by the mixing angle α.

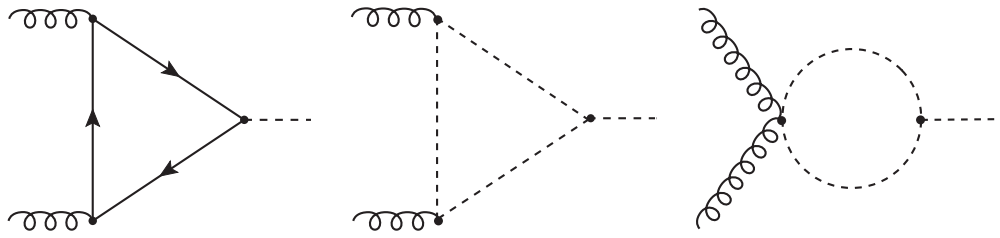

Figure 6.2: Lowest order diagrams for gluon-fusion Higgs production in the MSSM with real parameters.

[3]Note that this is not true for h in the decoupling region.

[4]Going beyond tree level, higher-order contributions can induce additional $\mathcal{CP}$-conserving mixings between the Higgs states, as was described in Section 5.3.

The LO diagrams for the process $gg \to \phi$ with $\phi \in \{h, H, A\}$ are depicted in Fig. 6.2[5]. In this section, we will present only the lowest order results for the gluon-fusion cross section in the MSSM with real parameters. The leading contributions arise from the third generation quarks and squarks: i.e. the top, bottom, stop and sbottom loops. We defer the discussion of higher-order corrections to Section 6.4.

The procedure for calculating the amplitudes for stop- and sbottom-induced loops is similar to what was outlined in Section 6.2. The matrix elements can be obtained by using the Feynman rules for the squark–gluon and squark–Higgs vertex for the $\mathcal{CP}$-even and $\mathcal{CP}$-odd Higgses, which can be found, for e.g., in Ref. [188].

The tensor structures of the loop amplitudes for the $\mathcal{CP}$-even Higgses $\phi^e \in \{h, H\}$ are given by [153]:

$$i\epsilon_\mu(k_1)\epsilon_\nu(k_2)\mathcal{M}_{ab}^{\mu\nu}(gg \to \phi^e) \propto \delta_{ab}\epsilon_\mu(k_1)\epsilon_\nu(k_2)\left(g^{\mu\nu}k_1\cdot k_2 - k_1^\nu k_2^\mu\right)\times \left\{\sum_{q\in\{t,b\}} g_q^{\phi^e}\tau_q^{\phi^e}\left[1+(1-\tau_q^{\phi^e})f(\tau_q^{\phi^e})\right] - \frac{1}{4}\sum_{q\in\{t,b\}}\tau_q^{\phi^e}\sum_{i=1}^{2} g_{\tilde{q}ii}^{\phi^e}\left[1-\tau_{\tilde{q}_i}^{\phi^e}f(\tau_{\tilde{q}_i}^{\phi^e})\right]\right\}. \tag{6.23}$$

The tensor structure for the $\mathcal{CP}$-odd Higgs boson A is

$$i\epsilon_\mu(k_1)\epsilon_\nu(k_2)\mathcal{M}_{ab}^{\mu\nu}(gg \to A) \propto \delta_{ab}\epsilon_\mu(k_1)\epsilon_\nu(k_2)\times \left\{i\epsilon^{\mu\nu\rho\sigma}k_{1\rho}k_{2\sigma}\sum_{q\in\{t,b\}} g_q^A\left[\tau_q^A f(\tau_q^A)\right]\right\}. \tag{6.24}$$

The definitions for momentum, colour and, spin follow the same conventions as in Section 6.2. Here $\tau_q^\phi = \frac{4m_q^2}{m_\phi^2}$ and $\tau_{\tilde{q}_i}^{\phi^e} = \frac{4m_{\tilde{q}_i}^2}{m_{\phi^e}^2}$. The g_q^ϕ are the relative Higgs–quark couplings as specified in Table 3.3 for $\phi \in \{h, H, A\}$. The Higgs–squark couplings $g_{\tilde{q}ij}^{\phi^e}$ for this case can be obtained from Appendix A by setting all the parameters to be real. Needless to say, the SM results are recovered by setting the Higgs–squark couplings to zero, and the relative Higgs–quark couplings g_q^ϕ to 1. Notice that there is no contribution from squarks in the amplitude for the $\mathcal{CP}$-odd Higgs boson A. This is because in the $\mathcal{CP}$-conserving MSSM, the squarks do not couple to the $\mathcal{CP}$-odd Higgs A at LO due to $\mathcal{CP}$ invariance; only couplings involving $\tilde{f}_i - \tilde{f}_j - A$ with $i \neq j$ are non-vanishing, which do not enter the LO calculation. Averaging over all the polarisations and colours, the LO partonic cross section in Eq. (6.19) for $\phi \in \{h, H, A\}$ can be written in the form

$$\sigma_0^\phi = \frac{G_F\alpha_s^2(\mu_R)}{288\sqrt{2}\pi}\left|\mathcal{A}^\phi\right|^2, \tag{6.25}$$

[5]Here we denote the $\mathcal{CP}$-eigenstates by ϕ, in a convention that differs from our notation for the tree-level mass eigenstates i in Chapter 5, in order to avoid confusion with the squark index $\tilde{q}_{ii}$.

where the loop amplitude is the sum of the individual quark and squark contributions:

$$\mathcal{A}^{\phi} = \sum_{q\in\{t,b\}} \left(a_q^{\phi} + \tilde{a}_q^{\phi}\right) . \tag{6.26}$$

The quark contributions to the amplitude for the $\mathcal{CP}$-even Higgses are the same as for the SM Higgs boson, barring the Higgs–quark couplings that contain the mixing angles for the $\mathcal{CP}$-even Higgs bosons. On the other hand, the amplitude for the $\mathcal{CP}$-odd Higgs has a much simpler form factor:

$$a_q^{\phi^e} = g_q^{\phi^e} \frac{3\tau_q^{\phi^e}}{2} \left[1 + (1-\tau_q^{\phi^e}) f(\tau_q^{\phi^e})\right] , \tag{6.27}$$

$$a_q^{A} = g_q^{A} \frac{3\tau_q^{A}}{2} f(\tau_q^{A}) . \tag{6.28}$$

Similarly, the individual squark contributions are

$$\tilde{a}_q^{\phi^e} = -\frac{3\tau_q^{\phi^e}}{8} \sum_{i=1}^{2} g_{\tilde{q}ii}^{\phi^e} \left[1 - \tau_{\tilde{q}_i}^{\phi^e} f(\tau_{\tilde{q}_i}^{\phi^e})\right] , \tag{6.29}$$

$$\tilde{a}_q^{A} = 0 . \tag{6.30}$$

6.3.2 Cross section in the MSSM with complex parameters

For the case of the MSSM with complex parameters we need to compute cross sections for the three neutral mass eigenstates h_1, h_2 and h_3, which are admixtures of the lowest-order mass eigenstates h, H and A. The leading order diagrams for the production of $h_{1,2,3}$ via gluon fusion therefore additionally include the loop-induced $\mathcal{CP}$-violating mixings as depicted in Fig. 6.3. Differences with respect to the calculation in the MSSM with real parameters are induced due to the following reasons:

1. $\mathcal{CP}$-violating couplings between the $\mathcal{CP}$-odd Higgs A and the squarks $g_{\tilde{f}ii}^{A}$ give rise to a non-zero amplitude: $\tilde{a}_q^{A} \neq 0$ in Eq. (6.30).

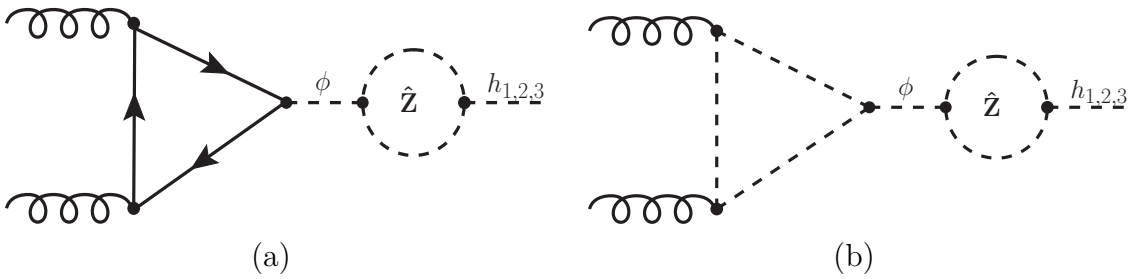

(a) (b)

Figure 6.3: Feynman diagrams for the LO cross section with (a) quark and (b) squark contributions in the MSSM with complex parameters.

2. Different left- and right-handed quark couplings, $g^{\phi}_{q_L}$ and $g^{\phi}_{q_R} = (g^{\phi}_{b_L})^*$ with $\phi \in \{h, H, A\}$ result in non-zero contributions to the quark loop amplitudes for the three neutral Higgses proportional to $(g^{\phi}_{q_L} - g^{\phi}_{q_R})$. In the $b/\bar{b}$ sector, we take into account higher-order corrections to the relation between the bottom-quark mass and the bottom-Yukawa coupling [189–194]. These corrections, known as the Δ_b corrections, are a function of the complex gluino and Higgsino mass parameters M_3 and μ. Therefore, we cannot use the relation $g^{\phi}_{b_R} = (g^{\phi}_{b_L})^* = g^{\phi}_b$ for the bottom-quark coupling to the Higgs as we did for the cross section calculation in the SM and the MSSM with real parameters. A detailed description of these SUSY QCD contributions will be given in Section 6.4.1.

3. $\hat{\mathbf{Z}}$ factors, which determine the $\mathcal{CP}$-violating mixings between the $\mathcal{CP}$-eigenstates, relate the amplitude for an external on-shell Higgs h_a in the mass eigenstate basis to the amplitudes of the $\mathcal{CP}$-even lowest-order states h and H and the $\mathcal{CP}$-odd state A (recall the discussion in Section 5.4). The cross section $pp \to h_a$, which involves one-loop diagrams in the production process $pp \to \phi$, is denoted as "LO cross section" despite the fact that it contains higher-order effects through the application of the $\hat{\mathbf{Z}}$ factors (Fig. 6.3).

In order to clearly see how $\mathcal{CP}$ violation affects the cross section due to these three factors, we will investigate each effect one at a time and subsequently build up the final cross section.

6.3.2.1 Effect of non-zero couplings $g^A_{\tilde{f}ii}$

When we allow $\mathcal{CP}$ invariance to be violated, a non-zero $g^A_{\tilde{f}ii}$ coupling gives rise to an additional term in the loop amplitude. A first analysis of this effect was presented in Ref. [153]. Assuming, at this point, that there is no mixing between the neutral $\mathcal{CP}$-eigenstates, and neglecting SUSY QCD corrections at the vertex, the tensor structure of the loop amplitude in Eq. (6.24) is modified by an additional term,

$$i\epsilon_\mu(k_1)\epsilon_\nu(k_2)\mathcal{M}^{\mu\nu}_{ab}(gg \to A) \propto \delta_{ab}\epsilon_\mu(k_1)\epsilon_\nu(k_2)\times$$
$$\left\{ i\epsilon^{\mu\nu\rho\sigma}k_{1\rho}k_{2\sigma}\sum_{q\in\{t,b\}} g^A_q\left[\tau^A_q f(\tau^A_q)\right] - \frac{1}{4}\sum_{q\in\{t,b\}}\tau^A_q\left(g^{\mu\nu}k_1\cdot k_2 - k_1^\nu k_2^\mu\right)\sum_{i=1}^{2} g^A_{\tilde{q}ii}\left[1 - \tau^A_{\tilde{q}i}f(\tau^A_{\tilde{q}i})\right]\right\}. \tag{6.31}$$

Notice that the tensor structure of the squark contributions to the amplitude of the $\mathcal{CP}$-odd Higgs is similar to that of the squark contributions to the $\mathcal{CP}$-even Higgs. Furthermore, there is an antisymmetric part containing the Levi-Civita tensor ϵ associated to the quark contributions and a symmetric part associated to the squark contributions. As a result, there are no interference terms between the quark and squark loop contributions for the $\mathcal{CP}$-odd Higgs production. As we will see in the next sections, this

will no longer be true when we take into account SUSY QCD corrections that make the bottom-Yukawa coupling complex or when an admixture with $\mathcal{CP}$-even states is induced. The squark loop amplitude for $\tilde{q}$, averaging over all spins and colours, is

$$\tilde{a}_q^A = -\frac{3}{8}\tau_q^A \sum_{i=1}^{2} g_{\tilde{q}ii}^A \left[1 - \tau_{\tilde{q}i}^A f(\tau_{\tilde{q}i}^A)\right] . \tag{6.32}$$

The amplitudes of the $\mathcal{CP}$-even Higgses at this stage have the same expression as given in Eq. (6.27) and Eq. (6.29).

6.3.2.2 Effect of complex Yukawa couplings

In the following, we will present the expressions for the quark-loop amplitudes of h, H and A for a general case of complex Yukawa couplings, without limiting ourselves to just the complex bottom-Yukawa couplings resulting from Δ_b corrections[6]. As mentioned earlier, when the Yukawa couplings are complex, the relation $g_{q_L}^{\phi} = g_{q_R}^{\phi} = g_q^{\phi}$ we have used in the expressions for the amplitudes so far is invalid, and there are additional contributions that modify the quark loop amplitude which need to be considered. For the $\mathcal{CP}$-even Higgses $\phi^e \in \{h, H\}$, the quark loop amplitudes now consist of two parts, written as

$$a_{q,+}^{\phi^e} = \frac{1}{2}\left(g_{q_L}^{\phi^e} + g_{q_R}^{\phi^e}\right)\frac{3}{2}\tau_q^{\phi^e}\left[1 + (1 - \tau_q^{\phi^e}) f(\tau_q^{\phi^e})\right] , \tag{6.33}$$

$$a_{q,-}^{\phi^e} = \frac{i}{2}\left(g_{q_R}^{\phi^e} - g_{q_L}^{\phi^e}\right)\frac{3}{2}\tau_q^{\phi^e} f(\tau_q^{\phi^e}) , \tag{6.34}$$

where the subscripts $+$ and $-$ denote amplitude components proportional to the sum and difference of the left- and right-handed couplings respectively. Similarly, the quark loop amplitudes for the $\mathcal{CP}$-odd Higgs also contain an additional contribution:

$$a_{q,+}^{A} = \frac{1}{2}\left(g_{q_L}^{A} + g_{q_R}^{A}\right)\frac{3}{2}\tau_q^{A} f(\tau_q^{A}) , \tag{6.35}$$

$$a_{q,-}^{A} = \frac{i}{2}\left(g_{q_L}^{A} - g_{q_R}^{A}\right)\frac{3}{2}\tau_q^{A}\left[1 + (1 - \tau_q^{h_a}) f(\tau_q^{A})\right] . \tag{6.36}$$

Terms in $a_{q,+}^{\phi}$ do not interfere with terms in $a_{q,-}^{\phi}$, due to the fact that they are associated with symmetric and antisymmetric terms, respectively, in the tensor structure of the loop amplitude for the scalars ϕ^e, and vice versa in case of the $\mathcal{CP}$-odd Higgs A. Furthermore, it is easy to see that in the limit where all the Yukawa couplings are real we retrieve the results obtained in Section 6.3.1 and Section 6.3.2.1.

[6] In Section 6.4.1 we will point towards a possibility of redefining (s)quark fields such that their phase is rotated away. However, here we will stick with the most general description of complex Yukawa couplings.

6.3.2.3 Effect of the $\hat{\mathbf{Z}}$ factor matrix

So far we have studied how the individual amplitudes for the lowest-order mass eigenstates h, H and A are affected by $\mathcal{CP}$-violating interactions and contributions. The next step is to obtain the amplitudes for the mass eigenstates h_a, $a = 1, 2, 3$ as admixtures of h, H and A using the non-unitary $\hat{\mathbf{Z}}$ matrix. Recall that the full mixing takes place not just between the tree-level Higgs mass eigenstates but also with the Goldstone boson and the electroweak gauge bosons. However, following the discussion in Section 5.1, we only consider the 3×3 mixing between $\{h, H, A\}$. The LO hadronic production cross section of the mass eigenstates h_a can be written as

$$\sigma_{\text{LO}}(pp \to h_a) = \sigma_0^{h_a} \tau_{h_a} \mathcal{L}^{gg}(\tau_{h_a}) \quad \text{with} \quad \mathcal{L}^{gg}(\tau) = \int_\tau^1 \frac{dx}{x} g(x) g(\tau/x)\,, \tag{6.37}$$

where $\tau_{h_a} = M_{h_a}^2/s$, and M_{h_a} is the loop-corrected mass of the eigenstate h_a. Accordingly, the partonic LO cross section for $gg \to h_a$ is given by

$$\begin{aligned} \sigma_0^{h_a} &= \frac{G_F \alpha_s^2(\mu_R)}{288\sqrt{\pi}} \left[\left| \mathcal{A}^{h_a,\text{e}} \right|^2 + \left| \mathcal{A}^{h_a,\text{o}} \right|^2 \right] \\ &\text{with} \quad \mathcal{A}^{h_a,\text{e}} = \hat{\mathbf{Z}}_{ah} \mathcal{A}_+^h + \hat{\mathbf{Z}}_{aH} \mathcal{A}_+^H + \hat{\mathbf{Z}}_{aA} \mathcal{A}_-^A \\ &\text{and} \quad \mathcal{A}^{h_a,\text{o}} = \hat{\mathbf{Z}}_{ah} \mathcal{A}_-^h + \hat{\mathbf{Z}}_{aH} \mathcal{A}_-^H + \hat{\mathbf{Z}}_{aA} \mathcal{A}_+^A\,, \end{aligned} \tag{6.38}$$

where $\hat{\mathbf{Z}}_{a\phi}$ are the elements of the $\hat{\mathbf{Z}}$ matrix from Eq. (5.39). We see from Eq. (6.38) that the final polarisation and colour averaged squared loop amplitude for a mass eigenstate h_a consists of two non-interfering terms. This is a consequence of the different tensor structures of various contributions, as we have illustrated in previous sections. In the effective field theory approach of heavy quark and SUSY masses, where the gluon–gluon–Higgs interaction is condensed into a single vertex, the amplitudes of the first term in Eq. (6.38) can be identified with a contribution that stems from $\mathcal{L} \supset G^{\mu\nu} G_{\mu\nu} \phi$ with the gluon field strength $G^{\mu\nu}$. The amplitudes of the second term stem from $\mathcal{L} \supset \tilde{G}^{\mu\nu} G_{\mu\nu} \phi$, which involves the dual of the gluon field strength tensor $\tilde{G}^{\mu\nu}$. This results in the cross section being expressible as the sum of two non-interfering squared amplitudes. This also explains the naming of the first and the second term with $\mathcal{A}^{h_a,\text{e}}$ and $\mathcal{A}^{h_a,\text{o}}$, respectively: the terms in $\mathcal{A}^{h_a,\text{e}}$ possess a tensor structure similar to the quark and squark contributions to the $\mathcal{CP}$-even amplitude in Eq. (6.23), while the terms in $\mathcal{A}^{h_a,\text{o}}$ possess a tensor structure similar to the quark contributions to the $\mathcal{CP}$-odd amplitude in Eq. (6.24). Similarly, we can split σ_{LO} into $\sigma_{\text{LO}}^{\text{e}}$ and $\sigma_{\text{LO}}^{\text{o}}$. Each of $\mathcal{A}^{h_a,\text{e}}$ and $\mathcal{A}^{h_a,\text{o}}$ is comprised of the individual quark and squark loop contributions to amplitudes of h, H and A, now evaluated on the mass shell of h_a. For the two $\mathcal{CP}$-even lowest-order mass eigenstates $\phi^e \in \{h, H\}$ we

obtain the amplitudes

$$\mathcal{A}_{+}^{\phi^e} = \sum_{q\in\{t,b\}} \left(a_{q,+}^{\phi^e} + \tilde{a}_q^{\phi^e}\right), \quad \mathcal{A}_{-}^{\phi^e} = \sum_{q\in\{t,b\}} a_{q,-}^{\phi^e} \tag{6.39}$$

with

$$\begin{aligned} a_{q,+}^{\phi^e} &= \frac{1}{2}\left(g_{q_L}^{\phi^e} + g_{q_R}^{\phi^e}\right)\frac{3}{2}\tau_q^{h_a}\left[1 + (1-\tau_q^{h_a})f(\tau_q^{h_a})\right], \quad a_{q,-}^{\phi^e} = \frac{i}{2}\left(g_{q_R}^{\phi^e} - g_{q_L}^{\phi^e}\right)\frac{3}{2}\tau_q^{h_a} f(\tau_q^{h_a}), \\ \tilde{a}_q^{\phi^e} &= -\frac{3}{8}\tau_q^{h_a}\sum_{i=1}^{2} g_{\tilde{q}ii}^{\phi^e}\left[1 - \tau_{\tilde{q}i}^{h_a} f(\tau_{\tilde{q}i}^{h_a})\right]. \end{aligned} \tag{6.40}$$

Similarly, for the $\mathcal{CP}$-odd Higgs boson A we have

$$\mathcal{A}_{-}^{A} = \sum_{q\in\{t,b\}} \left(a_{q,-}^{A} + \tilde{a}_q^{A}\right), \quad \mathcal{A}_{+}^{A} = \sum_{q\in\{t,b\}} a_{q,+}^{A} \tag{6.41}$$

with

$$\begin{aligned} a_{q,+}^{A} &= \frac{1}{2}\left(g_{q_L}^{A} + g_{q_R}^{A}\right)\frac{3}{2}\tau_q^{h_a} f(\tau_q^{h_a}), \quad a_{q,-}^{A} = \frac{i}{2}\left(g_{q_L}^{A} - g_{q_R}^{A}\right)\frac{3}{2}\tau_q^{h_a}\left[1 + (1-\tau_q^{h_a})f(\tau_q^{h_a})\right], \\ \tilde{a}_q^{A} &= -\frac{3}{8}\tau_q^{A}\sum_{i=1}^{2} g_{\tilde{q}ii}^{A}\left[1 - \tau_{\tilde{q}_i}^{h_a} f(\tau_{\tilde{q}_i}^{h_a})\right]. \end{aligned} \tag{6.42}$$

We checked that this result is consistent with Ref. [153], which however assumes $g_{q_L}^{\phi} = g_{q_R}^{\phi}$ and does not take into account the mixing among the tree-level mass eigenstates $\phi \in \{h, H, A\}$. All squark contributions, i.e. $\tilde{a}_q^{\phi^e}$ and $\tilde{a}_q^{A}$, enter the first term, $\mathcal{A}^{h_a,\mathrm{e}}$, in Eq. (6.38). Quark contributions to $\mathcal{A}^{h_a,\mathrm{e}}$ which couple to the $\mathcal{CP}$-odd lowest-order mass eigenstate A are proportional to the difference between the left- and right-handed quark couplings. The same holds for the quark contributions to the second term $\mathcal{A}^{h_a,\mathrm{o}}$ in Eq. (6.38) which couple to the $\mathcal{CP}$-even lowest-order mass eigenstates ϕ^e. All these terms are therefore denoted with the subscript $\mathcal{A}_{-}$. It should be noted that the quark contributions in $\mathcal{A}_{-}^{\phi_e,A}$ only arise due to the complex nature of the Yukawa couplings, which is a consequence of the incorporation of higher-order contributions entering via the Δ_b corrections, and our choice of working with a complex Yukawa coupling. Consequently, they vanish in the MSSM with real parameters.

The expressions in Eq. (6.38)–Eq. (6.42) contain the central result of this chapter. This analytical form of the leading order gluon-fusion cross section for the loop-corrected mass eigenstates h_1, h_2 and h_3 of the MSSM, taking into account complex Yukawa couplings, $\mathcal{CP}$-violating Higgs–squark couplings, and a 3×3 mixing for the general case of complex parameters has been presented for the first time in our publication Ref. [1].

6.4 Higher-order contributions

6.4.1 Resummation of SUSY QCD contributions

At tree level in the MSSM, there is no $\bar{b}_L h_u^0 b_R$ coupling, only the neutral component of the Higgs doublet $\mathcal{H}_1$, h_d^0 couples to the bottom quark. However, a coupling of the form $\bar{b}_L h_u^0 b_R$ can be induced by corrections from gluino–squark loops, such as the one shown in Fig. 6.4.

The leading parts of such SUSY QCD corrections arising from gluino–squark loops, as well as leading electroweak corrections, can be absorbed into the effective bottom-Yukawa coupling to the Higgs bosons [189–194]. For a heavy SUSY mass scale, the leading corrections are obtained from an effective Lagrangian

$$\mathcal{L}_{\text{eff}} = -y_b \bar{b}_R \left[h_d^0 + \frac{\Delta_b}{t_\beta} h_u^{0*} \right] b_L + h.c. \tag{6.43}$$

This loop induced correction shifts the b-quark mass from its tree-level value and is described by

$$m_b \to y_b v_d \, (1 + \Delta_b) \, . \tag{6.44}$$

It also results in a shift of the bottom-Yukawa couplings from the tree level relations. Following the treatment in Ref. [32], and inserting the expression for the bottom-Yukawa coupling from Eq. (6.44) into Eq. (6.43) for the general case of a complex Δ_b results in

$$\begin{aligned} \mathcal{L}_{\text{eff}} = & -\frac{1}{1+\Delta_b} \frac{m_b}{v_d} \bar{b}_R \left[h_d^0 + \frac{\Delta_b}{t_\beta} h_u^{0*} \right] b_L + h.c. \\ = & \frac{1 - ix}{1+y} \frac{m_b}{v_d} \bar{b}_R \left[h_d^0 + \frac{\Delta_b}{t_\beta} h_u^{0*} \right] b_L + h.c. \end{aligned} \tag{6.45}$$

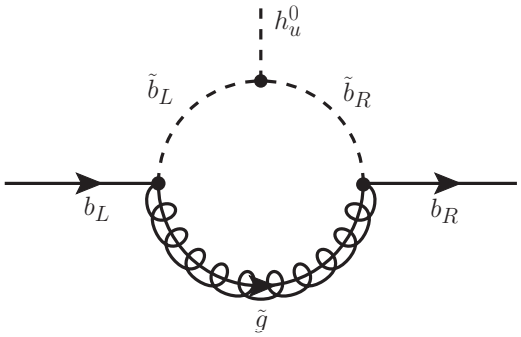

Figure 6.4: Feynman diagram that induces an effective coupling of the bottom quarks to the Higgs field component h_u^0.

where the quantities x and y are defined as

$$x = \frac{\mathrm{Im}\Delta_b}{1+\mathrm{Re}\Delta_b}\,, \tag{6.46}$$

$$y = \mathrm{Re}\Delta_b + x\mathrm{Im}\Delta_b\,. \tag{6.47}$$

Neglecting terms involving Goldstone bosons, the effective Lagrangian reads [51]

$$\begin{aligned}\mathcal{L}_{\text{eff}} = \bar{b}\frac{1}{1+y}\Bigg(&\left[1-\frac{1}{t_\alpha t_\beta}y + i\gamma_5 x\left(1+\frac{1}{t_\alpha t_\beta}\right)\right] v^{\text{tree}}_{hb\bar{b}} h \\ &+\left[1+\frac{t_\alpha}{t_\beta}y + i\gamma_5 x\left(1-\frac{t_\alpha}{t_\beta}\right)\right] v^{\text{tree}}_{Hb\bar{b}} H \\ &+\left[1-\frac{1}{t_\beta^2}y + i\gamma_5 x\left(1+\frac{1}{t_\beta^2}\right)\right] v^{\text{tree}}_{Ab\bar{b}} A\Bigg) b + \cdots\,,\end{aligned} \tag{6.48}$$

where $t_\alpha \equiv \tan\alpha$.

Finally, $v^{\text{tree}}_{hb\bar{b}}, v^{\text{tree}}_{Hb\bar{b}}, v^{\text{tree}}_{Ab\bar{b}}$ are given by

$$\begin{aligned}\mathcal{L}^{\text{tree}} &= \bar{b}\left[v^{\text{tree}}_{hb\bar{b}} h + v^{\text{tree}}_{Hb\bar{b}} H + v^{\text{tree}}_{Ab\bar{b}} A\right] b + \cdots \\ &= \bar{b}\left[-\frac{y^0_b}{\sqrt{2}}(-s_\alpha)h - \frac{y^0_b}{\sqrt{2}}(c_\alpha)H - \frac{y^0_b}{\sqrt{2}}(i\gamma_5)(-s_\beta)A\right] b + \cdots\,,\end{aligned} \tag{6.49}$$

with

$$\frac{y^0_b}{\sqrt{2}} = \frac{m_b}{v_d} = \frac{m_b}{v c_\beta} = \frac{m_b e}{(2 c_\beta s_W m_W)}\,, \tag{6.50}$$

where we have used $v = \frac{2m_W}{g_2}$ and $g_2 = \frac{e}{s_W}$ from Eq. (2.3), Eq. (2.13) and Eq. (2.15). Substituting the expressions from Eq. (6.46), Eq. (6.47) and Eq. (6.49) into Eq. (6.48) we obtain the following expression for the effective Lagrangian,

$$\mathcal{L}_{\text{eff}} = \frac{m_b}{v}\sum_{\phi^e\in\{h,H\}} \bar{b}\left[g^{\phi^e}_{b_L} P_L + (g^{\phi^e}_{b_L})^* P_R\right] b\phi^e + i\frac{m_b}{v}\bar{b}\left[g^A_{b_L} P_L - (g^A_{b_L})^* P_R\right] bA \tag{6.51}$$

in terms of the left-handed and right-handed couplings $g^\phi_{b_L}$ and $g^\phi_{b_R} = (g^\phi_{b_L})^*$, where $P_{L/R} = \frac{1}{2}(1 \mp \gamma_5)$ are the left- and right-handed projection operators, respectively. The explicit form of the couplings can then be deduced to be

$$g^h_{b_L} = \frac{f^h_{\alpha\beta}}{1+\Delta_b}\left[1-\frac{\cot\alpha}{\tan\beta}\Delta_b\right],\; g^H_{b_L} = \frac{f^H_{\alpha\beta}}{1+\Delta_b}\left[1+\frac{\tan\alpha}{\tan\beta}\Delta_b\right],\; g^A_{b_L} = \frac{f^A_{\alpha\beta}}{1+\Delta_b}\left[1-\frac{\Delta_b}{\tan^2\beta}\right], \tag{6.52}$$

with $f^h_{\alpha\beta} = \sin\alpha/\cos\beta$, $f^H_{\alpha\beta} = \cos\alpha/\cos\beta$ and $f^A_{\alpha\beta} = \tan\beta$ (see also Refs. [51, 195]).

The effective Lagrangian therefore provides a resummation of leading $\tan\beta$-enhanced contributions entering via the quantity Δ_b. The leading QCD contribution to Δ_b has the form

$$\Delta_b = \frac{2}{3}\frac{\alpha_s(\mu_d)}{\pi} M_3^* \mu^* \tan\beta \, I(m^2_{\tilde{b}_1}, m^2_{\tilde{b}_2}, m^2_{\tilde{g}}) \,, \tag{6.53}$$

$$I(a,b,c) = -\frac{ab\mathrm{Log}\left(\frac{b}{a}\right) + ac\mathrm{Log}\left(\frac{a}{c}\right) + bc\mathrm{Log}\left(\frac{c}{b}\right)}{(a-c)(c-b)(b-a)} \tag{6.54}$$

where α_s is typically evaluated at an averaged SUSY scale $\mu_d = (m_{\tilde{b}_1} + m_{\tilde{b}_2} + m_{\tilde{g}})/3$. As one can see from Eq. (6.53), the leading contribution to Δ_b has an explicit dependence on the complex parameters M_3 and μ. In the numerical analysis in this thesis the value for Δ_b is obtained from `FeynHiggs` (see Ref. [196]), which includes additional QCD and electroweak contributions [197–200].

We will use the expression for the bottom-quark Yukawa coupling according to the effective Lagrangian of Eq. (6.51) and Eq. (6.52) in our leading-order expressions for the (loop-induced) gluon-fusion process. For bottom-quark annihilation and the implementation of higher-order corrections to the gluon-fusion process, we will use as a simplified version [51]

$$g_b^\phi \equiv g_{b_L}^\phi = g_{b_R}^\phi = \frac{1}{|1+\Delta_b|} f_{\alpha\beta}^\phi \,, \tag{6.55}$$

in which the left- and right-handed couplings to bottom quarks are identical to each other. We will compare the numerical impact of the two implementations at LO in Chapter 8. The effective Yukawa coupling in Eq. (6.51) is complex. The phase of this coupling could be rotated away by an appropriate redefinition of the (s)quark fields, as described e.g. in Ref. [197]. This redefinition could be used to avoid having to explicitly differentiate between $g_{b_L}^\phi$ and $g_{b_R}^\phi$. Still, we prefer to use the most general expression for a complex Yukawa coupling. In the phenomenological discussion in Chapter 8 we compare the effect of the complex Yukawa coupling of Eq. (6.51) with the simplified real coupling of Eq. (6.55) (which are not equivalent to each other) and subsequently show that the numerical differences are small.

6.4.2 Gluon fusion at higher orders

Gluon fusion receives sizeable corrections at higher orders. Higher-order corrections have been calculated for the production of the SM Higgs boson, as well for the Higgs bosons of the MSSM with real parameters, in various orders of perturbation theory and expansions. In the following, we provide a brief overview of status of higher-order calculations for the gluon-fusion process involving both the SM, and SUSY particles for the case of real parameters. In the next sections, we will discuss to what degree they have been

implemented in SusHi. Subsequently, we will explain how they can be modified and incorporated into the cross sections for Higgs production in the MSSM with complex parameters, as well the scope of their implementation in SusHiMi.

The total effect of the next-to-leading order (NLO) real and virtual corrections for the SM quark contributions is the increase of the LO cross section by a factor of 1.5–1.7, with a residual dependence on renormalisation and factorisation scales of about 30%. These NLO QCD contributions have been known for arbitrary quark masses since the late 1990s and early 2000s [182, 201–205]. Their sizeable effect motivated the calculation of next-to-next-to-leading order (NNLO) SM QCD contributions which were calculated in the limit of a heavy top-quark mass [206–208]. The NNLO QCD corrections are smaller than the NLO ones, but are still significant and improve the stability against renormalisation and factorisation scale dependence. Finite top-quark mass effects at NNLO are known in an expansion of inverse powers of the top-quark mass [209–216].

More recently, N^{3}LO contributions for a $\mathcal{CP}$-even Higgs boson in an expansion around the threshold of Higgs production [217–221] were published, also in the heavy quark mass limit[7]. We will later discuss in more detail for which Higgs mass ranges these corrections are applicable, which also explains why the above mentioned N^{3}LO contributions will only be employed for the $\mathcal{CP}$-even component of the light Higgs boson.

Higher-order corrections to the gluon-fusion process are not just limited to QCD effects. Electroweak (EW) NLO corrections have been accounted for as well. In Refs. [224, 225] they were calculated in the infinite top mass limit, and the corrections to the gluon-fusion cross section were found to be less than 1%. However, contributions from diagrams with a closed loop of light fermions were more sizeable. These contributions have been evaluated in a closed analytic form in terms of generalised harmonic polylogarithms (GHPLs) in Refs. [226, 227]. In the intermediate Higgs mass range between 114 GeV up to the threshold of $2m_W$ these corrections can lead to an increase from the LO cross section by 4–9%. For masses of the Higgs boson above the $2m_W$ threshold, the light fermion corrections change sign and decrease the LO cross section by up to 2%. In Ref. [228], the remaining EW corrections from top quark contributions were evaluated in a Taylor expansion in $m^2_{H^0}/(4m_W)^2$, with a valid result in the $m_{H^0} < 2m_W$ range. However these corrections were found to be very small in size, reaching at most 15% of the light fermion contributions. Electroweak corrections as discussed in Ref. [226] can be added as well.

For the production of $\mathcal{CP}$-even MSSM Higgs bosons h and H, the QCD effects from the quarks can be adapted from the SM calculation by using the rescaled Yukawa couplings shown in Table 3.3. NNLO QCD corrections to the quark induced cross section for the $\mathcal{CP}$-odd Higgs boson A were calculated in Refs. [229, 230] in addition to Ref. [214]. In the MSSM with real parameters, NLO corrections from real radiation arising from Higgs production in association with a quark or gluon jet at one loop, mediated by

[7] Most recently the N^{3}LO QCD corrections for $\mathcal{CP}$-odd Higgs bosons have also become available [222, 223]. In the analysis presented in this thesis, those contributions are neglected.

quarks and squarks, can be expressed in terms of Passarino-Veltman functions [186], as presented in Ref. [231]. The analytical NLO virtual contributions involving squarks, quarks and gluinos are either known in the limit of a vanishing Higgs mass [232–235] or in an expansion of heavy SUSY masses [236–238][8]. Even NNLO corrections of stop-induced contributions to gluon fusion are known [242–244]. We neglect the latter contributions in our analysis for the MSSM with complex parameters.

6.4.2.1 NLO contributions

In this section, we will describe the numerically relevant NLO corrections to the LO cross section. A brief discussion of electroweak contributions will follow.

As explained in Section 6.4.1, a complex Yukawa coupling is only induced for the bottom quark through the incorporation of Δ_b contributions. According to this approach, for the top-quark Yukawa coupling g_t^ϕ, left- and right-handed components are identical also in the MSSM with complex parameters. Therefore we can directly take over the known higher-order QCD corrections to the top-quark loop contribution for the MSSM with complex parameters. For the incorporation of the bottom-quark contribution at NLO (SM) QCD, on the other hand, we will rely on the simplified version of the Δ_b corrections to the bottom-Yukawa coupling as specified in Eq. (6.55). This approximation ensures that the higher-order quark contributions, both real and virtual, are of the same structure as in the $\mathcal{CP}$-conserving MSSM.

The hadronic cross section for $h_a, a \in \{1,2,3\}$ at NLO can be written as

$$\sigma^{\mathrm{e/o}}_{\mathrm{NLO}}(pp \to h_a + X) = \sigma_0^{h_a,\mathrm{e/o}} \tau_{h_a} \mathcal{L}^{gg}(\tau_{h_a}) \left[1 + C^{\mathrm{e/o}} \frac{\alpha_s}{\pi}\right] + \Delta\sigma^{\mathrm{e/o}}_{gg} + \Delta\sigma^{\mathrm{e/o}}_{gq} + \Delta\sigma^{\mathrm{e/o}}_{q\bar{q}} \,. \tag{6.56}$$

At NLO in the MSSM with complex parameters, supersymmetric contributions are present both in virtual and real corrections. The terms $\Delta\sigma$ denote the real corrections. They arise from the hard gg, gq and $g\bar{q}$ scattering and are regular as $\hat{s} \to M_{h_a}$ in the partonic cross section. They are one-loop processes where the Higgs boson is produced with a gluon or quark jet. In the MSSM, the loop can be mediated by quarks as well as squarks. Example processes are depicted in Fig. 6.5.

The real corrections show a similar behaviour as observed for the LO cross section. Working with Eq. (6.55) implies that the left- and right-handed Yukawa couplings are equal and terms in the cross section proportional to their difference are absent. Therefore in the real corrections the only new ingredients arising due to complex parameters are Higgs–squark couplings to the $\mathcal{CP}$-odd, $g^A_{\tilde{q}ii}$. These squark induced contributions of $\mathcal{CP}$-odd components proportional to $g^A_{\tilde{q}ii}$ are added as a complex component to the $\mathcal{CP}$-even couplings. Consequently, the real corrections can be split in $\Delta\sigma^{\mathrm{e}}$ and $\Delta\sigma^{\mathrm{o}}$ since no

[8] Exact numerical and for certain contributions analytical results for NLO virtual contributions were presented in Refs. [204, 205, 239–241].

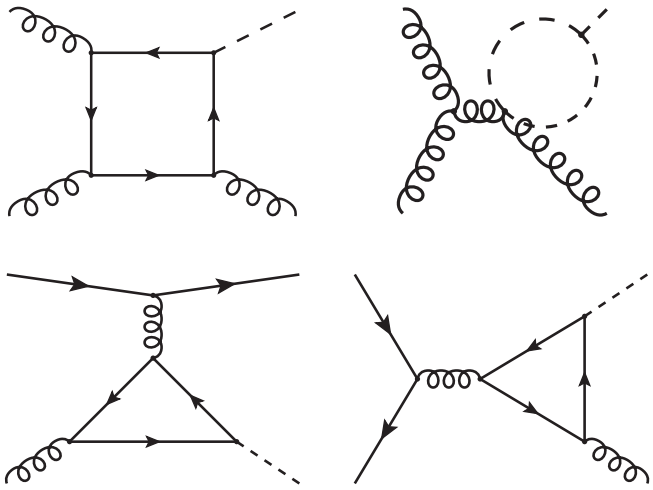

Figure 6.5: Sample Feynman diagrams contributing to real corrections at NLO in gluon-fusion Higgs production. The loops containing quarks can also be mediated by squarks.

interference terms arise. In `SusHiMi`, the real corrections have been taken over from the implementation in `SusHi` which uses the full analytical expressions presented in Ref. [231].

The factors $C^{e/o}$ in Eq. (6.56) contain the NLO virtual corrections to the gg process, regularised by the infrared singular part. They also contain counterterms to the LO quantities. For the quark induced contributions `SusHi` incorporates the full analytical formulas of Ref. [203]. These results are directly taken over for the complex case in `SusHiMi`. The NLO virtual contributions from supersymmetric particles can arise from diagrams containing gluon–squark or gluino–quark–squark loops. In order to preserve supersymmetry, the purely squark induced terms need to be evaluated in combination with the mixed gluino–quark-squark terms. Some example diagrams for the NLO virtual contributions are shown in Fig. 6.6.

In `SusHi`, these contributions are implemented for the case of real parameters in two limits [161]. The expansions in those limits hold if the Higgs mass is not much larger in comparison to the SUSY masses. For very large Higgs masses, only the numerical result of Ref. [239] is known so far.

1. The first limit is $m_\phi, m_q \ll m_{\tilde{q}_{1,2}}, m_{\tilde{g}}$ [231, 236–238], which can be applied to the bottom–sbottom sector and the top–stop sector, and is valid when $m_\phi < \min(2m_{\tilde{q}}, m_{\tilde{q}} + m_{\tilde{g}})$. `SusHi` uses the formulas of Refs. [237, 238] in these cases.

2. The limit $m_\phi \ll m_q, m_{\tilde{q}_{1,2}}, m_{\tilde{g}}$ [232, 233, 235] is valid for $m_\phi < \min(2m_q, 2m_{\tilde{q}}, m_{\tilde{q}} + m_q + m_{\tilde{g}})$ and is applied to the top–stop sector as long as ϕ is not too heavy. These corrections are incorporated in `SusHi` using the subroutine `evalcsusy.f` [245].

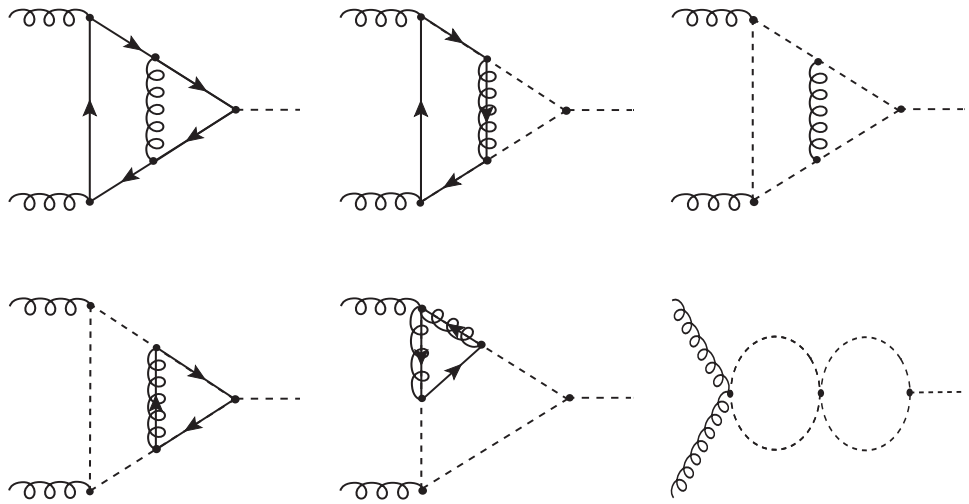

Figure 6.6: Example Feynman diagrams for virtual corrections at NLO in gluon-fusion Higgs production. Apart from quarks and gluons, squarks and gluinos can also participate in the loops.

The approach using the second limit in `evalcsusy.f` uses the tree-level coupling α explicitly in the amplitudes, and therefore is not compatible with the implementation of $\hat{\mathbf{Z}}$ factors used for the amplitudes according to Eq. (5.43) in `SusHiMi`. Consequently, we will use the first approach in our computation of NLO virtual contributions to h_1, h_2, h_3 production and its implementation in `SusHiMi`.

However, the NLO virtual contributions from supersymmetric particles as described above are not easily adjustable to the MSSM with complex parameters. We therefore interpolate the NLO virtual contributions between phases 0 and π of the various MSSM parameters using a cosine interpolation [246, 247]. This interpolation makes use of on-shell stop- and sbottom-quark masses defined at phases 0 and π. Thus, within the interpolated result we have to ensure the correct subtraction of the NLO contributions that have already been taken into account through Δ_b effects in the bottom-quark Yukawa coupling. This is done by expanding the Δ_b correction to next-to-leading order in the subtraction term.

For a certain value of the phase ϕ_z of a complex parameter z, the virtual NLO amplitude $\mathcal{A}^{\phi}_{\text{NLO}}(\phi_z)$ can be approximated using

$$\mathcal{A}^{\phi}_{\text{NLO}}(\phi_z) = \frac{1+\cos\phi_z}{2}\mathcal{A}^{\phi}_{\text{NLO}}(0) + \frac{1-\cos\phi_z}{2}\mathcal{A}^{\phi}_{\text{NLO}}(\pi) \tag{6.57}$$

for each of the lowest-order mass eigenstates $\phi \in \{h, H, A\}$. Here $\mathcal{A}^{\phi}_{\text{NLO}}(0)$ is the analytical result for the MSSM with real parameters, and $\mathcal{A}^{\phi}_{\text{NLO}}(\pi)$ is the analytical result with $z \to -z$. Using the factors $\cos\phi_z$ ensures a smooth interpolation such that the known results for a vanishing phase are recovered. Whereas a dependence on the phases of A_q

and μ is already apparent in the lowest-order diagrams of $gg \to \phi$, the phase of M_3 only enters through the NLO virtual corrections. Besides the Δ_b contributions, where the full phase dependence is incorporated, the treatment of the phase of M_3 therefore relies on the performed interpolation. While the implemented routines for the MSSM with real parameters are expressed in terms of the gluino mass, they can also be used for a negative soft-breaking parameter M_3, such that we can obtain interpolated results for a complex-valued parameter M_3. We note that the NLO virtual amplitudes with a negative M_3 are identical to the virtual amplitudes for positive M_3 with opposite signs of the parameters A_t, A_b and μ. This can be understood from the structure of the NLO diagrams involving the squark–quark–gluino couplings. It should however be noted in this context that due to the generation of Higgs–squark couplings $g^A_{\tilde{q}ii}$ for non-vanishing phases, a new class of NLO virtual diagrams arises which is not present in the MSSM with real parameters. Since the interpolation is based on the result for the MSSM with real parameters as input for the predictions at the phases 0 and π, the additional set of diagrams may not be adequately approximated in this way and therefore remain unaccounted for.

Despite this fact, we expect that the interpolation of the virtual two-loop contributions involving squarks and gluinos to the gluon-fusion amplitude provides a reasonable approximation, for the following reasons (we discuss the theoretical uncertainty associated with the interpolation in Section 8.6 and assign a conservative estimate of the uncertainty in our numerical analysis). We focus here on the gluon-fusion amplitude without $\hat{\mathbf{Z}}$ factors, since in the $\hat{\mathbf{Z}}$ factors the full phase dependence is incorporated without approximations. Gluino contributions are generally suppressed for gluino masses that are sufficiently heavy to be in accordance with the present bounds from LHC searches, while gluon-exchange contributions do not add an additional phase dependence compared to the dependence on the phases of A_q and μ in the LO cross section, which is fully taken into account. The dependence of the NLO amplitude on the phases of A_q and μ is therefore expected to follow a similar pattern as the LO amplitude, which is also what we find in the application of the interpolation method.

One can also compare the higher-order corrections to the gluon-fusion process with the ones to the Higgs boson masses and $\hat{\mathbf{Z}}$ factors. In fact, a similar interpolation was applied in the prediction for Higgs boson masses in the MSSM with complex parameters, see e.g. Refs. [144, 247–249], where the phase dependence of sub-leading two-loop contributions beyond $\mathcal{O}(\alpha_t\alpha_s)$ were approximated with an interpolation before the full phase dependence of the corresponding two-loop corrections at $\mathcal{O}(\alpha_t^2)$ was calculated [250, 251]. Generally good agreement was found between the full result and the approximation [250, 251]. In order to investigate the interpolation of the phase of M_3 we performed a similar check concerning the phase dependence of two-loop squark and gluino loop contributions. We numerically compared the full result for the Higgs mass prediction at this order from `FeynHiggs` with an approximation where the phases at the two-loop level are interpolated. Despite the fact that for the Higgs mass calculation new diagrams proportional

to $g^A_{\tilde{q}ii}$ arise away from phases 0 and π as well, the phase dependence of the interpolated results generically follows the behaviour of the full results very well.

Based on the NLO amplitude that has been obtained as described above, we can construct the NLO cross sections $\sigma^{\mathrm{e}}_{\mathrm{NLO}}$ and $\sigma^{\mathrm{o}}_{\mathrm{NLO}}$ individually, following Ref. [161], by defining the NLO correction factors C^{e} and C^{o}:

$$C^{\mathrm{e/o}} = 2\mathrm{Re}\left[\frac{\mathcal{A}^{h_a,\mathrm{e/o}}_{\mathrm{NLO}}}{\mathcal{A}^{h_a,\mathrm{e/o}}}\right] + \pi^2 + \beta_0 \log\left(\frac{\mu^2_{\mathrm{R}}}{\mu^2_{\mathrm{F}}}\right) . \tag{6.58}$$

The amplitudes are given by $\mathcal{A}^{h_a,\mathrm{e}}_{\mathrm{NLO}} = \hat{\mathbf{Z}}_{ah}\mathcal{A}^{h}_{\mathrm{NLO}} + \hat{\mathbf{Z}}_{aH}\mathcal{A}^{H}_{\mathrm{NLO}}$ and $\mathcal{A}^{h_a,\mathrm{o}}_{\mathrm{NLO}} = \hat{\mathbf{Z}}_{aA}\mathcal{A}^{A}_{\mathrm{NLO}}$, μ_{F} denotes the factorisation scale, and $\beta_0 = 11/2 - n_f/3$ with $n_f = 5$. Note that the LO amplitudes $\mathcal{A}^{h_a,\mathrm{e/o}}$ entering Eq. (6.58) are taken in the limit of large stop and sbottom masses, see Ref. [161].

6.4.2.2 Electroweak corrections

The full NLO electroweak corrections are known only in the Standard Model [252]. Consequently, for the MSSM, we can construct the EW amplitude only for the $\mathcal{CP}$-even eigenstates h and H. Since the $\mathcal{CP}$-odd Higgs A does not couple to gauge bosons, EW corrections to the $\mathcal{CP}$-odd Higgs production are expected to be negligible. This follows from the fact that important EW corrections arise from two-loop diagrams containing an internal light quark loop where the Higgs couples to the W and Z bosons. An example diagram is depicted in Fig. 6.7. These light quark diagrams are not suppressed by quark Yukawa couplings and therefore have a multiplicity enhancement from summing over the light quarks.

The electroweak effects of this kind are incorporated into the cross section in terms of a correction factor that multiplies the NLO cross section[9]:

$$\sigma^{\mathrm{e}}_{\mathrm{NLO,\,EW}} = \sigma^{\mathrm{e}}_{\mathrm{NLO}}(1 + \delta^{\mathrm{lf}}_{\mathrm{EW}}) . \tag{6.59}$$

The factor $\delta^{\mathrm{lf}}_{\mathrm{EW}}$ parametrises the contribution from light quarks, which can be reweighted

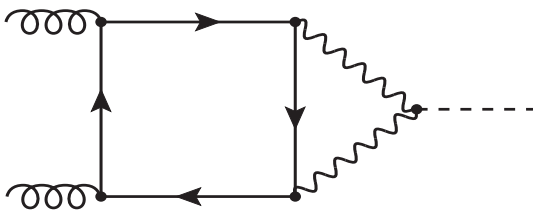

Figure 6.7: Example two-loop light-quark diagram contributing to the gluon-fusion cross section.

[9] This assumes factorisation of electroweak and QCD effects.

to the MSSM with complex parameters. We follow Ref. [253] and define the correction factor

$$\delta_{\rm EW}^{\rm lf} = \frac{\alpha_{\rm EM}}{\pi} \frac{2{\rm Re}\left(\mathcal{A}^{h_a,{\rm e}}\mathcal{A}^{h_a,{\rm EW}*}\right)}{|\mathcal{A}^{h_a,{\rm e}}|^2}\,, \tag{6.60}$$

where $\mathcal{A}^{h_a,{\rm e}}$, which has been given in Eq. (6.38), denotes the $\mathcal{CP}$-even part of the LO amplitude including quark and squark contributions. Accordingly, this electroweak correction factor is only applied to the $\mathcal{CP}$-even component of the LO and NLO cross section. The electroweak amplitude is given by [226]

$$\begin{aligned}\mathcal{A}^{h_a,{\rm EW}} = -\frac{3}{8}\,\frac{1}{x_W s_W^2}\left[\frac{2}{c_W^4}\left(\frac{5}{4}-\frac{7}{3}s_W^2+\frac{22}{9}s_W^4\right)A_1[x_Z]+4A_1[x_W]\right] \\ \cdot\left(-\hat{\mathbf{Z}}_{ah}\sin\alpha\cos\beta+\hat{\mathbf{Z}}_{aH}\cos\alpha\sin\beta\right)\,,\end{aligned} \tag{6.61}$$

with the abbreviation

$$x_V = \frac{M_{h_a}^2}{\left(m_V - i\frac{\Gamma_V}{2}\right)^2}\,, \qquad V\in\{W,Z\}\,. \tag{6.62}$$

In Eq. (6.60) $\alpha_{\rm EM}$ denotes the electro-magnetic coupling. Γ_V and m_V are the mass and the width of the heavy gauge bosons $V\in\{W,Z\}$. The function $A_1[x]$ is expressed in terms of the GHPLs defined in Ref. [226] as follows,

$$\begin{aligned}A_1[x] = &-4+2\left(1+\frac{1}{x}\right)G(-1;x)+\frac{2}{x}G(0,-1;x)+2\left(1+\frac{3}{x}\right)G(0,0,-1,x)\\ &+\left(1+\frac{2}{x}\right)\left[2G(0,-r,-r;x)-3G(-r,-r,-1;x)\right]-\sqrt{x(x+4)}\left\{\frac{2}{x}G(-r;x)\right.\\ &\left.+\frac{x+2}{x^2}\left[2G(-r,-r,-r;x)+2G(-r,0,-1;x)-3G(-4,-r,-1;x)\right]\right\}\,.\end{aligned} \tag{6.63}$$

The numerical evaluation of this function is very involved, and in `SusHi` the $\delta_{\rm EW}^{\rm lf}$ are implemented through an interpolation grid in M_{h_a} using fixed values for the masses and widths of the gauge bosons and the weak mixing angle,

$$\begin{aligned}m_W &= 80.385\ {\rm GeV}\,, \quad \Gamma_W = \ 2.085\ {\rm GeV}\,, \quad \sin^2\theta_W = \ 0.22295\\ m_Z &= 91.1896\ {\rm GeV}\,, \quad \Gamma_Z = \ 2.4952\ {\rm GeV}\,.\end{aligned} \tag{6.64}$$

Thus, the electroweak input values to `SusHi` for these correction factors are ignored.

Until now, we have presented how the gluon-fusion cross section in the MSSM is calculated considering all the different effects arising from the presence of complex parameters in the theory. We discussed the addition of higher-order contributions from various sectors and their adaptation and generalisation to the case of MSSM with complex pa-

rameters. In Chapter 7, we will describe how these components of the cross section, including NNLO and N^{3}LO contributions, are assembled in the numerical code `SusHiMi`.

6.5 Cross section for bottom-quark annihilation

The Higgs boson can be produced in association with bottom quarks ($b\bar{b}\phi$), similar to the process $t\bar{t}\phi$. In the SM, an increased phase space for $b\bar{b}\phi$ can compensate for the suppression by smaller Yukawa couplings. Depending on the centre-of-mass energy and the Higgs mass, this can result in the $b\bar{b}\phi$ cross section being even greater than that for $t\bar{t}\phi$ [254]. However, its experimental significance is reduced due to an enormous QCD background. In theories with extended Higgs sectors such as the 2HDM or the MSSM, the bottom-Yukawa couplings can be enhanced relative to the SM one so that $b\bar{b}\phi$ can become a dominant production channel for the Higgs bosons.

The theoretical prediction for this process can be made in two approaches. The first is called the four-flavour scheme (4FS) [255–257], where the leading order partonic processes are $q\bar{q} \to b\bar{b}\phi$ and $gg \to b\bar{b}\phi$, with $q \in \{u, d, c, s\}$. Here, the bottom quark appears as a final state particle and is not associated with a PDF. An example leading order diagram for this is depicted in Fig. 6.8 (a). In the 4FS, the cross section is known at NLO QCD in the SM. However, integration over phase space can lead to divergences arising from kinematic regions where the bottom quarks are collinear to the incoming partons which result in potentially large logarithms $\ln m_b/m_\phi$.

Ideally, these can be dealt with by resumming the large perturbative coefficients. This can be done in the five-flavour scheme (5FS) [258, 259], which introduces bottom-quark PDFs such that bottom quarks appear in the initial state (Fig. 6.8 (b)). The PDFs implicitly resum the momenta of the bottom quarks through DGLAP evolution[10]. `SusHi` employs the 5FS for the bottom-quark annihilation process for a SM Higgs boson at NNLO QCD. In the employed five-flavour scheme, where the bottom quarks are understood as

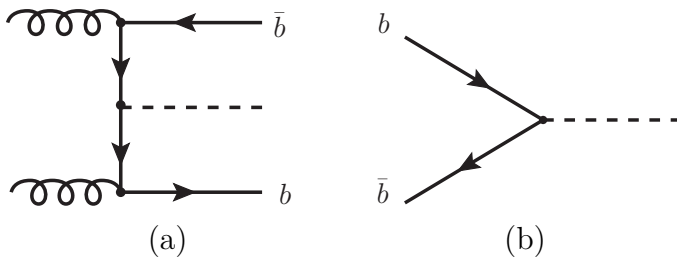

Figure 6.8: Leading order diagrams for bottom-quark annihilation in the (a) four-flavour scheme and (b) five-flavour scheme.

[10] Recently, calculations that perform a resummation of the logarithms combining the 4FS and 5FS are available, see e.g. Refs. [260–263].

partons, the result equals the cross section of a $\mathcal{CP}$-odd Higgs A (in a 2HDM with $\tan\beta = 1$). In the MSSM with real parameters, `SusHi` links to the program `bbh@nnlo` [264] for obtaining the inclusive cross section $\sigma_{b\bar{b}H^0}$ in the SM at NNLO QCD which uses $m_b^{\overline{\text{MS}}}(\mu_R)$ for the bottom-Yukawa coupling. This is subsequently reweighted by the resummed SUSY coupling g_b^ϕ.

For the production of the Higgs boson h_a in the MSSM with complex parameters, as implemented in `SusHiMi`, the results for the SM Higgs boson are further reweighted to the MSSM with $|\hat{\mathbf{Z}}_{ah} g_b^h + \hat{\mathbf{Z}}_{aH} g_b^H|^2 + |\hat{\mathbf{Z}}_{aA} g_b^A|^2$, which includes $\tan\beta$-enhanced squark effects through Δ_b according to the simplified resummation of Eq. (6.55). This procedure equals the application of a K-factor on the full LO cross section including $\hat{\mathbf{Z}}$ factors. In case of non-equal left- and right-handed couplings g_{b_L} and g_{b_R} due to the application of the full resummation in Eq. (6.52), the SM cross section has to be multiplied with

$$\begin{aligned} &|\hat{\mathbf{Z}}_{ah}(g_{bL}^h + g_{bR}^h) + \hat{\mathbf{Z}}_{aH}(g_{bL}^H + g_{bR}^H) + i\hat{\mathbf{Z}}_{aA}(g_{bL}^A - g_{bR}^A)|^2 \\ &+ |i\hat{\mathbf{Z}}_{ah}(g_{bR}^h - g_{bL}^h) + i\hat{\mathbf{Z}}_{aH}(g_{bR}^H - g_{bL}^H) + \hat{\mathbf{Z}}_{aA}(g_{bL}^A + g_{bR}^A)|^2 \,. \end{aligned} \tag{6.65}$$

We only discuss Higgs production through bottom-quark annihilation with simplified Δ_b resummation in this thesis.

Chapter 7

The program SusHi and its extension SusHiMi

This chapter describes the code SusHi *and its extension* SusHiMi*, which incorporates the results for cross sections for neutral Higgs bosons in the MSSM with explicit $\mathcal{CP}$ violation presented in Chapter 6. The summary of the computational framework for* SusHi *is based on the manual Ref. [161]. The description of* SusHiMi *closely follows Ref. [1], reflecting the author's contribution.*

7.1 Introduction

Studying the phenomenology of BSM models with high precision is a challenging task, especially since it can involve complex computations of mass matrices, interaction vertices, cross sections, and decay rates in a large number of processes. For this reason, it is essential to develop computational tools that can automate complicated and time consuming calculations and get robust numerical predictions to a high degree of precision. Such precise predictions are indeed required to discriminate between different models, or constrain the parameter space of new physics models at the level of accuracy delivered by the experiments.

One such computer code, whose development and extension this thesis is largely concerned with, is SusHi. SusHi is a numerical FORTRAN code [161, 162] which combines analytical results for the calculation of Higgs boson cross sections through gluon fusion and heavy-quark annihilation in models beyond the Standard Model up to the highest known orders in perturbation theory. It harbours several extensions, such as aMCSusHi [265, 266], a script for generating events for Higgs production at the LHC via gluon fusion which is used within MadGraph, and MoRe-SusHi (MOmentum REsummed SusHi) [266–268], which allows for the calculation of the transverse momentum distribution of a Higgs boson in the SM, the 2HDM, the MSSM, and the NMSSM by applying the formalism of analytic resummation to the gluon fusion-process. However, SusHi up to now did not allow for $\mathcal{CP}$ violation in the Higgs sector. Following our discussion in Chapter 6 we present the calculation of Higgs boson production in the context of the

MSSM with complex parameters, which we have included in an extension of SusHi named SusHiMi.

7.2 Workflow of SusHi

The input of SusHi is controlled by an SLHA-inspired [269, 270] input file. For the MSSM, the Higgs mass can be calculated by FeynHiggs or input by the user. The renormalisation scheme to be used is chosen in the input file, using which SusHi initialises the internal parameters. Various choices for the bottom-quark Yukawa coupling are supported, including the resummation of $\tan\beta$-enhanced sbottom effects. Subsequently the cross sections for gluon fusion and bottom-quark annihilation are calculated up to the order specified in the input file. The link to LHAPDF [271] takes place at various stages in the internal calculation. The output is generated in an output file as well as printed on the screen. The workflow for SusHi has been summarised in Fig. 7.1.

The external codes ggh@nnlo and bbh@nnlo are integrated into SusHi and are a part of the distribution. However, it must, especially for the MSSM with complex parameters, be linked to FeynHiggs, which is used to calculate the Higgs boson masses and mixings, and to LHAPDF, which provides the PDF sets that are used within SusHi.

7.3 The extension SusHiMi

The extension SusHiMi allows for complex values for the trilinear couplings of the Higgs with third generation sfermions $A_{t,b}$, the Higgsino mass parameter μ, and the gluino mass parameter M_3. While it is possible to also take into account $\mathcal{CP}$ violation in other sectors, we focus on the parameters that most affect the production cross sections through gluon fusion and bottom-annihilation.

We proceed along the lines of Fig. 7.2, which depicts the SusHiMi workflow, and calculate the Higgs boson production cross section through gluon fusion as follows: SusHiMi calls SusHi twice and in these two calls performs a "$\mathcal{CP}$-even" calculation for $\sigma^{\mathrm{e}}_{\mathrm{NLO}}$ and a "$\mathcal{CP}$-odd" calculation for $\sigma^{\mathrm{o}}_{\mathrm{NLO}}$ according to Eq. (6.56). Thus, the total gluon-fusion cross section is the sum of the two parts

$$\sigma_{\mathrm{N^kLO}}(pp \to h_a + X) = \sigma^{\mathrm{e}}_{\mathrm{N^kLO}}(pp \to h_a + X) + \sigma^{\mathrm{o}}_{\mathrm{N^kLO}}(pp \to h_a + X)\,. \tag{7.1}$$

We obtain the result beyond LO QCD through[1]

$$\sigma^{\mathrm{e}}_{\mathrm{N^kLO}} = \sigma^{\mathrm{e}}_{\mathrm{NLO}}(1+\delta^{\mathrm{lf}}_{\mathrm{EW}}) + \left(\sigma^{t,\mathrm{e}}_{\mathrm{N^kLO,\ EFT}} - \sigma^{t,\mathrm{e}}_{\mathrm{NLO,\ EFT}}\right) \tag{7.2}$$

$$\sigma^{\mathrm{o}}_{\mathrm{N^kLO}} = \sigma^{\mathrm{o}}_{\mathrm{NLO}} + \left(\sigma^{t,\mathrm{o}}_{\mathrm{N^kLO,\ EFT}} - \sigma^{t,\mathrm{o}}_{\mathrm{NLO,\ EFT}}\right)\,, \tag{7.3}$$

[1] These formulas equal the master formulas employed in previous SusHi releases [161, 162].

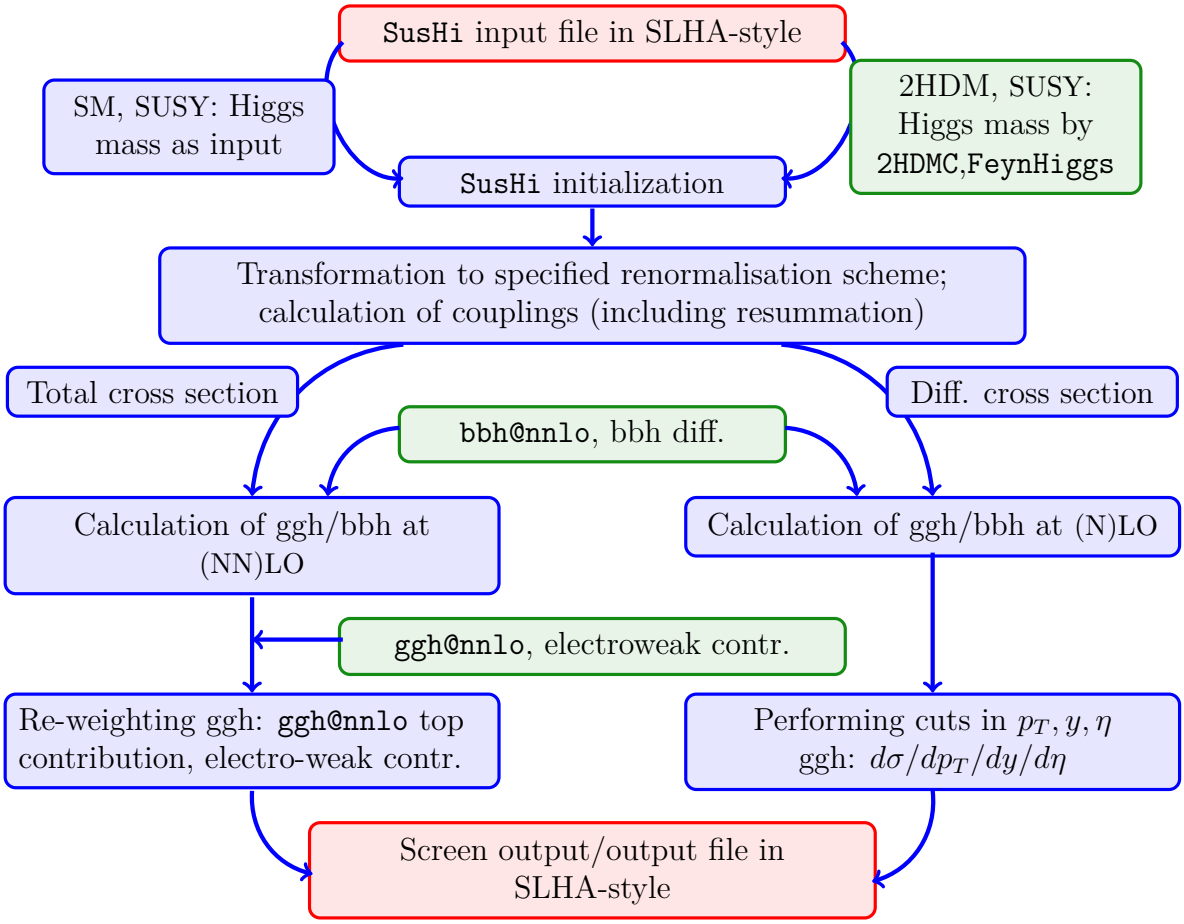

Figure 7.1: Internal workflow of SusHi. Red boxes indicate interaction with the user while green boxes refer to external code (see text), which is linked to/included in SusHi. Figure from Ref. [161].

whereas $\sigma^{\text{e/o}}_{\text{LO}}$ was specified in Section 6.3.2, and $k \in \{1,2,3\}$. The $\mathcal{CP}$-odd component $\sigma^{t,\text{o}}_{\text{N}^k\text{LO, EFT}}$ is only implemented up to $k=2$ (see below). In the previous formulas $\sigma^{\text{e/o}}_{\text{NLO}}$ are the NLO cross sections including real contributions and the interpolated NLO virtual corrections as discussed in Section 6.4.2.1. They employ the simplified Δ_b resummation according to Eq. (6.55), named Δ_{b1}. $\sigma^{t,\text{e}}_{\text{N}^k\text{LO, EFT}}$ and $\sigma^{t,\text{o}}_{\text{N}^k\text{LO, EFT}}$ are cross sections including the top-quark contribution only. They are based on a K-factor calculated in the EFT approach of an infinitely heavy top-quark obtained for a SM Higgs boson H and a $\mathcal{CP}$-odd A (in a 2HDM with $\tan\beta = 1$) with mass M_{h_a}, respectively.

This K-factor is subsequently reweighted with the exact LO cross section. For this purpose the employed LO cross sections $\sigma^{t,\text{e}}_{\text{LO}}$ and $\sigma^{t,\text{o}}_{\text{LO}}$ are again evaluated as discussed in Section 6.3.2 with full $\hat{\mathbf{Z}}$ factors, but include only the top-quark contribution. They are multiplied with the K-factors in $\sigma^{t,\text{e}}_{\text{N}^k\text{LO, EFT}}$ and $\sigma^{t,\text{o}}_{\text{N}^k\text{LO, EFT}}$, respectively. Due to their small numerical impact in $\sigma^{t,\text{e/o}}_{\text{N}^k\text{LO, EFT}}$ we do not take into account top-quark mass effects beyond NLO even though they are implemented in SusHi. An alternative approach,

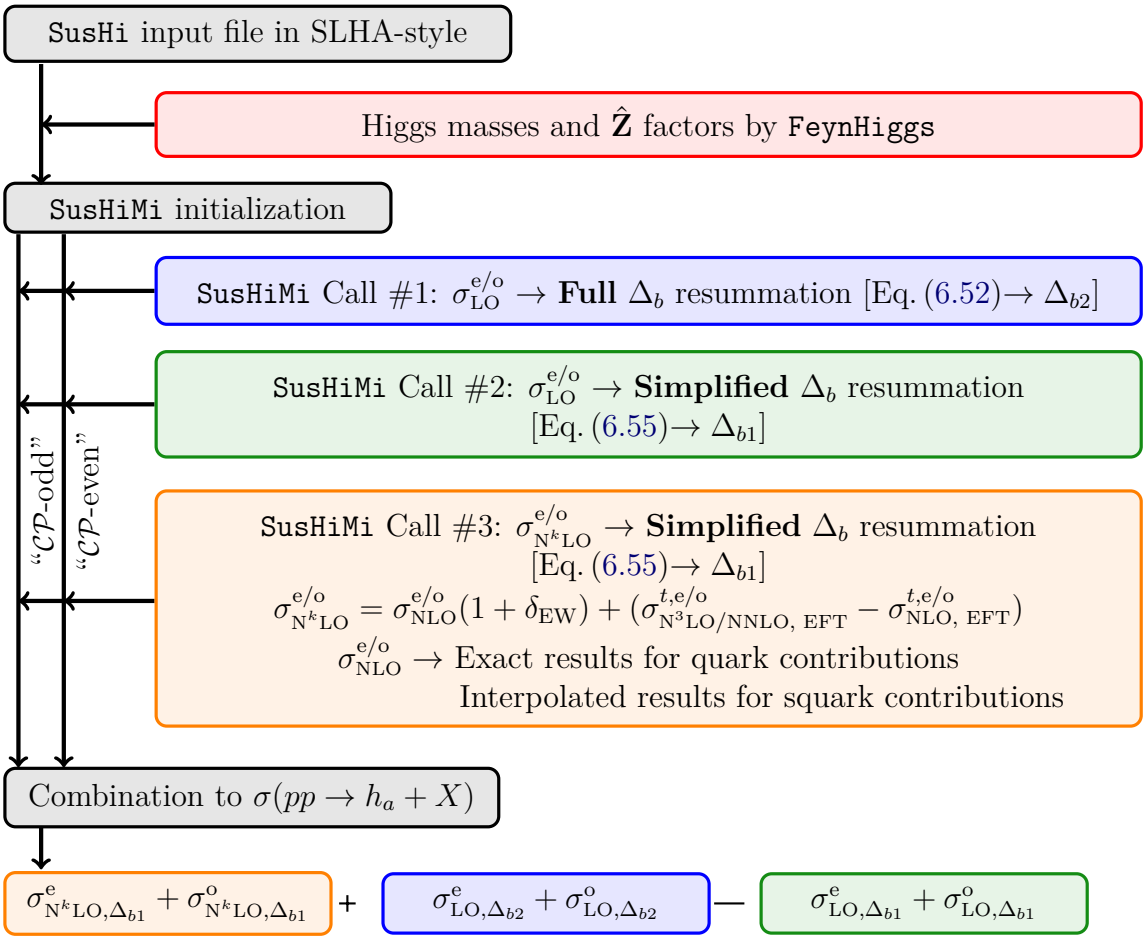

Figure 7.2: Pictorial view of the gluon-fusion cross section calculation in SusHiMi.

which is not discussed in this thesis but can be implemented in SusHiMi, is to include the relative couplings g_t^ϕ and the $\hat{\mathbf{Z}}$ factors into the complex-valued Wilson coefficients of the EFT directly.

As already mentioned in Section 6.4.2, the N^{3}LO QCD corrections are only taken into account for the $\mathcal{CP}$-even component of the light Higgs boson, which allows us to match the precision of the light Higgs boson cross section in the SM employed in up-to-date predictions. This is motivated by the fact that the light Higgs boson that is identified with the observed signal at 125 GeV is usually assumed to have a dominant $\mathcal{CP}$-even component, which is also the case in the scenarios which are considered in the numerical discussion that will follow in Chapter 8. For the $\mathcal{CP}$-odd component of the light Higgs and the heavy Higgs bosons we employ the NNLO corrections for the top-quark induced contributions to gluon fusion in the effective theory of a heavy top-quark, i.e. we do not take into account top-quark mass effects beyond NLO, but only factor out the LO QCD cross sections $\sigma_{\text{LO}}^{t,\text{e}}$ and $\sigma_{\text{LO}}^{t,\text{o}}$.

The strategy to employ the EFT result at NNLO beyond the top-quark mass threshold can be justified from the comparison of NLO corrections, which are known in the EFT approach and exactly with full quark-mass dependence and agree also beyond the top-quark mass threshold. On the other hand, the N^{3}LO QCD corrections that were obtained for the top-quark contribution are only known in the EFT approach and for an expansion around the threshold of Higgs production at $x = M_{h_a}^2/s \to 1$, which we can take into account up to $\mathcal{O}(1-x)^{16}$. Since the combination of the EFT approach and the threshold expansion becomes questionable above the top-quark mass threshold, we apply N^{3}LO QCD corrections only for the $\mathcal{CP}$-even component of the light Higgs boson and thus match the precision of the SM prediction. Finally, the electroweak correction factor $\delta_{\text{EW}}^{\text{lf}}$ multiplied in the "$\mathcal{CP}$-even" run is obtained from Eq. (6.60).

As shown in Fig. 7.2 we call SusHiMi three times in order to take into account the different possibilities of the resummation of $\tan\beta$-enhanced sbottom effects in the LO QCD contributions. We add the results as follows

$$\sigma(pp \to h_a + X) = \sigma_{\text{N}^k\text{LO}}^{\Delta_{b1}} + \sigma_{\text{LO}}^{\Delta_{b2}} - \sigma_{\text{LO}}^{\Delta_{b1}} \,, \tag{7.4}$$

where in the N^{k}LO QCD cross section following Eq. (7.1) the simplified resummation according to Eq. (6.55) is employed, indicated through the index Δ_{b1}. We add and subtract the LO QCD cross section using the full resummation according to Eq. (6.52), named Δ_{b2}, and the simplified resummation, respectively. As we will demonstrate, the differences between the two versions of resummation are small, which can partially be understood from a possible rephasing of complex Yukawa couplings by a redefinition of all (s)quark fields (see the discussion in Section 6.4.1).

The cross section for the bottom-quark annihilation process is implemented in the 5FS at NNLO QCD by modifying the bottom-Yukawa couplings as in Eq. (6.65).

SusHi also allows one to obtain differential cross sections as a function of the transverse

momentum or the (pseudo-)rapidity of the Higgs boson. These effects can be studied also in the MSSM with complex parameters. In the case of non-vanishing transverse momentum, which is only possible through additional radiation, i.e. real corrections, the precision for massive quark contributions in extended Higgs sectors is currently limited to the LO prediction [266,272]. The predictions of the p_T distributions in SusHiMi have been obtained from the LO contributions with arbitrary complex parameters, and in contrast to the total cross sections are therefore not affected by additional interpolation uncertainties from higher orders in comparison to the case of the MSSM with real parameters.

In Chapter 8, we will discuss the applications of SusHiMi for the Higgs boson phenomenology of the MSSM with complex parameters and study the effects of the phase of the complex parameters A_t and M_3 on the masses, mixings and cross sections of the three neutral Higgs bosons. In Chapter 9, we will discuss the $\mathcal{CP}$-violating interference factors that arise in a process of production and decay of the Higgs states $h_a, a \in \{1,2,3\}$ and describe their implementation in SusHiMi. We will then employ our cross section predictions along with the interference factors from SusHiMi to study how such interference effects can modify exclusion bounds for the MSSM from collider searches.

Chapter 8

Phenomenology of $\mathcal{CP}$ violation in MSSM Higgs production

In this chapter we address the phenomenological implications of the $\mathcal{CP}$-violating parameters in the Higgs sector of the MSSM using the results from Chapter 6 and their implementation into the code described in Chapter 7. The results presented in this chapter have been published in Ref. [1].

8.1 Introduction

In the previous chapters we studied how to calculate the production cross sections of neutral Higgs bosons for the gluon fusion and bottom-quark annihilation processes in the MSSM with explicit $\mathcal{CP}$ violation, and described their implementation in `SusHiMi`. After these methodological studies, we will now investigate the phenomenological implications of the complex parameters on various aspects of the Higgs sector. In particular, we will focus on the role played by the $\mathcal{CP}$-violating phases of the trilinear couplings of the Higgs with third generation sfermions, specifically A_t, and of the gluino mass parameter M_3 in affecting the predictions for mixings and cross sections of the heavy Higgs bosons h_2 and h_3. In the context of $\mathcal{CP}$-violating mixing, loop contributions can lead to large interference effects in the cross sections of the highly admixed heavy Higgses. Such interferences can lead to significant enhancement or suppression of the heavy Higgs cross sections, giving rise to modified exclusion bounds from collider searches as compared to the MSSM with real parameters.

As a first step, we will study scenarios where ϕ_{A_t} and ϕ_{M_3} substantially alter the phenomenology of Higgs bosons via $\mathcal{CP}$-violating effects from the squark and gluino sectors. The scenarios presented in this chapter were originally published before the latest updates on exclusion bounds for SUSY particle masses were released by CMS and ATLAS using data from Run II of the LHC. While the phenomenological viability of these scenarios may be under pressure in view of the latest exclusion bounds from the SUSY searches, they are useful for illustrating the possible effects of the $\mathcal{CP}$-violating phases. Note also that the cross section predictions in this chapter are for the individual Higgs

states h_a, and the interference between the production and decay contributions of the different Higgs bosons have not been taken into account. In Chapter 9, we will explore scenarios that are up to date with the most recent experimental results, and incorporate the effects of interference terms in our studies.

8.2 Definition of scenarios

For our numerical analysis we slightly modify two standard MSSM scenarios introduced in Ref. [130], namely the $m_h^{\text{mod+}}$ and the light-stop scenario[1]. As mentioned above, the scenarios have been chosen for illustration, featuring relatively large squark and gluino contributions to the gluon-fusion process. The corresponding effects will be relevant in our discussion of the associated theoretical uncertainties.

The light-stop inspired scenario that we use for our numerical analysis is defined for vanishing phases as follows

$$\begin{aligned} &M_1 = 340\,\text{GeV}, \quad M_2 = \mu = 400\,\text{GeV}, \quad M_3 = 1.5\,\text{TeV}\,, \\ &X_t = X_b = X_\tau = 1.0\,\text{TeV}, \quad A_q = A_l = 0\,, \\ &\tilde{m}_{Q_2} = \tilde{m}_L = 1\,\text{TeV}, \quad \tilde{m}_{Q_3} = 0.5\,\text{TeV}\,, \end{aligned} \tag{8.1}$$

where the modified values of M_1 and M_2 have been chosen to avoid direct bounds from stop searches obtained in LHC Run I (assuming R-parity conservation). For the $m_h^{\text{mod+}}$-inspired scenario we choose for vanishing phases of the complex parameters:

$$\begin{aligned} &M_1 = 250\,\text{GeV}, \quad M_2 = 500\,\text{GeV}, \quad M_3 = 1.5\,\text{TeV}\,, \\ &X_t = X_b = X_\tau = 1.5\,\text{TeV}, \quad A_q = A_l = 0\,, \\ &\mu = \tilde{m}_Q = \tilde{m}_L = 1\,\text{TeV}\,. \end{aligned} \tag{8.2}$$

The values of the SM parameters for both the scenarios are

$$\begin{aligned} &m_t^{\text{OS}} = 173.20\,\text{GeV}, \qquad m_b^{\overline{\text{MS}}}(m_b) = 4.16\,\text{GeV}, \\ &m_b^{\text{OS}} = 4.75\,\text{GeV}\,, \qquad \alpha_s(m_Z) = 0.119. \end{aligned} \tag{8.3}$$

The on-shell bottom-quark mass is used as internal mass for propagators and for the bottom-quark Yukawa coupling in the gluon-fusion process. The specified value of α_s is only used for the evaluations of `FeynHiggs`, for the cross sections the value of α_s associated with the employed PDF set is taken. We employ the `MMHT2014` PDF sets at LO, NLO, NNLO and N^{3}LO QCD [273]. The central choice for the renormalisation and factorisation scales μ_{R}^0 and μ_{F}^0, respectively, is $(\mu_{\text{R}}^0, \mu_{\text{F}}^0) = (M_{h_a}/2, M_{h_a}/2)$ for gluon fusion and $(\mu_{\text{R}}^0, \mu_{\text{F}}^0) = (M_{h_a}, M_{h_a}/4)$ for bottom-quark annihilation. More details are described

[1] A detailed documentation of the parameters for each scenario presented here is given in Appendix B.

in Section 8.6.

For the $m_h^{\text{mod+}}$-inspired scenario we choose the heavy Higgs boson masses through $M_{H^\pm} = 900\,\text{GeV}$ with $\tan\beta = 10$ and 40 for the study of Δ_b effects, while for the light-stop inspired scenario we set $M_{H^\pm} = 500\,\text{GeV}$ with $\tan\beta = 16$. A detailed discussion of squark effects for the Higgs boson cross sections in the light-stop scenario in the MSSM with real parameters can also be found in Ref. [274]. For the chosen parameter point the squark effects are sizeable, both for the light Higgs boson and in particular also for the heavy $\mathcal{CP}$-even Higgs boson, where they reduce the gluon-fusion cross section by about $\sim 90\%$. The Higgs boson masses and the $\hat{\mathbf{Z}}$ factors are obtained from `FeynHiggs 2.11.2`. The cross sections are evaluated with `SusHiMi`, which is based on the latest release of `SusHi`. We will mostly focus on the gluon-fusion cross section and present the bottom-quark annihilation cross section only for the $m_h^{\text{mod+}}$-inspired scenario with $\tan\beta = 40$.

In order to isolate the effects of individual phases, we vary them one a time, keeping the rest of the parameters real. For the parameter points associated with the mentioned scenarios, the absolute value of A_t is set using $A_t = X_t - \mu^*/\tan\beta$, and we set the values $A_b = A_\tau = |A_t|$. Therefore, we will vary the phases of $A_t = |A_t|e^{i\phi_{A_t}}$, and similarly $M_3 = m_{\tilde{g}}e^{i\phi_{M_3}}$, leaving the absolute values constant in order to address various aspects in the phenomenology of Higgs boson production. The phases of A_b and μ do not introduce new phenomenological features, and we do not display results for the variation of those phases. A variation of the phase of X_t leads to very similar cross sections for all Higgs bosons as observed for the variation of the phase of A_t. This can be understood from the fact that the chosen values of μ and $\tan\beta \geq 10$ are not too large, and so $X_t \approx A_t$. Note that the stop masses are constant as a function of the phase of X_t, if the absolute value of X_t is fixed.

Recall that in Section 3.3 we discussed bounds on the phases of complex parameters resulting from limits on EDMs of heavy quarks and the neutron. We had concluded from that discussion that the phases of A_t and M_3 still offer large room for variation and therefore, in the plots shown in this chapter, we will consider the full range of ϕ_{A_t} and ϕ_{M_3}, from 0 to 2π radians, as is done frequently in such studies. It should be noted in this context that in particular the variation of A_t affects the values of the stop masses. Additionally, the Higgs boson masses are a function of the phases of the complex parameters. The impact of the phases can be particularly pronounced for the mass of the light Higgs boson. A significant part of the observed phase variation of the cross sections can be a kinematic effect from the variation of mass. In general h_1 is almost fully $\mathcal{CP}$-even in the decoupling limit. In order to factor out the impact of phase space effects, we normalise the prediction for the cross section of the light Higgs boson in the MSSM to the cross section of a SM Higgs boson having the same mass M_{h_1} as the light Higgs h_1. In case of the heavy Higgs bosons for which the phase space effects are much less severe, we stick to the inclusive cross sections without such a normalisation. The

predicted value for the Higgs boson mass M_{h_1} deviates from 125 GeV by up to a few GeV in our studies. Deviations from the experimental value in this ballpark are still commensurate with the remaining theoretical uncertainties from unknown higher-order corrections of current state-of-the-art calculations of the light Higgs boson mass in the MSSM [65, 68, 92, 275, 276].

In the studies that follow, we will discuss three aspects: We start by investigating the effect of squark loops on the Higgs boson production cross sections. They are of relevance both for the heavy Higgs bosons and the light Higgs boson. Second, we focus on the admixture of the two heavy Higgs bosons (described through $\hat{\mathbf{Z}}$ factors) and its effect on production cross sections. Lastly we discuss Δ_b corrections in the context of the $m_h^{\text{mod}+}$-inspired scenario with large $\tan\beta$, for which the bottom-quark annihilation process for the heavy Higgs bosons is relevant as well.

Note that given the large admixture of the two heavy Higgs bosons in the MSSM with complex parameters, interference effects in the full processes of production and decay can be large. The results for the cross sections obtained in this chapter can be employed in a generalised narrow-width approximation as described in Refs. [137, 277] in order to incorporate interference effects. This issue will be addressed in the next chapter.

The prediction for Higgs boson cross sections is affected by various theoretical uncertainties, which will be discussed in detail in Section 8.6. In order to demonstrate the improvement in precision through the inclusion of higher-order corrections, all subsequent figures which show the LO cross section and our best prediction cross section according to Eq. (7.1) include renormalisation and factorisation scale uncertainties. The procedure for obtaining these scale uncertainties is outlined in Section 8.6.

8.3 Squark contributions in the light-stop inspired scenario

We start with a discussion of squark effects on the Higgs boson cross section $\sigma(gg \to h_a)$ for all three Higgs bosons h_a within the light-stop inspired scenario with $M_{H^\pm} = 500\,\text{GeV}$ and $\tan\beta = 16$. The variation of the light Higgs boson mass M_{h_1} as well as the stop masses is depicted in Fig. 8.1 (a) as a function of ϕ_{A_t}. The light Higgs mass in this scenario may appear to be too light to be compatible with the signal observed at the LHC, however we regard it as sufficiently close in view of the issue that our discussion should demonstrate phenomenological effects only, and that on the other hand there are still sizeable theoretical uncertainties in the MSSM prediction for the light Higgs boson mass. The lightest stop mass has its minimum at around 308 GeV. For the heavy Higgs bosons with masses between 492 and 494 GeV, which are shown in the Fig. 8.2, the NLO squark–gluino contributions [236–238] which assume squarks and gluinos to be heavier than half the Higgs mass are thus well applicable. The variation of the heavy Higgs boson masses as a function of the phases of ϕ_{A_t} (as well as ϕ_{M_3}) turns out to be small,

namely within 0.6 GeV. Due to the strong admixture of the left- and right-handed stops through a large value of A_t, also a phase dependence of the stop masses is observed, see Fig. 8.1. We checked that we obtain constant stop masses upon varying the phase of X_t for a constant value of $|X_t|$.

Fig. 8.1 (b) shows the production cross section through gluon fusion for the light Higgs boson h_1. The black, dot-dashed curve depicts the cross section with only top-quark and bottom-quark contributions and electroweak corrections in the production amplitudes, i.e. in the formulas of Chapter 7 we omit all squark contributions which enter either directly or through Δ_b. Note however that squark contributions are always part of the $\hat{\mathbf{Z}}$ factors.

Due to the decoupling with large values of $M_{H^\pm}$ in our scenarios, the light Higgs h_1 has mostly SM-like couplings to quarks and gauge bosons. Thus, thanks to the inclusion of N^{3}LO QCD contributions for the top-quark induced contribution, our prediction of the gluon-fusion cross section omitting the squark contributions (black, dot-dashed curve

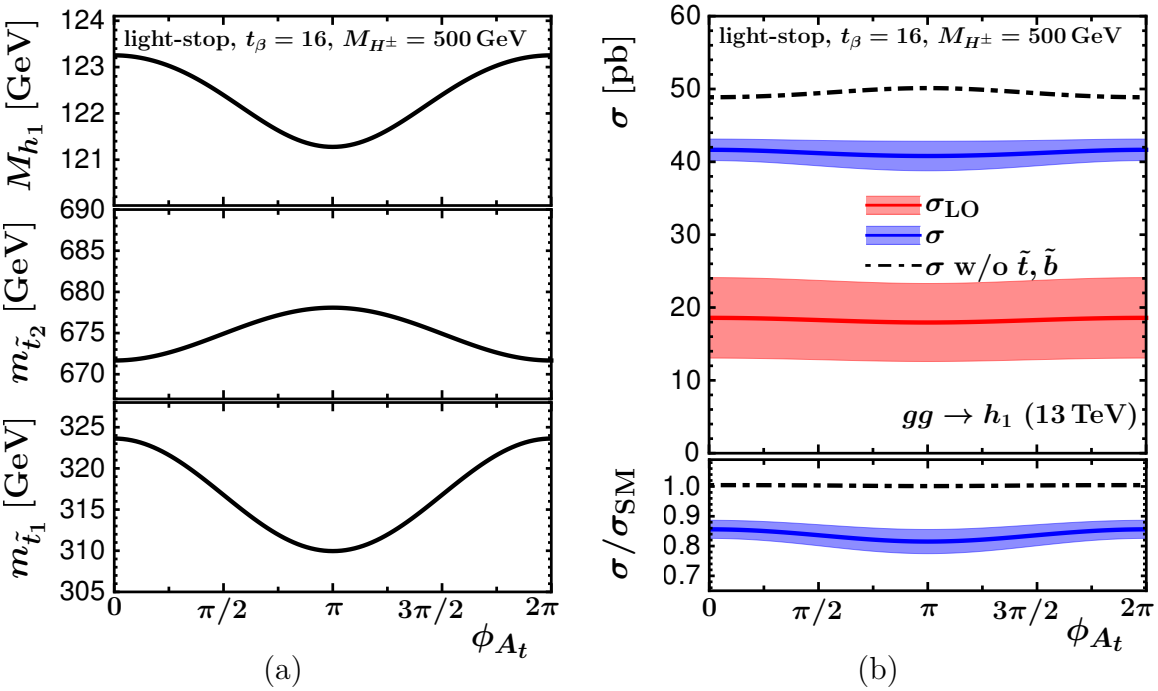

Figure 8.1: (a) Mass of h_1 and stop masses in GeV as a function of ϕ_{A_t}; (b) LO (red) and best prediction for the gluon-fusion cross section (blue) for the light Higgs h_1 in pb as a function of ϕ_{A_t}. The results are shown for the light-stop inspired scenario as specified in Eq. (8.1). The black, dot-dashed curve depicts the best prediction cross section without squark contributions (except through $\hat{\mathbf{Z}}$ factors). The depicted uncertainties are scale uncertainties. In the lower panel we normalise to the cross section of a SM Higgs boson with the same mass M_{h_1}.

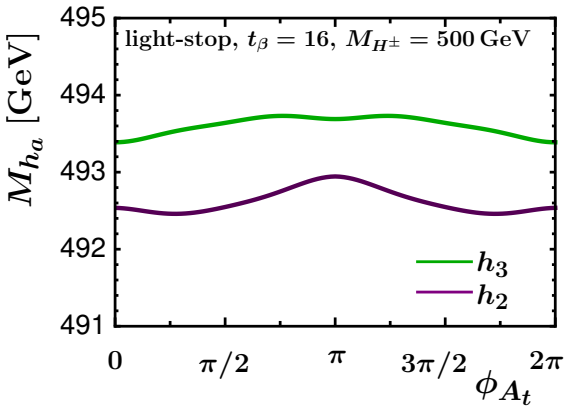

Figure 8.2: Variation of masses (in GeV) of the heavy Higgs bosons h_2 (violet) and h_3 (green) with ϕ_{A_t} in the light-stop inspired scenario specified in Eq. (8.1).

in Fig. 8.1 (b)) is very close to the one for the SM Higgs boson with the same mass as provided by the LHC Higgs Cross Section Working Group [92, 278]. The inclusion of squark contributions explicitly and through Δ_b resummation lowers the gluon-fusion cross section by about 20%, as can be inferred from the blue, solid curve, which is shown together with its renormalisation and factorisation scale uncertainty (to be discussed in Section 8.6). For completeness we also show the LO cross section calculated according to Eq. (6.37) including squark effects as the red curve. It is apparent that the scale uncertainties are significantly reduced from LO QCD to our best prediction cross section calculated according to Eq. (7.1).

Fig. 8.1 (b) also includes the cross section for h_1 normalised to the cross section of a SM Higgs boson with the same mass. Here the $\sim 20\%$ reduction due to squark effects is apparent once again, while the quark-induced cross section shows the decoupling behaviour. Not shown in the figures are the following effects, which are stated here for completeness: The variation of ϕ_{M_3} leads to a very similar picture, even though the light Higgs mass variation is not as pronounced and the stop masses are unaffected. Moreover, in the comparison of the simplified and the full resummation of Δ_b contributions in the LO gluon-fusion cross section of h_1, we observe a well-known behaviour, namely the simplified resummation of Eq. (6.55) does not yield a decoupled bottom-quark Yukawa coupling, whereas the full resummation of Eq. (6.52) does.

Fig. 8.3 (a) and (b) show the gluon-fusion cross sections of the heavy Higgs bosons h_2 and h_3, respectively, as a function of ϕ_{A_t}. The colour coding is identical to Fig. 8.1 except for the fact that the lower panel depicts the K-factor of our best prediction for the cross section with respect to the LO cross section, σ/σ_{LO}, rather than a cross section normalised to the SM Higgs boson cross section. Since the heavy Higgs masses change only slightly as a function of the phase ϕ_{A_t}, the associated phase space effect is small. For vanishing phase $\phi_{A_t} = 0$ it is known that squark effects are huge and reduce the

cross section by $\sim 89\%$ (h_2) and $\sim 22\%$ (h_3) [274]. These squark effects are strongly dependent on the phase ϕ_{A_t} and induce a large positive correction at phase $\phi_{A_t} = \pi$ in case of h_2. For h_3 the effects are not as pronounced, but still sizeable. The K-factor for both processes $gg \to h_2$ and $gg \to h_3$ remains within $[1, 1.6]$, i.e. higher-order corrections mainly follow the phase dependence of the LO cross section. The dependence of the K-factor on ϕ_{A_t} follows the black, dot-dashed curve, which shows the cross section with quark contributions only. The significant dependence of the cross section where only quark contributions are included on the phase ϕ_{A_t} is induced by the admixture of the two Higgs bosons through $\hat{\mathbf{Z}}$ factors. We will discuss this feature in detail for the $m_h^{\text{mod+}}$-inspired scenario in Section 8.4.

The phase dependence on ϕ_{M_3} is less pronounced. The corresponding cross sections for the two heavy Higgs bosons h_2 and h_3 are shown in Fig. 8.4. As in previous figures, we observe a significant reduction in the scale dependence from LO QCD to our best prediction for the cross section. The inclusion of squark and gluino contributions through the $\hat{\mathbf{Z}}$ factors and through Δ_b induces a dependence on the gluino phase already for the

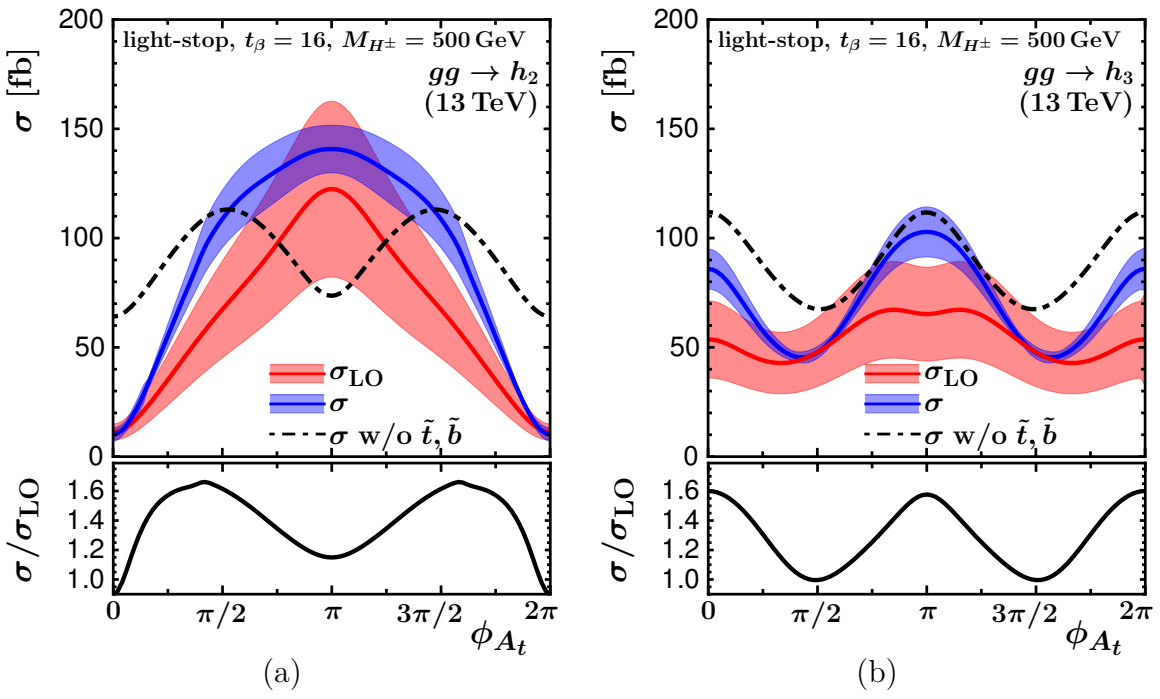

Figure 8.3: LO (red) and best prediction for the gluon-fusion cross section (blue) for (a) h_2 and (b) h_3 in fb as a function of ϕ_{A_t}. The results are shown for the light-stop inspired scenario as specified in Eq. (8.1). The black, dot-dashed curve depicts the best prediction cross section without squark contributions (except through $\hat{\mathbf{Z}}$ factors). The depicted uncertainties are scale uncertainties. In the lower panel we show the K-factor σ/σ_{LO}.

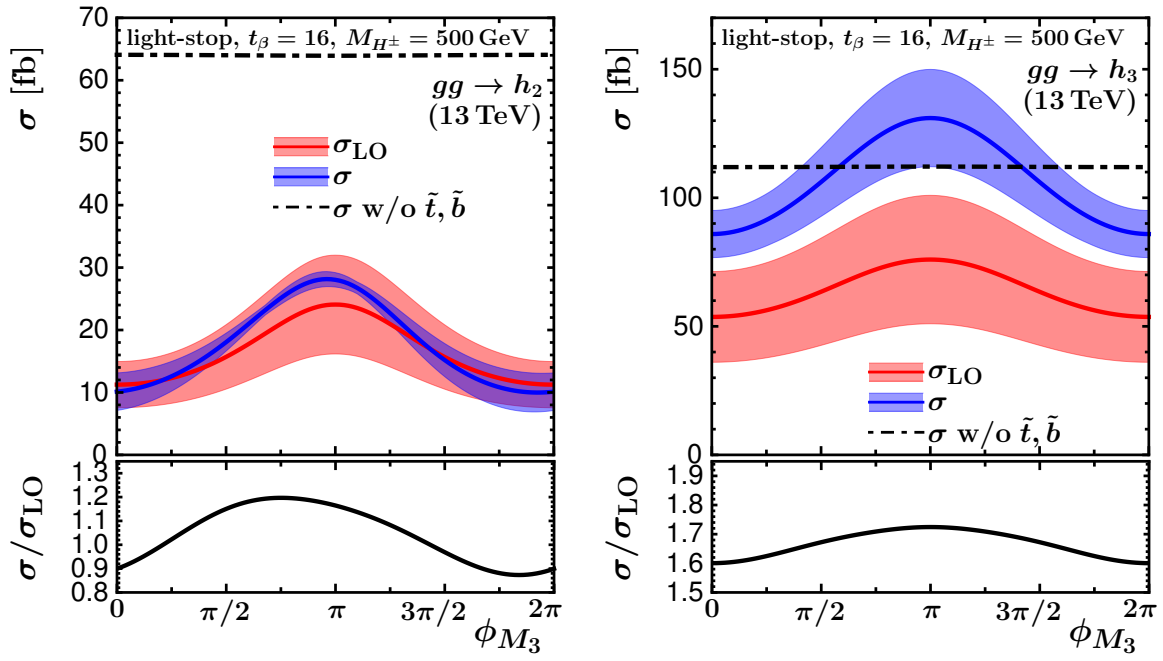

(a) (b)

Figure 8.4: LO (red) and best prediction for the gluon-fusion cross section (blue) for (a) h_2 and (b) h_3 in fb as a function of ϕ_{M_3}. The results are shown for the light-stop inspired scenario as specified in Eq. (8.1). The black, dot-dashed curve depicts the best prediction cross section without squark contributions (except through $\hat{\mathbf{Z}}$ factors). The depicted uncertainties are scale uncertainties. In the lower panel we show the K-factor σ/σ_{LO}.

LO cross section. The almost flat black dot-dashed curves show the cross section with quark contributions only, and any variation with ϕ_{M_3} is an effect of the $\hat{\mathbf{Z}}$ factors, which in this case is negligible since ϕ_{M_3} only enters at the two-loop level. The K-factor, which takes into account our interpolated NLO virtual corrections, only shows a relatively mild dependence on the phase. We will discuss the interpolation uncertainty for this scenario in Section 8.6, since we obtain the largest relative interpolation uncertainty in the cross section variation with phases for the interpolation of the gluino phase ϕ_{M_3}.

8.4 Admixture of Higgs bosons in the $m_h^{\text{mod+}}$-inspired scenario

In this section we discuss the $m_h^{\text{mod+}}$-inspired scenario with $\tan\beta = 10$ and $M_{H^\pm} = 900\,\text{GeV}$. Since the squark masses are at the TeV level in this scenario, the numerical effect of the squark loops in the gluon-fusion vertex contributions is rather small for the

production cross section of the light Higgs boson h_1. We will not discuss the results for h_1 in this section, however the considered scenario is typical for the decoupling region of supersymmetric theories, where a light SM-like Higgs boson is interpreted as the signal observed at about 125 GeV, as can be seen in Fig. 8.5. The predicted mass of h_1 in this scenario is close to the experimental value of the observed signal. It is accompanied by additional heavy Higgs bosons that are nearly mass degenerate. The results for the two heavy Higgs bosons are displayed in Fig. 8.6 and Fig. 8.7. The effects from squark loops are at the level of about $\pm 20\%$ for the cross sections of h_2 and h_3. In the general case where the possibility of $\mathcal{CP}$-violating interactions is taken into account, there can be a large mixing between the $\mathcal{CP}$-even and $\mathcal{CP}$-odd neutral Higgs states. This feature is clearly visible in Fig. 8.6. The dependence on the phase ϕ_{A_t} is seen to be closely correlated to the mixing character of the two neutral heavy Higgs bosons.

Fig. 8.6 depicts the masses of the two heavy Higgs bosons h_2 and h_3 as a function of ϕ_{A_t} together with the $\mathcal{CP}$-odd character of h_2 and h_3, being defined as $|\hat{\mathbf{Z}}_{aA}|^2$. For illustration here and in the following we call the mass eigenstates h_2 and h_3 either h_e or h_o, depending on their mixing character: if $|\hat{\mathbf{Z}}_{aA}|^2 \gtrsim 1/2$ the mass eigenstate h_a is called h_o, otherwise it is called h_e. It can be seen in Fig. 8.7 (a) and (b) that the behaviour of the cross sections as a function of ϕ_{A_t} closely follows the variation in the $\mathcal{CP}$-even and $\mathcal{CP}$-odd character of the Higgs states. A similar effect was already apparent in the top- and bottom-quark induced cross sections depicted in the light-stop inspired scenario, see Fig. 8.3, however there the effects of squark contributions are dominant. As above, also in Fig. 8.7, the uncertainty of our best prediction for the cross section is significantly reduced in comparison with the prediction in LO QCD. The variation of the K-factors between about 1.2 and 1.5 with the phase ϕ_{A_t} follows the modification of the mixing character of the two neutral heavy Higgs bosons.

Since the heavy Higgs bosons are nearly mass degenerate, it may not be possible in such a case to experimentally resolve the two heavy neutral Higgs bosons as separate signals.

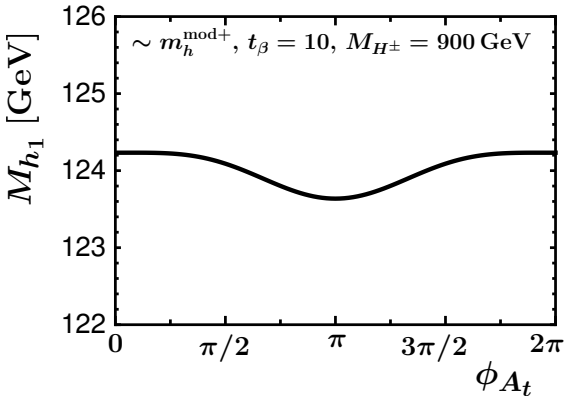

Figure 8.5: M_{h_1} in GeV as a function of ϕ_{A_t} in the $m_h^{\text{mod+}}$-inspired scenario specified in Eq. (8.2) with $\tan\beta = 10$.

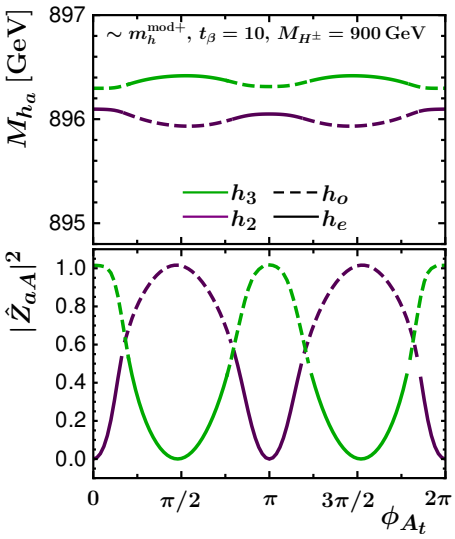

Figure 8.6: Masses of h_2 and h_3 in GeV as well as $\mathcal{CP}$-odd character $|\hat{\mathbf{Z}}_{aA}|^2$ as a function of ϕ_{A_t} in the $m_h^{\text{mod+}}$-inspired scenario specified in Eq. (8.2) with $\tan\beta = 10$. The solid and dashed curves depict regions in ϕ_{A_t} where h_2 and h_3 are predominantly $\mathcal{CP}$-even (h_e) or odd (h_o), respectively, corresponding to $|\hat{\mathbf{Z}}_{aA}|^2$ being below or above 0.5 as shown in the lower panel.

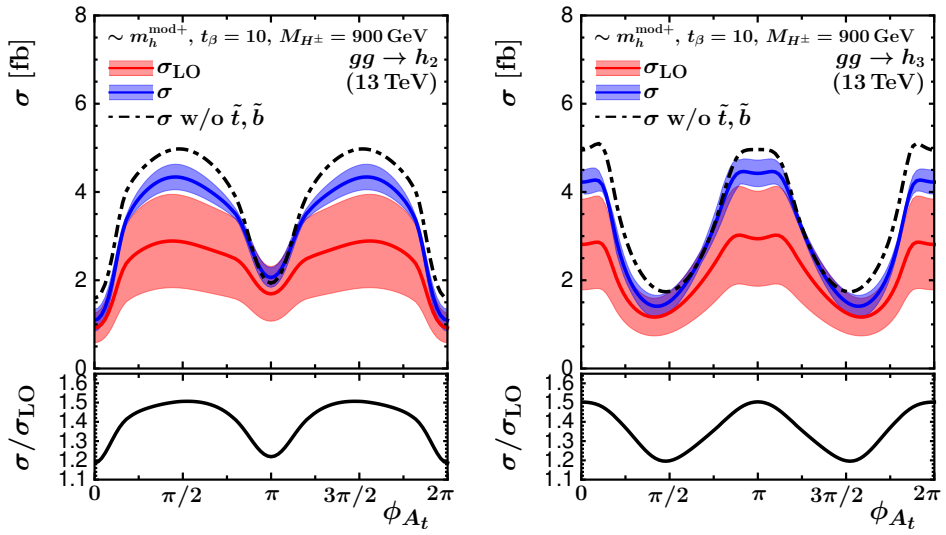

(a) (b)

Figure 8.7: LO (red) and best prediction for the gluon-fusion cross section (blue) for (a) h_2 and (b) h_3 in fb as a function of ϕ_{A_t} in the same scenario as Fig. 8.6. The black, dot-dashed curve depicts the best prediction for the cross section without squark contributions (except through $\hat{\mathbf{Z}}$ factors). In the lower panel we show the K-factor σ/σ_{LO}. The depicted uncertainties are scale uncertainties.

Rather than the individual cross sections times their respective branching ratios, the experimentally measurable quantity then consists of the sum of the cross sections of the two Higgs states times their respective branching ratios together with the interference contribution involving the two Higgs states. The latter can be particularly important if the mass difference between the two Higgs states is smaller than the sum of their total widths [137]. The incorporation of such interference effects into the prediction for the production and decay process will be discussed in Chapter 9. One can already infer from the plots of Fig. 8.7 (a) and (b) that in the overall contribution there will be sizeable cancellations between the phase dependencies of the separate contributions.

8.5 Δ_b corrections in the $m_h^{\text{mod+}}$-inspired scenario

We finally discuss the impact of Δ_b effects, which have been investigated for the two heavy Higgs bosons in the $m_h^{\text{mod+}}$-inspired scenario with $\tan\beta = 40$. In this scenario the admixture between the two heavy Higgs bosons, h_2 and h_3, is sizeable both as a function of ϕ_{A_t} and as a function of ϕ_{M_3}. This even leads to mass crossings as seen in Fig. 8.8. Since the mass eigenstates are defined such that $M_{h_3} \geq M_{h_2}$, for a case where the masses are degenerate and their hierarchy varies as we scan through ϕ_{A_t,M_3}, we observe a continuous mass curve only when we plot both the masses together. It is therefore convenient to discuss the results in terms of the predominantly $\mathcal{CP}$-even mass eigenstate h_e and the predominantly $\mathcal{CP}$-odd mass eigenstate h_o, as defined in Section 8.4, as for those states a smooth behaviour of the cross section as function of the phases is obtained. The masses of the two heavy Higgs bosons and their $\mathcal{CP}$ character (defining h_o and h_e) are shown in Fig. 8.8 as a function of ϕ_{A_t} and ϕ_{M_3}. One can see that the states h_2 and h_3 drastically change their $\mathcal{CP}$ character upon variation of the phases ϕ_{A_t} and ϕ_{M_3}, while on the other hand the state h_e is almost purely $\mathcal{CP}$-even and h_o is almost purely $\mathcal{CP}$-odd for the whole range of phase values, unlike what we saw in Section 8.4. Thus the mixing between the tree-level mass eigenstates is not very pronounced. It should be kept in mind in this context that $|\hat{\mathbf{Z}}_{aA}|^2$ arises from a non-unitary matrix and can therefore have values above 1. For vanishing phases the mass eigenstate h_2 corresponds to h_e and h_3 to h_o. This can also be seen in Fig. 8.9 (a) and (b), where we show the LO (red) and our best prediction cross section for gluon fusion (blue) for the Higgs states h_2 (solid curve) and h_3 (dotted curve) as a function of ϕ_{A_t} and ϕ_{M_3}, respectively, with their K-factors depicted in the lower panel. These plots further illustrate the discontinuities in the cross sections of h_2 and h_3 that occur due to the mass crossings and the jumps in their $\mathcal{CP}$-character as discussed for Fig. 8.8. Continuous curves are obtained only when the cross sections for h_2 and h_3 are plotted together. The lower red and blue curves in Fig. 8.9 (a) and (b) correspond to h_e and the upper red and blue curves to h_o. In order to demonstrate the discontinuities encountered in the cross sections of h_2 and h_3, they have been plotted without uncertainty bands.

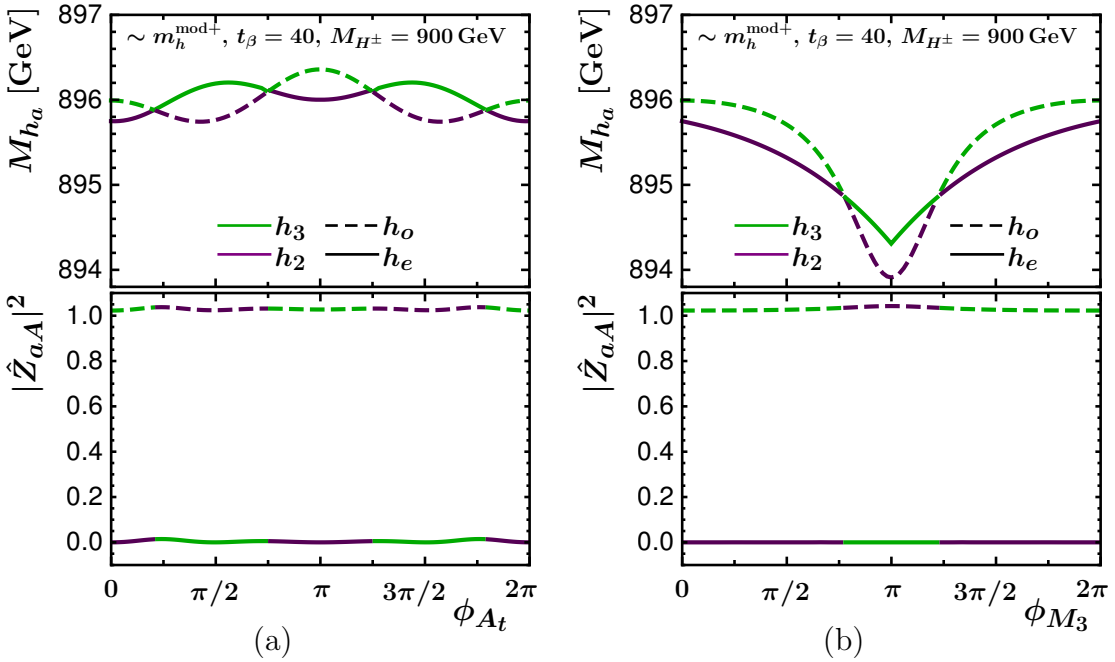

Figure 8.8: Masses of h_2 and h_3 in GeV and $\mathcal{CP}$-odd character as a function of (a) ϕ_{A_t} and (b) ϕ_{M_3} in the $m_h^{\mathrm{mod+}}$-inspired scenario specified in Eq. (8.2) with $\tan\beta = 40$. As in Fig. 8.6, the solid and dashed curves refer to h_e and h_o, respectively.

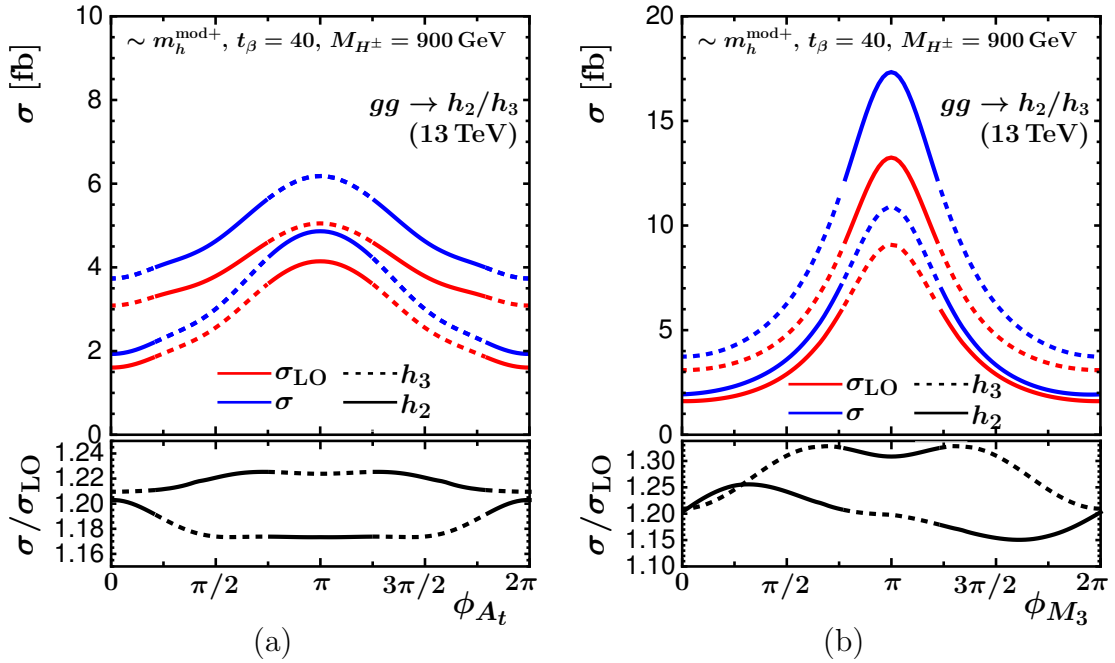

Figure 8.9: LO (red) and best prediction for the gluon-fusion cross section (blue) of h_2 and h_3 in fb as a function of (a) ϕ_{A_t} and (b) ϕ_{M_3} in the $m_h^{\mathrm{mod+}}$-inspired scenario specified in Eq. (8.2) with $\tan\beta = 40$. The solid curves specify the cross section for h_2 whereas the dotted curves denote the cross section for h_3. In the lower panel we show the K-factor σ/σ_{LO}.

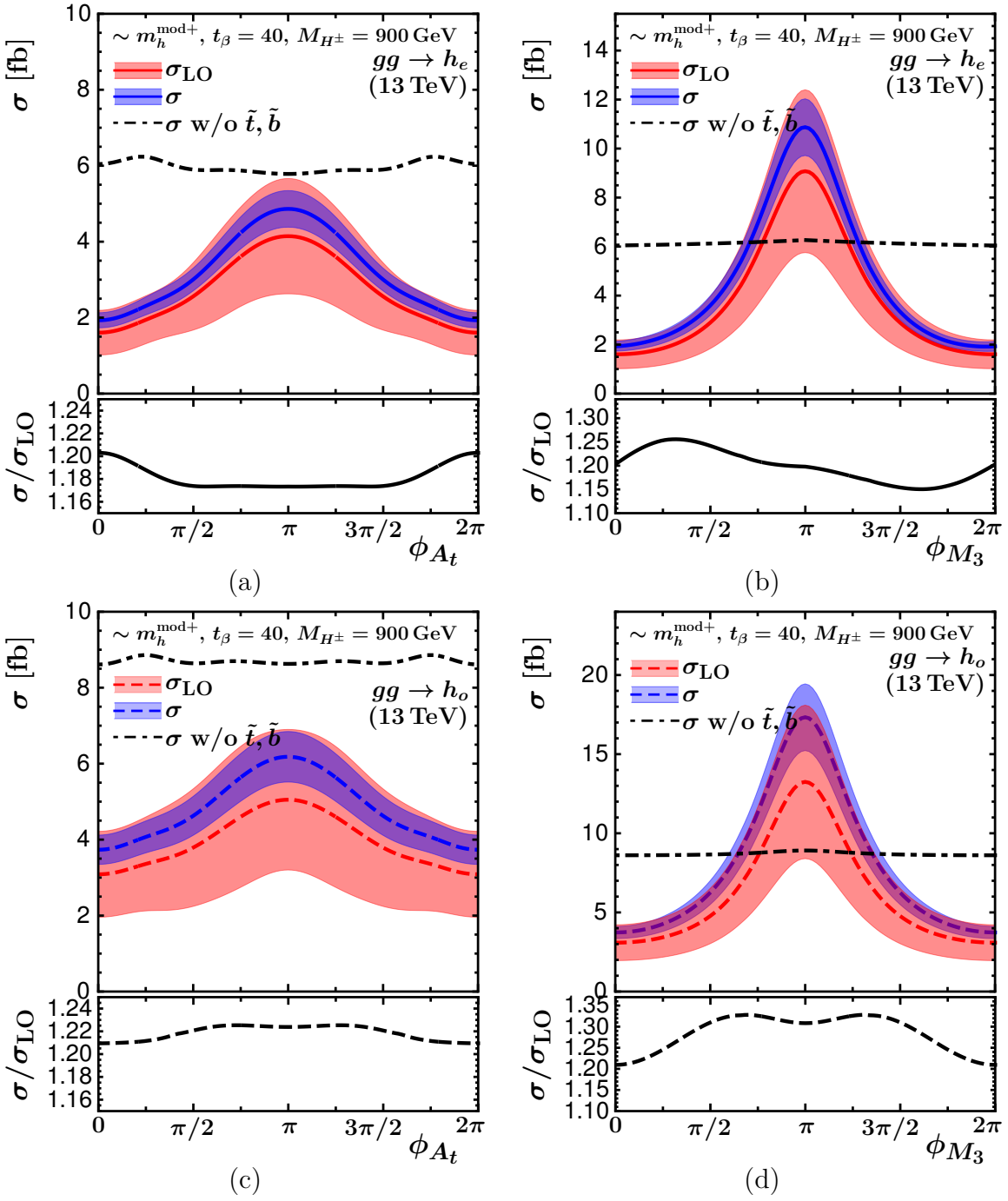

Figure 8.10: LO (red) and best prediction gluon-fusion cross section (blue) for h_e in fb as a function of (a) ϕ_{A_t} and (b) ϕ_{M_3} in the $m_h^{\text{mod+}}$-inspired scenario specified in Eq. (8.2) with $\tan\beta = 40$. The black dot-dashed curves depict the best prediction cross section without squark contributions (except through $\hat{\mathbf{Z}}$ factors). In the lower panel we show the K-factor σ/σ_{LO}. The depicted uncertainties are scale uncertainties. Figures (c) and (d) show the corresponding results for h_o.

In the following we mainly describe the results for the predominantly $\mathcal{CP}$-even mass eigenstate h_e. The observations for h_o are very similar. We will only add comments where appropriate, though they are presented for completeness in Fig. 8.10 (c) and (d). In Fig. 8.10 (a) and (b) we show the gluon-fusion cross section for h_e as a function of the phases ϕ_{A_t} and ϕ_{M_3}. Fig. 8.10 (c) and (d) show the corresponding results for h_o. The behaviour for the full prediction, including the squark contributions, is dominated by Δ_b corrections. For vanishing phases those corrections significantly reduce the cross sections compared to the case where only quark contributions are taken into account. For phase values around π, however, the Δ_b corrections can also give rise to a substantial enhancement of the cross section. In particular, for ϕ_{M_3} the quantity Δ_b changes sign between $\phi_{M_3} = 0$ and $\phi_{M_3} = \pi$, such that the bottom-Yukawa coupling is suppressed for small values of ϕ_{M_3} and enhanced for ϕ_{M_3} values close to π as a consequence of the resummation of the Δ_b corrections. The reduction of the scale uncertainties from LO QCD to our best prediction for the cross section is similar as in the previous plots. The K-factors in the lower panel show that the dependence of the NLO cross sections on the phases ϕ_{A_t} and ϕ_{M_3} follows a similar trend as the LO cross section.

In Fig. 8.11 we separately analyse the squark contributions for the LO cross section of h_e. The prediction omitting the squark loop contributions (black dot-dashed curves) is compared with the ones where first the pure LO squark contributions are added (depicted in cyan), and then the resummation of the Δ_b contributions to the bottom-quark Yukawa coupling is taken into account. For the latter both the results for the full (Δ_{b2} from Eq. (6.52), blue) and the simplified (Δ_{b1} from Eq. (6.55), red) resummation are shown. While the pure LO squark contributions are seen to have a moderate effect, it can be seen that the incorporation of the resummation of the Δ_b contribution leads to a significant enhancement of the squark loop effects. Looking at the blue and red curves, it can be confirmed that for the heavy neutral Higgs bosons considered here the simplified resummation approximates the full resummation of the Δ_b contribution very well. The curves corresponding to Δ_{b2} and Δ_{b1} hardly differ from each other both for the variation of ϕ_{A_t} and ϕ_{M_3}. As mentioned before all curves include the same $\hat{\mathbf{Z}}$ factors obtained from `FeynHiggs`. The results for h_o, which are not shown here, are qualitatively very similar. The LO squark contributions are less relevant for the h_o cross section, since those contributions are absent in the MSSM with real parameters. We also note that the curves for h_o follow a similar behaviour as the ones for h_e, which implies that there are no large cancellations expected in the sum of the cross sections for the two heavy Higgs bosons times their respective branching ratios. Thus, the phases entering Δ_b could potentially lead to observable effects in the production of the two heavy Higgs bosons even if the two states cannot be experimentally resolved as separate signals.

Having discussed the three different sources for $\mathcal{CP}$-violating effects relevant for Higgs boson production through gluon fusion in the MSSM — squark loop contributions, admixtures through $\hat{\mathbf{Z}}$ factors and resummation of Δ_b contributions — for completeness we

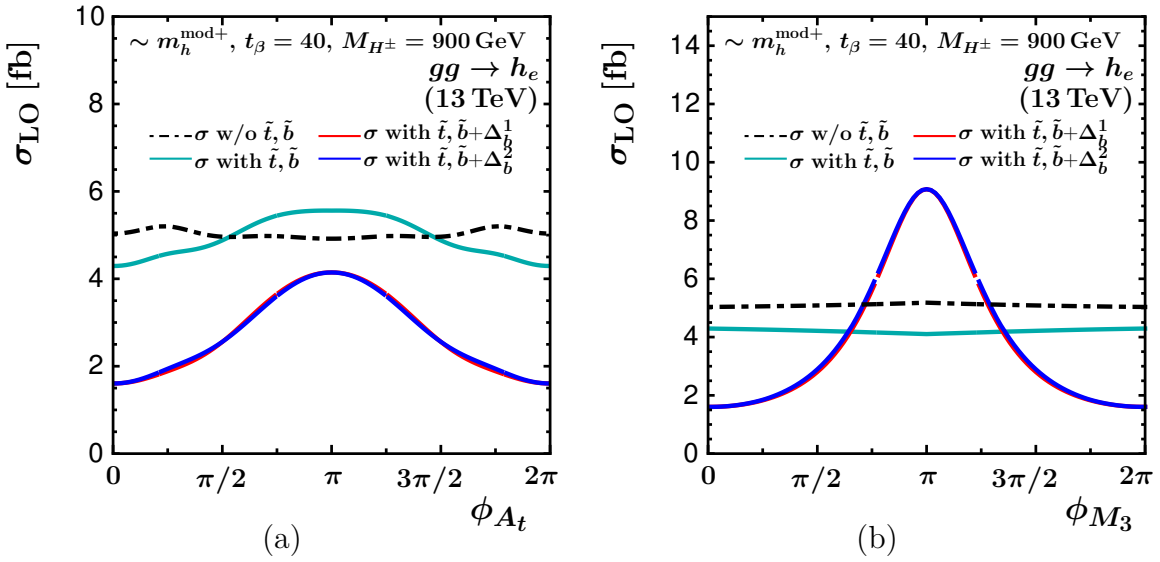

Figure 8.11: Effect of Δ_b contributions on the LO cross sections of h_e as a function of (a) ϕ_{A_t} and (b) ϕ_{M_3} in the $m_h^{\text{mod+}}$-inspired scenario specified in Eq. (8.2) with $\tan\beta = 40$. The black dot-dashed curves depict the prediction without squark contributions (except through $\hat{\mathbf{Z}}$ factors), while the cyan lines correspond to the prediction where the squark loop contributions at the one-loop level are included. In the red (blue) curves furthermore the simplified (full) resummation of the Δ_b contributions is included.

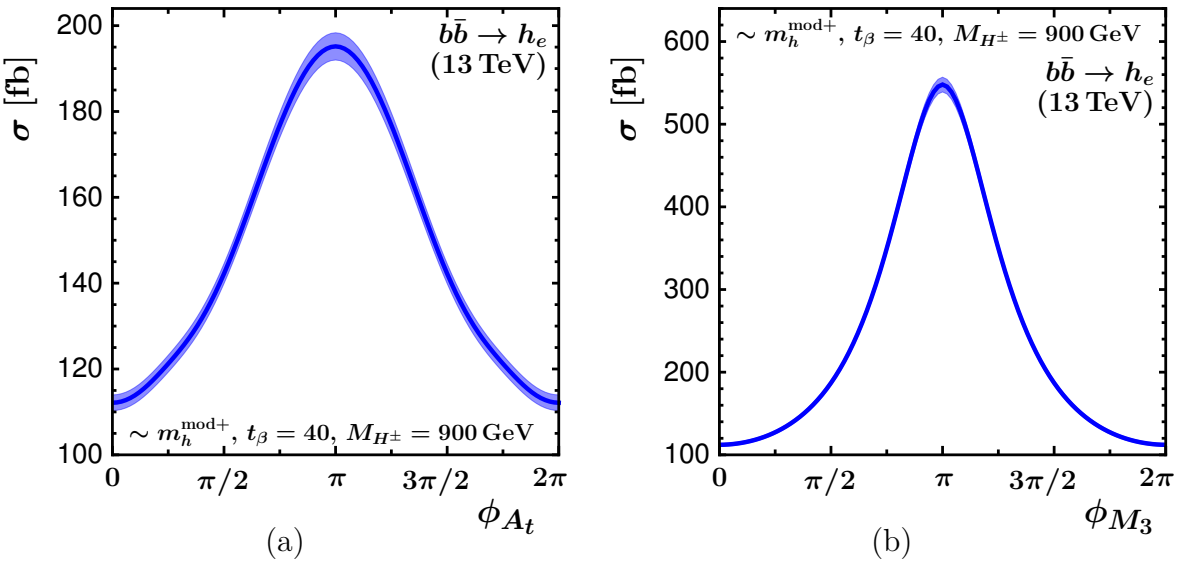

Figure 8.12: Bottom-quark annihilation cross section for h_e in fb as a function of (a) ϕ_{A_t} and (b) ϕ_{M_3} in the $m_h^{\text{mod+}}$-inspired scenario specified in Eq. (8.2) with $\tan\beta = 40$. The depicted uncertainties are scale uncertainties.

also briefly discuss the bottom-quark annihilation cross section for the $m_h^{\text{mod+}}$-inspired scenario with $\tan\beta = 40$. The corresponding cross section is shown in Fig. 8.12 as a function of ϕ_{A_t} and ϕ_{M_3}. For such a large value of $\tan\beta$ this cross section exceeds the gluon-fusion cross section by far. It shows a very significant dependence on the phases ϕ_{A_t} and ϕ_{M_3}, which is mainly induced by the Δ_b contribution.

8.6 Theoretical uncertainties

In the previous section we analysed the behaviour of our cross section predictions with $\mathcal{CP}$-violating effects entering via squark loop contributions, $\hat{\mathbf{Z}}$ factors and Δ_b contributions. Therein, we included renormalisation and factorisation scale uncertainties, which as expected are reduced upon inclusion of higher-order corrections. However, the cross section predictions are also affected by other relevant theoretical uncertainties, which will be discussed in detail in this section.

Some of the theoretical uncertainties of cross sections in the MSSM with complex parameters are very similar to the ones in the MSSM with real parameters as discussed in Ref. [274]. Therefore, we can directly transfer the discussion of PDF+α_s uncertainties as well as the uncertainty associated with the renormalisation prescription for the bottom-quark Yukawa coupling from the case of the MSSM with real parameters.

PDF+α_s uncertainties

The inexact knowledge of the proton PDFs affects the cross section predictions at the hadron level. Uncertainties due to PDFs can arise not only due to the fact that the PDFs are fitted from experimental data whose experimental errors permeates the prediction of any PDF-dependent quantity, but they also arise from the fitting methodology and mathematical representation used, which can create an ambiguity in the predictions. PDF uncertainties are of particular significance for the prediction of bottom-quark annihilation cross sections. The bottom mass effects need to be included consistently in the evolution of the PDFs according to the DGLAP equations. The transition between the 4FS and 5FS occurs at a matching scale set to the bottom mass, on which the bottom density in the proton is dependent. This consequently affects the cross section prediction.

The uncertainty due to experimental errors in the data from which the PDFs are extracted are estimated as follows: The PDF collaborations introduce N different replicas of PDF sets which can equivalently describe the data from a statistical point of view. To get the uncertainty associated with the experimental data and the fitting methodology, an observable must then be computed N different times to obtain the spread in its values. Moreover, there is an additional source of uncertainty arising from the choice for the input value of the strong coupling constant α_s. The recommended central value of $\alpha_s(m_Z)$ is different for each PDF set, which also results in a spread of calculated values

depending on the PDF set employed. Since the gluon-fusion cross section is proportional to α_s^2 at LO with QCD corrections of $\mathcal{O}(\alpha_s^3)$ at NLO, these uncertainties are very relevant.

Ref. [279] first discussed the correlation and combination of PDF and α_s (PDF+α_s) uncertainties. In Refs. [164, 274] it was observed that the relative size of PDF+α_s uncertainties does not depend on the details of the partonic process, but only on the Higgs mass, even upon inclusion of supersymmetric effects of squarks. We will therefore not discuss them in more detail, since – similar to the prescription for MSSM Higgs boson cross sections by the LHC Higgs Cross Section Working Group [92] – relative uncertainties can be taken over from tabulated relative uncertainties obtained for the SM Higgs boson or a $\mathcal{CP}$-odd Higgs (in a 2HDM with $\tan\beta = 1$) as a function of its mass.

In our calculation we employ the `MMHT2014` PDF sets at LO, NLO, NNLO and N^{3}LO [273], which can be used for both gluon fusion and bottom-quark annihilation. For Higgs masses in the range between 50 GeV and 1 TeV the typical size of PDF+α_s uncertainties for gluon fusion is $\pm(3-5)\%$ following the prescription of Ref. [280]. They increase up to $\pm 10\%$ for Higgs masses up to 2 TeV. For bottom-quark annihilation they are in the range $\pm(3-8)\%$ for Higgs masses between 50 GeV and 1 TeV and up to $\pm 16\%$ for Higgs masses below 2 TeV.

Renormalisation of the bottom-quark mass and definition of the bottom-Yukawa coupling

In our calculation, the bottom-quark mass is renormalised on-shell, and the bottom-Yukawa coupling is obtained from the bottom-quark mass as described in Section 6.4.1. The renormalisation of the bottom-quark mass and the freedom in the definition of the bottom-Yukawa coupling are known to have a sizeable numerical impact on the cross section predictions. This is in particular the case for large values of $\tan\beta$ where the bottom-Yukawa coupling of the heavy Higgs bosons is significantly enhanced and the top-quark Yukawa coupling is suppressed. On the other hand, in these regions of parameter space bottom-quark annihilation is the dominant process, for which there is less ambiguity regarding an appropriate choice for the renormalisation scale. The described uncertainties in the MSSM with complex parameters are analogous to the case of real parameters. We therefore refer to the discussion in Ref. [274] and references therein for further details.

8.6.1 Remaining theoretical uncertainties

The approximate NNLO stop-quark contributions and accordingly the uncertainty associated with the approximation of the involved Wilson coefficients, which was discussed in Ref. [274], are neglected in our analysis. The impact of the NNLO stop-quark contributions for the case of the MSSM with real parameters can be compared with our estimate for the renormalisation and factorisation scale uncertainty of our calculation.

As an example, the NNLO stop-quark contributions lower the inclusive cross section for the light Higgs boson by about 2 pb for zero phases in the light-stop inspired scenario, which is at the lower edge of the scale uncertainty depicted in Fig. 8.1 (b).

Other uncertainties discussed in Ref. [274] are renormalisation and factorisation scale uncertainties and an uncertainty related to higher-order contributions to Δ_b. Moreover, we add another uncertainty related to the performed interpolation of supersymmetric NLO QCD contributions. We discuss in the following our estimates for the three previously mentioned uncertainties:

Scale uncertainties: The complete all-order result for a hadronic cross section would be independent of the renormalisation and factorisation scales[2] μ_R and μ_F. However, the cross section at a fixed order of perturbation has a dependence on μ_R and μ_F, which is usually one order higher than the accuracy of the calculation. For a calculation at a given order, the choice of scales is usually arbitrary, and is fixed at some central value for μ_R and μ_F which is characteristic for the hard process. The variation of scales around the central values gives us an estimate of the size of the excluded higher-order contributions. We obtain the renormalisation and factorisation scale uncertainty as follows: The central scale choice is $(\mu_\mathrm{R}^0, \mu_\mathrm{F}^0) = (M_{h_a}/2, M_{h_a}/2)$ for gluon fusion and $(\mu_\mathrm{R}^0, \mu_\mathrm{F}^0) = (M_{h_a}, M_{h_a}/4)$ for bottom-quark annihilation. We obtain the scale uncertainty by taking the maximal deviation from the central scale choice $\Delta\sigma$ obtained from the additional scale choices:

$$(\mu_\mathrm{R}, \mu_\mathrm{F}) \in \{(2\mu_\mathrm{R}^0, 2\mu_\mathrm{F}^0), (2\mu_\mathrm{R}^0, \mu_\mathrm{F}^0), (\mu_\mathrm{R}^0, 2\mu_\mathrm{F}^0), (\mu_\mathrm{R}^0, \mu_\mathrm{F}^0/2), (\mu_\mathrm{R}^0/2, \mu_\mathrm{F}^0), (\mu_\mathrm{R}^0/2, \mu_\mathrm{F}^0/2)\}$$

We perform this procedure individually for all three cross sections in Eq. (7.4) and then obtain the overall absolute uncertainty through

$$\Delta\sigma^\mathrm{scale} = \sqrt{\left(\Delta\sigma_{\mathrm{N}^k\mathrm{LO}}^{\Delta_{b1}}\right)^2 + \left(\Delta\sigma_\mathrm{LO}^{\Delta_{b2}} - \Delta\sigma_\mathrm{LO}^{\Delta_{b1}}\right)^2}, \tag{8.4}$$

where we assume the two LO cross sections to be fully correlated. The uncertainty bands that we have displayed in the plots shown in the previous sections correspond to the cross section range covered by $\sigma \pm \Delta\sigma^\mathrm{scale}$.

Δ_b uncertainty: Here we largely follow the discussion presented in Ref. [274]. The value for Δ_b used in our analysis is obtained from `FeynHiggs`, which also contains electroweak contributions to Δ_b. One can improve the calculation of Δ_b corrections by including other one-loop contributions such as those arising from diagrams with stops and charginos, controlled by the top-Yukawa coupling. The calculation of Δ_b effects can further be extended by including dominant two-loop contributions. Refs. [198, 199, 281] showed that the one-loop result for Δ_b is quite sensitive to the scales at which the strong, gauge, and top-Yukawa couplings are expressed. This can be stabilised by including two-loop contributions. The one-loop sbottom-gluino and stop-chargino contributions to Δ_b

[2] While this is true in principle, note however that since the PDFs are fitted from data it is hard to get rid of the μ_F dependence fully.

vary by around ±10% when the renormalisation scales are lowered or raised by a factor of two around their central values.

Therefore, in order to display the propagation of an uncertainty arising from higher-order contributions to Δ_b to our cross section calculation, we vary the value of Δ_b obtained from `FeynHiggs` by ±10%. We label the obtained uncertainty as $\Delta\sigma^{\text{resum}}$ and assign an uncertainty band of $\sigma \pm \Delta\sigma^{\text{resum}}$.

Interpolation uncertainty: The employed interpolation for the two-loop virtual squark–gluino contributions following Eq. (6.57) leads to a further uncertainty. A conservative estimate for it can be obtained as follows: We determine the cross section $\sigma(\phi_z)$ following Eq. (7.1) not only for the correct phase ϕ_z in Eq. (6.57), but also leave the phase within Eq. (6.57) constant, i.e. fixed to 0 and π. We call the obtained cross sections $\sigma(0)$ and $\sigma(\pi)$. For each value of ϕ_z we take the difference $\Delta\sigma^{\text{int}} = \sin^2(\phi_z)|\sigma(0) - \sigma(\pi)|/2$. It is reweighted with $\sin^2(\phi_z)$, since we know that our result is correct at phases 0 and π. The obtained uncertainty band is given by $\sigma \pm \Delta\sigma^{\text{int}}$.

In the following we display the effects of the estimated uncertainties for certain scenarios, where we choose the displayed scenarios and the displayed cross sections such that the effect of the uncertainties is largest. While the scale uncertainties were included in all previous figures for the LO prediction as well as for our best prediction already, we will discuss the interpolation uncertainty for the light-stop inspired scenario with $\tan\beta = 16$ and the resummation uncertainty for the $m_h^{\text{mod+}}$-inspired scenario with $\tan\beta = 40$.

Fig. 8.13 shows the renormalisation and factorisation scale uncertainties $\Delta\sigma^{\text{scale}}$ as before and in addition the above described interpolation uncertainty $\Delta\sigma^{\text{int}}$, which in case of the variation of ϕ_{M_3} can be substantial. As can be seen in Fig. 8.13, the interpolation uncertainty obtained from our conservative estimate can in this scenario even exceed the scale uncertainty for the gluon-fusion cross section of h_2. It should be noted that this is an extreme case, while the interpolation uncertainty, which is an NLO effect related to the squark and gluino loop contributions, remains small for the other previously described scenarios (which we do not show here explicitly). This is simply a consequence of the fact that the relative impact of the squark and gluino contributions in the other scenarios is much smaller than in the light-stop inspired scenario.

The interpolation uncertainty for the gluon-fusion cross section of h_3 in Fig. 8.13 is much less pronounced than for h_2, since as discussed above the squark loop corrections are significantly smaller in this case and would vanish if h_3 were a pure $\mathcal{CP}$-odd state. The behaviour in the lower panels of Fig. 8.13 displays the fact that by construction the assigned interpolation uncertainty vanishes for the phases 0 and π, where the interpolated result in the MSSM with complex parameters merges the known result of the MSSM with real parameters and thus reflects the $\sin^2\phi_z$ behaviour. For the variation of ϕ_{A_t} the LO cross section incorporating squark contributions already includes the dominant effect on the cross section, such that the uncertainty due to the interpolated NLO contributions is also less pronounced than in case of the variation of ϕ_{M_3}.

The described Δ_b uncertainties are depicted in Fig. 8.14. Since Δ_b crosses 0 as a function of ϕ_{M_3} twice, the uncertainty that we have associated to it according to the prescription discussed above also vanishes there, as can be seen in the lower panel of Fig. 8.14(b). Even for the large value of $\tan\beta$ chosen here the assigned Δ_b uncertainty of $\pm 10\%$ is much smaller than the scale uncertainty of the displayed cross sections. Despite the different behaviour with the phases ϕ_{A_t} and ϕ_{M_3} displayed in the lower panel of Fig. 8.14 the qualitative effect of the resummation uncertainties on the Higgs boson production cross sections is nevertheless rather similar. The latter is also true for the bottom-quark annihilation cross section, which is not depicted here. The resummation uncertainties are of most relevance for large values of $\tan\beta$, where the cross section of bottom-quark annihilation exceeds the gluon-fusion cross section.

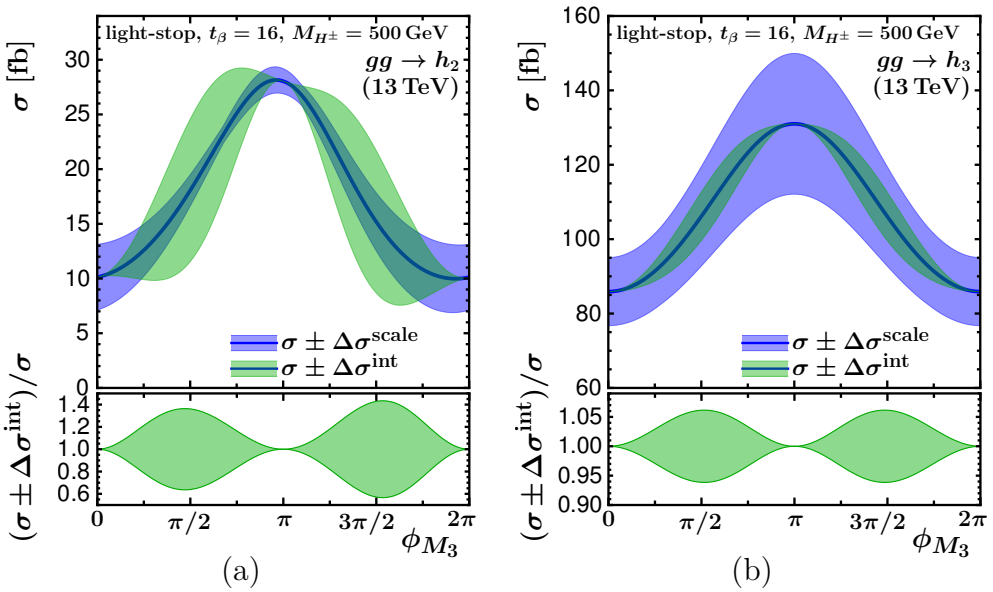

Figure 8.13: Renormalisation and factorisation scale uncertainties $\Delta\sigma^{\text{scale}}$ (blue) and interpolation uncertainties $\Delta\sigma^{\text{int}}$ (green) for the gluon-fusion cross section of (a) h_2 and (b) h_3 as a function of ϕ_{M_3} in the light-stop inspired scenario specified in Eq. (8.1). In the lower panel the upper and lower edge of the band of the cross section prediction with the assigned interpolation uncertainty is normalised to the cross section without this uncertainty.

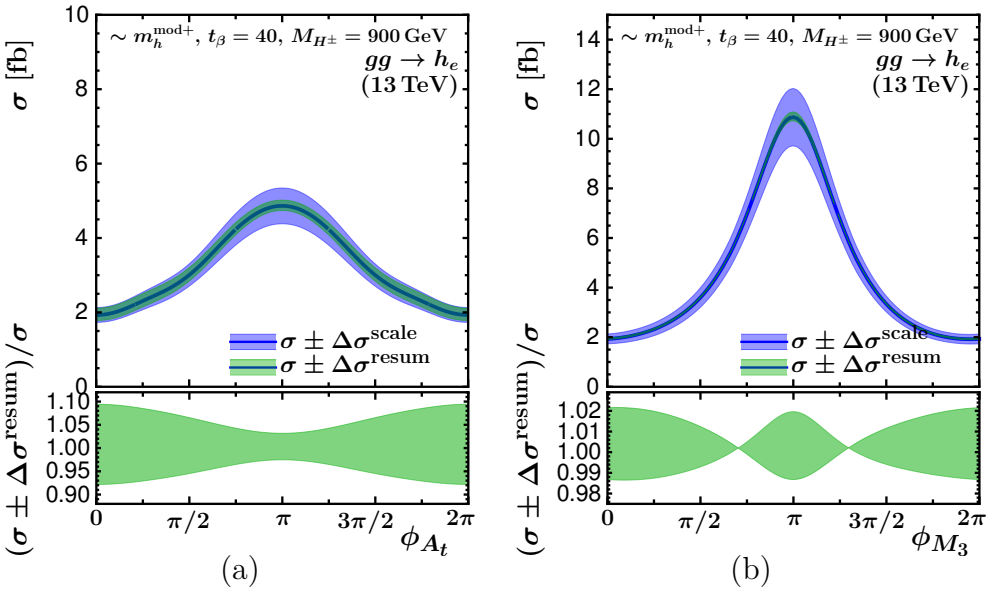

Figure 8.14: Renormalisation and factorisation scale uncertainties $\Delta\sigma^{\text{scale}}$ (blue) and resummation uncertainties $\Delta\sigma^{\text{resum}}$ (green) for the gluon-fusion cross section of h_e as a function of (a) ϕ_{A_t} and (b) ϕ_{M_3} in the $m_h^{\text{mod+}}$-inspired scenario specified in Eq. (8.2) for $\tan\beta = 40$. In the lower panel the upper and lower edge of the band of the cross section prediction with the assigned resummation uncertainty is normalised to the cross section without this uncertainty.

Chapter 9

Impact of interference effects on MSSM Higgs searches

This chapter discusses the effects of $\mathcal{CP}$-violating mixing and interference between the Higgs bosons of the MSSM with complex parameters on exclusion limits from the LHC. We will set up the analytical framework for calculating the interference terms in the full process of Higgs production and decay, following Refs. [32,33,138,277], and describe their implementation in `SusHiMi`*. Finally, we will present a numerical study of interference effects with a proposed benchmark scenario for $\mathcal{CP}$-violating MSSM Higgs searches at the LHC. The results presented in this chapter are based on ongoing work.*

9.1 Introduction

So far we have focussed our studies on effects of the complex parameters of the MSSM on individual cross sections of the neutral Higgs bosons h_1, h_2 and h_3. These parameters impact the cross section predictions through $\mathcal{CP}$-violating Higgs–sfermion couplings, complex Yukawa couplings, and the mixing of tree-level Higgs states described by the application of $\hat{\mathbf{Z}}$ factors to the external Higgs bosons. However, as we saw in Section 8.4, in scenarios where the two heavy Higgs bosons, h_2 and h_3, are nearly mass degenerate and strongly admixed, it may no longer be possible to experimentally resolve the two states as discernible signals. The measured quantity in this case is the total cross section times branching ratio ($\sigma\times$BR) of h_2 and h_3 combined. The amplitude of the full process of production and decay of the two Higgs states contains non-zero interference terms, which would vanish for the case where all the parameters of the theory are real.

In order to accurately interpret the experimental limits on $\sigma\times$BR from Higgs searches at the LHC, it is therefore crucial to also account for these interference contributions in their predictions, which could significantly enhance or diminish the value of $\sigma\times$BR in comparison to their values for the $\mathcal{CP}$-conserving case. At the LHC, all searches for additional heavy Higgs bosons that are interpreted in specific scenarios assume that the signal contributions from different Higgs bosons can be added incoherently, i.e. without any interference effects. In the MSSM with real parameters, where the physical states

are the $\mathcal{CP}$-eigenstates h, H and A, interference can occur only between the $\mathcal{CP}$-even Higgs bosons h and H, and any interference contributions between the $\mathcal{CP}$-even and $\mathcal{CP}$-odd Higgs states are absent. However, if we allow for $\mathcal{CP}$ violation, the tree-level mass eigenstates can mix and all three loop-corrected mass eigenstates can interfere. Such interference effects are especially significant when the mass splitting between the Higgs bosons is smaller than the sum of their total widths and they are strong admixtures of $\mathcal{CP}$-even and $\mathcal{CP}$-odd states, as is the case for h_2 and h_3 in the $m_h^{\text{mod}+}$-inspired scenario with $\tan\beta = 10$ in Section 8.4. In this chapter, we present the calculation of these interference effects and discuss their impact on the MSSM Higgs searches carried out at the LHC. In particular, we will study the modification of current exclusion bounds when $\mathcal{CP}$-violating interference effects are taken into account in the predictions for Higgs production and decay.

9.2 Use of $\hat{\mathbf{Z}}$ factors for internal Higgs bosons

In Chapters 5 and 6, we discussed the use of the $\hat{\mathbf{Z}}$ factors to calculate amplitudes and cross sections of *external*, on-shell Higgs bosons. Although the $\hat{\mathbf{Z}}$ matrix was introduced for the correct normalisation of external Higgs bosons, it is also applicable to *internal* Higgs bosons appearing between two vertices, in order to account for higher-order mixing properties [277]. For this, we employ the formalism developed in Refs. [33, 138, 277]. Recall the propagator matrix $\boldsymbol{\Delta}_{hHA}(p^2)$ defined in Eq. (5.6). The elements of $\boldsymbol{\Delta}_{hHA}$ are the propagators $\Delta_{ij}(p^2)$, which start as Higgs state i and end on Higgs state j, with all permutations of mixings in between. The off-diagonal propagators of the propagator matrix can be expanded around the three complex poles $\mathcal{M}_a^2, \mathcal{M}_b^2$ and $\mathcal{M}_c^2$. First, we carry out the expansion around $p^2 \simeq \mathcal{M}_a^2$ as follows [33],

$$\Delta_{ij}(p^2) = \frac{\Delta_{ij}(p^2)}{\Delta_{ii}(p^2)}\Delta_{ii}(p^2) \simeq \hat{Z}_{aj}\hat{\mathbf{Z}}_{ai}^2\Delta_a^{\text{BW}}(p^2) = \hat{\mathbf{Z}}_{aj}\hat{\mathbf{Z}}_{ai}\Delta_a^{\text{BW}}(p^2)\,, \tag{9.1}$$

where we use the Breit-Wigner propagator with constant width defined as

$$\Delta_a^{\text{BW}}(p^2) := \frac{i}{p^2 - \mathcal{M}_a^2} = \frac{i}{p^2 - M_{h_a}^2 + iM_{h_a}\Gamma_{h_a}}\,. \tag{9.2}$$

The second equivalence in Eq. (9.1) is obtained through the expansion of the diagonal propagator around $p^2 \simeq \mathcal{M}_a^2$ derived in Eq. (5.34),

$$\Delta_{ii}(p^2) = \frac{i}{p^2 - \mathcal{M}_a^2} \cdot \frac{1}{1 + \hat{\Sigma}_{ii}^{\text{eff}\prime}(\mathcal{M}_a^2)}\,. \tag{9.3}$$

We can recognise the first term on the right-hand side of Eq. (9.3) as the Breit-Wigner propagator from Eq. (9.2). Furthermore, we use the index notation defined in Eq. (5.37)

to identify the second term as $\hat{Z}_a$. This results in the expression

$$\Delta_{ii}(p^2) \simeq \Delta_a^{\mathrm{BW}}(p^2)\hat{Z}_a = \Delta_a^{\mathrm{BW}}(p^2)\hat{\mathbf{Z}}_{ai}^2 \,. \tag{9.4}$$

For the final equivalence $\hat{Z}_{aj}\hat{\mathbf{Z}}_{ai}^2\Delta_a^{\mathrm{BW}}(p^2) = \hat{\mathbf{Z}}_{aj}\hat{\mathbf{Z}}_{ai}\Delta_a^{\mathrm{BW}}(p^2)$ in Eq. (9.1), we make use of the fact that $\hat{\mathbf{Z}}_{ai} = \sqrt{\hat{Z}_a}$ and $\hat{\mathbf{Z}}_{aj} = \sqrt{\hat{Z}_a}\hat{Z}_{aj}$, following Eq. (5.37).

Similarly, $\Delta_{ij}(p^2)$ can also be expanded around the poles $\mathcal{M}_b^2$ and $\mathcal{M}_c^2$. Since the $\hat{\mathbf{Z}}$ factors are scheme invariant [33], for the expansion around the poles $p^2 \simeq \mathcal{M}_b^2$ and $p^2 \simeq \mathcal{M}_c^2$, we switch to a scheme where the index i is associated with state b, and c, respectively,

$$\Delta_{ij}(p^2) = \hat{\mathbf{Z}}_{bi}\Delta_b^{\mathrm{BW}}(p^2)\hat{\mathbf{Z}}_{bj} \,, \tag{9.5}$$

$$\Delta_{ij}(p^2) = \hat{\mathbf{Z}}_{ci}\Delta_c^{\mathrm{BW}}(p^2)\hat{\mathbf{Z}}_{cj} \,. \tag{9.6}$$

It is therefore possible to approximate the resonant contribution to the propagators close to one of the poles by a combination of the corresponding Breit-Wigner propagator and the $\hat{\mathbf{Z}}$ factors calculated at that pole. In order to account for possibly overlapping resonances, the approximation can be extended to a general case by summing all three expansions of the propagators,

$$\Delta_{ij}(p^2) \simeq \sum_{a=1}^{3} \hat{\mathbf{Z}}_{ai}\Delta_a^{\mathrm{BW}}(p^2)\hat{\mathbf{Z}}_{aj} \,, \tag{9.7}$$

as visualised in Fig. 9.1. Here the non-unitary $\hat{\mathbf{Z}}$ factors quantify the transition between the states i and h_a. From Eq. (9.7), we see that the main momentum dependence is contained in the Breit-Wigner propagators $\Delta_a^{\mathrm{BW}}(p^2)$, $a \in \{1, 2, 3\}$. Furthermore, Eq. (9.7) also covers the possibilities where $\mathcal{CP}$ is conserved and only the $\mathcal{CP}$-even eigenstates mix, in which case $\hat{\mathbf{Z}}_{3h}$ and $\hat{\mathbf{Z}}_{3H}$ are zero. Similarly, if $\mathcal{CP}$ is violated but the theory is in the decoupling regime such that h_1 is mostly $\mathcal{CP}$-even and the mass splitting between h_1 and $h_{2,3}$ is very large, then $\hat{\mathbf{Z}}_{1H}$ and $\hat{\mathbf{Z}}_{1A}$ are close to zero.

Consider a physical process involving the production and decay of Higgs bosons, where they appear as internal particles exchanged between the production vertex X and decay

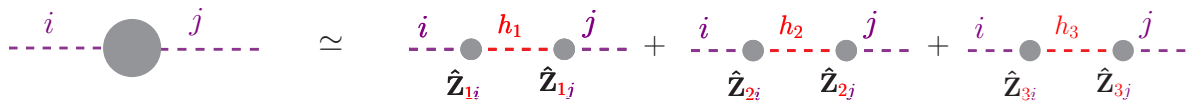

Figure 9.1: The full mixing propagators illustrated as a sum of the Breit-Wigner propagators combined with $\hat{\mathbf{Z}}$ factors to account for the change of state from lowest-order mass eigenstate i to loop-corrected mass eigenstate h_a. See also Ref. [138].

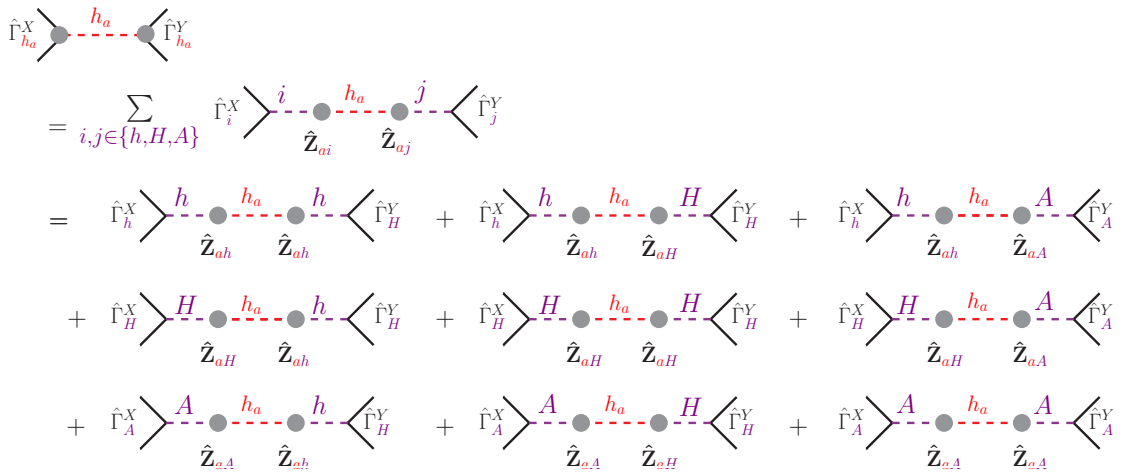

Figure 9.2: Pictorial representation of the amplitude for a process containing an internal exchange of Higgs boson h_a. All the diagrams contributing to the sum in Eq. (9.12) are shown, with the Breit-Wigner propagator $\Delta_a^{\mathrm{BW}}(p^2)$ for the state h_a denoted by the internal red line. Its transition from and into the tree-level states i and j is represented by the violet lines connected to the vertices [138].

vertex Y. In such a process, contributions from all permutations of the mixing propagators $\Delta_{ij}(p^2)$ need to be taken into account when calculating the full amplitude. From Fig. 9.1, we can count 27 diagrams that would contribute to the amplitude if we account for all possible combinations of i and j. The total amplitude is expressed as a sum over the irreducible vertex functions for a coupling of the Higgs i at the first vertex X ($\hat{\Gamma}_i^X$) and the irreducible vertex functions for a coupling of the Higgs j at the second vertex Y ($\hat{\Gamma}_j^Y$), combined with the momentum-dependent mixing propagators $\Delta_{ij}(p^2)$ from Eq. (9.7) [138]:

$$\mathcal{A} = \sum_{i,j\in\{h,H,A\}} \hat{\Gamma}_i^X \Delta_{ij}(p^2) \hat{\Gamma}_j^Y \simeq \sum_{i,j\in\{h,H,A\}} \hat{\Gamma}_i^X \left[\sum_{a=1}^{3} \hat{\mathbf{Z}}_{ai} \Delta_a^{\mathrm{BW}}(p^2) \hat{\mathbf{Z}}_{aj}\right] \hat{\Gamma}_j^Y \tag{9.8}$$

$$= \sum_{a=1}^{3} \left(\sum_{i\in\{h,H,A\}} \hat{\mathbf{Z}}_{ai} \hat{\Gamma}_i^X\right) \Delta_a^{\mathrm{BW}}(p^2) \left(\sum_{j\in\{h,H,A\}} \hat{\mathbf{Z}}_{aj} \hat{\Gamma}_j^Y\right) \tag{9.9}$$

$$= \sum_{a=1}^{3} \hat{\Gamma}_{h_a}^X \Delta_a^{\mathrm{BW}}(p^2) \hat{\Gamma}_{h_a}^Y . \tag{9.10}$$

In the last line we have expressed the one-particle irreducible vertex functions $\hat{\Gamma}_{h_a}$ as a linear combination of the vertex functions of the lowest-order states using $\hat{\mathbf{Z}}$ factors, analogous to Eq. (5.43),

$$\hat{\Gamma}_{h_a} = \hat{\mathbf{Z}}_{ah} \hat{\Gamma}_h + \hat{\mathbf{Z}}_{aH} \hat{\Gamma}_H + \hat{\mathbf{Z}}_{aA} \hat{\Gamma}_A + \cdots , \tag{9.11}$$

where the ellipsis denotes additional mixing contributions from Goldstone and vector bosons, which are neglected here. From Eq. (9.10), the contribution of a single resonance h_a can be expressed as

$$\mathcal{A}_{h_a} = \hat{\Gamma}^X_{h_a} \Delta^{\mathrm{BW}}_a(p^2) \hat{\Gamma}^Y_{h_a} \tag{9.12}$$

$$= \sum_{i,j\in\{h,H,A\}} \left(\hat{\Gamma}^X_i \hat{\mathbf{Z}}_{ai}\right) \Delta^{\mathrm{BW}}_a(p^2) \left(\hat{\mathbf{Z}}_{aj} \hat{\Gamma}^Y_j\right) \tag{9.13}$$

$$= \sum_{i,j\in\{h,H,A\}} \hat{\Gamma}^X_i \left(\hat{\mathbf{Z}}_{ai} \Delta^{\mathrm{BW}}_a(p^2) \hat{\mathbf{Z}}_{aj}\right) \hat{\Gamma}^Y_j \,. \tag{9.14}$$

Eq. (9.12)–Eq. (9.14) can be pictorially represented as shown in Fig. 9.2.

9.3 Interference effects in Higgs production and decay

In the previous section, we discussed the treatment of Higgs bosons appearing as internal propagators between two vertices X and Y. We now consider a full process of Higgs production and decay and calculate the interference of amplitudes in an s-channel exchange of the Higgses h_1, h_2 and h_3 in a generic $2 \to 2$ parton level process

$$I \to h_1, h_2, h_3 \to F \,, \tag{9.15}$$

with the initial state I denoting the production process and final state F denoting the decay products. Later on, we will apply this to specific production and decay mechanisms.

The calculation of the interference factors is carried out at leading order taking into account Higgs masses, total widths, and $\hat{\mathbf{Z}}$ factors from `FeynHiggs` computed with full one-loop and leading two-loop contributions. State-of-the-art higher-order contributions are taken into account in the computation for production cross sections for I and branching ratios for F. For the QCD corrections, a factorisation of higher-order corrections between initial and final states is often justified. This only misses corrections connecting initial and final state particles. Therefore it is well motivated to apply the interference factor calculated at LO only, with the full process containing higher-order corrections.

The interference term for a process $I \to F$ with $h_{1,2,3}$ Higgs exchange is obtained from the difference between the coherent and incoherent sum of the $2 \to 2$ amplitudes,

$$|\mathcal{A}|^2_{\mathrm{int}} = |\mathcal{A}|^2_{\mathrm{coh}} - |\mathcal{A}|^2_{\mathrm{incoh}} \tag{9.16}$$

$$= \sum_{a<b} 2 \,\mathrm{Re}\left[\mathcal{A}_{h_a} \mathcal{A}^*_{h_b}\right] \tag{9.17}$$

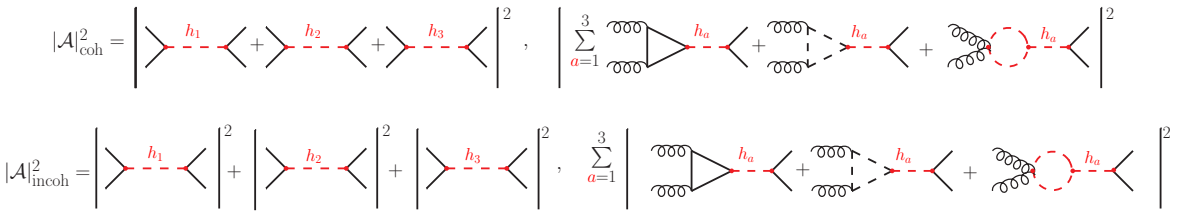

Figure 9.3: A pictorial representation of coherent and incoherent amplitudes in Eq. (9.18).

where the coherent and incoherent sums are defined as

$$|\mathcal{A}|^2_{\text{coh}} = \left|\sum_{a=1}^{3} \mathcal{A}_{h_a}\right|^2 , \qquad |\mathcal{A}|^2_{\text{incoh}} = \sum_{a=1}^{3} \left|\mathcal{A}_{h_a}\right|^2 . \tag{9.18}$$

The coherent sum of the partonic amplitudes therefore accounts for the interference between the amplitudes for production and decay of the three Higgs bosons h_1, h_2 and h_3. The coherent and incoherent sums of amplitudes are depicted for two example production processes in Fig. 9.3. Using the expression for $\mathcal{A}_{h_a}$ from Eq. (9.12) in Eq. (9.17) we obtain

$$|\mathcal{A}|^2_{\text{int}} = 2\text{Re}\left[\mathcal{A}_{h_1}\mathcal{A}^*_{h_2} + \mathcal{A}_{h_2}\mathcal{A}^*_{h_3} + \mathcal{A}_{h_1}\mathcal{A}^*_{h_3}\right] \tag{9.19}$$

$$\begin{aligned} = 2\text{Re}\Big[&\left(\hat{\Gamma}^I_{h_1}\Delta^{\text{BW}}_1(p^2)\hat{\Gamma}^F_{h_1}\right)\left(\hat{\Gamma}^I_{h_2}\Delta^{\text{BW}}_2(p^2)\hat{\Gamma}^F_{h_2}\right)^* \\ &+ \left(\hat{\Gamma}^I_{h_2}\Delta^{\text{BW}}_2(p^2)\hat{\Gamma}^F_{h_2}\right)\left(\hat{\Gamma}^I_{h_3}\Delta^{\text{BW}}_3(p^2)\hat{\Gamma}^F_{h_3}\right)^* \\ &+ \left(\hat{\Gamma}^I_{h_1}\Delta^{\text{BW}}_1(p^2)\hat{\Gamma}^F_{h_1}\right)\left(\hat{\Gamma}^I_{h_3}\Delta^{\text{BW}}_3(p^2)\hat{\Gamma}^F_{h_3}\right)^* \Big], \end{aligned} \tag{9.20}$$

where each vertex function $\hat{\Gamma}^{I,F}_{h_a}$ is expanded according to

$$\hat{\Gamma}^{I,F}_{h_a} = \sum_{i\in\{h,H,A\}} \hat{\mathbf{Z}}_{ai}\hat{\Gamma}^{I,F}_i . \tag{9.21}$$

For a scenario where we only consider mixing between the two heavy Higgses h_2 and h_3, Eq. (9.19) reduces to

$$|\mathcal{A}|^2_{\text{int}} = 2\text{Re}\left[\left(\hat{\Gamma}^I_{h_2}\Delta^{\text{BW}}_2(\hat{s})\hat{\Gamma}^F_{h_2}\right)\left(\hat{\Gamma}^I_{h_3}\Delta^{\text{BW}}_3(\hat{s})\hat{\Gamma}^F_{h_3}\right)^*\right], \tag{9.22}$$

which can be evaluated at the momentum $p^2 = \hat{s} = \left(\frac{M_{h_2}+M_{h_3}}{2}\right)^2$. However, this approach of evaluating the Breit-Wigner propagators at the squared average of the masses of the two heavy Higgses may not adequately account for all the phase space effects. For this reason, at partonic level we integrate Eq. (9.22) over s with

$$\sqrt{s}_{\text{min}} = \sqrt{\hat{s}} - 5\left(\frac{\hat{\Gamma}_{h_2}+\hat{\Gamma}_{h_3}}{2}\right), \quad \sqrt{s}_{\text{max}} = \sqrt{\hat{s}} + 5\left(\frac{\hat{\Gamma}_{h_2}+\hat{\Gamma}_{h_3}}{2}\right), \tag{9.23}$$

so that the interference term is given by the integral

$$\sigma(|\mathcal{A}|^2_{\text{int}}) = \int_{s_{\min}}^{s_{\max}} ds\ 2\text{Re}\left[\ \left(\hat{\Gamma}^I_{h_2}\Delta_2^{\text{BW}}(s)\hat{\Gamma}^F_{h_2}\right)\left(\hat{\Gamma}^I_{h_3}\Delta_3^{\text{BW}}(s)\hat{\Gamma}^F_{h_3}\right)^*\right]. \tag{9.24}$$

This covers the dominant fraction of a squared Breit-Wigner propagator. Similarly we define $\sigma_{\text{coh}} \equiv \sigma(|\mathcal{A}|^2_{\text{coh}})$ and $\sigma_{\text{incoh}} \equiv \sigma(|\mathcal{A}|^2_{\text{incoh}})$. Note that these cross sections miss a proper normalisation and the convolution with proton densities. However, those effects drop out in the subsequently discussed ratios of cross sections. The relative interference term for each production mode I and decay mode F is defined as

$$\eta^{IF} = \frac{\sigma^{IF}_{\text{int}}}{\sigma^{IF}_{\text{incoh}}}\,. \tag{9.25}$$

We can separate the total cross section for a given production mode I and decay channel F into the individual contribution from each Higgs boson σ_{h_a}, $a \in \{1,2,3\}$, and the contribution from the interference terms $\sigma_{\text{int}_{ab}}$, $a \neq b \in \{1,2,3\}$,

$$\sigma^{IF} = \sigma^{IF}_{h_1} + \sigma^{IF}_{h_2} + \sigma^{IF}_{h_3} + \sigma^{IF}_{\text{int}_{12}} + \sigma^{IF}_{\text{int}_{23}} + \sigma^{IF}_{\text{int}_{13}}\,. \tag{9.26}$$

We define the *relative* contribution to the cross section for a single Higgs h_a from its interference with the Higgses h_b and h_c as

$$\eta^{IF}_a = \frac{\sigma^{IF}_{\text{int}_{ab}}}{\sigma^{IF}_{h_a} + \sigma^{IF}_{h_b}} + \frac{\sigma^{IF}_{\text{int}_{ac}}}{\sigma^{IF}_{h_a} + \sigma^{IF}_{h_c}}\,. \tag{9.27}$$

With this definition the relative interference term is stable even when one of the contributions $\sigma^{IF}_{h_a}$ is suppressed. Using Eq. (9.27) in Eq. (9.26) results in the expression

$$\sigma^{IF} = \sigma^{IF}_{h_1}(1+\eta^{IF}_1) + \sigma^{IF}_{h_2}(1+\eta^{IF}_2) + \sigma^{IF}_{h_3}(1+\eta^{IF}_3)\,, \tag{9.28}$$

such that the total cross section for the full process is a sum of the cross sections of the individual Higgs bosons rescaled by their relative interference contributions. Therefore, the relative interference contributions η^{IF}_a can be used to approximately predict the experimentally measurable (coherent) $\sigma\times$BR as follows,

$$\sigma(pp \to I \to h_{1,2,3} \to F) \simeq \sum_{a=1}^{3} \sigma(pp \to I \to h_a)\cdot(1+\eta^{IF}_a)\cdot \text{BR}(h_a \to F)\,. \tag{9.29}$$

In the studies conducted in the following section, we make use of cross sections and interference factors obtained from `SusHiMi` and branching ratios from `FeynHiggs-2.13.0`. Currently `SusHiMi` implements the relative interference factors for the heavy Higgs bosons, η^{IF}_2 and η^{IF}_3, for the case where only h_2 and h_3 interfere using Eq. (9.27). The squared amplitude $|\mathcal{A}|^2_{\text{int}}$ used to obtain $\sigma_{\text{int}_{23}}$ is implemented using the expression from

Eq. (9.22) with the vertex functions expanded according to Eq. (9.21), and a numerical integration of $|\mathcal{A}|^2_{\text{int}}$ is performed using the limits described in Eq. (9.23).

At the current level of implementation in `SusHiMi`, it is possible to choose the production mode $I = b\bar{b}$ and the decay mode $F \in \{\tau^+\tau^-, b\bar{b}, t\bar{t}\}$. In our studies, we will consider the process $b\bar{b} \to h_2, h_3 \to \tau^+\tau^-$ where each h_a is an admixture of h, H, A. For this choice of I and F, the interference contribution to the squared amplitude is proportional to [32, 277]

$$|\mathcal{A}|^2_{\text{int}} \propto c_\beta^{-4}\ 2\text{Re}\left[(c_\alpha^2 \hat{\mathbf{Z}}_{2H}\hat{\mathbf{Z}}^*_{3H} + s_\beta^2 \hat{\mathbf{Z}}_{2A}\hat{\mathbf{Z}}^*_{3A})^2 \Delta_2^{\text{BW}}(s)\Delta_3^{\text{BW}}(s)\right] . \tag{9.30}$$

In the decoupling region, where the two heavy Higgses tend to be nearly mass-degenerate, i.e. $M_{h_2} \simeq M_{h_3}$ with similar widths $\Gamma_{h_2} \simeq \Gamma_{h_3}$, the product $\Delta_2^{\text{BW}}(s)\Delta_3^{\text{BW}*}(s) \simeq |\Delta_2^{\text{BW}}|^2$ is approximately real and $\cos\alpha \to \sin\beta$. Moreover, in this limit we get $\hat{\mathbf{Z}}_{2H} \simeq \hat{\mathbf{Z}}_{3A}$, $\hat{\mathbf{Z}}_{2A} \simeq -\hat{\mathbf{Z}}_{3H}$. Therefore, Eq. (9.30) simplifies to

$$|\mathcal{A}|^2_{\text{int}} \propto -8\tan^4\beta\ (\text{Im}\hat{\mathbf{Z}}_{2H}\text{Re}\hat{\mathbf{Z}}_{2A} - \text{Re}\hat{\mathbf{Z}}_{2H}\text{Im}\hat{\mathbf{Z}}_{2A})^2 |\Delta_2^{\text{BW}}(s)|^2 . \tag{9.31}$$

A non-zero interference term requires non-vanishing imaginary parts of the $\hat{\mathbf{Z}}$ factors. Furthermore, if $\mathcal{CP}$ is conserved, the interference term vanishes since $\hat{\mathbf{Z}}_{2A} = \hat{\mathbf{Z}}_{3H} = 0$. Notice also that $|\mathcal{A}|^2_{\text{int}}$ in Eq. (9.31) is negative, which means that in this limit the interference is expected to be destructive. In the next section, we will study scenarios which fulfil these conditions, and give rise to large interference contributions between the two heavy Higgs bosons.

9.4 Phenomenological effects of interference contributions

9.4.1 Definition of benchmark scenarios

In order to investigate the impact of $\mathcal{CP}$-violating interference contributions in $\sigma\times$BR calculations and their effect on the exclusion limits for heavy Higgs bosons at the LHC, we start by defining a benchmark scenario in accordance with the latest bounds on the masses of SUSY particles by ATLAS and CMS. This benchmark scenario, which we call the "$\mathcal{CP}$Int" scenario, contains two strongly admixed neutral heavy Higgs bosons h_2 and h_3, while the lightest neutral Higgs h_1 is interpreted to be the discovered Higgs state with a mass of about 125 GeV. We present our studies for two variations of the benchmark scenario. In each version of the scenario, the phases of complex parameters are kept fixed, and the behaviour of quantities such as the lightest Higgs mass, stop and sbottom masses, $\bar{b}b$ production cross sections and interference factors η is analysed in the $(M_{H^\pm}, \tan\beta)$ plane. For the first version of the scenario, denoted as "$\mathcal{CP}\text{Int}_1$" we choose the parameter values[1]

$$\begin{aligned}
&M_{\text{SUSY}} = 1.5\,\text{TeV}\,, \quad \mu = 1.5\,\text{TeV}\,,\\
&M_1 = 0.5\,\text{TeV}, \quad M_2 = 1\,\text{TeV}, \quad M_3 = 2.5\,\text{TeV}\,,\\
&A_t = \left(\tfrac{\mu}{\tan\beta} + 1.5\,M_{\text{SUSY}}\right)\cdot e^{i\frac{\pi}{4}}, \quad A_b = A_t, \quad A_\tau = |A_t|\,,\\
&M_{U_3} = M_{Q_3} = M_{D_3} = M_{L_{1,2}} = M_{E_{1,2}} = M_{\text{SUSY}}
\end{aligned} \tag{9.32}$$

and for the second version, denoted as "$\mathcal{CP}\text{Int}_2$", we choose

$$\begin{aligned}
&M_{\text{SUSY}} = 1.5\,\text{TeV}\,, \quad \mu = 1.5\,\text{TeV}\,,\\
&M_1 = 0.5\,\text{TeV}, \quad M_2 = 1\,\text{TeV}, \quad M_3 = 2.5\cdot e^{i\frac{\pi}{3}}\,\text{TeV}\,,\\
&A_t = \left(\tfrac{\mu}{\tan\beta} + 1.8\,M_{\text{SUSY}}\right)\cdot e^{i\frac{\pi}{4}}, \quad A_b = A_t, \quad A_\tau = |A_t|\,,\\
&M_{U_3} = M_{Q_3} = M_{D_3} = M_{\text{SUSY}}\,,\\
&M_{L_{1,2}} = M_{E_{1,2}} = 0.5\,\text{TeV}\,.
\end{aligned} \tag{9.33}$$

The Standard Model input parameters for both versions are

$$\begin{aligned}
&m_t = 172.5\,\text{GeV}, \qquad m_b = 4.18\,\text{GeV},\\
&M_W = 80.385\,\text{GeV}, \quad M_Z = 91.1876\,\text{GeV},\\
&\alpha_s(m_Z) = 0.118\,,
\end{aligned} \tag{9.34}$$

[1] A detailed record of the parameter values for each scenario can be found in Appendix B.

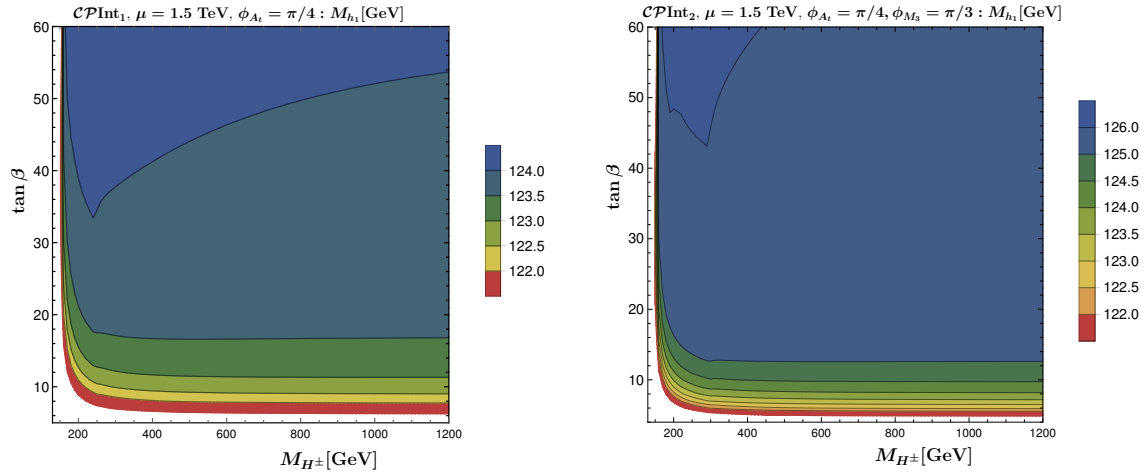

Figure 9.4: Mass of the lightest neutral Higgs h_1 in GeV as a function of $M_{H^\pm}$ and $\tan\beta$ for the $\mathcal{CP}\text{Int}_1$ and $\mathcal{CP}\text{Int}_2$ scenarios.

in accordance with the recommendations in Ref. [92]. In both the scenarios, the phases of the parameters $A_t = A_b$ and M_3 have been chosen to be non-maximal in view of the impact of bounds from EDMs. Fig. 9.4 depicts the mass of the lightest Higgs boson h_1 for the two scenarios in the $(M_{H^\pm}, \tan\beta)$ plane, obtained with `FeynHiggs-2.13.0` at two-loop level with NNLL resummation. In both cases, the mass M_{h_1} is within 125 ± 3 GeV for most of the $(M_{H^\pm}, \tan\beta)$ plane except for very low values of $\tan\beta$ and $M_{H^\pm}$. A mass prediction in this region appears to be phenomenologically viable in view of the current theoretical uncertainties from unknown higher-order corrections [65, 68, 92, 275, 276]. While for the $\mathcal{CP}\text{Int}_1$ scenario the predicted mass stays equal to or below 124 GeV throughout the $(M_{H^\pm}, \tan\beta)$ plane, for $\mathcal{CP}\text{Int}_2$ it reaches a maximum of about 126 GeV for the region of large $\tan\beta$ and small $M_{H^\pm}$.

In view of the latest experimental bounds on stop masses, the scenarios have been defined such that these masses are well above a TeV. For the $\mathcal{CP}\text{Int}_1$ and $\mathcal{CP}\text{Int}_2$ scenarios, the lightest stop mass varies with $\tan\beta$ by a couple of GeV around the values of 1.37 TeV and 1.34 TeV, respectively. The small variation in the stop masses with $\tan\beta$ can be understood from the fact that we choose a phase for A_t but not for μ, such that $|X_t|$ is not constant. Moreover, the lightest sbottom mass, $m_{\tilde{b}_1}$, in the $\mathcal{CP}\text{Int}$ scenarios is well above 1.3 TeV, which is in accordance with the latest search results, see for e.g. Refs. [96, 282]. In the $\mathcal{CP}\text{Int}_1$ scenario, the sbottom mass ranges from 1.38–1.5 TeV, a variation of 120 GeV. Similarly, in the $\mathcal{CP}\text{Int}_2$ scenario the sbottom mass varies up to a 100 GeV with $\tan\beta$. This relatively large variation with $\tan\beta$ takes place because in the sbottom sector the relevant parameter entering the mass matrix is $(\mu \tan\beta)$.

9.4.2 $b\bar{b}$ cross sections and interference terms in the $\mathcal{CP}$Int scenarios

Having seen the properties of $M_{h_1}, m_{\tilde{t}_1}$ and $m_{\tilde{b}_1}$ in the $\mathcal{CP}$Int scenarios, we compare the individual production cross sections $\sigma(b\bar{b} \to h_a)$ in the case where the mass eigenstates h_a undergo a full 3×3 mixing between h, H and A, with the case of a $\mathcal{CP}$-conserving 2×2 mixing. We will only show these cross sections for the Higgs h_2, with the plots for h_3 being qualitatively very similar. Due to the non-unitarity of the $\hat{\mathbf{Z}}$ factor matrix, individual cross sections of the admixed Higgs bosons can undergo significant enhancement in comparison to the case where no $\mathcal{CP}$-violating mixing takes place. This is in particular true when the admixture between the Higgs bosons is large, and the off-diagonal and imaginary parts of the $\hat{\mathbf{Z}}$ matrix become substantial, as is the case in the scenarios considered here. In the decoupling limit, where the lightest Higgs is mostly $\mathcal{CP}$-even and its mixing with the heavy Higgses can be neglected, the cross sections of h_2 and h_3 scale as $|\hat{\mathbf{Z}}_{aH}|^2|\mathcal{A}_H|^2 + |\hat{\mathbf{Z}}_{aA}|^2|\mathcal{A}_A|^2$ for $a \in \{2, 3\}$. Since the elements of the $\hat{\mathbf{Z}}$ matrix can be greater than one, this can lead to the cross section of h_a being larger than that of H and A individually.

This effect can be seen in Fig. 9.5 (a)–(d), which depict the bottom-quark annihilation cross sections for h_2. Fig. 9.5 (a) shows the $b\bar{b}$ cross section for h_2 in the $\mathcal{CP}\text{Int}_1$ scenario where all parameters are real and only a 2×2 mixing is allowed between the $\mathcal{CP}$-even states h and H. On the other hand, Fig. 9.5 (b) shows the $b\bar{b}$ cross section for h_2 with the full 3×3 mixing in the $\mathcal{CP}\text{Int}_1$ scenario with complex phase $\phi_{A_t} = \pi/4$. Fig. 9.5 (c) and (d) show the same quantities for the $\mathcal{CP}\text{Int}_2$ scenario, where in Fig. 9.5 (c) all phases are zero and in Fig. 9.5 (d) we have $\phi_{A_t} = \pi/4$ and $\phi_{M_3} = \pi/3$. In both scenarios, we observe an enhancement of the cross sections in comparison to the real case in certain areas of the parameter space. For the $\mathcal{CP}\text{Int}_1$ scenario, in the region around $\tan\beta = 18$ and $M_{H^\pm} = 550$ GeV, the cross section is doubled as compared to the case with 2×2 mixing. A similar effect is seen for the $\mathcal{CP}\text{Int}_2$ scenario, where for the region around $\tan\beta = 18$ and $M_{H^\pm} = 570$ GeV an enhancement in the cross section by almost a factor of 2 is observed yet again. Note that the small disconnected regions observed in the cross section contours depicted in Fig. 9.5 (b) and Fig. 9.5 (d) are an artefact of the sampling density of points in the $(M_{H^\pm}, \tan\beta)$ plane, and a smooth contour can be obtained for a finer scan of the parameters.

For the $\mathcal{CP}$Int scenarios, the factors $\eta^{b\bar{b}}$ taking into account the interference between h_2 and h_3 for the process $b\bar{b} \to h_2, h_3 \to \tau^+\tau^-$, computed using Eq. (9.27), are plotted in the $(M_{H^\pm}, \tan\beta)$ in Fig. 9.6 (a) and (b)[2]. Recalling our discussion following Eq. (9.31), we note that since the chosen scenarios lie in the decoupling region, the interference contribution is *negative* throughout the plane. For both the $\mathcal{CP}\text{Int}_1$ and $\mathcal{CP}\text{Int}_2$ scenarios, the heavy Higgs states are nearly mass degenerate and have sizeable $H - A$ mixing. This

[2]When we consider interference between just h_2 and h_3, $\eta_2^{IF} = \eta_3^{IF} \equiv \eta^{IF}$. We have dropped "$\tau\tau$" in the superscript of $\eta^{b\bar{b}}$ for ease of notation.

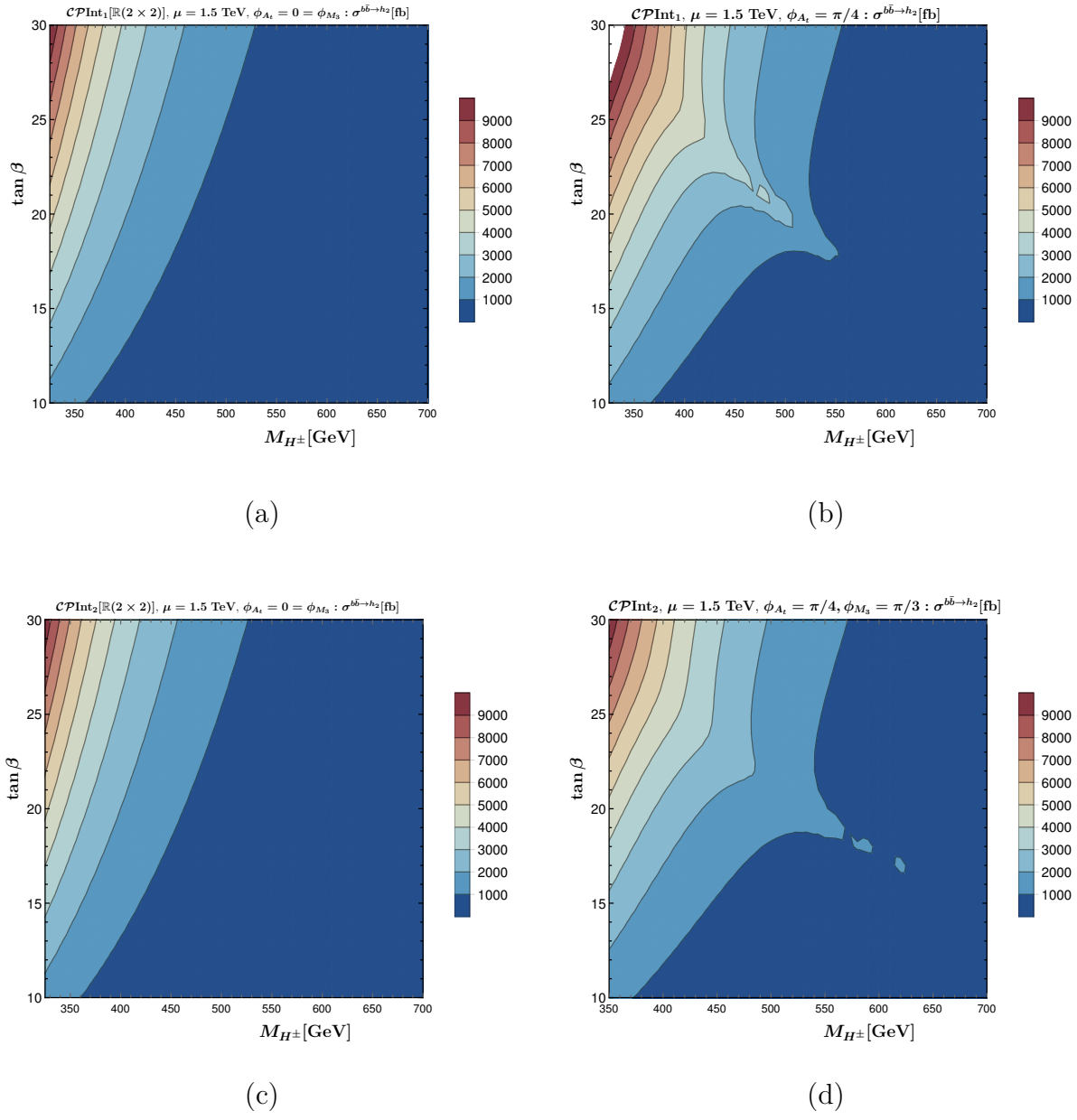

Figure 9.5: Production cross section in fb for h_2 via bottom-quark annihilation plotted in the $(M_{H^\pm}, \tan\beta)$ plane in the $\mathcal{CP}\text{Int}_1$ scenario in the case of (a) real parameters with only a $\mathcal{CP}$-conserving 2×2 mixing and (b) complex parameters with a full 3×3 mixing. In (c) and (d), the same quantities are depicted for the $\mathcal{CP}\text{Int}_2$ scenario.

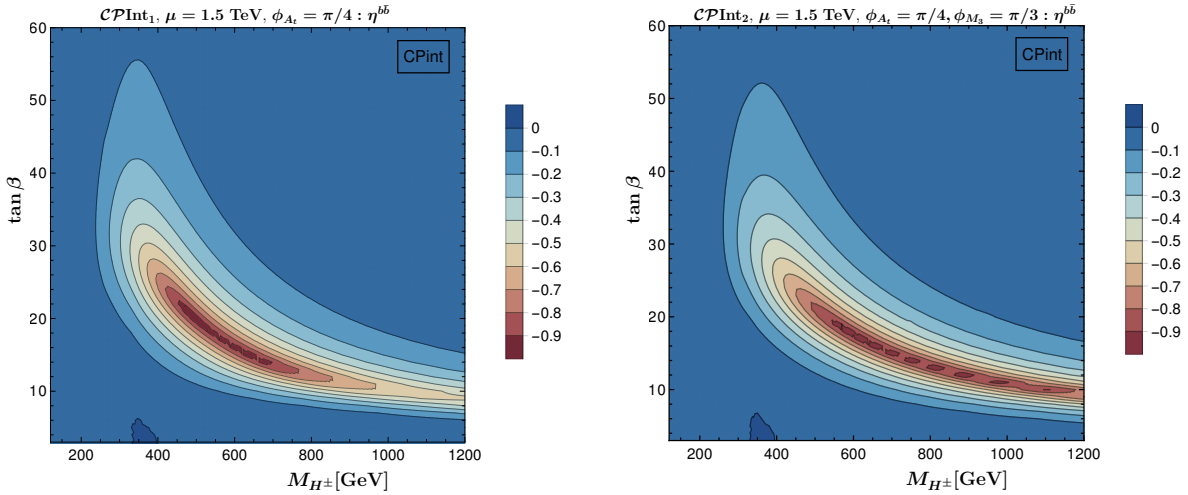

(a) (b)

Figure 9.6: Relative interference contribution of the Higgs bosons h_2 and h_3 decaying into $\tau^+\tau^-$ for the $b\bar{b}$ production mode in the (a) $\mathcal{CP}\text{Int}_1$ scenario with $\phi_{A_t} = \pi/4$ and (b) $\mathcal{CP}\text{Int}_2$ scenario with $\phi_{A_t} = \pi/4$ and $\phi_{M_3} = \pi/3$.

results in large interference contributions, with $\eta^{b\bar{b}}$ reaching a minimum of almost -98% in parts of the parameter space. In the $\mathcal{CP}\text{Int}_1$ scenario depicted in Fig. 9.6 (a), we observe a valley of strong destructive interference of about -90% starting from around the points (450 GeV, 23) to (670 GeV, 14) in the $(M_{H^\pm}, \tan\beta)$ plane whereas in the $\mathcal{CP}\text{Int}_2$ scenario depicted in Fig. 9.6 (b) the valley of strongest interference contributions exceeding -90% extends from around (550 GeV, 20) to (1000 GeV, 11) in the parameter plane.

9.4.3 Modified predictions with coherent cross sections

In the previous sections we defined a benchmark scenario and studied two consequences of $\mathcal{CP}$-violating mixing: the resonant enhancement of production cross sections of the Higgs states h_2 and h_3, and the destructive interference that results from the coherent sum of the amplitudes of the full process $b\bar{b} \to h_2, h_3 \to \tau^+\tau^-$. In this section, we will compare the theoretical predictions for $\sigma\times$BR of h_2 and h_3 obtained using the formulation described in Section 9.3, which accounts for the relative interference term in the prediction, with the experimental limits from searches for additional heavy neutral Higgs bosons produced via bottom-quark annihilation and decaying into $\tau^+\tau^-$ final state at Run II of the LHC [283].

All the searches for heavy Higgs bosons carried out at the LHC so far, including the ones presented in Fig. 4.6 in Chapter 4, assume in their interpretation in particular scenarios that $\mathcal{CP}$-symmetry is conserved. This means that exclusion limits on model parame-

ters are set based on predictions in which the $\sigma\times$BR are added incoherently for closely occurring resonances, i.e. without any interference terms. However, $\mathcal{CP}$ conservation is an ad-hoc assumption in this context. In this section, our goal is to examine how the exclusion bounds obtained under the assumption of $\mathcal{CP}$ conservation are modified in the most general case where mixing and interference effects arising from $\mathcal{CP}$ violation are taken into account.

The phenomenological impact of $\mathcal{CP}$-violating effects in the MSSM Higgs sector had already been investigated for Higgs searches at LEP [284,285]. The analyses in Refs. [51, 139,284,285] studied the effect of the phases of the trilinear couplings $A_{t,b}$ and the mixing between the $\mathcal{CP}$-eigenstates in the CPX scenario [286] which led to unexcluded parameter regions at relatively small values of the mass of the lightest Higgs. Furthermore, an analysis of interference in the $\mathcal{CP}$-conserving case between the light and heavy neutral MSSM Higgs bosons h and H produced via decays of heavy neutralinos was carried out in Ref. [137]. Such effects were studied for $gg \to h/H \to VV, V = W, Z$ with background contributions within a 2HDM in Ref. [287], and for the singlet extension of the SM in Ref. [288]. Ref. [289] discusses the $\mathcal{CP}$-violating interference between two light Higgs bosons decaying to two photons in the NMSSM. Studies of interference effects between heavy neutral Higgs bosons and with the background at low $\tan\beta$ in the $t\bar{t}$ final state have been made in Refs. [290–292].

Our studies in this section provide a follow-up to the analysis in Ref. [277], which examined the effects of $\mathcal{CP}$-violating mixing and interference between h_2 and h_3 decaying to two τ-leptons for gluon fusion and bottom-quark annihilation production channels and the impact of the interference factors on LHC exclusion limits from Run I. Here, we will examine these effects on Run II exclusion limits, wherein the cross sections have been augmented by the state-of-the-art cross section predictions described in Chapter 6, and the computation of the interference factors has also been automated by an implementation in `SusHiMi`.

In Fig. 9.7 (a) and (b) we show the theoretical predictions for $\sigma(pp \to b\bar{b} \to h_2, h_3 \to \tau^+\tau^-)$ as a function of the mass M_{h_a} of a neutral scalar resonance h_a for the two $\mathcal{CP}$Int scenarios, along with the respective experimental limits for the production of a single resonance ϕ at mass M_ϕ obtained from ATLAS searches for neutral Higgs bosons in Run II at 13 TeV with $\int \mathcal{L} = 13.3$ fb^{-1} reported in Ref. [283]. The black curves present essentially model-independent upper limits on the $b\bar{b}$ production cross section times the $\tau^+\tau^-$ branching ratio of a scalar boson versus its mass. The solid black line represents the observed exclusion bound and the dotted black line depicts the expected bound. The theoretical predictions have been obtained using Eq. (9.29) with $a = 2, 3$ with $\tan\beta$ and $M_{H^\pm}$ as input parameters:

$$\begin{aligned}\sigma(pp \to b\bar{b} \to h_{2,3} \to \tau^+\tau^-) = {} & \sigma(pp \to b\bar{b} \to h_2) \cdot (1 + \eta_2^{b\bar{b}}) \cdot \mathrm{BR}(h_2 \to \tau^+\tau^-) \\ & + \sigma(pp \to b\bar{b} \to h_3) \cdot (1 + \eta_3^{b\bar{b}}) \cdot \mathrm{BR}(h_3 \to \tau^+\tau^-)\,. \end{aligned} \tag{9.35}$$

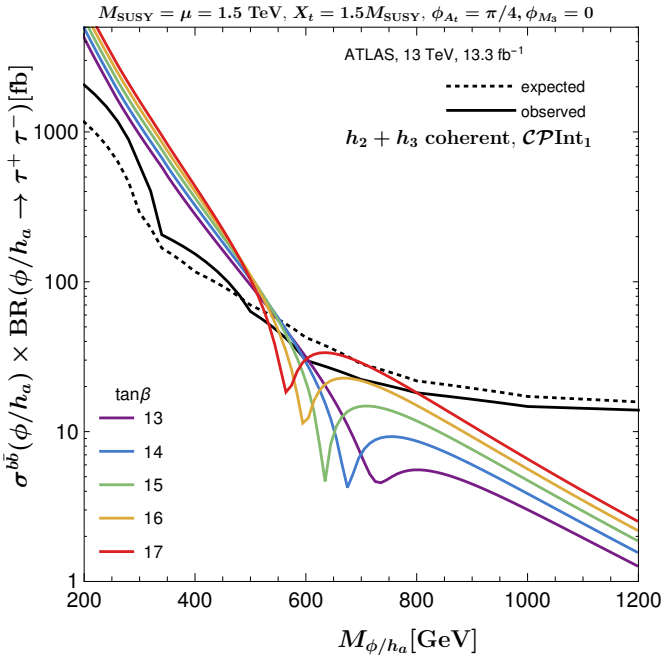

(a)

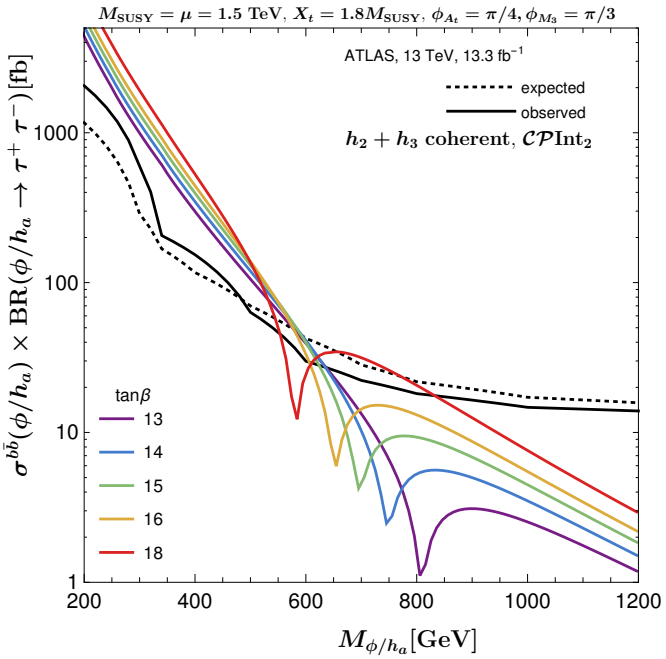

(b)

Figure 9.7: Comparison of coherent h_2 and h_3 cross sections times branching ratio (in fb) for $b\bar{b} \to \tau^+\tau^-$ in the $\mathcal{CP}$Int scenarios with the 95 % CL exclusion bounds obtained by ATLAS at 13 TeV for 13.3 fb^{-1} integrated luminosity from Ref. [283]. The colour coding for (a) $\tan\beta = 13, 14, 15, 16, 17$ for the $\mathcal{CP}$Int$_1$ scenario and (b) $\tan\beta = 13, 14, 15, 16, 18$ for the $\mathcal{CP}$Int$_2$ scenario is depicted in the respective plots.

The theoretical predictions have been plotted for a sample of $\tan\beta$ values in Fig. 9.7 as a function of $M_{h_a} = M_{h_3}$, where in the relevant regions we also have $M_{h_3} \simeq M_{h_2}$. The values of $\tan\beta$ have been chosen to display the regions of strongest interference, which is destructive. When we compare theoretical predictions with the cross section limits presented in the ATLAS measurement, M_{h_a} values for which the predicted $\sigma\times$BR is larger than the observed limit are excluded at 95% CL for the given value of $\tan\beta$. Therefore, the lower bound on M_{h_a} for a particular value of $\tan\beta$ is set by the point where the curve for the theoretical prediction crosses the observed limit. In general, the inclusion of the interference contribution in the full process can reduce this lower bound for a given $\tan\beta$ value compared to the $\mathcal{CP}$-conserving case, as was shown in Ref. [277]. For a given $\tan\beta$, the suppression of the predicted $\sigma\times$BR due to interference contributions can result in a range of M_{h_a} values, that would have been excluded if we assumed $\mathcal{CP}$ conservation, which escape the exclusion limits. In Fig. 9.7 (a) and (b) we examine this effect for the scenarios $\mathcal{CP}\text{Int}_1$ and $\mathcal{CP}\text{Int}_2$.

In Fig. 9.7 (a), the plotted curves show the interference-corrected $\sigma\times$BR for $\tan\beta = 13, 14, 15, 16, 17$ in the $\mathcal{CP}\text{Int}_1$ scenario, compared to the roughly model-independent cross section limits by ATLAS in black. We see the strongest suppression in the predicted values of $\sigma\times$BR for $\tan\beta = 15$, with slightly shallower valleys for values of $\tan\beta \pm 2$. Fig. 9.7 (b) shows the corresponding quantities for the $\mathcal{CP}\text{Int}_2$ scenario with $\phi_{A_t} = \pi/4$ and $\phi_{M_3} = \pi/3$. Here the $\tan\beta$ values for the depicted curves are 13,14,15,16 and 18. In contrast to Fig. 9.7 (a) where we saw the steepest valley for one value of $\tan\beta$ with the trough of the valleys tapering off for the neighbouring values of $\tan\beta$, in this case the destructive interference contributing to the suppression of cross section times branching ratios is about equally strong for all the values of $\tan\beta$ that have been sampled. Consequently, in these scenarios one can expect that even if future analyses continue to increase the lower bound of excluded M_{h_a}, the dips in the $\sigma\times$BR due to strong destructive interference will have the effect that certain ranges of Higgs bosons masses, depending on the considered value of $\tan\beta$, will remain unexcluded in comparison to the case where $\mathcal{CP}$ conservation is assumed.

In our preliminary analysis, we refrain from a detailed discussion on the theoretical and experimental uncertainties that can affect this comparison of predictions for cross sections times branching ratios including interference with observed limits, since we primarily want to display the qualitative effects of the $\mathcal{CP}$-violating mixing and interference terms. A discussion on the theoretical uncertainties in our cross section prediction was already provided in Section 8.6. A detailed analysis of theory uncertainties can be found in Ref. [92], and a discussion of experimental uncertainties for the displayed exclusion limits is presented in Ref. [283]. A closer examination of the uncertainties involved in the calculation of interference contribution is deferred to a future publication [2].

9.4.4 Impact on LHC exclusion bounds

In the previous sections, we encountered large $\mathcal{CP}$-violating interference effects which modified the predictions for $\sigma\times$BR of $b\bar{b}$ Higgs production and decay to $\tau^+\tau^-$ significantly. Comparing these predictions to the roughly model-independent experimental limits on the cross sections resulted in a range of unexcluded values for M_{h_a}. Experimental exclusion bounds on the parameter space of the MSSM are therefore affected by interference contributions between h_1, h_2 and h_3. We now analyse the exclusion limits in the $(M_{H^\pm}, \tan\beta)$ plane for the $\mathcal{CP}$Int scenarios using `HiggsBounds-5.1.1beta` [177–180]. For any particular model, `HiggsBounds` takes a selection of Higgs sector predictions as input and uses the experimental topological cross section limits from Higgs searches at LEP, the Tevatron and the LHC to determine whether this parameter point has been excluded at 95% CL.

In order to incorporate the interference effects into the prediction of $\sigma(b\bar{b} \to h_a)$ times the respective branching ratio, the ratio of production cross sections which are used as input to `HiggsBounds` are rescaled with the interference factor. Given that the exclusion is driven by the $\tau^+\tau^-$ final state, for simplicity we apply $\eta^{b\bar{b}\tau\tau}$ to all $b\bar{b}$ production cross sections and redefine

$$\frac{\sigma^{\mathrm{MSSM}}(b\bar{b} \to h_a)}{\sigma^{\mathrm{SM}}(b\bar{b} \to h_a)} \longrightarrow \frac{\sigma^{\mathrm{MSSM}}(b\bar{b} \to h_a)}{\sigma^{\mathrm{SM}}(b\bar{b} \to h_a)} \cdot (1 + \eta_a^{b\bar{b}})\,, \tag{9.36}$$

where the $\eta_a^{b\bar{b}}$ values are computed via our implementation in `SusHiMi`, and plotted in Fig. 9.6. The quantity $\sigma^{\mathrm{SM}}(b\bar{b} \to h_a)$ is the SM production cross section for a Higgs with mass M_{h_a}. The rescaled production ratio multiplied to the branching ratio of $h_a \to \tau^+\tau^-$ is then compared by `HiggsBounds` with the observed experimental limit for each point in the $(M_{H^\pm}, \tan\beta)$ plane.

In Fig. 9.8 (a) and (b), we show the exclusion bounds in the $(M_{H^\pm}, \tan\beta)$ plane for the $\mathcal{CP}$Int scenarios with non-zero $\mathcal{CP}$-violating phases in blue, together with the exclusion bounds in red for the same scenarios where all the parameters are real, i.e. no $\mathcal{CP}$-violating phases or resulting interference effects are present. In these plots we see the effects of the reduced $\sigma\times$BR rates that we described in Section 9.4.3. Certain parameter points in the $(M_{H^\pm}, \tan\beta)$ plane, that appear to be excluded when $\mathcal{CP}$ conservation is assumed, have a predicted cross section times branching ratio that is smaller than the observed limit when we include the $\mathcal{CP}$-violating interference term in the prediction. As a result, those parameter points become unexcluded when the interference-corrected prediction is compared with the experimental limits.

In Fig. 9.8 (a), we show the exclusion for the $\mathcal{CP}$-conserving and the $\mathcal{CP}$-violating case in red and blue, respectively, for the $\mathcal{CP}\mathrm{Int}_1$ scenario. The blue region corresponds to the scenario where $\phi_{A_t} = \pi/4$. Here we see that accounting for the interference term and the complex parameters in the $\sigma\times$BR prediction leads to a "wedge" of destructive interference in the region between $M_{H^\pm} \sim 500$ GeV and 750 GeV for $\tan\beta \sim 12$ to 20

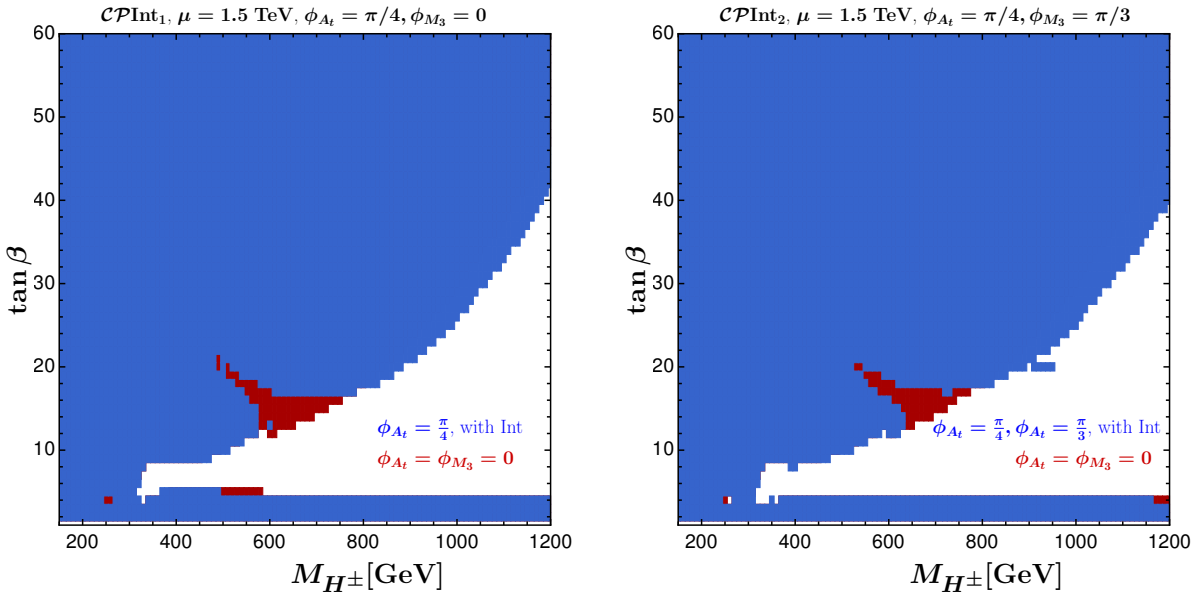

Figure 9.8: Exclusion bounds in the $(M_{H^\pm}, \tan\beta)$ plane of the MSSM obtained with `HiggsBounds5.1.1beta` for (a) the $\mathcal{CP}$Int$_1$ and (b) the $\mathcal{CP}$Int$_2$ scenario. The blue region depicts the exclusion bounds when interference terms in the production and decay of h_2 and h_3 are taken into account for $b\bar{b} \to \tau^+\tau^-$. The red contour depicts the additional region that is considered to be excluded when all the parameters are assumed to be real and no $\mathcal{CP}$-violating interferences occur.

that remains unexcluded, in contrast to the $\mathcal{CP}$-conserving case. In Fig. 9.8 (b), where the blue region corresponds to the $\mathcal{CP}$Int$_2$ scenario with $\phi_{A_t} = \pi/4$ and $\phi_{M_3} = \pi/3$, such a wedge occurs between $M_{H^\pm} \sim 550$ GeV and 800 GeV for $\tan\beta \sim 13$ to 20. In the above plots one can also notice disconnected red points that appear in the low $\tan\beta$ region in Fig. 9.8 (a) and blue points that appear around $\tan\beta = 20$ and $M_{H^\pm} \sim 900$ GeV in Fig. 9.8 (b). These occurrences seem to result from numerical instabilities.

In the light of these results which show that accounting for the effects of $\mathcal{CP}$ violation in the MSSM Higgs sector can lead to significant modifications of the exclusion contours, we assert that interpretations of exclusion limits from the searches for heavy Higgs bosons should account for the possibility that the Higgs sector of the MSSM is not $\mathcal{CP}$-conserving.

9.5 Summary and outlook

In this chapter, we investigated the effects of $\mathcal{CP}$-violating interference contributions on the predictions for the full process of production and decay of the MSSM Higgs bosons. We used an approximation of the 3×3 propagator matrix that employs the $\hat{\mathbf{Z}}$ factors evaluated at the complex poles along with the Breit-Wigner propagators to calculate the interference terms in the amplitudes of the full process. Furthermore, we reviewed a formalism to incorporate relative interference factors into the prediction for the on-shell production and decay of the Higgs states h_a, $a \in \{1, 2, 3\}$, and described the implementation for the calculation of these interference factors into `SusHiMi`.

In order to study the phenomenology of the Higgs sector in parameter regions where the interference effects are important, we defined a benchmark scenario ("$\mathcal{CP}$Int"). Note that these interference effects arise generically in the theory, and it was not necessary to fine-tune the benchmark scenario to a particular set of parameters in order to make them visible. Focussing on the interference between h_2 and h_3 in the process $b\bar{b} \to \tau^+\tau^-$ in the $\mathcal{CP}$Int scenario, we highlighted four aspects. First, we showed that nearly mass degenerate heavy Higgs states leads to a substantial $H - A$ mixing and there is a resonant enhancement in the individual $b\bar{b}$ cross sections of h_2 and h_3. The strong mixing in this resonant region also gives rise to a large destructive interference, which overcompensates the enhancement in cross sections. We showed that in the considered scenarios strongly destructive interference of up to ∼98% occurs in significant regions of the studied $(M_{H^\pm}, \tan\beta)$ plane, which leads to modified predictions for $\sigma\times$BR in the process of h_2, h_3 production and decay. Our cross section predictions described in previous chapters and implemented in `SusHi` were used to obtain the modified predictions. We compared the values of $\sigma\times$BR, which take the interference contributions into account, to the roughly model-independent experimental limits for the considered process. The suppression in the predicted $\sigma\times$BR in the resonance region due to destructive interference resulted in significant regions of Higgs masses that remain unexcluded while they would appear to be excluded under the assumption of $\mathcal{CP}$ conservation. Lastly, we analysed the modification of exclusion bounds in the $(M_{H^\pm}, \tan\beta)$ plane using production rates rescaled by the interference factors as an input to `HiggsBounds`. We found that in the case where $\mathcal{CP}$ violation is allowed and interference effects are accounted for, a region of unexcluded parameter points opens up.

In our preliminary analysis, we only considered one process of Higgs production and decay. In future investigations, we will incorporate interference factors for the gg production channel into `SusHiMi`, such that the gluon-fusion cross section predictions can be directly used to obtain values for $\sigma\times$BR with interference effects included. Furthermore, a detailed study of the modified exclusions with a variation in the phases of A_t, A_b, M_3 and μ will be performed.

Chapter 10

Conclusions

Precise theory predictions are indispensable for testing deviations, or lack thereof, from the Standard Model. They are also essential for increasing the sensitivity to signatures of new physics. We have seen that BSM theories with extended Higgs sectors provide viable solutions to some of the shortcomings of the SM. For the search of these additional Higgs bosons, not only do we need an accurate knowledge of their production cross sections, branching ratios, and potential interference effects, but a meaningful comparison of the predictions to the experimental data is also important for the proper interpretation of the new results from Run II of the LHC.

The year 2016 ended on an exceptional note for the LHC, with the ATLAS and CMS experiments receiving an integrated luminosity of almost 40 fb^{-1} as compared to the 25 fb^{-1} that was originally planned. In the spring of 2017, the physics runs at LHC restarted and promised to deliver even greater statistics. With higher energies than Run I and a remarkable amount of data available in Run II, this translates to improved and more decisive constraints on physics beyond the Standard Model.

While the non-observation of the heavier Higgs bosons of the MSSM has been used for confining the SUSY parameter space, scenarios that allow $\mathcal{CP}$ violation are more difficult to restrict using the Higgs search data. The MSSM predicts three neutral mass eigenstates at lowest-order: the $\mathcal{CP}$-even h and H, and the $\mathcal{CP}$-odd A. At tree level, and at higher orders for vanishing phases, the Higgs sector is $\mathcal{CP}$-conserving and only the $\mathcal{CP}$-even Higgs states h and H mix. So far, experimental investigations have been carried out under the assumption that the MSSM is $\mathcal{CP}$-conserving. However, $\mathcal{CP}$ is not an inherent symmetry of nature. In fact, an explanation for the baryon asymmetry in the universe demands additional sources of $\mathcal{CP}$ violation not contained in the SM. While allowing for $\mathcal{CP}$ violation does increase the number of free parameters in the MSSM, there is no a priori physical reason to assume that all parameters of the MSSM must be real. Complex parameters in the MSSM can enter the Higgs sector via loop induced $\mathcal{CP}$-violating corrections and result in three new $\mathcal{CP}$-admixed neutral mass eigenstates h_1, h_2 and h_3 with $M_{h_1} \leq M_{h_2} \leq M_{h_3}$. This leads to interesting deviations from the phenomenology of the $\mathcal{CP}$-conserving MSSM.

In this thesis, we studied the relevance of these $\mathcal{CP}$-violating phases in searches for

neutral Higgs bosons of the MSSM. The investigation of the effects of the complex parameters of the theory giving rise to additional $\mathcal{CP}$ violation beyond the single phase of the SM was carried out in two steps, summarised in the following.

On-shell Higgs production in the MSSM with complex parameters

In Chapter 6, we presented the theoretical predictions for inclusive cross sections for h_1, h_2 and h_3 production via gluon fusion and bottom-quark annihilation in the MSSM with complex parameters. The cross section predictions for the gluon-fusion process at leading order are based on an explicit calculation taking into account the dependence on all complex parameters in the MSSM. The complete form of the analytical formulae for the general $\mathcal{CP}$-violating case including Higgs mixing has been presented in the literature for the first time. The 3×3 mixing of the lowest-order mass eigenstates of the Higgs bosons $\{h, H, A\}$ into the loop-corrected mass eigenstates $\{h_1, h_2, h_3\}$ was described in Chapter 5 with full propagator-type corrections using the $\hat{\mathbf{Z}}$ factors of the neutral Higgs bosons, which are provided by the code `FeynHiggs`. Moreover, we discussed how the predictions for the gluon-fusion process in the MSSM with complex parameters deviate from those of the MSSM with real parameters due to non-zero couplings of the squarks to the $\mathcal{CP}$-odd Higgs boson A and potentially different left- and right-handed bottom-Yukawa couplings arising from the resummation of $\tan\beta$-enhanced sbottom contributions in Δ_b.

The LO computation of the cross section was further supplemented by higher-order contributions. Using a simplified version of the Δ_b resummation for the treatment of the higher-order corrections, we included the full massive top- and bottom-quark contributions at NLO QCD and interpolated the NLO SUSY QCD corrections from the amplitudes in the MSSM with real parameters. The uncertainties involved in using such an interpolation were discussed in Chapter 8. The interpolation uncertainty at NLO is most relevant in scenarios where the squarks and the gluino are relatively light, which are under tension from the present limits from LHC searches. This uncertainty could be avoided if an explicit result for the squark–gluino contributions at NLO QCD in the MSSM becomes available for the general case of complex parameters. For the top-quark contribution in the effective theory of a heavy top-quark, we added NNLO QCD contributions for all Higgs bosons, and N^{3}LO QCD contributions in an expansion around the threshold of Higgs production for the $\mathcal{CP}$-even component of the amplitude of the light Higgs boson h_1 to match the precision of the predictions for the SM Higgs boson. Finally, electroweak corrections which include two-loop contributions with couplings of the heavy gauge bosons to the Higgs bosons mediated by light quarks were added to the gluon-fusion cross section. The results for cross sections presented in this thesis are currently the state of the art for neutral Higgs production in the MSSM with complex parameters.

In Chapter 7 we described the implementation of the cross section calculations in an extension of the code `SusHi`, called `SusHiMi`, which is linked to `FeynHiggs`. Using

SusHiMi, we investigated the phenomenological effects of $\mathcal{CP}$-violating phases on the production of Higgs bosons in the MSSM with complex parameters in two scenarios, inspired by the light-stop and $m_h^{\text{mod+}}$ benchmark scenarios. We found in our analysis of Higgs boson production through gluon fusion that a proper description of squark and gluino loop contributions is essential, in particular if their masses are light. This refers both to the loop contributions to the gluon–gluon–Higgs vertex and to the corrections entering through Δ_b. Squark and gluino loop contributions furthermore enter the wave function normalisation factors that are necessary to ensure the correct on-shell properties of the produced Higgs boson. In regions where squark and gluino contributions are sizeable, the production cross sections show a significant dependence on the $\mathcal{CP}$-violating phases. We discussed the remaining theoretical uncertainties in the cross section predictions taking into account renormalisation and factorisation scale uncertainties, a resummation uncertainty for Δ_b and an uncertainty due to the performed interpolation of NLO SUSY QCD corrections, in addition to other uncertainties that can directly be taken over from the case of the MSSM with real parameters or the SM.

In the $m_h^{\text{mod+}}$-inspired scenario, which features a slightly heavier squark spectrum, an important feature in the production processes of the two heavy states h_2 and h_3 was the large mixing between the nearly mass-degenerate states. Their mixing effects are incorporated in the wave function normalisation factors for the external Higgs bosons. In a scenario such as this, we note that the signals of the two Higgs bosons cannot be experimentally resolved and the measured quantity is the sum of their cross sections times branching ratios. For an accurate interpretation of experimental exclusion limits arising from MSSM Higgs searches, which so far have only been analysed in the framework of the $\mathcal{CP}$-conserving MSSM, it is important to take into account the interference effects in the full process of Higgs production and decay arising from $\mathcal{CP}$-violating interactions. Such interference contributions are especially large when the mixing is large and the heavy Higgses have a very small mass splitting. Our results for the cross sections for on-shell Higgs bosons can be directly used in the formalism of a generalised narrow-width approximation to incorporate these interference effects.

Impact of interference effects on LHC Higgs searches

In Chapter 9, we reviewed the formalism to incorporate interference terms in the factorisation of a full process into the on-shell production and decay of an intermediate particle. Interference effects between Higgs bosons can be crucial in assessing allowed and excluded parameter regions. $\mathcal{CP}$-conserving interference between the $\mathcal{CP}$-even Higgs states h and H becomes relevant when their mass difference is smaller than the sum of their total widths. However, in such scenarios both these Higgs states are light, which is under pressure from experimental limits. In this thesis we have mainly investigated scenarios where the lightest Higgs h_1 is mostly $\mathcal{CP}$-even and SM-like, having a large mass splitting from the Higgses h_2 and h_3 which are nearly mass-degenerate. This is typical

in the decoupling regions of models with an extended Higgs sector. Since h_2 and h_3 are $\mathcal{CP}$-admixed states in the MSSM with complex parameters, the total matrix element of their production and decay has non-zero interference terms, and the $\sigma\times$BR of these two Higgs states cannot be added incoherently. This interference term in the coherent sum of $\sigma\times$BR is dependent on the diagonal and off-diagonal elements of the $\hat{\mathbf{Z}}$ matrix and the Breit-Wigner propagators of h_2 and h_3. We described the implementation of the relative interference factors in `SusHiMi` for the $b\bar{b}$ initial state, which is planned to be extended to the gg initial state as well. Therefore, a `SusHiMi` run outputs not just the relevant Higgs cross section for a chosen initial state, but also the interference factor that must be multiplied to it for a given final state while calculating the $\sigma\times$BR for the chosen Higgs. This provides a tool for systematically incorporating and accounting for the effects of $\mathcal{CP}$-violating phases in the process of production and decay of a Higgs boson.

A $\mathcal{CP}$-violating scenario ("$\mathcal{CP}$Int") with non-zero phases for the trilinear coupling A_t and gluino mass parameter M_3 was defined in order to investigate the impact of complex parameters giving rise to interference in the process $b\bar{b} \to h_2, h_3 \to \tau^+\tau^-$. We found that the interference between h_2 and h_3 was strongly destructive with values of up to 98%. For sample values of $\tan\beta$, this interference was found to reduce the theoretical prediction for the cross section times branching ratio of the considered process significantly below the experimentally observed limits. Consequently, it opened up parameter regions that were regarded as excluded in Higgs searches that assume $\mathcal{CP}$-conservation and do not account for such $\mathcal{CP}$-violating interferences. The two versions of the defined scenario within which we analysed the interference effects are proposed to serve as benchmarks for neutral Higgs searches with $\mathcal{CP}$ violation in future analyses by ATLAS and CMS.

Run II of the LHC promises to vastly improve the reach of searches for new physics, including supersymmetry. In this thesis we have presented precise predictions for the production of Higgs bosons in the $\mathcal{CP}$-violating MSSM for two prominent production channels at the LHC, and developed a tool for systematically studying the effects of complex parameters in the full process of Higgs production and decay in the MSSM. We look forward to utilising these results in the light of the upcoming Higgs search data from the LHC.

Appendix A

Formulas: Higgs–quark and Higgs–squark couplings

In SusHiMi the Higgs–(s)quark couplings are expressed in terms of the $\mathcal{CP}$-even and $\mathcal{CP}$-odd neutral gauge eigenstates $\phi_g \in \{\phi_1^0, \phi_2^0\}$ and $\chi_g \in \{\chi_1^0, \chi_2^0\}$, respectively. In order to obtain the couplings of the squarks with the lowest-order mass eigenstates $\phi \in \{h, H, A, G\}$ the gauge eigenstates are rotated using the tree-level mixing matrix $\mathcal{R}$ as depicted in the following Feynman diagrams

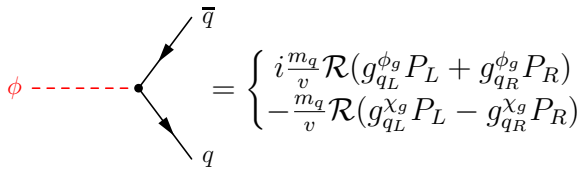

(A.1)

with $v = 2m_W/g_2 = 1/\sqrt{\sqrt{2}G_F}$ and the tree-level mixing matrix $\mathcal{R}$ given in Eq. (3.46). At the amplitude level the results will then also be multiplied with the corresponding $\hat{\mathbf{Z}}$ factor.

The couplings between the gauge eigenstates and the third generation quarks are $g_{q_L} = 1/\cos\beta$ for ϕ_1^0 and χ_1^0 and $g_{q_L} = 1/\sin\beta$ for ϕ_2^0 and χ_2^0. For Δ_b corrections we refer to Eq. (6.52) and Eq. (6.55).

The couplings between the gauge eigenstates and the third generation squarks contain terms from the squark mass diagonalisation matrix $U_{\tilde{q}}$ (see Eq. (3.18)) which is a unitary matrix with real diagonal elements and complex off-diagonal elements, i.e. it can be written as follows

$$U_{\tilde{q}} = \begin{pmatrix} U_{\tilde{q}11} & U_{\tilde{q}12} \\ -U_{\tilde{q}12}^* & U_{\tilde{q}22} \end{pmatrix} . \tag{A.2}$$

They are obtained with MaCoR [184, 293]. For the $\mathcal{CP}$-even state ϕ_1^0 we have the stop couplings (using $s_\beta \equiv \sin\beta$, $c_\beta \equiv \cos\beta$, $t_\beta \equiv \tan\beta$, $s_W \equiv \sin\theta_W$ and $c_W \equiv \cos\theta_W$):

$$
\begin{aligned}
g^{\phi_1^0}_{\tilde{t},11} &= U^*_{\tilde{t}12}\left[-\frac{U_{\tilde{t}11}m_t\mu}{s_\beta}+\frac{4}{3}U_{\tilde{t}12}c_\beta m_Z^2 s_W^2\right]-U^*_{\tilde{t}11}\left[\frac{U_{\tilde{t}12}m_t\mu^*}{s_\beta}+c_\beta m_Z^2 U_{\tilde{t}11}\left(\frac{1}{3}s_W^2-c_W^2\right)\right]\\
g^{\phi_1^0}_{\tilde{t},12} &= U^*_{\tilde{t}12}\left[-\frac{U_{\tilde{t}21}m_t\mu}{s_\beta}+\frac{4}{3}U_{\tilde{t}22}c_\beta m_Z^2 s_W^2\right]-U^*_{\tilde{t}11}\left[\frac{U_{\tilde{t}22}m_t\mu^*}{s_\beta}+c_\beta m_Z^2 U_{\tilde{t}21}\left(\frac{1}{3}s_W^2-c_W^2\right)\right]\\
g^{\phi_1^0}_{\tilde{t},21} &= U^*_{\tilde{t}22}\left[-\frac{U_{\tilde{t}11}m_t\mu}{s_\beta}+\frac{4}{3}U_{\tilde{t}12}c_\beta m_Z^2 s_W^2\right]-U^*_{\tilde{t}21}\left[\frac{U_{\tilde{t}12}m_t\mu^*}{s_\beta}+c_\beta m_Z^2 U_{\tilde{t}11}\left(\frac{1}{3}s_W^2-c_W^2\right)\right]\\
g^{\phi_1^0}_{\tilde{t},22} &= U^*_{\tilde{t}22}\left[-\frac{U_{\tilde{t}21}m_t\mu}{s_\beta}+\frac{4}{3}U_{\tilde{t}22}c_\beta m_Z^2 s_W^2\right]-U^*_{\tilde{t}21}\left[\frac{U_{\tilde{t}22}m_t\mu^*}{s_\beta}+c_\beta m_Z^2 U_{\tilde{t}21}\left(\frac{1}{3}s_W^2-c_W^2\right)\right].
\end{aligned}
\tag{A.3}
$$

For the $\mathcal{CP}$-even state ϕ_2^0, the couplings are:

$$
\begin{aligned}
g^{\phi_2^0}_{\tilde{t},11} &= U^*_{\tilde{t}12}\left[\frac{U_{\tilde{t}11}m_tA_t^*}{s_\beta}+U_{\tilde{t}12}\left(\frac{2m_t^2}{s_\beta}-\frac{4}{3}s_\beta m_z^2 s_W^2\right)\right]\\
&\quad+U^*_{\tilde{t}11}\left[\frac{U_{\tilde{t}12}m_tA_t}{s_\beta}+\frac{2U_{\tilde{t}11}m_t^2}{s_\beta}+s_\beta m_Z^2 U_{\tilde{t}11}\left(\frac{1}{3}s_W^2-c_W^2\right)\right]\\
g^{\phi_2^0}_{\tilde{t},12} &= U^*_{\tilde{t}12}\left[\frac{U_{\tilde{t}21}m_tA_t^*}{s_\beta}+U_{\tilde{t}22}\left(\frac{2m_t^2}{s_\beta}-\frac{4}{3}s_\beta m_z^2 s_W^2\right)\right]\\
&\quad+U^*_{\tilde{t}11}\left[\frac{U_{\tilde{t}22}m_tA_t}{s_\beta}+\frac{2U_{\tilde{t}21}m_t^2}{s_\beta}+s_\beta m_Z^2 U_{\tilde{t}21}\left(\frac{1}{3}s_W^2-c_W^2\right)\right]\\
g^{\phi_2^0}_{\tilde{t},21} &= U^*_{\tilde{t}22}\left[\frac{U_{\tilde{t}11}m_tA_t^*}{s_\beta}+U_{\tilde{t}12}\left(\frac{2m_t^2}{s_\beta}-\frac{4}{3}s_\beta m_z^2 s_W^2\right)\right]\\
&\quad+U^*_{\tilde{t}21}\left[\frac{U_{\tilde{t}12}m_tA_t}{s_\beta}+\frac{2U_{\tilde{t}11}m_t^2}{s_\beta}+s_\beta m_Z^2 U_{\tilde{t}11}\left(\frac{1}{3}s_W^2-c_W^2\right)\right]\\
g^{\phi_2^0}_{\tilde{t},22} &= U^*_{\tilde{t}22}\left[\frac{U_{\tilde{t}21}m_tA_t^*}{s_\beta}+U_{\tilde{t}22}\left(\frac{2m_t^2}{s_\beta}-\frac{4}{3}s_\beta m_z^2 s_W^2\right)\right]\\
&\quad+U^*_{\tilde{t}21}\left[\frac{U_{\tilde{t}22}m_tA_t}{s_\beta}+\frac{2U_{\tilde{t}21}m_t^2}{s_\beta}+s_\beta m_Z^2 U_{\tilde{t}21}\left(\frac{1}{3}s_W^2-c_W^2\right)\right].
\end{aligned}
\tag{A.4}
$$

Similarly for the $\mathcal{CP}$-odd states χ_1^0 and χ_2^0 the stop couplings are given as:

$$
\begin{aligned}
g^{\chi_1^0}_{\tilde{t},11} &= i\frac{m_t}{s_\beta}\left[-\mu U^*_{\tilde{t}12}U_{\tilde{t}11}+\mu^*U^*_{\tilde{t}11}U_{\tilde{t}12}\right] \quad g^{\chi_2^0}_{\tilde{t},11} = i\frac{m_t}{s_\beta}\left[-A_t^*U^*_{\tilde{t}12}U_{\tilde{t}11}+A_tU^*_{\tilde{t}11}U_{\tilde{t}12}\right]\\
g^{\chi_1^0}_{\tilde{t},12} &= i\frac{m_t}{s_\beta}\left[-\mu U^*_{\tilde{t}12}U_{\tilde{t}21}+\mu^*U^*_{\tilde{t}11}U_{\tilde{t}22}\right] \quad g^{\chi_2^0}_{\tilde{t},12} = i\frac{m_t}{s_\beta}\left[-A_t^*U^*_{\tilde{t}12}U_{\tilde{t}21}+A_tU^*_{\tilde{t}11}U_{\tilde{t}22}\right]\\
g^{\chi_1^0}_{\tilde{t},21} &= i\frac{m_t}{s_\beta}\left[-\mu U^*_{\tilde{t}22}U_{\tilde{t}11}+\mu^*U^*_{\tilde{t}21}U_{\tilde{t}12}\right] \quad g^{\chi_2^0}_{\tilde{t},21} = i\frac{m_t}{s_\beta}\left[-A_t^*U^*_{\tilde{t}22}U_{\tilde{t}11}+A_tU^*_{\tilde{t}21}U_{\tilde{t}12}\right]\\
g^{\chi_1^0}_{\tilde{t},22} &= i\frac{m_t}{s_\beta}\left[-\mu U^*_{\tilde{t}22}U_{\tilde{t}21}+\mu^*U^*_{\tilde{t}21}U_{\tilde{t}22}\right] \quad g^{\chi_2^0}_{\tilde{t},22} = i\frac{m_t}{s_\beta}\left[-A_t^*U^*_{\tilde{t}22}U_{\tilde{t}21}+A_tU^*_{\tilde{t}21}U_{\tilde{t}22}\right].
\end{aligned}
\tag{A.5}
$$

Analogously, the Higgs–sbottom couplings for the $\mathcal{CP}$-even state ϕ_1^0 are:

$$\begin{aligned}
g^{\phi_1^0}_{\tilde{b},11} &= U^*_{\tilde{b}12}\left[\frac{U_{\tilde{b}11}A_b^* m_b}{c_\beta} + U_{\tilde{b}12}\left(\frac{2m_b^2}{c_\beta} - \frac{2}{3}c_\beta m_Z^2 s_W^2\right)\right] \\
&\quad + U^*_{\tilde{b}11}\left[\frac{U_{\tilde{b}12}A_b m_b}{c_\beta} + \frac{2U_{\tilde{b}11}m_b^2}{c_\beta} - c_\beta m_Z^2 U_{\tilde{b}11}\left(\frac{1}{3}s_W^2 + c_W^2\right)\right] \\
g^{\phi_1^0}_{\tilde{b},12} &= U^*_{\tilde{b}12}\left[\frac{U_{\tilde{b}21}A_b^* m_b}{c_\beta} + U_{\tilde{b}22}\left(\frac{2m_b^2}{c_\beta} - \frac{2}{3}c_\beta m_Z^2 s_W^2\right)\right] \\
&\quad + U^*_{\tilde{b}11}\left[\frac{U_{\tilde{b}22}A_b m_b}{c_\beta} + \frac{2U_{\tilde{b}21}m_b^2}{c_\beta} - c_\beta m_Z^2 U_{\tilde{b}21}\left(\frac{1}{3}s_W^2 + c_W^2\right)\right],
\end{aligned}$$

$$\begin{aligned}
g^{\phi_1^0}_{\tilde{b},21} &= U^*_{\tilde{b}22}\left[\frac{U_{\tilde{b}11}A_b^* m_b}{c_\beta} + U_{\tilde{b}12}\left(\frac{2m_b^2}{c_\beta} - \frac{2}{3}c_\beta m_Z^2 s_W^2\right)\right] \\
&\quad + U^*_{\tilde{b}21}\left[\frac{U_{\tilde{b}12}A_b m_b}{c_\beta} + \frac{2U_{\tilde{b}11}m_b^2}{c_\beta} - c_\beta m_Z^2 U_{\tilde{b}11}\left(\frac{1}{3}s_W^2 + c_W^2\right)\right] \\
g^{\phi_1^0}_{\tilde{b},22} &= U^*_{\tilde{b}22}\left[\frac{U_{\tilde{b}21}A_b^* m_b}{c_\beta} + U_{\tilde{b}22}\left(\frac{2m_b^2}{c_\beta} - \frac{2}{3}c_\beta m_Z^2 s_W^2\right)\right] \\
&\quad + U^*_{\tilde{b}21}\left[\frac{U_{\tilde{b}22}A_b m_b}{c_\beta} + \frac{2U_{\tilde{b}21}m_b^2}{c_\beta} - c_\beta m_Z^2 U_{\tilde{b}21}\left(\frac{1}{3}s_W^2 + c_W^2\right)\right].
\end{aligned} \tag{A.6}$$

For the $\mathcal{CP}$-even state ϕ_0^2 they are given as:

$$\begin{aligned}
g^{\phi_2^0}_{\tilde{b},11} &= U^*_{\tilde{b}12}\left[-\frac{U_{\tilde{b}11}m_b\mu}{c_\beta} + \frac{2}{3}U_{\tilde{b}12}s_\beta m_z^2 s_W^2\right] + U^*_{\tilde{b}11}\left[-\frac{U_{\tilde{b}12}m_b\mu^*}{c_\beta} + s_\beta m_Z^2 U_{\tilde{b}11}\left(\frac{1}{3}s_W^2 + c_W^2\right)\right] \\
g^{\phi_2^0}_{\tilde{b},12} &= U^*_{\tilde{b}12}\left[-\frac{U_{\tilde{b}21}m_b\mu}{c_\beta} + \frac{2}{3}U_{\tilde{b}22}s_\beta m_z^2 s_W^2\right] + U^*_{\tilde{b}11}\left[-\frac{U_{\tilde{b}22}m_b\mu^*}{c_\beta} + s_\beta m_Z^2 U_{\tilde{b}21}\left(\frac{1}{3}s_W^2 + c_W^2\right)\right] \\
g^{\phi_2^0}_{\tilde{b},21} &= U^*_{\tilde{b}22}\left[-\frac{U_{\tilde{b}11}m_b\mu}{c_\beta} + \frac{2}{3}U_{\tilde{b}12}s_\beta m_z^2 s_W^2\right] + U^*_{\tilde{b}21}\left[-\frac{U_{\tilde{b}12}m_b\mu^*}{c_\beta} + s_\beta m_Z^2 U_{\tilde{b}11}\left(\frac{1}{3}s_W^2 + c_W^2\right)\right] \\
g^{\phi_2^0}_{\tilde{b},22} &= U^*_{\tilde{b}22}\left[-\frac{U_{\tilde{b}21}m_b\mu}{c_\beta} + \frac{2}{3}U_{\tilde{b}22}s_\beta m_z^2 s_W^2\right] + U^*_{\tilde{b}21}\left[-\frac{U_{\tilde{b}22}m_b\mu^*}{c_\beta} + s_\beta m_Z^2 U_{\tilde{b}21}\left(\frac{1}{3}s_W^2 + c_W^2\right)\right].
\end{aligned} \tag{A.7}$$

Finally, for the $\mathcal{CP}$-odd states χ_1^0 and χ_2^0 the Higgs–sbottom couplings are:

$$
\begin{aligned}
g^{\chi_1^0}_{\tilde{b},11} &= i\frac{m_b}{c_\beta}\left[-A_b^* U^*_{\tilde{b}12} U_{\tilde{b}11} + A_b U^*_{\tilde{b}11} U_{\tilde{b}12}\right] & g^{\chi_2^0}_{\tilde{b},11} &= i\frac{m_b}{c_\beta}\left[-\mu U^*_{\tilde{b}12} U_{\tilde{b}11} + \mu^* U^*_{\tilde{b}11} U_{\tilde{b}12}\right] \\
g^{\chi_1^0}_{\tilde{b},12} &= i\frac{m_b}{c_\beta}\left[-A_b^* U^*_{\tilde{b}12} U_{\tilde{b}21} + A_b U^*_{\tilde{b}11} U_{\tilde{b}22}\right] & g^{\chi_2^0}_{\tilde{b},12} &= i\frac{m_b}{c_\beta}\left[-\mu U^*_{\tilde{b}12} U_{\tilde{b}21} + \mu^* U^*_{\tilde{b}11} U_{\tilde{b}22}\right] \\
g^{\chi_1^0}_{\tilde{b},21} &= i\frac{m_b}{c_\beta}\left[-A_b^* U^*_{\tilde{b}22} U_{\tilde{b}11} + A_b U^*_{\tilde{b}21} U_{\tilde{b}12}\right] & g^{\chi_2^0}_{\tilde{b},21} &= i\frac{m_b}{c_\beta}\left[-\mu U^*_{\tilde{b}22} U_{\tilde{b}11} + \mu^* U^*_{\tilde{b}21} U_{\tilde{b}12}\right] \\
g^{\chi_1^0}_{\tilde{b},22} &= i\frac{m_b}{c_\beta}\left[-A_b^* U^*_{\tilde{b}22} U_{\tilde{b}21} + A_b U^*_{\tilde{b}21} U_{\tilde{b}22}\right] & g^{\chi_2^0}_{\tilde{b},22} &= i\frac{m_b}{c_\beta}\left[-\mu U^*_{\tilde{b}22} U_{\tilde{b}21} + \mu^* U^*_{\tilde{b}21} U_{\tilde{b}22}\right] .
\end{aligned}
\tag{A.8}
$$

Appendix B

Parameter points in MSSM scenarios

In the following we summarise the parameter values in GeV for scenarios used or referenced in this thesis. We use the relation $A_t = (X_t + \mu^* \cot\beta) \cdot e^{i\phi_{A_t}}$ as the input to `SusHiMi` in all the scenarios and X_t is given in the on-shell scheme. The GUT relation is given by Eq. (3.16):

$$M_1 = \frac{5}{3}\frac{s_W^2}{c_W^2} M_2 \,.$$

Table B.1: An overview of the MSSM scenarios used in this thesis. All quantities except for the ratios are in GeV.

Scenario Parameter	**light-stop** [130]	$\mathbf{m_h^{mod+}}$ [130]	**light-stop inspired** [1]	$\mathbf{m_h^{mod+}}$ **inspired** [1]	$\mathcal{CP}$**Int**$_1$ [2]	$\mathcal{CP}$**Int**$_2$ [2]
m_t	173.2	173.2	173.2	173.2	172.5	172.5
$M_{H^\pm}$(or M_A)	*Varied*	*Varied*	*Varied*	*Varied*	*Varied*	*Varied*
$\tan\beta$	*Varied*	*Varied*	*Varied*	*Varied*	*Varied*	*Varied*
M_{SUSY}	500	1000	500	1000	1500	1500
M_{l_3}	1000	1000	1000	1000	M_{SUSY}	M_{SUSY}
X_t/M_{SUSY}	2	1.5	2	1.5	1.5	1.8
A_b	A_t	A_t	$\lvert A_t\rvert$	$\lvert A_t\rvert$	A_t	A_t
A_τ	A_t	A_t	$\lvert A_t\rvert$	$\lvert A_t\rvert$	$\lvert A_t\rvert$	$\lvert A_t\rvert$
μ	350	200	400	1000	1500	1500
M_1	*GUT*	*GUT*	340	250	500	500
M_2	350	200	400	500	1000	1000
M_3	1500	1500	$1500e^{i\phi_{M_3}}$	$1500e^{i\phi_{M_3}}$	$2500e^{i\phi_{M_3}}$	$2500e^{i\phi_{M_3}}$
$M_{\tilde{q}_{1,2}}$	1500	1500	1500	M_{SUSY}	M_{SUSY}	M_{SUSY}
$M_{\tilde{l}_{1,2}}$	500	500	1500	M_{SUSY}	M_{SUSY}	500
$A_{f\neq t,b,\tau}$	0	0	0	0	0	0

Appendix C

Renormalisation of the MSSM Higgs sector

Higher-order corrections to the MSSM Higgs sector have a significant impact on its phenomenology. Beyond tree level, the Higgs sector is affected by many more parameters in addition to $M_{A,H^\pm}$ and $\tan\beta$. In the following, we summarise the renormalisation of relevant quantities in the Higgs sector, for which a hybrid on-shell and $\overline{\text{DR}}$-renormalisation scheme is adopted as defined in Ref. [144].

C.1 Higgs potential

At one loop, the linear and bilinear terms in the MSSM Higgs potential (Eq. (3.33)) are renormalised by the following transformations

$$\mathbf{M}_{\phi\phi\chi\chi} \to \mathbf{M}_{\phi\phi\chi\chi} + \delta\mathbf{M}_{\phi\phi\chi\chi} \tag{C.1}$$

$$\mathbf{M}_{\phi^\pm\phi^\pm} \to \mathbf{M}_{\phi^\pm\phi^\pm} + \delta\mathbf{M}_{\phi^\pm\phi^\pm} \tag{C.2}$$

$$T_i \to T_i + \delta T_i, \quad i = h, H, A \tag{C.3}$$

$$\tan\beta \to \tan\beta(1 + \delta\tan\beta)\,. \tag{C.4}$$

Minimising the Higgs potential results in the one-loop tadpole coefficients to vanish,

$$T_i^{(1)} + \delta T_i = 0 \implies \delta T_i = -T_i, \quad i = h, H, A\,. \tag{C.5}$$

The mass counterterm matrices in the mass eigenbasis have the elements denoted by

$$\delta m_{ij}^2 = (\delta\mathbf{M}_{hHAG})_{ij} = (\mathbf{U}_n \delta\mathbf{M}_{\phi\phi\chi\chi}\mathbf{U}_n^\dagger)_{ij}\,. \tag{C.6}$$

$$\delta m_{ii}^2 \equiv \delta m_i^2, \qquad i, j = h, H, A, G\,, \tag{C.7}$$

and

$$\delta m^2_{kl} = (\delta \mathbf{M}_{H^\pm G^\pm})_{kl} = (\mathbf{U}_c \mathbf{M}_{\phi^\pm \phi^\pm} \mathbf{U}_c^\dagger)_{kl} \,, \tag{C.8}$$

$$\delta m^2_{kk} \equiv \delta m^2_k, \qquad k,l = H^\pm, G^\pm \,. \tag{C.9}$$

$\mathbf{U}_n(\alpha, \beta_n)$ and $\mathbf{U}_c(\beta_c)$ are the rotation matrices which stay unrenormalised. Furthermore, one field renormalisation constant is introduced for each Higgs doublet,

$$\mathcal{H}_{1,2} \to (1 + \frac{1}{2}\delta Z_{\mathcal{H}_{1,2}})\mathcal{H}_{1,2} \,. \tag{C.10}$$

The renormalisation constants $\delta Z_{ij}, \delta Z_{kl}$ of the physical fields are related to the above as

$$\begin{aligned}
\delta Z_{hh} &= s_\alpha^2 \delta Z_{\mathcal{H}_1} + c_\alpha^2 \delta Z_{\mathcal{H}_2} \,, && \text{(C.11)}\\
\delta Z_{AA} &= s_\beta^2 \delta Z_{\mathcal{H}_1} + c_\beta^2 \delta Z_{\mathcal{H}_2} && \text{(C.12)}\\
&= \delta Z_{H^- H^+} \,, && \text{(C.13)}\\
\delta Z_{hH} &= s_\alpha c_\alpha (\delta Z_{\mathcal{H}_2} - \delta Z_{\mathcal{H}_1}) \,, && \text{(C.14)}\\
\delta Z_{AG} &= s_\beta c_\beta (\delta Z_{\mathcal{H}_2} - \delta Z_{\mathcal{H}_1}) && \text{(C.15)}\\
&= \delta Z_{H^\pm G^\pm} \,, && \text{(C.16)}\\
\delta Z_{HH} &= c_\alpha^2 \delta Z_{\mathcal{H}_1} + s_\alpha^2 \delta Z_{\mathcal{H}_2} \,, && \text{(C.17)}\\
\delta Z_{GG} &= c_\beta^2 \delta Z_{\mathcal{H}_1} + s_\beta^2 \delta Z_{\mathcal{H}_2} && \text{(C.18)}\\
&= \delta Z_{G^- G^+} \,, && \text{(C.19)}
\end{aligned}$$

and all the $\mathcal{CP}$-violating terms are zero: $\delta Z_{hA} = \delta Z_{hG} = \delta Z_{HA} = \delta Z_{HG} = 0$.

C.2 Field and parameter renormalisation

There is no obvious physical observable to which we could relate $\tan\beta$ for an on-shell definition, therefore the $\overline{\text{DR}}$ scheme is adopted which has been shown to give numerically stable and gauge invariant results at one-loop order. The renormalisation constant for $\tan\beta$ is constructed from the field renormalisation constants for the Higgs doublets also defined in the $\overline{\text{DR}}$ scheme,

$$\begin{aligned}
\delta \tan\beta^{\overline{\text{DR}}} &= \frac{1}{2}(\delta Z_{\mathcal{H}_2}^{\overline{\text{DR}}} - \delta Z_{\mathcal{H}_1}^{\overline{\text{DR}}}) \qquad \text{with} \\
\delta Z_{\mathcal{H}_1}^{\overline{\text{DR}}} &= -\,\text{Re}\left[\Sigma'^{(\text{div})}_{HH}(m_H^2)\right]_{\alpha=0} \,, \\
\delta Z_{\mathcal{H}_2}^{\overline{\text{DR}}} &= -\,\text{Re}\left[\Sigma'^{(\text{div})}_{hh}(m_h^2)\right]_{\alpha=0} \,. && \text{(C.20)}\\
& && \text{(C.21)}
\end{aligned}$$

C.3 Higgs self-energies

The renormalised self-energies of the neutral Higgs bosons can be expressed in terms of the previously defined quantities as

$$\hat{\Sigma}_{ij}(p^2) = \Sigma_{ij}(p^2) + \delta Z_{ij} \left(p^2 - \frac{1}{2}(m_i^2 + m_j^2) \right) - \delta m_{ij}^2 \,, \tag{C.22}$$

$$\hat{\Sigma}_{ik}(p^2) = \Sigma_{ik}(p^2) - \delta m_{ik}^2 \,, \tag{C.23}$$

with $i, j \in \{h, H\}$ being the $\mathcal{CP}$-even eigenstates and $k = A$ being the $\mathcal{CP}$-odd one. Further, δZ_{ij} are the field renormalisation constants and $\delta m_{ij}^2, \delta m_{ik}^2$ are the mass counterterms defined earlier.

Bibliography

[1] S. Liebler, S. Patel and G. Weiglein, *Phenomenology of on-shell Higgs production in the MSSM with complex parameters*, *Eur. Phys. J.* **C77** (2017) 305, [1611.09308].

[2] E. Fuchs, S. Liebler, S. Patel and G. Weiglein, *The MSSM Higgs Sector with $\mathcal{CP}$ violation at the LHC Run 2*, in preparation.

[3] ATLAS collaboration, G. Aad et al., *Observation of a new particle in the search for the Standard Model Higgs boson with the ATLAS detector at the LHC*, *Phys. Lett.* **B716** (2012) 1–29, [1207.7214].

[4] CMS collaboration, S. Chatrchyan et al., *Observation of a new boson at a mass of 125 GeV with the CMS experiment at the LHC*, *Phys. Lett.* **B716** (2012) 30–61, [1207.7235].

[5] F. Englert and R. Brout, *Broken Symmetry and the Mass of Gauge Vector Mesons*, *Phys. Rev. Lett.* **13** (1964) 321–323.

[6] P. W. Higgs, *Broken Symmetries and the Masses of Gauge Bosons*, *Phys. Rev. Lett.* **13** (1964) 508–509.

[7] G. S. Guralnik, C. R. Hagen and T. W. B. Kibble, *Global Conservation Laws and Massless Particles*, *Phys. Rev. Lett.* **13** (1964) 585–587.

[8] M. Böhm, A. Denner and H. Joos, *Gauge theories of the strong and electroweak interaction*. Stuttgart, Germany: Teubner (2001).

[9] M. E. Peskin and D. V. Schroeder, *An Introduction to quantum field theory*. USA: Addison-Wesley (1995).

[10] Particle Data Group collaboration, C. Patrignani et al., *Review of Particle Physics*, *Chin. Phys.* **C40** (2016) 100001.

[11] D. Griffiths, *Introduction to elementary particles*. Weinheim, Germany: Wiley-VCH (2008).

[12] H. E. Logan, *TASI 2013 lectures on Higgs physics within and beyond the Standard Model*, 1406.1786.

[13] S. L. Glashow, *Partial symmetries of weak interactions*, *Nuclear Physics* **22** (1961) 579 – 588.

[14] A. Salam, *Weak and Electromagnetic Interactions*, *Conf. Proc.* **C680519** (1968) 367–377.

[15] S. Weinberg, *A model of leptons*, *Phys. Rev. Lett.* **19** (Nov, 1967) 1264–1266.

[16] S. L. Glashow, J. Iliopoulos and L. Maiani, *Weak interactions with lepton-hadron symmetry*, *Phys. Rev. D* **2** (Oct, 1970) 1285–1292.

[17] M. Gell-Mann, *Symmetries of baryons and mesons*, *Phys. Rev.* **125** (Feb, 1962) 1067–1084.

[18] M. Gell-Mann, *A schematic model of baryons and mesons*, *Physics Letters* **8** (1964) 214 – 215.

[19] Y. Ne'eman, *Derivation of strong interactions from a gauge invariance*, *Nuclear Physics* **26** (1961) 222 – 229.

[20] G. Zweig, *An SU(3) model for strong interaction symmetry and its breaking. Version 2*, in *Developments in the quark theory of hadrons Vol. 1. 1964 - 1978* (D. Lichtenberg and S. P. Rosen, eds.), pp. 22–101. 1964.

[21] P. W. Higgs, *Broken symmetries, massless particles and gauge fields*, *Phys. Lett.* **12** (1964) 132–133.

[22] Y. Nambu and G. Jona-Lasinio, *Dynamical Model of Elementary Particles Based on an Analogy with Superconductivity. 1.*, *Phys. Rev.* **122** (1961) 345–358.

[23] J. Goldstone, A. Salam and S. Weinberg, *Broken Symmetries*, *Phys. Rev.* **127** (1962) 965–970.

[24] Super-Kamiokande collaboration, Y. Fukuda et al., *Evidence for oscillation of atmospheric neutrinos*, *Phys. Rev. Lett.* **81** (1998) 1562–1567, [hep-ex/9807003].

[25] M. Kobayashi and T. Maskawa, *$\mathcal{CP}$ Violation in the Renormalizable Theory of Weak Interaction*, *Prog. Theor. Phys.* **49** (1973) 652–657.

[26] N. Cabibbo, *Unitary Symmetry and Leptonic Decays*, *Phys. Rev. Lett.* **10** (1963) 531–533.

[27] U. Amaldi, W. de Boer and H. Furstenau, *Comparison of grand unified theories with electroweak and strong coupling constants measured at LEP*, *Phys. Lett.* **B260** (1991) 447–455.

[28] WMAP collaboration, E. Komatsu et al., *Seven-Year Wilkinson Microwave Anisotropy Probe (WMAP) Observations: Cosmological Interpretation*, *Astrophys. J. Suppl.* **192** (2011) 18, [1001.4538].

[29] A. G. Cohen, A. De Rujula and S. L. Glashow, *A Matter - antimatter universe?*, *Astrophys. J.* **495** (1998) 539–549, [astro-ph/9707087].

[30] A. D. Sakharov, *Violation of $\mathcal{CP}$ Invariance, C Asymmetry, and Baryon Asymmetry of the Universe*, *Pisma Zh. Eksp. Teor. Fiz.* **5** (1967) 32–35.

[31] Planck collaboration, P. A. R. Ade et al., *Planck 2013 results. XVI. Cosmological parameters*, *Astron. Astrophys.* **571** (2014) A16, [1303.5076].

[32] A. Fowler, *Higher order and $\mathcal{CP}$-violating effects in the neutralino and Higgs boson sectors of the MSSM*. PhD thesis, Durham, IPPP, 2010.

[33] E. Fuchs, *Interference effects in new physics processes at the LHC*. PhD thesis, U. Hamburg, Dept. Phys., Hamburg, 2015. 10.3204/DESY-THESIS-2015-037.

[34] G. Weiglein, *Lectures on Higgs physics*, DESY Hamburg, 2014.

[35] G. Weiglein, *Lectures on physics beyond the Standard Model*, DESY Hamburg, 2014.

[36] S. P. Martin, *A Supersymmetry primer*, hep-ph/9709356.

[37] I. J. R. Aitchison, *Supersymmetry and the MSSM: An Elementary introduction*, hep-ph/0505105.

[38] J. F. Gunion, H. E. Haber, G. L. Kane and S. Dawson, *The Higgs Hunter's Guide*, *Front. Phys.* **80** (2000) 1–404.

[39] W. Pauli, *Dear radioactive ladies and gentlemen*, *Phys. Today* **31N9** (1978) 27.

[40] S. Coleman and J. Mandula, *All Possible Symmetries of the S Matrix*, *Phys. Rev.* **159** (Jul, 1967) 1251–1256.

[41] Yu. A. Golfand and E. P. Likhtman, *Extension of the Algebra of Poincare Group Generators and Violation of P Invariance*, *JETP Lett.* **13** (1971) 323–326.

[42] V. P. Akulov and D. V. Volkov, *Goldstone fields with spin 1/2*, *Theor. Math. Phys.* **18** (1974) 28.

[43] R. Haag, J. T. Lopuszanski and M. Sohnius, *All Possible Generators of Supersymmetries of the S Matrix*, *Nucl. Phys.* **B88** (1975) 257.

[44] J. Wess and B. Zumino, *Supergauge transformations in four dimensions*, *Nuclear Physics B* **70** (1974) 39 – 50.

[45] G. R. Farrar and P. Fayet, *Phenomenology of the Production, Decay, and Detection of New Hadronic States Associated with Supersymmetry*, *Phys. Lett.* **76B** (1978) 575–579.

[46] H. Goldberg, *Constraint on the photino mass from cosmology*, *Phys. Rev. Lett.* **50** (May, 1983) 1419–1422.

[47] J. Ellis, J. Hagelin, D. Nanopoulos, K. Olive and M. Srednicki, *Supersymmetric relics from the big bang*, *Nuclear Physics B* **238** (1984) 453 – 476.

[48] G. D'Ambrosio, G. F. Giudice, G. Isidori and A. Strumia, *Minimal flavor violation: An Effective field theory approach*, *Nucl. Phys.* **B645** (2002) 155–187, [hep-ph/0207036].

[49] A. J. Buras, *Minimal flavor violation*, *Acta Phys. Polon.* **B34** (2003) 5615–5668, [hep-ph/0310208].

[50] R. Barbieri, G. Isidori, J. Jones-Perez, P. Lodone and D. M. Straub, $U(2)$ *and Minimal Flavour Violation in Supersymmetry*, *Eur. Phys. J.* **C71** (2011) 1725, [1105.2296].

[51] K. E. Williams, H. Rzehak and G. Weiglein, *Higher order corrections to Higgs boson decays in the MSSM with complex parameters*, *Eur. Phys. J.* **C71** (2011) 1669, [1103.1335].

[52] T. Hahn, *Routines for the diagonalization of complex matrices*, physics/0607103.

[53] T. Takagi, *On an Algebraic Problem Related to an Analytic Theorem of Carathéodory and Fejér and on an Allied Theorem of Landau*, *Japanese journal of mathematics :transactions and abstracts* **1** (1924) 83–93.

[54] R. D. Peccei and H. R. Quinn, *Constraints imposed by $\mathcal{CP}$ conservation in the presence of instantons*, *Phys. Rev.* **D16** (1977) 1791–1797.

[55] R. D. Peccei and H. R. Quinn, *$\mathcal{CP}$ conservation in the presence of instantons*, *Phys. Rev. Lett.* **38** (1977) 1440–1443.

[56] N. Polonsky, *The μ parameter of supersymmetry*, in *Supersymmetry, supergravity and superstring. Proceedings, KIAS-CTP International Symposium, Seoul, Korea, June 23-26, 1999*, pp. 100–124, 1999. hep-ph/9911329.

[57] J. E. Kim and H. Nilles, *The μ-problem and the strong $\mathcal{CP}$-problem*, *Physics Letters B* **138** (1984) 150 – 154.

[58] OPAL, DELPHI, LEP Working Group for Higgs boson searches, ALEPH, L3 collaboration, R. Barate et al., *Search for the standard model Higgs boson at LEP*, *Phys. Lett.* **B565** (2003) 61–75, [hep-ex/0306033].

[59] J. Espinosa and M. Quirós, *Two-loop radiative corrections to the mass of the lightest Higgs boson in supersymmetric standard models*, *Physics Letters B* **266** (1991) 389 – 396.

[60] J. Ellis, G. Ridolfi and F. Zwirner, *On radiative corrections to supersymmetric Higgs boson masses and their implications for LEP searches*, *Physics Letters B* **262** (1991) 477 – 484.

[61] R. Barbieri and M. Frigeni, *The supersymmetric Higgs searches at LEP after radiative corrections*, *Physics Letters B* **258** (1991) 395 – 398.

[62] J. Ellis, G. Ridolfi and F. Zwirner, *Radiative corrections to the masses of supersymmetric Higgs bosons*, *Physics Letters B* **257** (1991) 83 – 91.

[63] H. E. Haber and R. Hempfling, *Can the mass of the lightest Higgs boson of the minimal supersymmetric model be larger than m_Z?*, *Phys. Rev. Lett.* **66** (Apr, 1991) 1815–1818.

[64] S. Heinemeyer, W. Hollik and G. Weiglein, *The Masses of the neutral $\mathcal{CP}$-even Higgs bosons in the MSSM: Accurate analysis at the two loop level*, *Eur. Phys. J.* **C9** (1999) 343–366, [hep-ph/9812472].

[65] H. Bahl, S. Heinemeyer, W. Hollik and G. Weiglein, *Reconciling EFT and hybrid calculations of the light MSSM Higgs-boson mass*, 1706.00346.

[66] H. Bahl and W. Hollik, *Precise prediction for the light MSSM Higgs boson mass combining effective field theory and fixed-order calculations*, *Eur. Phys. J.* **C76** (2016) 499, [1608.01880].

[67] T. Hahn, S. Heinemeyer, W. Hollik, H. Rzehak and G. Weiglein, *High-Precision Predictions for the Light $\mathcal{CP}$ -Even Higgs Boson Mass of the Minimal Supersymmetric Standard Model*, *Phys. Rev. Lett.* **112** (2014) 141801, [1312.4937].

[68] E. Bagnaschi, J. Pardo Vega and P. Slavich, *Improved determination of the Higgs mass in the MSSM with heavy superpartners*, *Eur. Phys. J.* **C77** (2017) 334, [1703.08166].

[69] J. Pardo Vega and G. Villadoro, *SusyHD: Higgs mass Determination in Supersymmetry*, *JHEP* **07** (2015) 159, [1504.05200].

[70] P. Bechtle, S. Heinemeyer, O. Stal, T. Stefaniak, G. Weiglein and L. Zeune, *MSSM Interpretations of the LHC Discovery: Light or Heavy Higgs?*, *Eur. Phys. J.* **C73** (2013) 2354, [1211.1955].

[71] T. Han, T. Li, S. Su and L.-T. Wang, *Non-Decoupling MSSM Higgs Sector and Light Superpartners*, *JHEP* **11** (2013) 053, [1306.3229].

[72] M. Drees, *A Supersymmetric Explanation of the Excess of Higgs–Like Events at the LHC and at LEP*, *Phys. Rev.* **D86** (2012) 115018, [1210.6507].

[73] R. Benbrik, M. Gomez Bock, S. Heinemeyer, O. Stal, G. Weiglein and L. Zeune, *Confronting the MSSM and the NMSSM with the discovery of a signal in the two Photon Channel at the LHC*, *Eur. Phys. J.* **C72** (2012) 2171, [1207.1096].

[74] K. Hagiwara, J. S. Lee and J. Nakamura, *Properties of 125 GeV Higgs boson in non-decoupling MSSM scenarios*, *JHEP* **10** (2012) 002, [1207.0802].

[75] J. F. Gunion, H. E. Haber and J. Wudka, *Sum rules for Higgs bosons*, *Phys. Rev. D* **43** (Feb, 1991) 904–912.

[76] J. F. Gunion and H. E. Haber, *$\mathcal{CP}$-conserving two-Higgs doublet model: The approach to the decoupling limit*, *Phys. Rev. D* **67** (Apr, 2003) 075019.

[77] P. Bechtle, H. E. Haber, S. Heinemeyer, O. Stål, T. Stefaniak, G. Weiglein et al., *The Light and Heavy Higgs Interpretation of the MSSM*, *Eur. Phys. J.* **C77** (2017) 67, [1608.00638].

[78] M. Carena, H. E. Haber, I. Low, N. R. Shah and C. E. M. Wagner, *Complementarity between Nonstandard Higgs Boson Searches and Precision Higgs Boson Measurements in the MSSM*, *Phys. Rev.* **D91** (2015) 035003, [1410.4969].

[79] M. Carena, I. Low, N. R. Shah and C. E. M. Wagner, *Impersonating the Standard Model Higgs Boson: Alignment without Decoupling*, *JHEP* **04** (2014) 015, [1310.2248].

[80] D. A. Demir, O. Lebedev, K. A. Olive, M. Pospelov and A. Ritz, *Electric dipole moments in the MSSM at large tan β*, *Nucl. Phys.* **B680** (2004) 339–374, [hep-ph/0311314].

[81] D. Chang, W.-Y. Keung and A. Pilaftsis, *New two loop contribution to electric dipole moment in supersymmetric theories*, *Phys. Rev. Lett.* **82** (1999) 900–903, [hep-ph/9811202].

[82] A. Pilaftsis, *Higgs boson two loop contributions to electric dipole moments in the MSSM*, *Phys. Lett.* **B471** (1999) 174–181, [hep-ph/9909485].

[83] W. Hollik, J. I. Illana, S. Rigolin and D. Stockinger, *One loop MSSM contribution to the weak magnetic dipole moments of heavy fermions*, *Phys. Lett.* **B416** (1998) 345–352, [hep-ph/9707437].

[84] W. Hollik, J. I. Illana, S. Rigolin and D. Stockinger, *Weak electric dipole moments of heavy fermions in the MSSM*, *Phys. Lett.* **B425** (1998) 322–328, [hep-ph/9711322].

[85] O. Lebedev, K. A. Olive, M. Pospelov and A. Ritz, *Probing $\mathcal{CP}$ violation with the deuteron electric dipole moment*, *Phys. Rev.* **D70** (2004) 016003, [hep-ph/0402023].

[86] V. D. Barger, T. Falk, T. Han, J. Jiang, T. Li and T. Plehn, *$\mathcal{CP}$-violating phases in SUSY, electric dipole moments, and linear colliders*, *Phys. Rev.* **D64** (2001) 056007, [hep-ph/0101106].

[87] Y. Li, S. Profumo and M. Ramsey-Musolf, *A Comprehensive Analysis of Electric Dipole Moment Constraints on $\mathcal{CP}$-violating Phases in the MSSM*, *JHEP* **08** (2010) 062, [1006.1440].

[88] Y. Nakai and M. Reece, *Electric Dipole Moments in Natural Supersymmetry*, 1612.08090.

[89] G. F. Giudice and A. Romanino, *Electric dipole moments in split supersymmetry*, *Phys. Lett.* **B634** (2006) 307–314, [hep-ph/0510197].

[90] M. Carena, J. Ellis, J. S. Lee, A. Pilaftsis and C. E. M. Wagner, *$\mathcal{CP}$ Violation in Heavy MSSM Higgs Scenarios*, *JHEP* **02** (2016) 123, [1512.00437].

[91] LHC Higgs Cross Section Working Group collaboration, J. R. Andersen et al., *Handbook of LHC Higgs Cross Sections: 3. Higgs Properties*, 1307.1347.

[92] LHC Higgs Cross Section Working Group collaboration, D. de Florian et al., *Handbook of LHC Higgs Cross Sections: 4. Deciphering the Nature of the Higgs Sector*, 1610.07922.

[93] ATLAS collaboration. See: https://twiki.cern.ch/twiki/bin/view/AtlasPublic/HiggsPublicResults, 2017.

[94] ATLAS collaboration. See: https://twiki.cern.ch/twiki/bin/view/AtlasPublic/SupersymmetryPublicResults, 2017.

[95] CMS collaboration. See: https://twiki.cern.ch/twiki/bin/view/CMSPublic/PhysicsResultsHIG, 2017.

[96] CMS collaboration. See: https://twiki.cern.ch/twiki/bin/view/CMSPublic/PhysicsResultsSUS, 2017.

[97] A. Djouadi, *The Anatomy of electro-weak symmetry breaking. II. The Higgs bosons in the minimal supersymmetric model*, *Phys. Rept.* **459** (2008) 1–241, [hep-ph/0503173].

[98] ATLAS collaboration, *Measurement of fiducial, differential and production cross sections in the $H \to \gamma\gamma$ decay channel with 13.3 fb^{-1} of 13 TeV proton-proton collision data with the ATLAS detector*, ATLAS-CONF-2016-067, CERN, Geneva, Aug, 2016.

[99] CMS collaboration, *Updated measurements of the Higgs boson at 125 GeV in the two photon decay channel*, CMS-PAS-HIG-13-001, 2013.

[100] ATLAS collaboration, *Measurements of the properties of the Higgs-like boson in the four lepton decay channel with the ATLAS detector using 25 fb^{-1} of proton-proton collision data*, ATLAS-CONF-2013-013, CERN, Geneva, Mar, 2013.

[101] CMS collaboration, S. Chatrchyan et al., *Measurement of the properties of a Higgs boson in the four-lepton final state*, *Phys. Rev.* **D89** (2014) 092007, [1312.5353].

[102] ATLAS, CMS collaboration, G. Aad et al., *Measurements of the Higgs boson production and decay rates and constraints on its couplings from a combined ATLAS and CMS analysis of the LHC pp collision data at $\sqrt{s} = 7$ and 8 TeV*, *JHEP* **08** (2016) 045, [1606.02266].

[103] ATLAS collaboration, G. Aad et al., *Evidence for the spin-0 nature of the Higgs boson using ATLAS data*, *Phys. Lett.* **B726** (2013) 120–144, [1307.1432].

[104] CMS collaboration, *Properties of the observed Higgs-like resonance using the diphoton channel*, CMS-PAS-HIG-13-016, 2013.

[105] CMS collaboration, V. Khachatryan et al., *Search for supersymmetry in the all-hadronic final state using top quark tagging in pp collisions at $\sqrt{s} = 13$ TeV*, 1701.01954.

[106] D. S. M. Alves, E. Izaguirre and J. G. Wacker, *Where the Sidewalk Ends: Jets and Missing Energy Search Strategies for the 7 TeV LHC*, *JHEP* **10** (2011) 012, [1102.5338].

[107] ATLAS collaboration, H. Okawa, *Interpretations of SUSY Searches in ATLAS with Simplified Models*, in *Particles and fields. Proceedings, Meeting of the Division of the American Physical Society, DPF 2011, Providence, USA, August 9-13, 2011*, 2011. 1110.0282.

[108] J. Alwall, P. Schuster and N. Toro, *Simplified Models for a First Characterization of New Physics at the LHC*, *Phys. Rev.* **D79** (2009) 075020, [0810.3921].

[109] CMS collaboration, S. Chatrchyan et al., *Interpretation of Searches for Supersymmetry with simplified Models*, *Phys. Rev.* **D88** (2013) 052017, [1301.2175].

[110] J. Alwall, M.-P. Le, M. Lisanti and J. G. Wacker, *Model-Independent Jets plus Missing Energy Searches*, *Phys. Rev.* **D79** (2009) 015005, [0809.3264].

[111] LHC New Physics Working Group collaboration, D. Alves, *Simplified Models for LHC New Physics Searches*, *J. Phys.* **G39** (2012) 105005, [1105.2838].

[112] C. Borschensky, M. Krämer, A. Kulesza, M. Mangano, S. Padhi, T. Plehn et al., *Squark and gluino production cross sections in pp collisions at $\sqrt{s}$ = 13, 14, 33 and 100 TeV*, *Eur. Phys. J.* **C74** (2014) 3174, [1407.5066].

[113] L. Zeune, *Constraining supersymmetric models using Higgs physics, precision observables and direct searches*. PhD thesis, U. Hamburg, Dept. Phys., Cham, 2014. 10.1007/978-3-319-22228-8.

[114] M. Drees, H. Dreiner, D. Schmeier, J. Tattersall and J. S. Kim, *CheckMATE: Confronting your Favourite New Physics Model with LHC Data*, *Comput. Phys. Commun.* **187** (2015) 227–265, [1312.2591].

[115] D. Dercks, N. Desai, J. S. Kim, K. Rolbiecki, J. Tattersall and T. Weber, *CheckMATE 2: From the model to the limit*, 1611.09856.

[116] J. M. Butterworth, D. Grellscheid, M. Krämer, B. Sarrazin and D. Yallup, *Constraining new physics with collider measurements of Standard Model signatures*, *JHEP* **03** (2017) 078, [1606.05296].

[117] D. Barducci, A. Belyaev, M. Buchkremer, J. Marrouche, S. Moretti and L. Panizzi, *XQCAT: eXtra Quark Combined Analysis Tool*, *Comput. Phys. Commun.* **197** (2015) 263–275, [1409.3116].

[118] D. Barducci, A. Belyaev, M. Buchkremer, G. Cacciapaglia, A. Deandrea, S. De Curtis et al., *Framework for Model Independent Analyses of Multiple Extra Quark Scenarios*, *JHEP* **12** (2014) 080, [1405.0737].

[119] M. Papucci, K. Sakurai, A. Weiler and L. Zeune, *Fastlim: a fast LHC limit calculator*, *Eur. Phys. J.* **C74** (2014) 3163, [1402.0492].

[120] S. Kraml, S. Kulkarni, U. Laa, A. Lessa, W. Magerl, D. Proschofsky-Spindler et al., *SModelS: a tool for interpreting simplified-model results from the LHC and its application to supersymmetry*, *Eur. Phys. J.* **C74** (2014) 2868, [1312.4175].

[121] F. Ambrogi, S. Kraml, S. Kulkarni, U. Laa, A. Lessa, V. Magerl et al., *SModelS v1.1 user manual*, 1701.06586.

[122] GAMBIT collaboration, P. Athron et al., *GAMBIT: The Global and Modular Beyond-the-Standard-Model Inference Tool*, 1705.07908.

[123] ATLAS collaboration, G. Aad et al., *Search for neutral Higgs bosons of the minimal supersymmetric standard model in pp collisions at* $\sqrt{s} = 8$ *TeV with the ATLAS detector*, *JHEP* **11** (2014) 056, [1409.6064].

[124] CMS collaboration, V. Khachatryan et al., *Search for neutral MSSM Higgs bosons decaying to a pair of tau leptons in pp collisions*, *JHEP* **10** (2014) 160, [1408.3316].

[125] CMS collaboration, *Search for charged Higgs bosons with the* $H^+ \to \tau\nu$ *decay channel in the fully hadronic final state at* $\sqrt{s} = 8$ *TeV*, CMS-PAS-HIG-14-020, 2014.

[126] ATLAS collaboration, G. Aad et al., *Search for charged Higgs bosons decaying via* $H^\pm \to \tau^\pm\nu$ *in fully hadronic final states using pp collision data at* $\sqrt{s} = 8$ *TeV with the ATLAS detector*, *JHEP* **03** (2015) 088, [1412.6663].

[127] ATLAS collaboration, *Search for additional heavy neutral Higgs and gauge bosons in the ditau final state produced in 36.1* fb^{-1} *of pp collisions at* $\sqrt{s} = 13$ *TeV with the ATLAS detector*, ATLAS-CONF-2017-050, CERN, Geneva, Jul, 2017.

[128] CMS collaboration, *Search for a neutral MSSM Higgs boson decaying into* $\tau\tau$ *with 12.9* fb^{-1} *of data at* $\sqrt{s} = 13$ TeV, CMS-PAS-HIG-16-037, CERN, Geneva, 2016.

[129] E. Bagnaschi, F. Frensch, S. Heinemeyer, G. Lee, S. R. Liebler, M. Muhlleitner et al., *Benchmark scenarios for low* $\tan\beta$ *in the MSSM*, LHCHXSWG-2015-002, CERN, Geneva, Aug, 2015.

[130] M. Carena, S. Heinemeyer, O. Stål, C. E. M. Wagner and G. Weiglein, *MSSM Higgs Boson Searches at the LHC: Benchmark Scenarios after the Discovery of a Higgs-like Particle*, *Eur. Phys. J.* **C73** (2013) 2552, [1302.7033].

[131] N. Kauer, *Narrow-width approximation limitations*, *Phys. Lett.* **B649** (2007) 413–416, [hep-ph/0703077].

[132] D. Berdine, N. Kauer and D. Rainwater, *Breakdown of the Narrow Width Approximation for New Physics*, *Phys. Rev. Lett.* **99** (2007) 111601, [hep-ph/0703058].

[133] C. F. Uhlemann and N. Kauer, *Narrow-width approximation accuracy*, *Nucl. Phys.* **B814** (2009) 195–211, [0807.4112].

[134] G. Cacciapaglia, A. Deandrea and S. De Curtis, *Nearby resonances beyond the Breit-Wigner approximation*, *Phys. Lett.* **B682** (2009) 43–49, [0906.3417].

[135] J. Reuter, *Off-Shell and Interference Effects for SUSY Particle Production*, *eConf* **C0705302** (2007) SUS14, [0709.0068].

[136] D. Barducci, A. Belyaev, J. Blamey, S. Moretti, L. Panizzi and H. Prager, *Towards model-independent approach to the analysis of interference effects in pair production of new heavy quarks*, *JHEP* **07** (2014) 142, [1311.3977].

[137] E. Fuchs, S. Thewes and G. Weiglein, *Interference effects in BSM processes with a generalised narrow-width approximation*, *Eur. Phys. J.* **C75** (2015) 254, [1411.4652].

[138] E. Fuchs and G. Weiglein, *Breit-Wigner approximation for propagators of mixed unstable states*, 1610.06193.

[139] K. E. Williams and G. Weiglein, *Precise predictions for $h_a \to h_b h_c$ decays in the complex MSSM*, *Phys. Lett.* **B660** (2008) 217–227, [0710.5320].

[140] A. C. Fowler and G. Weiglein, *Precise Predictions for Higgs Production in Neutralino Decays in the Complex MSSM*, *JHEP* **01** (2010) 108, [0909.5165].

[141] A. Bharucha, A. Fowler, G. Moortgat-Pick and G. Weiglein, *Consistent on shell renormalisation of electroweakinos in the complex MSSM: LHC and LC predictions*, *JHEP* **05** (2013) 053, [1211.3134].

[142] O. Brein, A. Djouadi and R. Harlander, *NNLO QCD corrections to the Higgs-strahlung processes at hadron colliders*, *Phys. Lett.* **B579** (2004) 149–156, [hep-ph/0307206].

[143] R. V. Harlander, S. Liebler and T. Zirke, *Higgsstrahlung at the Large Hadron Collider in the 2-Higgs-Doublet Model*, *JHEP* **02** (2014) 023, [1307.8122].

[144] M. Frank, T. Hahn, S. Heinemeyer, W. Hollik, H. Rzehak and G. Weiglein, *The Higgs Boson Masses and Mixings of the Complex MSSM in the Feynman-Diagrammatic Approach*, *JHEP* **02** (2007) 047, [hep-ph/0611326].

[145] P. H. Chankowski, S. Pokorski and J. Rosiek, *Complete on-shell renormalization scheme for the minimal supersymmetric Higgs sector*, *Nucl. Phys.* **B423** (1994) 437–496, [hep-ph/9303309].

[146] A. Dabelstein, *Fermionic decays of neutral MSSM Higgs bosons at the one loop level*, *Nucl. Phys.* **B456** (1995) 25–56, [hep-ph/9503443].

[147] S. Heinemeyer, W. Hollik, J. Rosiek and G. Weiglein, *Neutral MSSM Higgs boson production at e^+e^- colliders in the Feynman diagrammatic approach*, *Eur. Phys. J.* **C19** (2001) 535–546, [hep-ph/0102081].

[148] H. Lehmann, K. Symanzik and W. Zimmermann, *On the formulation of quantized field theories*, *Nuovo Cim.* **1** (1955) 205–225.

[149] S. Heinemeyer, W. Hollik and G. Weiglein, *FeynHiggs: A Program for the calculation of the masses of the neutral $\mathcal{CP}$ even Higgs bosons in the MSSM*, *Comput. Phys. Commun.* **124** (2000) 76–89, [hep-ph/9812320].

[150] G. Degrassi, S. Heinemeyer, W. Hollik, P. Slavich and G. Weiglein, *Towards high precision predictions for the MSSM Higgs sector*, *Eur. Phys. J.* **C28** (2003) 133–143, [hep-ph/0212020].

[151] LHC Higgs Cross Section Working Group collaboration, S. Dittmaier et al., *Handbook of LHC Higgs Cross Sections: 1. Inclusive Observables*, 1101.0593.

[152] S. Dittmaier et al., *Handbook of LHC Higgs Cross Sections: 2. Differential Distributions*, 1201.3084.

[153] A. Dedes and S. Moretti, *Effects of $\mathcal{CP}$-violating phases on Higgs boson production at hadron colliders in the minimal supersymmetric standard model*, *Nucl. Phys.* **B576** (2000) 29–55, [hep-ph/9909418].

[154] S. Y. Choi and J. S. Lee, *MSSM Higgs boson production at hadron colliders with explicit $\mathcal{CP}$ violation*, *Phys. Rev.* **D61** (2000) 115002, [hep-ph/9910557].

[155] S. Y. Choi, K. Hagiwara and J. S. Lee, *Observability of the lightest MSSM Higgs boson with explicit $\mathcal{CP}$ violation via gluon fusion at the LHC*, *Phys. Lett.* **B529** (2002) 212–221, [hep-ph/0110138].

[156] M. Carena, J. R. Ellis, S. Mrenna, A. Pilaftsis and C. E. M. Wagner, *Collider probes of the MSSM Higgs sector with explicit $\mathcal{CP}$ violation*, *Nucl. Phys.* **B659** (2003) 145–178, [hep-ph/0211467].

[157] A. Arhrib, D. K. Ghosh and O. C. W. Kong, *Observing $\mathcal{CP}$-violating MSSM Higgs bosons at hadron colliders?*, *Phys. Lett.* **B537** (2002) 217–226, [hep-ph/0112039].

[158] Q.-H. Cao, D. Nomura, K. Tobe and C. P. Yuan, *Enhancement of $\mathcal{CP}$-odd higgs boson production in the minimal supersymmetric standard model with explicit $\mathcal{CP}$ violation*, *Phys. Lett.* **B632** (2006) 688–694, [hep-ph/0508311].

[159] S. Hesselbach, S. Moretti, S. Munir and P. Poulose, *Exploring the Di-Photon Decay of a Light Higgs Boson in the MSSM With Explicit $\mathcal{CP}$ Violation*, *Eur. Phys. J.* **C54** (2008) 129–147, [0706.4269].

[160] S. Hesselbach, S. Moretti, S. Munir and P. Poulose, *Explicit $\mathcal{CP}$ violation in the MSSM through $gg \to H(1) \to \gamma\gamma$*, *Phys. Rev.* **D82** (2010) 074004, [0903.0747].

[161] R. V. Harlander, S. Liebler and H. Mantler, *SusHi: A program for the calculation of Higgs production in gluon fusion and bottom-quark annihilation in the Standard Model and the MSSM*, *Comput. Phys. Commun.* **184** (2013) 1605–1617, [1212.3249].

[162] R. V. Harlander, S. Liebler and H. Mantler, *SusHi Bento: Beyond NNLO and the heavy-top limit*, *Comput. Phys. Commun.* **212** (2017) 239–257, [1605.03190].

[163] R. V. Harlander, *Higgs production in heavy quark annihilation through next-to-next-to-leading order QCD*, *Eur. Phys. J.* **C76** (2016) 252, [1512.04901].

[164] S. Liebler, *Neutral Higgs production at proton colliders in the $\mathcal{CP}$-conserving NMSSM*, *Eur. Phys. J.* **C75** (2015) 210, [1502.07972].

[165] J. Küblbeck, M. Böhm and A. Denner, *FeynArts — computer-algebraic generation of Feynman graphs and amplitudes*, *Computer Physics Communications* **60** (1990) 165 – 180.

[166] A. Denner, H. Eck, O. Hahn and J. Küblbeck, *Feynman rules for fermion-number-violating interactions*, *Nuclear Physics B* **387** (1992) 467 – 481.

[167] T. Hahn, *Generating Feynman diagrams and amplitudes with FeynArts 3*, *Computer Physics Communications* **140** (2001) 418 – 431.

[168] J. Kublbeck, H. Eck and R. Mertig, *Computer algebraic generation and calculation of Feynman graphs using FeynArts and FeynCalc*, *Nucl. Phys. Proc. Suppl.* **29A** (1992) 204–208.

[169] T. Fritzsche, T. Hahn, S. Heinemeyer, F. von der Pahlen, H. Rzehak and C. Schappacher, *The implementation of the renormalized complex MSSM in FeynArts and FormCalc*, *Computer Physics Communications* **185** (2014) 1529 – 1545.

[170] T. Hahn and M. Perez-Victoria, *Automatized one loop calculations in four-dimensions and D-dimensions*, *Comput. Phys. Commun.* **118** (1999) 153–165, [hep-ph/9807565].

[171] T. Hahn, *Generating and calculating one loop Feynman diagrams with FeynArts, FormCalc, and LoopTools*, hep-ph/9905354.

[172] T. Hahn, *Automatic loop calculations with FeynArts, FormCalc, and LoopTools*, *Nuclear Physics B - Proceedings Supplements* **89** (2000) 231 – 236.

[173] T. Hahn and M. Rauch, *News from FormCalc and LoopTools*, *Nucl. Phys. Proc. Suppl.* **157** (2006) 236–240, [hep-ph/0601248].

[174] T. Hahn, *A Mathematica interface for FormCalc-generated code*, *Comput. Phys. Commun.* **178** (2008) 217–221, [hep-ph/0611273].

[175] V. Shtabovenko, R. Mertig and F. Orellana, *New Developments in FeynCalc 9.0*, *Comput. Phys. Commun.* **207** (2016) 432–444, [1601.01167].

[176] R. Mertig, M. Böhm and A. Denner, *FeynCalc - Computer-algebraic calculation of Feynman amplitudes*, *Computer Physics Communications* **64** (1991) 345 – 359.

[177] P. Bechtle, S. Heinemeyer, O. Stal, T. Stefaniak and G. Weiglein, *Applying Exclusion Likelihoods from LHC Searches to Extended Higgs Sectors*, *Eur. Phys. J.* **C75** (2015) 421, [1507.06706].

[178] P. Bechtle, O. Brein, S. Heinemeyer, O. Stål, T. Stefaniak, G. Weiglein et al., *HiggsBounds–4: Improved Tests of Extended Higgs Sectors against Exclusion Bounds from LEP, the Tevatron and the LHC*, *Eur. Phys. J.* **C74** (2014) 2693, [1311.0055].

[179] P. Bechtle, O. Brein, S. Heinemeyer, G. Weiglein and K. E. Williams, *HiggsBounds: Confronting Arbitrary Higgs Sectors with Exclusion Bounds from LEP and the Tevatron*, *Comput. Phys. Commun.* **181** (2010) 138–167, [0811.4169].

[180] P. Bechtle, O. Brein, S. Heinemeyer, O. Stal, T. Stefaniak, G. Weiglein et al., *Recent Developments in HiggsBounds and a Preview of HiggsSignals*, *PoS* **CHARGED2012** (2012) 024, [1301.2345].

[181] H. M. Georgi, S. L. Glashow, M. E. Machacek and D. V. Nanopoulos, *Higgs Bosons from Two Gluon Annihilation in Proton Proton Collisions*, *Phys. Rev. Lett.* **40** (1978) 692.

[182] M. Spira, A. Djouadi, D. Graudenz and P. M. Zerwas, *Higgs boson production at the LHC*, *Nucl. Phys.* **B453** (1995) 17–82, [hep-ph/9504378].

[183] S. Bentvelsen, E. Laenen and P. Motylinski, *Higgs production through gluon fusion at leading order*, NIKHEF 2005-007.

[184] S. R. Liebler, *LHC phenomenology and higher order electroweak corrections in supersymmetric models with and without R-parity*. PhD thesis, Wurzburg U., 2011.

[185] G. 't Hooft and M. Veltman, *Scalar one-loop integrals*, *Nuclear Physics B* **153** (1979) 365 – 401.

[186] G. Passarino and M. Veltman, *One-loop corrections for e^+e^- annihilation into $\mu^+\mu^-$ in the Weinberg model*, *Nuclear Physics B* **160** (1979) 151 – 207.

[187] V. D. Barger, M. S. Berger and P. Ohmann, *Supersymmetric grand unified theories: Two loop evolution of gauge and Yukawa couplings*, *Phys. Rev.* **D47** (1993) 1093–1113, [hep-ph/9209232].

[188] J. Rosiek, *Complete set of Feynman rules for the MSSM: Erratum*, hep-ph/9511250.

[189] T. Banks, *Supersymmetry and the Quark Mass Matrix*, *Nucl. Phys.* **B303** (1988) 172–188.

[190] L. J. Hall, R. Rattazzi and U. Sarid, *The Top quark mass in supersymmetric SO(10) unification*, *Phys. Rev.* **D50** (1994) 7048–7065, [hep-ph/9306309].

[191] R. Hempfling, *Yukawa coupling unification with supersymmetric threshold corrections*, *Phys. Rev.* **D49** (1994) 6168–6172.

[192] M. Carena, M. Olechowski, S. Pokorski and C. E. M. Wagner, *Electroweak symmetry breaking and bottom-top Yukawa unification*, *Nucl. Phys.* **B426** (1994) 269–300, [hep-ph/9402253].

[193] M. Carena, D. Garcia, U. Nierste and C. E. M. Wagner, *Effective Lagrangian for the $\bar{t}bH^+$ interaction in the MSSM and charged Higgs phenomenology*, *Nucl. Phys.* **B577** (2000) 88–120, [hep-ph/9912516].

[194] M. Carena, D. Garcia, U. Nierste and C. E. M. Wagner, $b \to s\gamma$ *and supersymmetry with large* $\tan\beta$, *Phys. Lett.* **B499** (2001) 141–146, [hep-ph/0010003].

[195] J. Baglio, R. Gröber, M. Mühlleitner, D. T. Nhung, H. Rzehak, M. Spira et al., *NMSSMCALC: A Program Package for the Calculation of Loop-Corrected Higgs Boson Masses and Decay Widths in the (Complex) NMSSM*, *Comput. Phys. Commun.* **185** (2014) 3372–3391, [1312.4788].

[196] M. Frank, L. Galeta, T. Hahn, S. Heinemeyer, W. Hollik, H. Rzehak et al., *Charged Higgs Boson Mass of the MSSM in the Feynman Diagrammatic Approach*, *Phys. Rev.* **D88** (2013) 055013, [1306.1156].

[197] L. Hofer, U. Nierste and D. Scherer, *Resummation of tan β-enhanced supersymmetric loop corrections beyond the decoupling limit*, *JHEP* **10** (2009) 081, [0907.5408].

[198] D. Noth and M. Spira, *Supersymmetric Higgs Yukawa Couplings to Bottom Quarks at next-to-next-to-leading Order*, *JHEP* **06** (2011) 084, [1001.1935].

[199] D. Noth and M. Spira, *Higgs Boson Couplings to Bottom Quarks: Two-Loop Supersymmetry-QCD Corrections*, *Phys. Rev. Lett.* **101** (2008) 181801, [0808.0087].

[200] A. Bauer, L. Mihaila and J. Salomon, *Matching coefficients for $\alpha(s)$ and m(b) to $O(\alpha^2(s))$ in the MSSM*, *JHEP* **02** (2009) 037, [0810.5101].

[201] A. Djouadi, M. Spira and P. M. Zerwas, *Production of Higgs bosons in proton colliders: QCD corrections*, *Phys. Lett.* **B264** (1991) 440–446.

[202] S. Dawson, *Radiative corrections to Higgs boson production*, *Nucl. Phys.* **B359** (1991) 283–300.

[203] R. Harlander and P. Kant, *Higgs production and decay: Analytic results at next-to-leading order QCD*, *JHEP* **12** (2005) 015, [hep-ph/0509189].

[204] C. Anastasiou, S. Beerli, S. Bucherer, A. Daleo and Z. Kunszt, *Two-loop amplitudes and master integrals for the production of a Higgs boson via a massive quark and a scalar-quark loop*, *JHEP* **01** (2007) 082, [hep-ph/0611236].

[205] U. Aglietti, R. Bonciani, G. Degrassi and A. Vicini, *Analytic Results for Virtual QCD Corrections to Higgs Production and Decay*, *JHEP* **01** (2007) 021, [hep-ph/0611266].

[206] R. V. Harlander and W. B. Kilgore, *Next-to-next-to-leading order Higgs production at hadron colliders*, *Phys. Rev. Lett.* **88** (2002) 201801, [hep-ph/0201206].

[207] C. Anastasiou and K. Melnikov, *Higgs boson production at hadron colliders in NNLO QCD*, *Nucl. Phys.* **B646** (2002) 220–256, [hep-ph/0207004].

[208] V. Ravindran, J. Smith and W. L. van Neerven, *NNLO corrections to the total cross-section for Higgs boson production in hadron-hadron collisions*, *Nucl. Phys.* **B665** (2003) 325–366, [hep-ph/0302135].

[209] R. V. Harlander, H. Mantler, S. Marzani and K. J. Ozeren, *Higgs production in gluon fusion at next-to-next-to-leading order QCD for finite top mass*, *Eur. Phys. J.* **C66** (2010) 359–372, [0912.2104].

[210] R. V. Harlander and K. J. Ozeren, *Finite top mass effects for hadronic Higgs production at next-to-next-to-leading order*, *JHEP* **11** (2009) 088, [0909.3420].

[211] R. V. Harlander and K. J. Ozeren, *Top mass effects in Higgs production at next-to-next-to-leading order QCD: Virtual corrections*, *Phys. Lett.* **B679** (2009) 467–472, [0907.2997].

[212] A. Pak, M. Rogal and M. Steinhauser, *Finite top quark mass effects in NNLO Higgs boson production at LHC*, *JHEP* **02** (2010) 025, [0911.4662].

[213] A. Pak, M. Rogal and M. Steinhauser, *Virtual three-loop corrections to Higgs boson production in gluon fusion for finite top quark mass*, *Phys. Lett.* **B679** (2009) 473–477, [0907.2998].

[214] A. Pak, M. Rogal and M. Steinhauser, *Production of scalar and pseudo-scalar Higgs bosons to next-to-next-to-leading order at hadron colliders*, *JHEP* **09** (2011) 088, [1107.3391].

[215] S. Marzani, R. D. Ball, V. Del Duca, S. Forte and A. Vicini, *Higgs production via gluon-gluon fusion with finite top mass beyond next-to-leading order*, *Nucl. Phys.* **B800** (2008) 127–145, [0801.2544].

[216] T. Neumann and C. Williams, *The Higgs boson at high p_T*, *Phys. Rev.* **D95** (2017) 014004, [1609.00367].

[217] C. Anastasiou, C. Duhr, F. Dulat, E. Furlan, T. Gehrmann, F. Herzog et al., *Higgs boson gluon–fusion production at threshold in N^3LO QCD*, *Phys. Lett.* **B737** (2014) 325–328, [1403.4616].

[218] Y. Li, A. von Manteuffel, R. M. Schabinger and H. X. Zhu, *Soft-virtual corrections to Higgs production at N^3LO*, *Phys. Rev.* **D91** (2015) 036008, [1412.2771].

[219] C. Anastasiou, C. Duhr, F. Dulat, E. Furlan, T. Gehrmann, F. Herzog et al., *Higgs Boson Gluon fusion Production Beyond Threshold in N^3LO QCD*, *JHEP* **03** (2015) 091, [1411.3584].

[220] C. Anastasiou, C. Duhr, F. Dulat, F. Herzog and B. Mistlberger, *Higgs Boson Gluon-Fusion Production in QCD at Three Loops*, *Phys. Rev. Lett.* **114** (2015) 212001, [1503.06056].

[221] C. Anastasiou, C. Duhr, F. Dulat, E. Furlan, T. Gehrmann, F. Herzog et al., *High precision determination of the gluon fusion Higgs boson cross-section at the LHC*, *JHEP* **05** (2016) 058, [1602.00695].

[222] T. Ahmed, M. C. Kumar, P. Mathews, N. Rana and V. Ravindran, *Pseudo-scalar Higgs boson production at threshold N^3LO and N^3LL QCD*, *Eur. Phys. J.* **C76** (2016) 355, [1510.02235].

[223] T. Ahmed, M. Bonvini, M. C. Kumar, P. Mathews, N. Rana, V. Ravindran et al., *Pseudo-scalar Higgs boson production at $N^3LO_A + N^3LL'$*, *Eur. Phys. J.* **C76** (2016) 663, [1606.00837].

[224] A. Djouadi and P. Gambino, *Leading electroweak correction to Higgs boson production at proton colliders*, *Phys. Rev. Lett.* **73** (1994) 2528–2531, [hep-ph/9406432].

[225] A. Djouadi, P. Gambino and B. A. Kniehl, *Two-loop electroweak heavy fermion corrections to Higgs boson production and decay*, *Nucl. Phys.* **B523** (1998) 17–39, [hep-ph/9712330].

[226] R. Bonciani, G. Degrassi and A. Vicini, *On the Generalized Harmonic Polylogarithms of One Complex Variable*, *Comput. Phys. Commun.* **182** (2011) 1253–1264, [1007.1891].

[227] U. Aglietti, R. Bonciani, G. Degrassi and A. Vicini, *Two-loop light fermion contribution to Higgs production and decays*, *Phys. Lett.* **B595** (2004) 432–441, [hep-ph/0404071].

[228] G. Degrassi and F. Maltoni, *Two-loop electroweak corrections to Higgs production at hadron colliders*, *Phys. Lett.* **B600** (2004) 255–260, [hep-ph/0407249].

[229] C. Anastasiou and K. Melnikov, *Pseudoscalar Higgs boson production at hadron colliders in NNLO QCD*, *Phys. Rev.* **D67** (2003) 037501, [hep-ph/0208115].

[230] R. V. Harlander and W. B. Kilgore, *Production of a pseudoscalar Higgs boson at hadron colliders at next-to-next-to leading order*, *JHEP* **10** (2002) 017, [hep-ph/0208096].

[231] R. V. Harlander, F. Hofmann and H. Mantler, *Supersymmetric Higgs production in gluon fusion*, *JHEP* **02** (2011) 055, [1012.3361].

[232] R. V. Harlander and M. Steinhauser, *Hadronic Higgs production and decay in supersymmetry at next-to-leading order*, *Phys. Lett.* **B574** (2003) 258–268, [hep-ph/0307346].

[233] R. V. Harlander and M. Steinhauser, *Supersymmetric Higgs production in gluon fusion at next-to-leading order*, *JHEP* **09** (2004) 066, [hep-ph/0409010].

[234] R. V. Harlander and F. Hofmann, *Pseudo-scalar Higgs production at next-to-leading order SUSY-QCD*, *JHEP* **03** (2006) 050, [hep-ph/0507041].

[235] G. Degrassi and P. Slavich, *On the NLO QCD corrections to Higgs production and decay in the MSSM*, *Nucl. Phys.* **B805** (2008) 267–286, [0806.1495].

[236] G. Degrassi and P. Slavich, *NLO QCD bottom corrections to Higgs boson production in the MSSM*, *JHEP* **11** (2010) 044, [1007.3465].

[237] G. Degrassi, S. Di Vita and P. Slavich, *NLO QCD corrections to pseudoscalar Higgs production in the MSSM*, *JHEP* **08** (2011) 128, [1107.0914].

[238] G. Degrassi, S. Di Vita and P. Slavich, *On the NLO QCD Corrections to the Production of the Heaviest Neutral Higgs Scalar in the MSSM*, *Eur. Phys. J.* **C72** (2012) 2032, [1204.1016].

[239] C. Anastasiou, S. Beerli and A. Daleo, *The Two-loop QCD amplitude $gg \to h, H$ in the Minimal Supersymmetric Standard Model*, *Phys. Rev. Lett.* **100** (2008) 241806, [0803.3065].

[240] M. Muhlleitner, H. Rzehak and M. Spira, *SUSY-QCD Corrections to MSSM Higgs Boson Production via Gluon fusion*, *PoS* **RADCOR2009** (2010) 043, [1001.3214].

[241] M. Muhlleitner and M. Spira, *Higgs Boson Production via Gluon Fusion: Squark Loops at NLO QCD*, *Nucl. Phys.* **B790** (2008) 1–27, [hep-ph/0612254].

[242] A. Pak, M. Steinhauser and N. Zerf, *Towards Higgs boson production in gluon fusion to NNLO in the MSSM*, *Eur. Phys. J.* **C71** (2011) 1602, [1012.0639].

[243] A. Pak, M. Steinhauser and N. Zerf, *Supersymmetric next-to-next-to-leading order corrections to Higgs boson production in gluon fusion*, *JHEP* **09** (2012) 118, [1208.1588].

[244] R. Harlander and M. Steinhauser, *Effects of SUSY QCD in hadronic Higgs production at next-to-next-to-leading order*, *Phys. Rev.* **D68** (2003) 111701, [hep-ph/0308210].

[245] R. Harlander. See: http://www.robert-harlander.de/software.

[246] S. Heinemeyer, W. Hollik, D. Stockinger, A. M. Weber and G. Weiglein, *Precise prediction for M(W) in the MSSM*, *JHEP* **08** (2006) 052, [hep-ph/0604147].

[247] T. Hahn, S. Heinemeyer, W. Hollik, H. Rzehak and G. Weiglein, *Higgs Masses and More in the Complex MSSM with FeynHiggs*, in *SUSY 2007 Proceedings, 15th International Conference on Supersymmetry and Unification of Fundamental Interactions, July 26 - August 1, 2007, Karlsruhe, Germany*, pp. 442–449, 2007. 0710.4891.

[248] S. Heinemeyer, W. Hollik, H. Rzehak and G. Weiglein, *The Higgs sector of the complex MSSM at two-loop order: QCD contributions*, *Phys. Lett.* **B652** (2007) 300–309, [0705.0746].

[249] T. Hahn, S. Heinemeyer, W. Hollik, H. Rzehak and G. Weiglein, *FeynHiggs: A program for the calculation of MSSM Higgs boson observables - Version 2.6.5*, *Comput. Phys. Commun.* **180** (2009) 1426–1427.

[250] W. Hollik and S. Paßehr, *Two-loop top-Yukawa-coupling corrections to the Higgs boson masses in the complex MSSM*, *Phys. Lett.* **B733** (2014) 144–150, [1401.8275].

[251] W. Hollik and S. Paßehr, *Higgs boson masses and mixings in the complex MSSM with two-loop top-Yukawa-coupling corrections*, *JHEP* **10** (2014) 171, [1409.1687].

[252] S. Actis, G. Passarino, C. Sturm and S. Uccirati, *NLO Electroweak Corrections to Higgs Boson Production at Hadron Colliders*, *Phys. Lett.* **B670** (2008) 12–17, [0809.1301].

[253] E. Bagnaschi, G. Degrassi, P. Slavich and A. Vicini, *Higgs production via gluon fusion in the POWHEG approach in the SM and in the MSSM*, *JHEP* **02** (2012) 088, [1111.2854].

[254] M. Spira, *QCD effects in Higgs physics*, *Fortsch. Phys.* **46** (1998) 203–284, [hep-ph/9705337].

[255] S. Dittmaier, M. Kramer, 1 and M. Spira, *Higgs radiation off bottom quarks at the Tevatron and the CERN LHC*, *Phys. Rev.* **D70** (2004) 074010, [hep-ph/0309204].

[256] S. Dawson, C. B. Jackson, L. Reina and D. Wackeroth, *Higgs production in association with bottom quarks at hadron colliders*, *Mod. Phys. Lett.* **A21** (2006) 89–110, [hep-ph/0508293].

[257] S. Dawson, C. B. Jackson, L. Reina and D. Wackeroth, *Exclusive Higgs boson production with bottom quarks at hadron colliders*, *Phys. Rev.* **D69** (2004) 074027, [hep-ph/0311067].

[258] R. M. Barnett, H. E. Haber and D. E. Soper, *Ultraheavy Particle Production from Heavy Partons at Hadron Colliders*, *Nucl. Phys.* **B306** (1988) 697–745.

[259] D. A. Dicus and S. Willenbrock, *Higgs Boson Production from Heavy Quark Fusion*, *Phys. Rev.* **D39** (1989) 751.

[260] M. Bonvini, A. S. Papanastasiou and F. J. Tackmann, *Resummation and matching of b-quark mass effects in $b\bar{b}H$ production*, *JHEP* **11** (2015) 196, [1508.03288].

[261] M. Bonvini, A. S. Papanastasiou and F. J. Tackmann, *Matched predictions for the $b\bar{b}H$ cross section at the 13 TeV LHC*, *JHEP* **10** (2016) 053, [1605.01733].

[262] S. Forte, D. Napoletano and M. Ubiali, *Higgs production in bottom-quark fusion in a matched scheme*, *Phys. Lett.* **B751** (2015) 331–337, [1508.01529].

[263] S. Forte, D. Napoletano and M. Ubiali, *Higgs production in bottom-quark fusion: matching beyond leading order*, *Phys. Lett.* **B763** (2016) 190–196, [1607.00389].

[264] R. V. Harlander and W. B. Kilgore, *Higgs boson production in bottom quark fusion at next-to-next-to leading order*, *Phys. Rev.* **D68** (2003) 013001, [hep-ph/0304035].

[265] H. Mantler and M. Wiesemann, *Hadronic Higgs production through NLO + PS in the SM, the 2HDM and the MSSM*, *Eur. Phys. J.* **C75** (2015) 257, [1504.06625].

[266] S. Liebler, H. Mantler and M. Wiesemann, *Distributions for neutral Higgs production in the NMSSM*, 1608.02949.

[267] R. V. Harlander, H. Mantler and M. Wiesemann, *Transverse momentum resummation for Higgs production via gluon fusion in the MSSM*, *JHEP* **11** (2014) 116, [1409.0531].

[268] H. Mantler and M. Wiesemann, *Top- and bottom-mass effects in hadronic Higgs production at small transverse momenta through LO+NLL*, *Eur. Phys. J.* **C73** (2013) 2467, [1210.8263].

[269] P. Z. Skands et al., *SUSY Les Houches accord: Interfacing SUSY spectrum calculators, decay packages, and event generators*, *JHEP* **07** (2004) 036, [hep-ph/0311123].

[270] B. C. Allanach et al., *SUSY Les Houches Accord 2*, *Comput. Phys. Commun.* **180** (2009) 8–25, [0801.0045].

[271] A. Buckley, J. Ferrando, S. Lloyd, K. Nordstroem, B. Page, M. Rüfenacht et al., *LHAPDF6: parton density access in the LHC precision era*, *Eur. Phys. J.* **C75** (2015) 132, [1412.7420].

[272] E. Bagnaschi, R. V. Harlander, H. Mantler, A. Vicini and M. Wiesemann, *Resummation ambiguities in the Higgs transverse-momentum spectrum in the Standard Model and beyond*, *JHEP* **01** (2016) 090, [1510.08850].

[273] L. A. Harland-Lang, A. D. Martin, P. Motylinski and R. S. Thorne, *Parton distributions in the LHC era: MMHT 2014 PDFs*, *Eur. Phys. J.* **C75** (2015) 204, [1412.3989].

[274] E. Bagnaschi, R. V. Harlander, S. Liebler, H. Mantler, P. Slavich and A. Vicini, *Towards precise predictions for Higgs-boson production in the MSSM*, *JHEP* **06** (2014) 167, [1404.0327].

[275] S. Paßehr and G. Weiglein, *Two-loop top and bottom Yukawa corrections to the Higgs-boson masses in the complex MSSM*, 1705.07909.

[276] P. Drechsel, R. Gröber, S. Heinemeyer, M. M. Muhlleitner, H. Rzehak and G. Weiglein, *Higgs-Boson Masses and Mixing Matrices in the NMSSM: Analysis of On-Shell Calculations*, *Eur. Phys. J.* **C77** (2017) 366, [1612.07681].

[277] E. Fuchs and G. Weiglein, *Impact of $\mathcal{CP}$-violating interference effects on MSSM Higgs searches*, 1705.05757.

[278] S. Forte, D. Gillberg, C. Hays, G. Petrucciani, A. Massironi, G. Zanderighi et al., *Gluon-gluon fusion*, LHCHXSWG-DRAFT-INT-2016-011, Jun, 2016.

[279] F. Demartin, S. Forte, E. Mariani, J. Rojo and A. Vicini, *The impact of PDF and α_s uncertainties on Higgs Production in gluon fusion at hadron colliders*, *Phys. Rev.* **D82** (2010) 014002, [1004.0962].

[280] J. Butterworth et al., *PDF4LHC recommendations for LHC Run II*, *J. Phys.* **G43** (2016) 023001, [1510.03865].

[281] L. Mihaila and C. Reisser, *$O(\alpha_s^2)$ corrections to fermionic Higgs decays in the MSSM*, *JHEP* **08** (2010) 021, [1007.0693].

[282] ATLAS collaboration, *Search for Supersymmetry in events with b-tagged jets and missing transverse energy in pp collisions at $\sqrt{s} = 13$ TeV with the ATLAS detector*, ATLAS-CONF-2017-038, CERN, Geneva, May, 2017.

[283] ATLAS collaboration, *Search for Minimal Supersymmetric Standard Model Higgs Bosons H/A in the $\tau\tau$ final state in up to 13.3 fb^{-1} of pp collisions at $\sqrt{s}$=13 TeV with the ATLAS Detector*, ATLAS-CONF-2016-085, CERN, Geneva, Aug, 2016.

[284] DELPHI, OPAL, ALEPH, LEP Working Group for Higgs Boson Searches, L3 collaboration, S. Schael et al., *Search for neutral MSSM Higgs bosons at LEP*, *Eur. Phys. J.* **C47** (2006) 547–587, [hep-ex/0602042].

[285] OPAL collaboration, G. Abbiendi et al., *Search for neutral Higgs boson in $\mathcal{CP}$-conserving and CP-violating MSSM scenarios*, *Eur. Phys. J.* **C37** (2004) 49–78, [hep-ex/0406057].

[286] M. Carena, J. R. Ellis, A. Pilaftsis and C. E. M. Wagner, *$\mathcal{CP}$-violating MSSM Higgs bosons in the light of LEP-2*, *Phys. Lett.* **B495** (2000) 155–163, [hep-ph/0009212].

[287] N. Greiner, S. Liebler and G. Weiglein, *Interference contributions to gluon initiated heavy Higgs production in the Two-Higgs-Doublet Model*, *Eur. Phys. J.* **C76** (2016) 118, [1512.07232].

[288] E. Maina, *Interference effects in Heavy Higgs production via gluon fusion in the Singlet Extension of the Standard Model*, *JHEP* **06** (2015) 004, [1501.02139].

[289] B. Das, S. Moretti, S. Munir and P. Poulose, *Two Higgs bosons near 125 GeV in the NMSSM: beyond the narrow width approximation*, 1704.02941.

[290] S. Jung, J. Song and Y. W. Yoon, *Dip or nothingness of a Higgs resonance from the interference with a complex phase*, *Phys. Rev.* **D92** (2015) 055009, [1505.00291].

[291] W. Bernreuther, P. Galler, C. Mellein, Z. G. Si and P. Uwer, *Production of heavy Higgs bosons and decay into top quarks at the LHC*, *Phys. Rev.* **D93** (2016) 034032, [1511.05584].

[292] M. Carena and Z. Liu, *Challenges and opportunities for heavy scalar searches in the $t\bar{t}$ channel at the LHC*, *JHEP* **11** (2016) 159, [1608.07282].

[293] S. Liebler and W. Porod, *Electroweak corrections to Neutralino and Chargino decays into a W-boson in the (N)MSSM*, *Nucl. Phys.* **B849** (2011) 213–249, [1011.6163].

Acknowledgements

First and foremost, I would like to thank my supervisor, Georg Weiglein, for the extremely rewarding three years at DESY, and for his encouragement, invaluable advice, and motivating discussions. I thank Jan Louis for agreeing to co-referee my work, and Günter Sigl, Géraldine Servant and Christian Sander for being the referees in my disputation committee. Along with Georg, I am grateful to Nigel Glover for affording me the chance to be a part of the HiggsTools Initial Training Network, which funded a part of my PhD.

My time at DESY would have been a lot less enjoyable or productive without Stefan Liebler, who has been a friend, teacher, mentor and tax advisor all rolled into one. I am indebted to his kindness, his willingness to patiently answer all my questions, and for all that he has taught me over the years. I am also immensely thankful to Elina Fuchs, for numerous discussions, for her timely advice on navigating my PhD whenever I needed help, and for the work on the HiggsBounds plots in the days before the submission of this thesis, among many other things. I am grateful to Stefan and Elina also for reading parts of the thesis draft and providing valuable feedback. I would like to thank Matías Rodríguez Vázquez, Juan M. Cruz Martínez, and Nigel for an insightful collaboration for the HiggsTools Handbook; and Frank Tackmann and Stefan for interesting `SCETlib` discussions.

The HiggsTools Network has been integral to my PhD life. I thank Nigel, Frank Krauss and Giampiero Passarino for making our time with HiggsTools as fruitful as possible; and to the coordinators of all the nodes for organising wonderful summer schools, conferences and workshops. Every HiggsTools meeting with Juan, Giulia, Matías, Raquel, Aga, Stephen, Hjalte, Davide×2, Jooseph, Theo, Marzieh, Cosimo, Giulio, Nicolas, Yaccine, Zahari, Elisa and Michele has been as much fun as it was inspiring, and I am grateful to have shared this time with them. A special thanks to Tim Wolf for his sincere friendship.

Next, a big thanks to DESY friends! I would like to thank Frank and Kerstin, not just for many fun hours of Robo-Rally (and cake!) but also for much needed encouragement and advice. To my many office-mates Shireen, Peter, Marco, Christian, Thibaud, Riccardo, Ibrahim and Johannes, thank you for your supply of food and good humour that made Room 3.206 in 1b such a welcoming and productive place to work. A special thanks to Markus Ebert who kindly lent me a template for typesetting this thesis, and has been my go-to person over the years whenever I found German bureaucracy too overwhelming. My heartfelt gratitude goes out to all the other members of the penthouse: So Young, Markus Diehl, Max, Jim, Maarten, Piotr, Zoltan, Alex, Sebastian; for such lively lunches, coffee breaks and movie nights.

My fondness for Hamburg is inseparable from the friends I found here, who have often played the role of an extended family. An utmost thanks goes to Alexandra and Rebekka, for being a constant part of my life in the last years. Then: To Ludovica, Annika and Ninja, for being my first friends in an unfamiliar country. To Marta, Lorena and Riccardo;

my most unforgettable experiences in Hamburg can undoubtedly be attributed to your company. For the seemingly endless debates and discussions which made my weekends so much fun, I thank Diana, Marco, Salvador, Trevor, and Johannes.

I would not be here if not for a family that has always supported my choices and encouraged me to follow them to the best of my abilities. Thank you: to Siddharth for always keeping me grounded; to mum, for constantly believing in me, sometimes more than I did myself; and to dad, for teaching me to be curious.

Last, a thanks to Shweta Nambiar, Shruti Bhagat and Vassiki Chauhan for friendships that have spanned a decade and several continents, and have been fundamental sources of comfort and motivation. Finally, I would like to thank Frederik for always being in my team and for making the universe a little less absurd.

Eidesstattliche Erklärung

Hiermit erkläre ich an Eides statt, dass ich die vorliegende Dissertationsschrift selbst verfasst und keine anderen als die angegebenen Quellen und Hilfsmittel benutzt habe.

Declaration on oath

I hereby declare, on oath, that I have written the present dissertation by my own and have not used other than the acknowledged resources and aids.

Hamburg, den 14.08.2017 Shruti Patel